Development of fractional step methods for compressible flow solvers using Variational Multiscale stabilized finite element formulations

A thesis submitted for the degree of
Doctor of Philosophy
Universitat Politècnica de Catalunya - Barcelona Tech

UNIVERSITAT POLITÈCNICA
DE CATALUNYA
BARCELONATECH

Doctoral Program in Civil Engineering
Department of Civil & Environmental Engineering
School of Civil Engineering

Samuel Parada Bustelo
Advisors: Ramon Codina Rovira – Joan Baiges Aznar

September 29, 2022

The financial support received from the Agència de Gestió d'Ajuts Universitaris i de Recerca through the predoctoral FI grant 2019-FI-B-00607 is gratefully acknowledged.

Dedicated to my sister

Contents

List of Figures

List of Tables

Acknowledgements

En esta página me gustaría incluir unas líneas de agradecimiento a todas aquellas personas que, de una manera u otra, han hecho posible que haya podido terminar mi tesis de doctorado con éxito.

Quiero empezar agradeciendo a mis dos tutores, a Ramon (sí, sin tilde) Codina y a Joan Baiges. Ha sido un placer haber podido realizar este proyecto de tesis con vosotros. Gracias a Ramon por tener siempre la puerta abierta (a veces literalmente) para contestar mis preguntas e inquietudes y por haberme dejado desarrollar este trabajo con la suficiente libertad. Joan, gracias por la ingente cantidad de horas que has dedicado a mi aprendizaje, sobre todo al principio, y también por hacerme entender el equilibrio práctico que debe existir entre lo que se tiene, lo que se quiere y lo que se necesita.

Al equipo de FEMUSS, gracias por todo el apoyo y ayuda durante todos estos años. Gracias también por haberme llenado el correo de mensajes ”tests failed in test server”. Mi vida sin esos correos ya no será la misma. Quiero mencionar especialmente a Ino y Laura, por haber sido compañeros de fatiga durante la pandemia a través de las reuniones online, lo cual creó un vínculo que va más allá de la oficina. Gracias a los @gbarbat, @aguirre, @afabra, @camoreira, @atello, @rreyes, @cbayona y @ecastillo. Sin duda esto no hubiese sido lo mismo sin vosotros y ha sido muy gratifiante compartir esta experiencia aunque en algunos casos solo fuese por poco tiempo. Especial mención también para David y Jordi, por todas las pausas para el café junto con Ino en la terraza CIMNE, para compartir nuestros pesares y alegrías doctorales.

No puedo olvidarme de mis amigos de Galicia. Gracias a Javier, por la confianza y ser mi compañero de aventuras ciclistas. Gracias a Alejandro, por hacerme ver lo importante que es seguir remando cuando las cosas se le ponen a uno verdaderamente difíciles. Gracias a Gonzalo y a Carlos, por el gran apoyo desde la distancia. También agradecer a mis primeros compañeros de piso, Arnau y Jordi, por haberme proporcionado un ambiente de convivencia tan bueno desde el momento en que llegué a Barcelona.

Finalmente, me gustaría dedicar unas líneas para mis seres queridos. Gracias, en primer lugar, a Claudia. Solo los dos sabemos todo lo que ha costado llegar hasta aquí. Gracias por tu apoyo incondicional desde el primer momento y por hacerme ver el vaso siempre medio lleno. Es una inmensa suerte tenerte cerca. Gracias por ser *mi casa*. Gracias a mi hermana, Fani, por ser siempre el perfecto espejo en el que mirarme, por ser una persona tan valiente, y por regalarme dos sobrinos fantásticos. Gracias a mis padres, por todos los sacrificios que han hecho a lo largo de sus vidas para darnos lo mejor. Y gracias a mis abuelos, sin los cuales hoy no estaría aquí.

Abstract

This thesis deals with finite element methods to solve compressible flow problems, an important branch of Computational Fluid Dynamics (CFD) whose applications are broad in many areas of engineering and science. In spite of the increasing amount of computational resources made available for the scientific and engineering research communities, the numerical simulation of complex compressible phenomena in many practical applications is still a challenge. These type of flow problems are extremely demanding in what concerns numerical computations and memory requirements.

In particular, in this thesis we investigate the possibility to solve the underlying algebraic systems in a decoupled manner, a technique usually called fractional step or segregation method. Although segregation techniques have been broadly studied and analyzed for the incompressible Navier-Stokes equations, allowing for the separate resolution of velocity and pressure unkonwns, much less has been explored for compressible problems. The interest on this type of technique not only comes from the fact that it permits a segregated calculation of the problem unkonwns (usually leading to better conditioned systems) but from the associated reduction of the computational cost.

We study three different problems inside the compressible CFD research branch in separated chapters: the isentropic Navier-Stokes equations, the Navier-Stokes problem written in primitive variables (velocity, pressure and temperature), and the Navier-Stokes problem written in the classical formulation with conservative variables (momentum, density, total energy). For each of these problems, first we propose a finite element stabilized formulation framed within the Variational MultiScale concept, which allows to use equal interpolation spaces for all the variables in play. Second, and once space and time discretizations are selected, we derive fractional step methods up to second order in time. Finally, all the schemes are implemented in a parallel multiphysics code and representative simulations are carried out in order to analyze the performance of the proposed techniques.

Notation

The notation employed in this work is fairly standard in the computational mechanics literature. In order to clarify the exposition, the matrix version of the abstract formulation of the problems studied in this thesis will be given, mainly because it will serve as a starting point for presenting the basic flow chart of the iterative algorithms.

As a general rule and with few exceptions stated in the text, tensors of rank greater than or equal to one are denoted by boldface characters and scalars by lightface italic characters. Moreover, we shall use standard Cartesian notation to refer to a particular coordinate system, hence denoting by $\mathbf{x}$ the position vector and (x_1, x_2, x_3) or (x, y, z) the Cartesian coordinates for the three-dimensional case.

When deriving the weak formulation of the problems in this thesis, we will use

$$\langle \bullet, \star \rangle_\omega$$

to denote the integral over a region ω of the product of two functions $(\bullet)$ and $(\star)$, assumed to be well defined. The subscript will be dropped when the region is the actual computational domain of the problem Ω.

Likewise, the classical gradient, divergence, and Laplacian operators have been denoted respectively by

$$\nabla(\bullet), \quad \nabla \cdot (\bullet), \quad \text{and} \quad \Delta(\bullet).$$

For the case of the temporal derivative and for the partial derivative with respect to a Cartesian coordinate x_i, we shall use any of the following symbols

$$\partial_t(\bullet) \equiv \frac{\partial(\bullet)}{\partial t}, \quad \partial_i(\bullet) \equiv \frac{\partial(\bullet)}{\partial x_i},$$

and, in addition, the symbol δt will stand for the time step size. In this regard, we make use of a superscript to denote the time step counter, indicating by n the time level up to which the solution is known. Then, f^n will denote an approximation to a certain time-dependent function $f(t)$ at time t^n.

Most of the problems in this thesis are nonlinear and the way in which we denote a certain iterative strategy is by a superscript with parentheses enclosing the nonlinear iteration counter, *e.g.*, $g^{(i)}$ denotes a general function g evaluated at iteration i.

Various integers have been employed in the text. The most important ones are

N_{sd} :	number of space dimensions
N_{el} :	number of elements in the discretization
N_{no} :	number of nodes per element
N_{tp} :	total number of nodes of the finite element mesh
N :	number of time steps

In the development of finite element formulations, the symbol

$$\Omega^{(e)}, \quad e = 1, \dots, N_{\text{el}}$$

has been used to denote a finite element partition of the computational domain Ω. It is understood that the subdomains $\Omega^{(e)}$ are open, non-overlapping and the union of their closures is the closure of Ω, *i. e.*

$$\overline{\Omega} = \bigcup_{e=1}^{N_{\text{el}}} \overline{\Omega}^{(e)} \quad \text{and} \quad \Omega^{(e)} \cap \Omega^{(f)} = \emptyset \quad \text{for } e \neq f.$$

Each subdomain $\Omega^{(e)}$ has a has a piecewise smooth boundary $\Gamma^{(e)} = \partial\Omega^{(e)}$. A function belonging to the finite element space is recognized by the subscript h, which also stands for the characteristic mesh size, such that

$$h = \max_{e} \left\{ h^{(e)} \right\}, \quad h^{(e)} = \operatorname{diam}\left(\Omega^{(e)}\right).$$

A generic shape function has been denoted by φ, usually with the addition of a superscript to indicate the node to which it is associated.

The rest of the notation is explained in the text.

Introduction 1

1.1 Prologue

After having spent his entire life dedicated to the study of mathematics and physics, with paramount contributions in the field of fluid mechanics, Leonhard Euler died in 1783 due to an ischemic disease. French engineer Claude-Louis Navier, carrying on the work previously developed by Euler, passed away just at the age of 51 in the 19th century. Now it is my turn to address the subject of fluid mechanics; specifically Computational Fluid Dynamics (CFD). Taking into account the previous statements, perhaps it would be a wise decision to approach the subject with extreme care.

All jokes aside, fluid mechanics has always been one the main areas of science which resulted more appealing to mathematicians, physicists and engineers. In the 18th century, Euler was able to completely describe the movement of a fluid by means of a set of Partial Differential Equations (PDEs), fully derived from basic physical principles such as conservation of mass, momentum and energy. Until then, the majority of the works in the field of fluid mechanics were devoted to hydraulic engineering, where the Archimede's principle and Pascal's law represented the most remarkable contributions. Hence, Euler was the first scientist who succeeded at providing a mathematical description which characterized the basic behavior of a fluid.

Although Euler equations were a huge accomplishment in themselves, they did not reproduce viscous effects, which are innate to a fluid motion. The inclusion and interpretation of viscosity effects were precisely the main findings of Navier and Irish mathematician and physicist George Stokes. Thereby, the socalled Navier-Stokes equations were born[1].

Nowadays, the mathematical set of Navier-Stokes equations serves as an starting point in many different fields of physics and engineering, specifically in aerodynamics [1, 2], as well as in the study of atmospheric and oceanic sciences [3] or even geophysical phenomena; a branch usually known as geophysical fluid dynamics (GFD) [4, 5]. However, from the

[1] Although in the literature many publications refer to the Navier-Stokes equations to those modeling just the incompressible behavior, in this thesis we refer to the complete set of PDEs including mass, momentum and energy conservation equations.

[1]: Anderson (2021), *Fundamentals of Aerodynamics*
[2]: Blazek (2015), *Computational Fluid Dynamics: principles and applications*
[3]: Vallis (2017), *Atmospheric and Oceanic Fluid Dynamics: Fundamentals and Large-Scale Circulation*
[4]: Cushman-Roisin et al. (2011), *Introduction to Geophysical Fluid Dynamics*
[5]: Vallis (2016), "Geophysical fluid dynamics: whence, whither and why?"

pure mathematical point of view, the Navier-Stokes equations are really challenging to tackle. They represent a mixed nonlinear parabolic-hyperbolic set of PDEs whose analytical solutions is unknown even when making use of simplification hypothesis. This is in fact one of the socalled millennium problems proposed by the Clay Mathematics Institute, whose solution could reward you a total prize of $1,000,000. Therefore, in practice, solutions to this problem are computed via numerical methods, a branch of mathematics whose early developments date back to the 17th century with the Newton-Raphson method.

Nevertheless, the boom of numerical methods took place in the 20th century mainly associated to the strengthening of computational calculus. This fact is nothing but a direct result of the technological advances in computer science, what made possible to deal with mathematical problems which were unaffordable until then. In this regard, many different methodologies were developed, such as the Finite Element Method (FEM), originally used in solid mechanics, and the Finite Volume Method (FVM), which emerged as the fluid mechanics counterpart. The cornerstone of these two techniques is the splitting of the domain where the problem is posed into a set of elements, forming a mesh in which the solution is approximated. The application of numerical or computational methods specifically in fluid mechanics is named CFD, whose developments were of significant impact in the Cold War and in particular in the Space Race. Doubtlessly, this is an area of continuous advance and innovation and this thesis is my very small contribution to the exciting field of CFD.

1.2 Compressibility

We shall start this introductory section by clarifying the concept of compressibility. The compressibility of a fluid is a measure of the density changes which occur as a response to specific changes in pressure. In general, it can be stated that gases are highly compressible whereas most liquids show a very low compressiblity. In a fluid flow, there might be changes in pressure associated, for instance, with changes in the flow velocity. Then, these pressure changes will, in general, induce density changes, which will have an influence on the flow features, *i.e.*, the compressibility of the fluid will have an influence on the flow. If these density changes are significant, the temperature changes in the flow, which may arise due to the kinetic energy variations, also affect the development of the flow. In other words, when compressibility is important, the temperature changes of the flow are also important.

There exist many different situations of practical relevance in which the effect of such density and/or temperature changes is negligible. Classical incompressible fluid mechanics deals with that kind of flows in which pressure and kinetic energy changes are so small that the effects of the induced density and temperature changes on the fluid flow are not accounted for. There also exist, however, many fluid flows in which the incompressible assumption is not adequate. Density and temperature changes can be so large that they can really influence the development of the flow. Under these circumstances, it is mandatory to analyze the dynamics of the flow together with its thermodynamics. The study of this type of flows is an entire discipline by itself in the vast field of fluid mechanics and it is usually termed compressible fluid flow or, sometimes, gas dynamics.

The traditional (and most important we shall say) application of compressible fluid flow theory is in the design of high speed aircrafts[2]. Likewise, compressible flow theory is required in the design and operation of many other devices commonly encountered in many engineering areas such as steam and gas turbines (the flow in the blades and nozzles is compressible) or reciprocating engines (the flow of the gases through the valves and in the intake and exhaust systems must be treated as compressible).

[2] The reader might remember the popular Aérospatiale/BAC Concorde, retired back in 2003, which was a passenger airliner with a maximum speed over twice the speed of sound.

1.3 Numerical methods

1.3.1 A brief historical note

The field of numerical methods experienced a huge step forward from the second half of the 20th century. The method of finite differences represents one of the oldest and most direct approaches to discretizing PDEs. In fact, it was already used by Euler for one-dimensional problems. However, although it can be a very efficient method for regular grids and provide high quality results, its applicability is reduced and hence usually left for academic purposes since it shows many inconveniences for complex problems with irregular geometries and the imposition of boundary conditions might also be problematic.

In the 50s, the Finite Element Method (FEM) was born. Initially, the formulation of the method emerged from a traditional structural engineering approach and the first applications of this technique were precisely in the field of solid mechanics. However, as the underlying mathematical foundation of the method was understood, its extension to other disciplines became possible. This fact represented a huge advance in many design and analysis procedures in different areas such as civil, mechanical and aerospace engineering. Professor Zienkiewicz[3], one of the early pioneers of the FEM and internationally recognized as a leading figure in its development, was precisely the one who became aware of the possible application of this technique outside the area of structural analysis. His book [6] is still viewed by many as ”the bible” of the FEM. In particular, he applied the FEM to fluid mechanics problems, being the first non-structural application the treatment of a groundwater flow problem. The finite element process as a methodology to solve continuum problems is based on the division of the continuum into a finite number of parts (known as finite elements, which form a mesh), whose response is specified by a finite number of parameters. From the mathematical viewpoint, the FEM is a variational (or energy) methodology based on the derivation of the socalled weak form, departing from the strong (or differential form). Then, the unknown quantities can be interpolated using polynomials over the elements of the mesh. Over the last 10 to 15 years, efficient numerical techniques for CFD simulations in the framework of FEM have been developed and become increasingly popular. Today, the FEM remains as a prosper research branch and its application has been considerably extended to new scientific areas, even including medicine (see *e.g.* [7, 8]).

Closely related to the FEM, and developed almost in parallel, the Finite Volume Method (FVM) has always been a widely used technique in CFD. In essence, the basic principle is the same as in the FEM, *i.e.*, the division of the continuum domain into a finite number of parts, yet in this case the term cell or control volume is used instead of element due to mathematical reasoning. In contrast to the FEM, the FVM departs from the integral form of the conservation laws, rather than

[3] He founded the first journal devoted to the subject of computational mechanics in 1968, the International Journal for Numerical Methods in Engineering (IJNME) which still remains nowadays as one of the preferred options for the publication of novel developments in computational mechanics and related areas.

[6]: Zienkiewicz et al. (2013), *The Finite Element Method: Its Basis and Fundamentals*

[7]: Magomedov et al. (2020), “Application of Finite Element Analysis in medicine”

[8]: Driscoll (2019), “The Impact of the Finite Element Method on Medical Device Design”

their differential form. It ensures local conservation at the cell level, and this is precisely why it has been the natural choice to solve problems in CFD (the Navier-Stokes equations represent nothing but conservation of mass, momentum and energy). One of the first and most important contributions in this area was proposed by Godunov [9], as he developed a conservative scheme for nonlinear hyperbolic systems where the solution is constant over each cell. Since then, many works have been developed within the FVM framework, in order to understand the difficulties lying on the application of the general procedure, the development of numerical strategies to overcome them and the extension to higher-order approximations.

In the 70s decade, one of the first meshless techniques appeared. This is the socalled Smooth Particle Hydrodynamics (SPH) method. This technique was novelly developed in [10] and simultaneously in [11] initially for problems in astrophysics. However, in the end it has been widely used in fluid mechanics problems especially when the required solution involves heterogeneous media or rapidly moving free surfaces [12]. The lack of a mesh in the classical sense simplifies the model implementation and its parallelization. However, the prescription of boundary conditions in inlets, outlets or walls is definitely more problematic than classical grid-based techniques and, specifically in CFD, it shows many difficulties when dealing with shock waves.

The advancement of numerical methods within the field of CFD has always been related to the development of higher order approximations. In this regard, it is worth mentioning the Discontinuous Galerkin (DG) method, which was first introduced in [13]. It is based on a element by element discontinuous aproximation but continuity is imposed in the weak form with proper numerical fluxes, which provide a natural stabilization to the solution. Successful applications of DG methods to flow problems were performed in the 90s, being very important contributions the works by Cockburn [14] for the Euler equations and Bassi [15] for the Navier-Stokes equations. However, DG methods have been considerably questioned mainly because for the same mesh and polynomial degree of the approximation, the number of globally coupled degrees of freedom of the DG methods is much bigger than that of the classical continuous method (FEM). In order to mitigate this inconvenience, the Hybridizable Discontinuous Galerkin (HDG) method emerged. Generally speak-

[9]: Godunov (1959), "A difference scheme for numerical solution of discontinuous solution of hydrodynamic equations"

[10]: Lucy (1977), "A numerical approach to the testing of the fission hypothesis."

[11]: Gingold et al. (1977), "Smoothed particle hydrodynamics: theory and application to non-spherical stars"

[12]: Violeau (2012), *Fluid Mechanics and the SPH Method: Theory and Applications*

[13]: Reed et al. (1973), *Triangular mesh methods for the neutron transport equation*

[14]: Cockburn (1999), "Discontinuous Galerkin Methods for Convection-Dominated Problems"

[15]: Bassi et al. (1997), "A High-Order Accurate Discontinuous Finite Element Method for the Numerical Solution of the Compressible Navier–Stokes Equations"

ing, the HDG methods are derived upon the discretization in terms of many local problems, especifically one for each element in the mesh, together with a single global problem posed over the skeleton of the mesh which imposes the transmission conditions. Clearly, HDG methods have been devised as a significantly less expensive alternative than classical DG methods, and they have been succesfully aplied to a wide range of problems in CFD [16–18].

[16]: Sevilla (2021), "An implicit HDG method for linear convection-diffusion with dual time stepping"
[17]: Cockburn et al. (2009), "The Derivation of Hybridizable Discontinuous Galerkin Methods for Stokes Flow"
[18]: Woopen et al. (2014), "A Hybridized Discontinuous Galerkin Method for Turbulent Compressible Flow"

1.3.2 State of the art

The numerical approximation of transient flow problems (particularly the compressible Navier-Stokes equations) involves complex numerical techniques particularly when the principal objective is to represent the flow features up to the smallest scales. To this end, researchers either focus on the application of high precision numerical methodologies or on the refinement of the mesh (and time step sizes for the time integration). The latter option is remarkably expensive from the computational point of view (and especially in large domains), since it leads to an algebraic system that contains a very large number of unknowns and whose solution is substantially difficult to obtain. In this regard, a possible alternative is to make use of Adaptive Mesh Refinement (AMR) techniques. Essentially, AMR faces the previous issue after dynamically reconfiguring an initial mesh and changing its structure by employing some type of criteria (see *e.g.* the technique previously developed in our group in [19] as an example in compressible flow simulations).

[19]: Bayona-Roa et al. (2018), "Variational multiscale error estimators for the adaptive mesh refinement of compressible flow simulations"

On the other hand, high order spatial methods have experienced a growing interest in scientific and engineering communities (and especially in CFD), due to their increased accuracy with respect to classical low-order methods [20]. This approach is generally cheaper from the computational viewpoint in contrast to the refinement technique, yet most high order spatial schemes are commonly restricted to simple domain configurations. For more challenging geometries, the aforementioned HDG method has become an engaging field of research [21]. However, the FVM and FEM still remain as the preferred choices in both industrial [22] and research [23, 24] CFD solvers mainly due to their demonstrated robustness, easy implementation and competitiveness. Particularly in this work, we favor finite element methodologies.

[20]: Wang et al. (2013), "High-order CFD methods: current status and perspective"
[21]: Vila-Pérez et al. (2021), "Hybridisable Discontinuous Galerkin Formulation of Compressible Flows"
[22]: Chalot et al. (2010), "Higher-Order Stabilized Finite Elements in an Industrial Navier-Stokes Code"
[23]: Sevilla et al. (2013), "An analysis of the performance of a high-order stabilised finite element method for simulating compressible flows"
[24]: Chassaing et al. (2013), "Accuracy assessment of a high-order moving least squares finite volume method for compressible flows"

The treatment of the transient term appearing in the flow equations also deserves some special comments. Of course, a different approach than the FEM or the FVM has to be selected, usually a finite difference scheme in time. In this case, and particularly in the field of compressible flows, a dichotomy is devised between explicit or implicit schemes. The former uses only known information from previous calculations in order to advance the solution in time whereas the latter requires information of the solution which still has to be determined, thus resulting in a nonlinear problem that needs to be treated with some numerical strategy at some point.

Explicit time integration schemes are usually selected to accurately describe the propagation of the smallest scales, and they have been extensively used in compressible flow simulations (see *e.g.* [25–27]). The properties of this type of methods are well understood and fairly efficient schemes from the computational viewpoint have been developed, since they require a small number of parallel communications compared to implicit schemes (yet this depends on the computational implementation strategy). However, the main drawback of explicit time integration schemes lies in the numerical limit of stability posed on the time step size for the computations; the well known Courant–Friedrichs–Lewy (CFL) condition. When the time step size exceeds such stability limit, numerical instabilities appear and the solution becomes unbounded in time. In addition, intermediate stages are often needed by higher order schemes, which results in several computational efforts that can be wasted in cumbersome calculations. On the contrary, the time step size can be prescribed for implicit schemes but some particular method for dealing with the nonlinear character of the underlying equations needs to be included, as pointed out previously. There is not a clear agreement on the choice of the time integration scheme for compressible flow problems. Although explicit schemes might be the standard procedure for transonic and supersonic simulations (*e.g.* [28]), at low Mach number flows the acoustic speed tends to infinity and this fact restricts explicit schemes to extremely small time step sizes. This restriction is avoided by using an implicit time integration scheme for the time derivatives of the unknowns of the problem [29]. In this thesis, we will make use of implicit time integration schemes.

The compressible Navier-Stokes equations, namely the con-

[25]: Jameson et al. (1981), “Numerical solution of the Euler equations by finite volume methods using Runge Kutta time stepping schemes”

[26]: Messahel et al. (2021), “A conservative multirate explicit time integration method for computation of compressible flows”

[27]: Buuren (1999), “Time integration methods for compressible flow”

[28]: Bayona et al. (2015), “Variational multi-scale finite element solution of the compressible Navier–Stokes equations”

[29]: Bayona et al. (2019), “Solution of low Mach number aeroacoustic flows using a Variational Multi-Scale finite element formulation of the compressible Navier–Stokes equations written in primitive variables”

servation of mass, momentum, and energy, together with the constitutive and thermodynamical closing equations, represent a physical model capable of describing compressible fluid flow phenomena. This model is able to represent the wide range of spatial and temporal flow scales typically encountered in engineering cases of interest, as pointed out in Section 1.2. After performing the space discretization via the FEM and selecting a time integration scheme to advance the solution in time, solving the underlying algebraic system of equations in a monolithic (coupled) manner is the classical strategy. However, despite of the several simplifications that might be introduced along the whole procedure, solving the resulting linear system might still be computationally expensive, specially in 3D geometries. The unknowns in compressible flow problems are highly coupled (mainly through the constitutive and thermodynamical relations) and nonlinearities need to be treated with some strategy too. An alternative to that standard approach is to advance the solution of the problem in time by means of a *fractional step or segregation method*. This technique consists in segregating or splitting the calculation of the unknowns, in such a way that they can be computed separately, yet this may involve the introduction of some correction steps during the computations. On the negative side, fractional step methods have an associated temporal error, frequently labeled as fractional or segregation error, and which precisely emanates from the splitting of the solution procedure. In this regard, it is indispensable to ensure that such error is at least of the same order than that of the time integration scheme used for the temporal discretization, because otherwise the global temporal accuracy of the method is broken.

Although some may think that fractional step methods are a novel solution approach, the truth is that this technique was developed in the 60s with the pioneering works published by Chorin and Teman in [30–33] for the incompressible Navier-Stokes problem. In these publications, a method to decouple the calculation of velocity and pressure unknowns was proposed, an originally labeled as pressure segregation methods. The original method made possible the segregation of the pressure unknown by means of a projection operator, and that is why the original scheme is also known in the literature as the projection method. In the projection method, an intermediate velocity obtained from the momentum equation without the pressure term is decomposed into a

[30]: Chorin (1967), "A numerical method for solving incompressible viscous problems"
[31]: Chorin (1968), "Numerical solution of the Navier-Stokes equations"
[32]: Teman (1969), "Sur l'approximation de la solution des equations de Navier–Stokes par la méthode des pas fractionaires (I)"
[33]: Teman (1969), "Sur l'approximation de la solution des equations de Navier–Stokes par la méthode des pas fractionaires (II)"

solenoidal field, the velocity, and the gradient of a scalar field, the pressure. Essentially, the main idea is that the approximation of the uncoupled continuous problem has a lower computational requirement than the one from the original coupled problem, what in turn permits to compute the solution more efficiently for large scale simulations. Those publications established the foundation of this segregated approach and, since then, many works have been devoted to a proper understanding of the original schemes, their numerical and stability properties, their extension to higher order approximations and to the design of adequate boundary conditions (we highlight *e.g.* [34–45] to name a few). Over the past two decades, fractional step methods have enjoyed an extensive recognition mainly due to two reasons: the aforementioned important reduction of computational time and the introduction of an intrinsic stability over the pressure gradient term, as explained in [46].

Although the first schemes were introduced at the continuous level, *i.e.* manipulating the continuous equations, a different approach to the classical projection methods was proposed by Perot in a discrete setting (both in space and time) in [47]. In this publication, the classical pressure segregation method is identified as an inexact factorization of the final algebraic system. In [48], Quarteroni further analyzed and generalized this approach, and Badia in [49] performed the convergence analysis of a first order algebraic method obtaining optimal results in space and in time. In this work we favor such algebraic viewpoint, introducing the splitting of the equations once space and time discretizations have been selected. Our choice is based on some of the points discussed in [50] (see Section 4 of that publication). First of all, continuous projection methods have been questioned regarding the imposition of Dirichlet and Neumann boundary conditions on the different steps of the scheme. However, any reference to the proper imposition of boundary conditions for the steps of the scheme can be skipped if the splitting at the purely algebraic level is performed. In addition to this, and for problems with open boundaries, Neumann boundary conditions are directly incorporated in the force term as it is the case of the coupled monolithic system. High order schemes designed at the continuous level are scarce and particularly difficult to obtain, but several third and even fourth order splitting methods obtained from the algebraic viewpoint can be found in the literature (see *e.g.* [51, 52]). It is also worth men-

[34]: Guermond et al. (2003), “A new class of truly consistent splitting schemes for incompressible flows”

[35]: Kan (1986), “A Second-Order Accurate Pressure-Correction Scheme for Viscous Incompressible Flow”

[36]: Prohl (1997), “Advances in Numerical Mathematics”

[37]: Guermond et al. (1998), “On the approximation of the unsteady Navier–Stokes equations by finite element projection methods”

[38]: Guermond et al. (2004), “On the error estimates for the rotational pressure-correction projection methods”

[39]: Karniadakis et al. (1991), “High-order splitting methods for the incompressible Navier-Stokes equations”

[40]: Codina et al. (2006), “On some pressure segregation methods of fractional-step type for the finite element approximation of incompressible flow problems”

[41]: Shen (1992), “On error estimates of some higher order projection and penalty-projection methods for Navier-Stokes equations”

[42]: Kim et al. (1985), “Application of a fractional-step method to incompressible Navier-Stokes equations”

[43]: Guermond et al. (1998), “On stability and convergence of projection methods based on pressure Poisson equation”

[44]: Guermond et al. (2006), “An overview of projection methods for incompressible flows”

[45]: Rebholz et al. (2020), “Analysis of Algebraic Chorin Temam splitting for incompressible NSE and comparison to Yosida methods”

[46]: Codina (2001), “Pressure stability in fractional step finite element methods for incompressible flows”

[47]: Perot (1993), “An analysis of the fractional step method”

tioning that pressure segregation methods introduced at the purely algebraic level also motivate effective preconditioners to be exploited for the monolithic Navier-Stokes system. Finally, the algebraic approach has been extensively and effectively applied to different test cases in computational physics in our research group, including the classical incompressible equations [53, 54] and the viscoelastic flow problem [55]. In this regard, this thesis can be seen as a continuation of those works, and with the objective of exploring the applicability of segregation techniques to compressible flow problems.

While the literature regarding fractional step or segregation schemes for incompressible flow applications is really vast, the application of this type of techniques to compressible flow simulations is rare. However, several innovative and diverse collections of uncoupling techniques have been published, which involve distinct spatial discretizations (finite differences, finite volumes, finite elements), temporal schemes (explicit, implicit, semi-implicit) and also different sets of unknowns (conservative, primitive and even combinations of both type of variables). In [56], Hauke and coworkers introduce a segregated method for non-isothermal compressible flows but preserving the thermodynamic coupling due to convergence reasons and Herárd [57] presents a fractional step algorithm in the context of the FVM for the computation of numerical approximations of a class of two-fluid two-phase flow model. A mixed method for a barotropic flow model is discussed in [58], which combines a segregation method of pressure-correction type to a space discretization associating low order non-conforming mixed finite elements and finite volumes. A sort of fractional step in the context of the second order central difference scheme for low Mach number flows was developed in [59]. Finally, it is also worth mentioning the work of Codina and coworkers [60], who proposed a general algorithm for both compressible and incompressible regimes by performing discretizations along the characteristics.

1.4 Conferences & publications

During the development of the present PhD thesis, the partial advances and results have been presented in several international and specialized conferences or workshops. The list of attended conferences is included down below:

[48]: Quarteroni et al. (2000), “Factorization methods for the numerical approximation of Navier–Stokes equations”

[49]: Badia et al. (2007), “Convergence analysis of the FEM approximation of the first order projection method for incompressible flows with and without the inf-sup condition”

[50]: Badia et al. (2007), “Algebraic Pressure Segregation Methods for the Incompressible Navier–Stokes Equations”

[51]: Gervasio et al. (2006), “Algebraic Fractional-Step Schemes for Time-Dependent Incompressible Navier–Stokes Equations”

[52]: Gervasio et al. (2006), “Algebraic fractional-step schemes with spectral methods for the incompressible Navier–Stokes equations”

[53]: Badia et al. (2008), “Pressure segregation methods based on a discrete pressure Poisson equation. An algebraic approach”

[54]: Folch et al. (1999), “A fractional-step finite-element method for the Navier–Stokes equations applied to magma-chamber withdrawal”

[55]: Castillo et al. (2015), “First, second and third order fractional step methods for the three-field viscoelastic flow problem”

[56]: Hauke et al. (2005), “A segregated method for compressible flow computation.Part II: General divariant compressible fows”

[57]: Hérard et al. (2012), “A fractional step method to compute a class of compressible gas-liquid flows”

[58]: Gallouët et al. (2008), “An unconditionally stable pressure correction scheme for the compressible barotropic Navier–Stokes equations”

[59]: Liu et al. (2007), “A fractional step method for solving the compressible Navier–Stokes equations”

- Joan Baiges, Ramon Codina and Samuel Parada. *A fractional step method for the isentropic Navier-Stokes problem.* 20th International Conference on Fluid Flow Problems (FEF–2019). March 31 – April 3, 2019, Chicago, IL, USA.
- Samuel Parada, Joan Baiges and Ramon Codina. *Weak imposition of Dirichlet boundary conditions in incompressible and isentropic flows using fractional step methods.* Congress on Numerical Methods in Engineering (CMN-2019). July 1–3, 2019, Guimarães, Portugal.
- Samuel Parada, Ramon Codina and Joan Baiges. *On the development of algebraic fractional step algorithms for the compressilbe Navier-Stokes equations.* 14th World Congress in Computational Mechanics (WCCM – ECCOMAS 2020). January 11 – February 4, 2021, Paris, France (online due to Covid-19 pandemic).

[60]: Codina et al. (1996), "A general algorithm for the compressible and incompressible flows. Part III: the semi–implicit form"

In addition to the above mentioned conferences, the results and findings of this thesis have been published in peer reviewed academic journals. The list of articles is provided down below:

- Samuel Parada, Joan Baiges and Ramon Codina. *A fractional step method for computational aeroacoustics using weak imposition of Dirichlet boundary conditions.* In *Computers & Fluids* (2020), p. 104374, vol. 197.
  DOI = https://doi.org/10.1016/j.compfluid.2019.104374.
- Samuel Parada, Ramon Codina and Joan Baiges. *Development of an algebraic fractional step scheme for the primitive formulation of the compressible Navier-Stokes equations.* In *Journal of Computational Physics* (2021), p. 111017, vol. 433.
  DOI = https://doi.org/10.1016/j.jcp.2020.110017
- Samuel Parada, Ramon Codina and Joan Baiges. *A VMS-based fractional step technique for the compressible Navier-Stokes equations using conservative variables.* In *Journal of Computational Physics* (2022), p. 111137, vol. 459.
  DOI = https://doi.org/10.1016/j.jcp.2022.111137

1.5 Outline

The work developed in this thesis can be enclosed in the main objective of investigating stabilized finite element formulations for compressible flows simulations, a new research line opened in our research group quite recently. The aim of this study is specifically the design and development of new numerical schemes to solve compressible flow problems with reduced computational cost in comparison to classical techniques by using fractional step methods.

All the numerical strategies that we develop are based on the FEM, and in order to avoid any possible instabilities that may appear when using the standard Galerkin methodology, a two-scale approximation is developed in the context of the Variational Multi-Scale (VMS) framework, which permits the same interpolation for all variables of the problem.

In particular, we will analyze in this thesis three different scenarios. As a first approach to compressible flows, we study the isentropic Navier-Stokes problem, which can be understood as an extension of the classical incompressible case with the addition of the pressure temporal derivative. After this, we examine the primitive formulation of the complete Navier-Stokes problem and, finally, we proceed similarly with the conservative formulation. The main goal for each problem is to develop fractional step schemes at least of second order in time, implement them in a High Performance Computing (HPC) environment and test them by simulating reference test cases.

The specific content of this work is divided into several subjects, which are studied and developed progressively, and that will be presented in the document as follows:

- Chapter 2 is an introductory chapter to present the basic equations in fluid mechanics (postulates, variables in play, definitions, *etc.*), which will serve as starting point for the upcoming developments.
- Chapter 3 is devoted to the VMS framework. Since all the numerical algorithms of this thesis are based precisely on this technique, a separated chapter is included. Here we apply the VMS framework to a general problem, which we then particularize in the subsequent chapters.
- Chapter 4 presents a development of a fractional step method for the isentropic Navier-Stokes problem within the VMS framework.
- Chapter 5 extends the work of the previous chapter and focuses on the solution of the complete Navier-Stokes equations written in pressure primitive variables by means

of a fractional step method in time. We focus here on low Mach simulations.

- Chapter 6 is devoted to the VMS formulation of the full compressible Navier-Stokes equations written in conservative variables. The design of the VMS stabilized formulation plus the derivation of a fractional step algorithm is the main objective of the chapter. The solution of supersonic cases with shock capturing methods is also investigated.

Let us finally mention that chapters are quite self contained even if this implies the need of repeating some information. This is due to the fact that Chapter 4, Chapter 5 and Chapter 6 are based on the above mentioned publications individually.

1.6 FEMUSS

All the algorithms developed in this thesis are implemented in FEMUSS[4]. This is an object-oriented and Fortran-based finite element code which follows a modular approach for multiphysics interaction and performs parallel computations under MPI directives, thus setting an HPC environment. The included modules range from fluid dynamics (classical incompressible and compressible equations, wave equations, low Mach models, *etc.*), solid mechanics (plates, shells, incompressible materials, *etc.*), fluid-structure interacion or coupled thermal problems among others.

FEMUSS makes use of PETSc[5] [61], a suite of data routines and algorithms for the scalable (parallel) solution of different applications modeled by PDEs. It includes a large set of parallel linear and nonlinear solvers that can be coupled to different application codes. Nowadays, FEMUSS relies on PETSC not only as a solver library, but also as a partitioner and communicator among subdomains, thanks to the PETSC broad set of capabilities. The interaction of FEMUSS with PETSc is achieved through an abstract and independent interface, what would allow to easily replace PETSc by another library if required (for example Trilinos).

For the preprocessing stage we use GID, a processing system for computer analysis in science and engineering developed here at CIMNE, whereas most of the postprocessing has been done with Paraview [62] through the VTK library [63].

[4] FEMUSS stands for Finite Element Method Using Subgrid Scales.

[5] PETSc stands for Portable, Extensible Toolkit for Scientific Computation.

[61]: Balay et al. (2015), *PETSc Web page*

[62]: Ayachit (2015), *The ParaView Guide: A Parallel Visualization Application*

[63]: Schroeder et al. (2006), *The Visualization Toolkit*

One of the main strengths of FEMUSS is the straightforward organization and accessibility of the code, which facilitates the introduction of new models and algorithms. Nevertheless, since it is mostly research-oriented and in constant development, the implementation of new formulations requires additional changes and improvements to reach the goals of the work.

Let us now provide some insights on the general structure of FEMUSS. The highest level structure in FEMUSS is named CASE. In each CASE, all processes taking place over the same finite element mesh are grouped. As a consequence, each CASE has a its own mesh (together with an adaptive refiner, yet this is out of the scope of this explanation), a file postprocessor and might have several physical problems inside. Hence, different CASEs could be defined so that the code is capable of dealing with, for instance, fluid-structure interaction where each problem is defined on a different computational domain and may involve different mesh requirements and procedures.

The most important object inside FEMUSS is the mesh object. This takes care of all the geometrical information including elements, connectivities, coordinates, shape functions, *etc.* File postprocessors are objects in charge of writing information to disk so that the results can be visualized later on.

Other important concepts in FEMUSS are the Physical Problems and the Physical Problem Drivers. The latter, as the name suggests, 'drives' or commands the Physical Problem while allowing for its interaction with external objects. Inside the Physical Problems part, the different modules are implemented. In this thesis, a compressible flow module was developed from scratch for the algorithms in Chapter 5 and Chapter 6, whereas the implementation of the algorithms in Chapter 4 relies in previous subroutines .

The Navier-Stokes equations of compressible flow 2

2.1 Introduction

The foundation of the subject of continuum mechanics is the establishment of a series of general postulates, holding under any type of condition. These are the socalled balance principles, namely, the conservation of mass, the balance of linear (and angular) momentum and the conservation of energy (also known as the first law of thermodynamics).

From this point, the fluid mechanics or general Navier-Stokes problem can be formally stated. This chapter is devoted to the presentation of the basic equations which allow to study the dynamic behavior of a fluid and which also serve as a starting point for the developments in Chapter 4, Chapter 5 and Chapter 6.

The material here presented is basic and the different parts of this chapter can be found in classical textbooks of fluid mechanics or continuum mechanics. Some of my favourite are [64–68].

[64]: Landau et al. (1987), *Fluid Mechanics*
[65]: Aris (1989), *Vectors, Tensors and the Basic Equations of Fluid Mechanics*
[66]: Batchelor (2000), *An Introduction to Fluid Dynamics*
[67]: Oliver et al. (2017), *Continuum Mechanics for Engineers. Theory and Problems*
[68]: Holzapfel (2000), *Nonlinear Solid Mechanics: A Continuum Approach for Engineering*

2.2 Balance principles

2.2.1 Introduction

In order to derive the equations which govern the motion of a fluid, two different viewpoints might be considered. One of these methods approach the question from the molecular point of view, considering the fluid as a collection of molecules whose motion is governed by the laws of dynamics. Although this statistical theory is well developed for light gases, it is known to be incomplete for liquids [69].

[69]: Hill (1986), *An introduction to statistical thermodynamics.*

The alternative to that statistical methodology is the continuum approach, which is the classically adopted viewpoint, where it is assumed that the fluid consists of continuous matter. Then, at each point, the fluid is to be characterized by unique values of velocity, pressure, density and/or other field variables. The continuous matter is required to satisfy the conservation laws of mass, momentum and energy, which state the basic set of PDEs for the field variables. The continuum assumption is valid when the mean free path between molecular collisions is much smaller than the characteristic length of the body under consideration, or equivalently, when the socalled Knudsen number, precisely the ratio between the mean free path between molecular collisions and a characteristic length, is much smaller than the unity[1].

2.2.2 Lagrangian vs Eulerian and computational aspects

The choice of a frame of reference to adequately formulate the conservation laws is a fact of paramount importance. As it is well known in continuum mechanics, the are two basic coordinate systems which might be employed, *i. e.*, the Eulerian and the Lagrangian coordinates, yet both descriptions can actually be combined and related by means of the Arbitrary Lagrangian Eulerian (ALE) methodology (see *e. g.* [70] for the fundamentals of this mixed technique).

In the Eulerian framework the independent variables are basically the spatial coordinates (position vector $\mathbf{x}$) and the time coordinate t. Hence, our attention is focused on the fluid passing through a certain control volume which is fixed in space. On the contrary, in the Lagrangian approach, we focus on a particular mass of fluid as it moves, thus considering always the same particles. Here, the independent variables correspond to the position vector $\mathbf{X}$, precisely the coordinates of a fluid mass at a time, say, t_0. The configuration at this time t_0 is called reference configuration, *i. e.*, the configuration where the equations are formally stated. Within this regard, two distinct Lagrangian approaches can be defined, namely total and updated Lagrangian configurations. On the one hand, in the total Lagrangian formulation the reference configuration coincides with the initial one and it is fixed in time. On the other hand, in the updated Lagrangian formulation, the reference configuration changes in time and it usually corresponds to the last known configuration [2]. See for instance, [71, 72], which solve the same mathematical problem from both total and updated descriptions.

The usual approach to derive the equations is to apply the conservation laws to a control volume consisting of the same fluid mass rather than one where different fluid particles pass, hence using a Lagrangian coordinate system. However, the

[1] A classical situation where the continuum approach is no longer valid is the atmospheric reentry of a space shuttle, where the flow is rarified. This is out of the scope of the present work

[70]: Donea et al. (2017), "Arbitrary Lagrangian–Eulerian methods"

[2] In the ALE description, the reference configuration is chosen with the aim of reducing the mesh distortion. Generally speaking, it does not coincide either with the material nor spatial configurations. The ALE technique pretends to exploit the advantages of both Lagrangian and Eulerian descriptions. However, it has been questioned in the literature due to certain inconveniences for very large domain deformations

[71]: Nemer et al. (2021), "Stabilized finite element method for incompressible solid dynamics using an updated Lagrangian formulation"

[72]: Castañar et al. (2020), "A stabilized mixed finite element approximation for incompressible finite strain solid dynamics using a total Lagrangian formulation"

Eulerian system is preferred for solving the majority of problems in fluid mechanics. In this regard, a relation between the two different approaches is established, the well known Reynold's transport theorem.

From the computational point of view, selecting Lagrangian or Eulerian frame of references implies a very different treatment of a certain problem. In solid mechanics, Lagrangian algorithms are usually preferred, since each individual node of the computational mesh is associated to a material particle during the motion. This makes possible to easily track different surfaces, whether they represent free surfaces or contact interfaces among different materials. On the contrary, the major weakness of the Lagrangian approach resides in its difficulty to describe large distortions of the computational domain without resorting to a remeshing strategy. This is precisely why the Eulerian methodology is extensively used in fluid mechanics problems. However, since the Eulerian formulation dissociates the mesh nodes from the material particles, convective effects appear in the definition of the time derivatives due to the relative motion between the deforming material and the computational grid. Hence, this type of terms need to be treated accordingly in order to avoid numerical instabilities in the solution. On top of this, the definition of evolving interfaces is not natural as in the Lagrangian approach, yet this might be circumvented by resorting to numerical techniques such as the level set (LS) method [73, 74].

2.2.3 Local spatial equations

For the sake of conciseness, we shall skip the whole derivation of the fundamental principles, which depart from a specific mass of fluid occupying a volume arbitrarily chosen, and then localizing the result via the Reynold's transport theorem (see e.g. [67, 68] or [75] for the whole procedure).

In order to describe the basic equations, let us consider a given physical domain Ω. The velocity of the fluid is denoted with the vector function $\mathbf{u}(\mathbf{x}, t)$. In order to provide a complete dynamic description of the fluid, the velocity needs to be supplemented with at least two thermodynamic variables. Usually, those might be selected from the set formed by the density $\rho(\mathbf{x}, t)$, the (thermodynamic) pressure $p(\mathbf{x}, t)$ and the temperature $\vartheta(\mathbf{x}, t)$, although others might be considered.

[73]: Osher et al. (2006), *Level set methods and dynamic implicit surfaces*

[74]: Castillo et al. (2015), "Approximation of the two-fluid flow problem for viscoelastic fluids using the level set method and pressure enriched finite element shape functions"

[75]: Currie (1976), *Fundamental mechanics of fluids*

The principle of conservation of mass states that the mass of a continuous medium remains unchanged. Mathematically, the socalled local spatial form of the principle of conservation of mass is expressed as

Conservation of mass

$$\frac{\partial \rho}{\partial t} + \nabla \cdot (\rho \mathbf{u}) = 0 \tag{2.1}$$

This expression is sometimes called continuity equation. In some practical cases, the variation of density might be negligible, for instance in many flow problems involving liquids. In such cases, the fluid is termed incompressible and pressure changes are not associated to density changes. This amounts to saying that

$$\frac{\mathrm{d}\rho}{\mathrm{d}t} = 0,$$

where the notation $\frac{\mathrm{d}\bullet}{\mathrm{d}t}$ stands for the material derivative [3] of $(\bullet)$. By expanding the divergence term, the differential form of the mass conservation equation is reduced to

$$\nabla \cdot \mathbf{u} = 0, \tag{2.2}$$

that is to say, the velocity field is solenoidal under the incompressibility regime.

The principle of linear momentum states that the following differential equation needs to be satisfied by the field variables so that the basic law of dynamics holds:

Conservation of momentum (I)

$$\frac{\partial (\rho \mathbf{u})}{\partial t} + \nabla \cdot (\rho \mathbf{u} \otimes \mathbf{u}) = \rho \mathbf{b} + \nabla \cdot \boldsymbol{\sigma}, \tag{2.3}$$

which is the usually named local spatial form of the principle of balance of linear momentum. Here and in what follows, $\rho \mathbf{b}(\mathbf{x}, t)$ are (external) body forces per unit of volume and $\boldsymbol{\sigma}(\mathbf{x}, t)$ is the Cauchy stress tensor.

Different external forcing terms can be considered on the right hand side of Equation 2.3. The most common type of body force acting on a fluid is the gravity force based on the

[3] The material derivative,

$$\frac{\mathrm{d}\bullet}{\mathrm{d}t} = \frac{\partial \bullet}{\partial t} + (\nabla \bullet)\mathbf{u}$$

represents the total change in a property $(\bullet)$ as seen by an observer following a particular fluid mass. The right-hand side of the equation is the total change of the property in an Eulerian frame.

gravity acceleration, $\mathbf{g}(\mathbf{x}, t)$. Likewise, there are many problems where electromagnetic effects are also important and need to be accounted for[4]. The external forcing term is in that case linked to the classical Lorentz force which relates the charge density, the electric field vector and the magnetic field vector, which in turn are related through Maxwell's equations. In these scenarios, the problem to be solved involves the equations of fluid mechanics and electromagnetism, jointly known as the magnetohydrodynamics problem (see *e.g.* [76, 77]). Moreover, sometimes it is of practical interest to consider a temperature-dependent external forcing term, as it is the case for instance of the classical Boussinesq approximation [78].

Making use of Einstein's notation, some authors also introduce the conservation of linear momentum principle as

$$\frac{\partial(\rho u_i)}{\partial t} = -\frac{\partial \Pi_{ik}}{\partial x_k} + \rho b_i,$$

where the second order tensor

$$\Pi_{ik} := -\sigma_{ik} + \rho u_i u_k, \quad i, k \in \{1, 2, 3\}$$

is termed momentum flux density tensor, and which physically represents the i-th component of the amount of momentum flowing through an unit area perpendicular to the x_k axis.

The left-hand side of Equation 2.3 might be simplified upon the expansion of the temporal and spatial derivatives. Then, taking into account the conservation of mass above stated, the conservation of momentum becomes now

Conservation of momentum (II)

$$\rho \frac{\partial \mathbf{u}}{\partial t} + \rho \left(\mathbf{u} \cdot \nabla\right) \mathbf{u} = \rho \mathbf{b} + \nabla \cdot \boldsymbol{\sigma}. \tag{2.4}$$

The principle of conservation of energy is the application of the first law of thermodynamics to a fluid element. It basically states that the change of internal energy due to a certain process equals the total work done on the system plus any heat which was possibly added. Denoting by $\iota(\mathbf{x}, t)$ the specific internal energy, the local spatial form of the internal energy balance (usually shortened to simply energy equation)

[4] This is the case in many problems of practical significance in computational physics and engineering, *e.g.*, liquid-metal cooling of nuclear reactors and electromagnetic casting among others.

[76]: Popa et al. (2003), "Fluid–Magnetic Splitting of the Magnetohydrodynamic Equations"

[77]: Codina et al. (2006), "Stabilized finite element approximation of the stationary MHD equations"

[78]: Codina et al. (2010), "Finite element approximation of turbulent thermally coupled incompressible flows with numerical sub-grid scale modelling."

can be finally written as

$$\frac{\partial}{\partial t}\left(\rho\iota + \frac{1}{2}\rho\mathbf{u}\cdot\mathbf{u}\right) + \nabla\cdot\left[\left(\rho\iota + \frac{1}{2}\rho\mathbf{u}\cdot\mathbf{u}\right)\mathbf{u}\right] = \nabla\cdot(\boldsymbol{\sigma}\cdot\mathbf{u} - \mathbf{q}) \\ + \rho\mathbf{u}\cdot\mathbf{b} + \rho r, \tag{2.5}$$

where $\mathbf{q}(\mathbf{x}, t)$ is the heat flux vector and $r(\mathbf{x}, t)$ is a possible heat source, which may include chemical reactions or even electromagnetic effects. Moreover, the quantity

$$\rho\iota + \frac{1}{2}\rho\mathbf{u}\cdot\mathbf{u},$$

is the total energy of the system per unit of volume, composed of intrinsic or internal energy and the kinetic energy. However, Equation 2.5 is not very handy as it is written and it shall be simplified by first expanding the derivatives and then by using both the conservation of mass and momentum equations. Thus, the equation which expresses conservation of thermal energy finally reads

Conservation of energy

$$\rho\frac{\partial\iota}{\partial t} + \rho\,(\mathbf{u}\cdot\nabla)\,\iota = \boldsymbol{\sigma} : \nabla\mathbf{u} - \nabla\cdot\mathbf{q} + \rho r \tag{2.6}$$

The entire left-hand side of the equation contains the rate of change in internal energy (temporal plus convective), whereas the right-hand side is composed of three main parts: the conversion of mechanical into thermal energy due to surface stresses, the rate at which heat is being added/subtracted by conduction from the outside, and finally other heat sources or sinks.

2.3 Constitutive equations in fluid mechanics

The basic conservation equations stated in the previous subsection account for three fundamental physical principles. Equation 2.1, Equation 2.3 and Equation 2.5 represent five scalar equations in the three-dimensional case. Nevertheless, there are many more unknown variables in play, exactly seventeen: the scalars ρ (1) and ι (1), the vectors $\mathbf{u}$ (3) and $\mathbf{q}$ (3) and the stress tensor $\boldsymbol{\sigma}$ which has, in general, nine independent components[5]. Thus, supplementary expressions are needed to complete the formulation of the problem. These are the so-called constitutive equations, which we discuss up next.

[5] However, the principle of conservation of angular momentum reduces to the fact that $\boldsymbol{\sigma}(\mathbf{x},t) = \boldsymbol{\sigma}^T(\mathbf{x},t)$, *i. e.* the stress tensor is symmetric and hence only six components shall be considered.

2.3.1 Thermo-mechanical constitutive equation

In the most general case, this equation expresses the dependency of the Cauchy stress tensor $\boldsymbol{\sigma}$ on thermodynamic variables: the thermodynamic pressure $p(\mathbf{x},t)$, the density $\rho(\mathbf{x},t)$, the absolute temperature $\vartheta(\mathbf{x},t)$ and on the strain rate tensor $\boldsymbol{\varepsilon}(\mathbf{x},t)$.

The strain rate tensor is an implicit function of the velocity, and it is formally defined as its symmetric gradient, *i. e.*

$$\boldsymbol{\varepsilon}(\mathbf{u}) := \frac{1}{2}\left(\nabla\mathbf{u} + \nabla^T\mathbf{u}\right). \tag{2.7}$$

Then, the thermo-mechanical constitutive equation is expressed in the most general case as

$$\boldsymbol{\sigma} = -p\mathbf{I}_{N_{\text{sd}}} + \boldsymbol{\mathfrak{F}}(\boldsymbol{\varepsilon},\rho,\vartheta),$$

where $\boldsymbol{\mathfrak{F}}$ is a symmetrical tensor function. If this tensor function is nonlinear on its arguments, the resulting model is termed *Stokesian* fluid model, whereas if $\boldsymbol{\mathfrak{F}}$ is linear, the result is the classical *Newtonian* fluid model. As a consequence, the stress components depend linearly on the rates of deformation. A classical example of non-Newtonian behavior is a type of fluid called *viscoelastic*, widely used in many industrial applications in chemical engineering [79, 80]. Hereinafter, only Newtonian fluids will be considered.

[79]: Moreno et al. (2021), “Numerical simulation of non-isothermal viscoelastic fluid flows using a VMS stabilized finite element formulation”

[80]: Castillo et al. (2021), “Stabilised Variational Multi-scale Finite Element Formulations for Viscoelastic Fluids”

The mechanical constitutive equation for a Newtonian fluid can be stated as

$$\boldsymbol{\sigma} = -p\mathbf{I}_{N_{\text{sd}}} + \mathbb{C} : \boldsymbol{\varepsilon}, \tag{2.8}$$

where $\mathbb{C}$ is a constant fourth-order constitutive tensor. For an *isotropic*[6] behavior (there is an absence of any internally preferred direction), the constitutive tensor $\mathbb{C}$ is an isotropic tensor, *i. e.* it maintains its components in any Cartesian coordinate system. The basic isotropic tensor is the (second order) Kronecker delta tensor. In the case of fourth-order

[6] Generally speaking, gases have a clear isotropic structure and so do simple liquids, whereas suspensions may exhibit some directional preference which depend on the past history of the motion [66].

tensors, the most general expression is demonstrated to be

$$\mathbb{C} = \lambda \mathbf{I}_{N_{\mathrm{sd}}} \otimes \mathbf{I}_{N_{\mathrm{sd}}} + 2\mu \mathbb{I},$$
$$[\mathbb{I}]_{ijkl} = \frac{1}{2}\left[\delta_{ik}\delta_{jl} + \delta_{il}\delta_{jk}\right], \qquad i,j,k,l \in \{1,2,3\}$$

where $\mathbf{I}_{N_{\mathrm{sd}}}$ is the second order identity tensor and $\mathbb{I}$ is the fourth-order symmetric (isotropic) unit tensor. If we now replace this expression in Equation 2.8, the mechanical constitutive equation yields

Mechanical constitutive equation

$$\boldsymbol{\sigma} = -p\mathbf{I}_{N_{\mathrm{sd}}} + \boldsymbol{\sigma}^{\mathrm{d}} = -p\mathbf{I}_{N_{\mathrm{sd}}} + \lambda \operatorname{tr}(\boldsymbol{\varepsilon})\mathbf{I}_{N_{\mathrm{sd}}} + 2\mu\boldsymbol{\varepsilon} \tag{2.9}$$

where $\boldsymbol{\sigma}^{\mathrm{d}}$ represents the viscous part of the constitutive tensor and tr(•) stands for the trace operation over (•).

A note on viscosity coefficients

The parameters λ and μ physically correspond to viscosities, which are understood as material properties. Usually, μ is termed *dynamic*, *molecular* or even *shear* viscosity and λ is referred to as *second* viscosity coefficient. It can be shown that these parameters are required to be non-negative. See *e.g.* the proof in [64]. In the most general case, they are non-constant and may depend on other thermodynamic variables, for example

$$\lambda = \lambda(p,\vartheta) \text{ and } \mu = \mu(p,\vartheta).$$

[81]: Sutherland (1893), "The viscosity of gases and molecular force"

A classical example is the dependency of the viscosity on the temperature, by means of the well known Sutherland's law [81]. It is based on the kinetic theory of ideal gases and an idealized intermolecular-force potential. The formula reads

$$\mu = \mu(\vartheta) = \mu_{\mathrm{ref}} \left(\frac{\vartheta}{\vartheta_{\mathrm{ref}}}\right)^{1/2} \frac{\vartheta_{\mathrm{ref}} + S}{\vartheta + S}, \tag{2.10}$$

where ϑ_{ref} is a reference temperature, μ_{ref} is the viscosity at the reference temperature and S is the usually termed Sutherland temperature.

In order to introduce some insights in the viscosity parameters, the mean pressure $\bar{p}$ is calculated, which is given by

$$\bar{p} := \frac{1}{3}\,\mathrm{tr}(\boldsymbol{\sigma}).$$

Let us now take the trace of the constitutive equation of a Newtonian fluid, *i. e.*

$$\begin{aligned}\mathrm{tr}(\boldsymbol{\sigma}) &= -p\mathrm{tr}(\mathbf{I}_{N_{\mathrm{sd}}}) + \lambda\,\mathrm{tr}(\boldsymbol{\varepsilon})\,\mathrm{tr}\Big(\mathbf{I}_{N_{\mathrm{sd}}}\Big) + 2\mu\,\mathrm{tr}(\boldsymbol{\varepsilon}) \\ &= -3p + (3\lambda + 2\mu)\,\mathrm{tr}(\boldsymbol{\varepsilon}).\end{aligned}$$

Then, it is easy to see that the relation between thermodynamic and mean pressures can be stated as

$$p = \bar{p} + \mu_{\mathrm{b}}\,\mathrm{tr}(\boldsymbol{\varepsilon}) = \bar{p} + \mu_{\mathrm{b}}\nabla\cdot\mathbf{u}$$

where μ_{b} denotes the *bulk* viscosity, which controls sound attenuation together with μ [82] and it is given by

$$\mu_{\mathrm{b}} = \lambda + \frac{2}{3}\mu. \tag{2.11}$$

[82]: Dukhin et al. (2009), "Bulk viscosity and compressibility measurement using acoustic spectroscopy"

A common practice in the analysis of the motion of compressible fluids is to make use of the well-known Stokes hypothesis, that is to say

$$\mu_{\mathrm{b}} = 0 \rightarrow \lambda = -\frac{2}{3}\mu.$$

Setting $\mu_{\mathrm{b}} = 0$ is supported by the kinetic theory of gases *for the case of a polyatomic gas.* This assumption renders the mathematical treatment of compressible flows notably easier, yet it has been the object of long-lasting discussions on compressible flows simulations[7].

2.3.2 Equations of state

These equations are the classical caloric equation of state, which define the specific internal energy $\iota(\mathbf{x}, t)$ (function of density and temperature in the most general case), and the kinetic equation of state, which provides an equation for the thermodynamic pressure p as a function of other thermodynamic variables. Mathematically, we can express these statements as

$$\iota = g(\rho, \vartheta), \tag{2.12a}$$

[7] According to experimental evidence, only in very particular conditions will the term $\mu_{\mathrm{b}}\mathrm{tr}(\boldsymbol{\varepsilon})$ be of practical significance. This may happen for instance when the fluid exhibits large values of μ_{b} (*e. g.* CO_2), or the motion is such that extremely large values of $\nabla\cdot\mathbf{u}$ occur, for example in hypersonic flows, which are out of the scope of the present work.

$$f(\rho, p, \vartheta) = 0. \tag{2.12b}$$

In this work, we shall consider a calorically perfect gas. As a result, the internal energy is a sole function of the temperature, and hence the caloric equation of state can be simplified to

$$\iota = \iota(\vartheta) := c_v \vartheta. \tag{2.13}$$

In the sequel, c_v denotes the specific heat at constant volume, and c_p stands for the specific heat at constant pressure. In this regard, we also define the ratio of specific heats

$$\gamma := c_p / c_v. \tag{2.14}$$

The most frequently encountered form of the thermal equation of state is the ideal-gas law[8],

$$f(\rho, p, \vartheta) \equiv p - \rho R_{\mathrm{g}} \vartheta = 0, \tag{2.15}$$

where R_{g} is the constant of the gas under consideration, defined as

$$R_{\mathrm{g}} = \frac{R^0}{M_{\mathrm{w}}}, \tag{2.16}$$

being $R^0 = 8.31$ J/(mol K) the universal constant and M_{w} the molecular weight.

However, there might be some conditions where simpler relations can be considered. For instance, if the fluid is considered to be *barotropic*, temperature does not intervene in the kinetic equation of state and thus we can simply write

$$f(\rho, p) = 0 \;\rightarrow\; \rho = g(p),$$

that is to say, the density is a sole function of the pressure. A very particular case of a barotropic fluid is the above mentioned incompressible fluid in which the density is constant

$$f(\rho, p) \equiv \rho - \mathscr{C} = 0, \;\; \mathscr{C} = \text{const.}, \tag{2.17}$$

and hence it does not depend on the pressure or the temperature.

Another particular case of the barotropic fluid arises when isentropic (reversible and adiabatic) ideal conditions are considered. In such a case

$$f(\rho, p) \equiv \frac{p}{\rho^{\gamma}} - \mathscr{C} = 0, \;\; \mathscr{C} = \text{const.} \tag{2.18}$$

[8] Dry air in the atmosphere behaves approximately as an ideal gas. However the situation is significantly different if water vapor is present. In such situation, the classical relation is modified by introducing a factor that varies with the specific humidity. See *e. g.* [3].

2.3.3 Thermal constitutive equation

The heat flux vector $\mathbf{q}(\mathbf{x}, t)$ is calculated using Fourier's law of heat conduction, which in general can be written as

$$\mathbf{q} = -\nabla g(\vartheta),$$

where g is a nonlinear function of the temperature $\vartheta(\mathbf{x}, t)$. Although nonlinear diffusion problems are often found in practice, we will restrict ourselves to the classical linear relation in order to ease the discussion. Hence we write

$$\mathbf{q} := -\mathbf{k} \cdot \nabla\vartheta, \tag{2.19}$$

where $\mathbf{k}$ is the (symmetrical second-order) tensor of thermal conductivity, which is a property of the fluid. For the isotropic case, the thermal conductivity tensor is a spherical tensor, *i. e.*

$$\mathbf{k} = \kappa \mathbf{I}_{N_{\mathrm{sd}}},$$

and it depends on the scalar parameter $\kappa(\mathbf{x}, t)$, which is the thermal conductivity of the fluid.

Remark 2.3.1 Although μ and κ might be assumed to be constant to ease the discussion, many other models can be introduced in order to reproduce more realistic conditions. Apart from the above mentioned classical Sutherland's law which makes the variables temperature dependent, other expressions based on the kinetic theory can be considered such as the Chapman-Cowling relation for μ or the modified Eucken correction formula for κ (see *e.g.* [83–85]).

[83]: Chapman et al. (1991), *The mathematical theory of non-uniform gases*
[84]: Hirschfelder et al. (1954), *Molecular theory of gases and liquids*
[85]: Hollis (1996), *Real-gas flow properties for NASA Langley research center aerothermodynamic facilities complex wind tunnels*

2.3.4 Dissipation function

Due to the symmetry of Cauchy's stress tensor, it is easy to see that

$$\boldsymbol{\sigma} : \boldsymbol{\varepsilon}(\mathbf{u}) = -p\,(\nabla \cdot \mathbf{u}) + 2\mu\boldsymbol{\varepsilon}(\mathbf{u}) : \boldsymbol{\varepsilon}(\mathbf{u}) - \frac{2}{3}\mu\,(\nabla \cdot \mathbf{u})^2,$$

where the remaining two terms correspond to the usually termed *dissipation* or Rayleigh function, denoted here as Φ and defined as

$$\Phi := 2\mu\boldsymbol{\varepsilon}(\mathbf{u}) : \boldsymbol{\varepsilon}(\mathbf{u}) - \frac{2}{3}\mu\,(\nabla \cdot \mathbf{u})^2.$$

This function represents the rate at which mechanical energy is being converted to thermal energy (Joule's effect).

Usually, this term in the energy equation is negligible for the Newtonian fluid model, and it might only be taken into account when highly viscous flows are considered. In particular, this term is fundamental when the flow of viscoplastic materials is studied but it is also of paramount importance in the small scales of turbulence in compressible flows.

2.4 Final problem statement

2.4.1 General fluid mechanics problem

The general (coupled) fluid mechanics problem is defined the general domain $\Omega \times \mathbb{R}^+$ domain. Then, the problem consists in computing the density $\rho(\mathbf{x}, t)$, the velocity $\mathbf{u}(\mathbf{x}, t)$, the pressure $p(\mathbf{x}, t)$, the temperature $\vartheta(\mathbf{x}, t)$, and the internal energy $\iota(\mathbf{x}, t)$ from the following set of equations:

General fluid mechanics problem

$$\frac{\partial \rho}{\partial t} + \nabla \cdot (\rho \mathbf{u}) = 0, \tag{2.20a}$$

$$\begin{aligned} \rho \frac{\partial \mathbf{u}}{\partial t} + \rho \left(\mathbf{u} \cdot \nabla\right) \mathbf{u} &= -\nabla p + 2\nabla \cdot \left[\mu \boldsymbol{\varepsilon}(\mathbf{u})\right] + \nabla \left(\lambda \nabla \cdot \mathbf{u}\right) \\ &\quad + \rho \mathbf{b} \end{aligned} \tag{2.20b}$$

$$\begin{aligned} \rho \frac{\partial \iota}{\partial t} + \rho \left(\mathbf{u} \cdot \nabla\right) \iota &= -p \nabla \cdot \mathbf{u} + \nabla \cdot (\kappa \nabla \vartheta) + \lambda (\nabla \cdot \mathbf{u})^2 \\ &\quad + 2\mu \boldsymbol{\varepsilon}(\mathbf{u}) : \boldsymbol{\varepsilon}(\mathbf{u}) + \rho r \end{aligned} \tag{2.20c}$$

$$\iota = \iota(\rho, \vartheta), \tag{2.20d}$$

$$p = p(\rho, \vartheta), \tag{2.20e}$$

The definitions from Equation 2.9, Equation 2.7 and Equation 2.19 are plugged into the mass, momentum and energy conservation equations. Furthermore, initial and boundary conditions need to be appended in order to ensure the well-possedness of the problem.

In the following chapters we will discuss different techniques to numerically solve this problem by making use of the finite element method. Particularly, in Chapter 4 we analyze the isentropic regime, for which the mechanical part can be uncoupled from the thermal part. This fact reduces the global size of the problem since only the momentum and mass conservation equations need to be solved. In Chapter 5 we deal with the complete set of equations considering the socalled *primitive* set of unknowns, *i. e.* the pressure, the velocity and the temperature. On the contrary, in Chapter 6 we reformulate the problem in terms of *conservative* variables, namely, the density, the linear momentum, and the total energy of the system.

2.4.2 Non-dimensional numbers

The description of the problem can be further complemented with the definition of some dimensionless numbers. The most remarkable ones in fluid mechanics are defined as follows:

Definition 2.4.1 *Dimensionless numbers in fluid mechanics*

$$\mathrm{Re} := \frac{\rho U L}{\mu} \qquad \textit{Reynolds number,} \tag{2.21a}$$

$$\mathrm{Pe} := \frac{\rho c_p U L}{\kappa} \qquad \textit{Péclet number,} \tag{2.21b}$$

$$\mathrm{Ma} := \frac{U}{a} \qquad \textit{Mach number,} \tag{2.21c}$$

$$\mathrm{Ra} := \frac{\|\mathrm{g}\|\rho^2 c_p \Delta\theta}{\mu\kappa} \qquad \textit{Rayleigh number,} \tag{2.21d}$$

$$\mathrm{Pr} := \frac{c_p \mu}{\kappa} \qquad \textit{Prandtl number,} \tag{2.21e}$$

$$\mathrm{Gr} := \frac{\|\mathrm{g}\|\rho^2 \Delta\theta}{\mu^2} \qquad \textit{Grashof number,} \tag{2.21f}$$

$$\mathrm{Nu} := \frac{\phi L}{\kappa} \qquad \textit{Nusselt number,} \tag{2.21g}$$

where L is a characteristic length (to be specified), U a characteristic velocity, $\Delta\theta$ a characteristic temperature difference (not to be confused here with the Laplacian of the temperature), g a buoyancy force vector, ϕ is the heat transfer coefficient, and a is the speed of sound in the considered medium. The rest of the variables were already defined. These numbers are related by

$$\begin{aligned}\mathrm{Ra} &= \mathrm{Gr}\mathrm{Pr},\\ \mathrm{Fr} &= \mathrm{Re}^2\mathrm{Gr}^{-1},\\ \mathrm{Re} &= \mathrm{Pe}\mathrm{Pr}^{-1}.\end{aligned}$$

Upon the introduction of the thermal diffusivity

$$K := \frac{\kappa}{\rho c_p}, \tag{2.22}$$

and the kinematic viscosity

$$\nu := \frac{\mu}{\rho}, \tag{2.23}$$

the Prandtl number might be simply written as

$$\mathrm{Pr} = \nu/K.$$

The Prandtl number is a measure for the similarity of the transport of heat and momentum. In addition, the Grashof number is a measure of the relative importance of the bouyancy forces to the viscous forces.

In compressible flows, the Mach number is of particular interest since it defines the *compressibility regime*. It can range from subsonic ($\mathrm{Ma} < 0.8$), transonic ($0.8 < \mathrm{Ma} < 1.2$), supersonic ($\mathrm{Ma} > 1.2$), and hypersonic ($\mathrm{Ma} \gg 1$) flow conditions.

2.4.3 Closure of the initial boundary value problem

Once the governing equations are defined, boundary and initial conditions must be adequately prescribed in order to close the statement of the problem and ensure well-possedness. Boundary conditions are still an open question for the complete set of Navier-Stokes equations [86].

[86]: Lions (1998), *Mathematical Topics in Fluid Dynamics, Volume 2. Compressible Models*

In general, three types of boundary conditions can be considered: Dirichlet (or essential), Neumann (or natural) and Robin (or mixed) conditions. Let us denote by $\Gamma = \partial\Omega$ the boundary of the domain Ω and consider the following disjoint splitting:

$$\begin{aligned}\overline{\Gamma_D \cup \Gamma_N \cup \Gamma_M} &= \Gamma,\\ \overline{\Gamma_D \cap \Gamma_N} &= \emptyset,\\ \overline{\Gamma_N \cap \Gamma_M} &= \emptyset,\\ \overline{\Gamma_D \cap \Gamma_M} &= \emptyset,\end{aligned}$$

where the subscripts refer to, respectively, the Dirichlet, Neumann and mixed parts of the boundary. Generally speaking, we shall require the following specifications in order to solve a problem:

- Dirichlet boundary conditions for the unknonwn variables at the boundary Γ_D.
- Neumann boundary conditions for the normal component of the fluxes of the variables at the boundary Γ_N.
- Robin boundary conditions at the boundary Γ_M, stated as a linear combination of given values of the unknowns and normal components of the fluxes.
- Initial conditions prescribed over whole domain Ω for all the variables in play at $t = 0$.

However, not all boundary conditions can be applied arbitrarily everywhere along the contours of the domain. For instance, in hyperbolic problems essential boundary conditions cannot be imposed on the whole boundary. In addition to this, boundary conditions might be prescribed using different sets of variables which complicates even more this fact. Many other times, the boundary conditions involve unknown variables and hence an iterative procedure has to be introduced (as we shall do for the problem analyzed in Chapter 6).

In the context of pure hyperbolic problems, a simplified analysis in one dimension can be done by assuming that viscosity and diffusion effects are removed and studying the problem from the viewpoint of a Fourier transformation, see the results in [87, 88]. The following general statements can be done for inflows and outflows at different Mach numbers in compressible flows:

- For the subsonic regime, *i. e.* when Ma<1, two conditions are imposed at inlets, usually the velocity and the temperature and only one condition is prescribed at the outlet, usually the pressure.

[87]: Huerta et al. (2003), *Finite Element Methods for flow problems*
[88]: Oliger et al. (1978), “Theoretical and Practical Aspects of Some Initial Boundary Value Problems in Fluid Dynamics”

- For supersonic conditions Ma≥1, three conditions are prescribed at the inlet, usually the density, the velocity and the temperature, and none at the outlet.

In addition to all this, solid boundaries can be represented as a slip condition (impermeable wall condition)

$$\mathbf{u} \cdot \mathbf{n} = 0,$$

as a no-slip condition

$$\mathbf{u} = \mathbf{0},$$

with a given velocity $\mathbf{u}_\mathrm{g}$

$$\mathbf{u} - \mathbf{u}_\mathrm{g} = \mathbf{0},$$

as an isothermal wall with a given temperature value ϑ_g

$$\vartheta - \vartheta_\mathrm{g} = 0,$$

or as a wall with a prescribed heat flux

$$-\kappa \mathbf{n} \cdot \nabla\vartheta = \overline{\varphi},$$

with $\overline{\varphi} = 0$ in the case of an adiabatic wall.

In Chapter 4, Chapter 5 and Chapter 6 we shall explicitly detail in each case the prescribed boundary conditions when formulating the corresponding problem.

Numerical fundamentals: the VMS framework 3

3.1 Introduction

The Variational Multi-Scale (VMS) concept was first introduced in the 90s by Hughes and coworkers in [89, 90]. Since then, it has served as a starting point for the development of stabilized finite element methods for the solution of problems where the stability of the standard Galerkin formulation is not guaranteed. In mixed problems, this is mainly due to some incompatibility restriction of the corresponding interpolating spaces[1]. Apart from this, the convective terms appearing in the governing equations of flow problems may render the solution unstable when using a finite element formulation, showing spurious oscillations. In general, this fluctuating behavior could be avoided setting a specific mesh size, but this approach if often disregarded as it is not computationally affordable.

[89]: Hughes (1995), "Multiscale phenomena : Green's functions, the Dirichlet-to-Neumann formulation, subgrid scale models, bubbles and the origins of stabilized methods"

[90]: Hughes et al. (1998), "The variational multiscale method–a paradigm for computational mechanics"

Both instabilities can be tackled by resorting to stabilized finite element methods. Although the term stabilization is really broad in the field of computational mechanics, since it includes many numerical techniques, here we refer to those methods based on the modification of the weak form obtained by the Galerkin approach by adding some mesh-dependent terms weighted by the residuals of the differential equations (or even part of these residuals).

Stabilized finite element methods were initially developed in the context of convection-dominated flow problems. It was soon understood that node-to-node numerical oscillations could be avoided by introducing some sort of numerical diffusion. The first successful attempt of this idea had already been tested in the context of the finite difference method [91]. Later, this idea evolved so as to introduce artificial diffusion but only along the streamline direction [92].

[91]: VonNeumann et al. (1950), "A Method for the Numerical Calculation of Hydrodynamic Shocks"

[92]: Kelly et al. (1980), "A note on upwinding and anisotropic balancing dissipation in finite element approximations to convective diffusion problems"

The widely known Streamline Upwind Petrov Galerkin (SUPG) method [93, 94] was originally introduced as an extension of the previously developed stabilization methods for convection-diffusion flow problems. The foundation of the method was to introduce numerical diffusion along the streamlines in an optimal manner by defining a certain stabilization term. This

[93]: Brooks et al. (1982), "Streamline Upwind/Petrov-Galerkin formulations for convection dominated flows with particular emphasis on the incompressible Navier-Stokes equations"

[94]: Tezduyar et al. (1983), "Finite element formulations for convection dominated flows with particular emphasis on the compressible Euler equations"

[1] The most well-known example of this situation in fluid mechanics is the Stokes problem where the approximating spaces need to satisfy the inf-sup (also named LBB) compatibility condition.

term was based on a matrix of algorithmic parameters, an operator applied to the test function, and the complete residual of the differential equation. Later, modifications to that operator applied to the test function were introduced, giving raise to the commonly named Galerkin Least Squares (GLS) method (see e.g., [95]). Other examples of similar stabilized methods are the Characteristic Galerkin method [96], and the Taylor-Galerkin method [97].

The key idea behind the VMS approach is to split the unknowns of the problem in hand into two scales, namely, the scale that can be approximated by the finite element mesh and the subgrid scale, the unresolvable one. The general methodology consists in finding an approximation for the subgrid scale so as to yield a stable formulation involving only the finite element scales, hence maintaining the number of degrees of freedom of the starting Galerkin variational problem. There are different ways to model the subgrid scale, provided a definition of the functional space where it belongs. In this thesis, we will assume the subgrid component to be L^2-orthogonal to the finite element space, what leads to the orthogonal subgrid scales method (named OSGS or simply OSS).

The OSGS approach was first introduced by Codina in [98] as an extension of the stabilized method earlier introduced for the Stokes problem and the convection-diffusion equation. Later, the natural extension of this technique to transient problems was elaborated in [99]. The OSS method is facilely extended to transient problems and the effect of the time discretization over the stabilization method is also explained in that publication.

After performing the decomposition of the unknown of the problem into the finite element and subgrid scale, some modelling considerations have to be taken into account in order to be able to numerically compute the subscales [2]. Different approaches have been proposed in the literature of VMS. In [100], the approach for the subgrid problem is to consider a finer finite element space and the introduction of numerical diffusion. A different possibility is to consider the subscales as bubble functions [101, 102]. A more recent development in based on a multiscale discontinuous Galerkin [103], where the coarse scale is considered continuous and the subgrid scale discontinuous.

[95]: Hauke et al. (1998), "A comparative study of different sets of variables for solving compressible and incompressible flows"

[96]: Douglas et al. (1982), "Numerical Methods for Convection-Dominated Diffusion Problems Based on Combining the Method of Characteristics with Finite Element or Finite Difference Procedures"

[97]: Donea (1984), "A Taylor–Galerkin method for convective transport problems"

[98]: Codina (2001), "A stabilized finite element method for generalized stationary incompressible flows"

[99]: Codina (2002), "Stabilized finite element approximation of transient incompressible flows using orthogonal subscales"

[2] This is due to the fact that the space of subscales is, in principle, infinite dimensional and hence, some modelling is needed.

[100]: Guermond (1999), "Stabilization of Galerkin approximations of transport equations by subgrid modeling"

[101]: Brezzi et al. (1992), "A relationship between stabilized finite element methods and the Galerkin method with bubble functions"

[102]: Brezzi et al. (2000), "Residual-free bubbles for advection-diffusion problems: the general error analysis"

[103]: Hughes et al. (2006), "A multiscale discontinuous Galerkin method with the computational structure of a continuous Galerkin method"

The classical techniques within the VMS framework neglect the time derivatives of the subgrid scales when solving the associated subscale problem. The subscales resulting from this assumption are labeled as quasi-static [99]. For such an approximation, it turns out that the inequality

$$\delta t > Ch^2$$

needs to be satisfied in order to obtain stable solutions, being δt the time step size, C a certain positive constant and h the spatial grid size. In this regard, and as it is explained in [104], anisotropic space-time discretizations [3] cannot guarantee stable solutions. Moreover, these instabilities usually appear in the early stages of the time integration procedure. In that publication, the basic features of considering time-dependent subscales are exposed, *e.g.*, the resolution of inconsistencies, to perform the simulation of turbulent flows and the reductions of the computational effort since the number of nonlinear iterations needed to solve each time step decreases too. In essence, accounting for the time derivative of the subgrid scales has become an effective feature in order to eliminate numerical oscillations originated by initial transients while minimizing numerical dissipation (see *e.g.* [105]).

[104]: Codina et al. (2007), “Time dependent subscales in the stabilized finite element approximation of incompressible flow problems”

[3] Partitions in which h and δt are independently refined.

[105]: Codina et al. (2007), “Dynamic subscales in the finite element approximation of thermally coupled incompressible flows”

The multi-scale concept was first presented in the context of compressible Navier-Stokes formulations as a turbulence model. For this reason, it originally played the role of a numerical artifact to account for the effect of the unresolved scales rather than a stabilization method *per se*. In this regard, [106] introduced a mixed formulation to approximate the solution by separating in advance the resolved and unresolved turbulent scales, whose effect is modeled using a Reynolds stress tensor. This initial work was contrasted in [107], specifically in the definition of the unresolved scales, proposing a Fourier-Spectral projector, which could be implemented with a discontinuous Galerkin method. Likewise, [108] proposed a GLS methodology for the solution of the compressible Navier-Stokes problem written in the socalled entropy variables, which includes a filtering procedure with subgrid entropy variables and where the authors modeled the effects of subscales into the resolved scales with a turbulence model. In [109] conservative variables are used, but then velocity, pressure and temperature were selected in the mixed terms that resulted after averaging the compressible equations. The influence of the subscales was modeled using the

[106]: Koobus et al. (2004), “A variational multiscale method for the large eddy simulation of compressible turbulent flows on unstructured meshes–application to vortex shedding”

[107]: Bos et al. (2007), “A multiscale formulation for compressible turbulent flows suitable for general variational discretization techniques”

[108]: Levasseur et al. (2006), “An entropy-variable-based VMS/GLS method for the simulation of compressible flows on unstructured grids”

[109]: Dahmen et al. (2011), “Adaptive multiresolution finite volume discretization of the Variational Multiscale Method. General Framework.”

Smagorinsky turbulence model.

Specifically in the context of compressible flows, [110] presents a review of different stabilized methods for compressible flow computations with a historical perspective from initial developments to modern approaches. In addition, [111] was the first attempt to introduce stabilization techniques strictly in the frame of VMS methods. In these references, VMS-based formulations previously developed for the incompressible case are satisfactorily extended to its compressible counterpart. More recently, in [112] the VMS method was applied in order to stabilize the Euler equations, where the authors demonstrated the convergence of the numerical method in a wide range of stratified flows, yet they restricted the explicit formulation to a linear Euler time integration scheme.

[110]: Hughes et al. (2010), "Stabilized Methods for Compressible Flows"

[111]: Rispoli et al. (2006), "A stabilized finite element method based on SGS models for compressible flows"

[112]: Marras et al. (2013), "Simulations of moist convection by a variational multiscale stabilized finite element method"

The purpose of this chapter is to present the basic numerical ingredients for the upcoming developments in Chapter 4, Chapter 5 and Chapter 6. We will depart from a general initial and boundary value problem, and then expose the basic features of the VMS framework and how to apply it to this standard case.

3.2 General initial and boundary value problem

The majority of problems in fluid mechanics may be conveniently cast in a unified manner as a system of nonlinear convection-diffusion-reaction evolution equations, as it is the case of the problem in Equation 2.20a–Equation 2.20c. Let then Ω be an open, bounded and polyhedral domain of $\mathbb{R}^{N_{\mathrm{sd}}}$ ($N_{\mathrm{sd}} = 2$ or 3 is the number of space dimensions) and $[0, t_{\mathrm{f}}]$ the time interval of analysis. The strong form of the problem consists in finding a vector function $\mathbf{y} \in \mathbb{R}^{N_{\mathrm{sd}}+2}$ such that

$$\mathscr{M}(\mathbf{y})\partial_t \mathbf{y} + \mathscr{L}(\mathbf{y};\mathbf{y}) = \mathscr{F} \quad \text{in } \Omega \times (0, t_{\mathrm{f}}), \tag{3.1}$$

where $\mathscr{M}$ is an operator containing coefficients related to the temporal derivatives (nonlinear in the most general case), and $\mathscr{F}$ is an external forcing term. The remaining spatial operator $\mathscr{L}(\mathbf{y};\mathbf{y})$, linear in the second argument, is clearly a convection-diffusion-reaction operator for the problems of interest described in Chapter 4, Chapter 5, Chapter 6. It is defined as

$$\mathscr{L}(\mathbf{y}_\star;\mathbf{y}) := \mathscr{A}_j(\mathbf{y}_\star)\partial_j\mathbf{y} - \partial_j(\mathscr{K}_{jk}(\mathbf{y}_\star)\partial_k\mathbf{y}) - \mathscr{S}(\mathbf{y}_\star)\mathbf{y}, \quad (3.2)$$

where $\mathscr{A}_j$, $\mathscr{K}_{jk}$ and $\mathscr{S}$ are the classical $(N_{\text{sd}}+2) \times (N_{\text{sd}}+2)$ convective, diffusive and reactive matrices.

In general, this problem corresponds to a nonlinear initial and boundary value problem of parabolic-hyperbolic type which needs to be supplemented with appropriate initial and boundary conditions. Usually, these can be expressed in the following vector form after setting $\Gamma = \overline{\Gamma_{\text{D}} \cup \Gamma_{\text{N}}}$ [4]:

$$\begin{aligned} n_j\left(\mathscr{K}_{jk}(\mathbf{y})\partial_k\mathbf{y}\right) &= \bar{\mathbf{t}}_{\text{N}} && \text{on } \Gamma_{\text{N}}, t \in (0,t_{\text{f}}), && (3.3\text{a}) \\ \mathfrak{D}\mathbf{y} &= \mathfrak{D}\mathbf{y}_{\text{D}} && \text{on } \Gamma_{\text{D}}, t \in (0,t_{\text{f}}), && (3.3\text{b}) \\ \mathbf{y} &= \mathbf{y}_0(\mathbf{x}), && \text{in } \Omega, t = 0, && (3.3\text{c}) \end{aligned}$$

where $\mathbf{y}_0$ denotes the prescribed initial conditions over the whole domain Ω. Furthermore, the Dirichlet boundary operator $\mathfrak{D}$ is used to impose the Dirichlet boundary conditions from given values $\mathbf{y}_{\text{D}}$. The normal vector to Γ is denoted by $\mathbf{n}$, whose j-th component is n_j, and $\bar{\mathbf{t}}_{\text{N}}$ is the prescribed "traction" (in general, a flux) over the Neumann boundary. For the sake of simplicity, let us assume $\bar{\mathbf{t}}_{\text{N}} = \mathbf{0}$ in this chapter, as well as $\mathfrak{D}\mathbf{y} = \mathbf{0}$ [5].

3.3 Variational formulation

Let us denote by $\mathbb{Y}$ the proper functional space where each component of the unknown vector $\mathbf{y}$ is well defined for each fixed time $t \in (0,t_{\text{f}})$, with appropriate regularity and satisfying the Dirichlet boundary conditions. The weak form of the problem is obtained by testing Equation 3.1 against an arbitrary set of test functions $\mathbf{z}$ which we consider to be time independent and such that they vanish on the Dirichlet part of the boundary. Then the weak or variational form of the problem consists in solving for $\mathbf{y} : (0,t_{\text{f}}) \to \mathbb{Y}$ such that

$$\int_\Omega \mathbf{z}^T \cdot [\mathscr{M}(\mathbf{y})\partial_t\mathbf{y} + \mathscr{L}(\mathbf{y};\mathbf{y})]\, \text{d}\Omega = \int_\Omega \mathbf{z}^T \cdot \mathscr{F}\, \text{d}\Omega, \quad (3.4\text{a})$$

$$\int_\Omega \mathbf{z}^T \cdot \mathbf{y} = \int_\Omega \mathbf{z}^T \cdot \mathbf{y}_0\, \text{d}\Omega, \quad (3.4\text{b})$$

for all $\mathbf{z} \in \mathbb{Y}$.

[4] For the sake of simplicity in the discussion, we skip mixed type of boundary conditions.

[5] Although we have grouped Neumann conditions on Γ_{N} and Dirichlet conditions on Γ_{D}, a combination of boundary equations could be applied to different variables on the same part of the boundary, and hence they may overlap, *e.g.*, we may prescribe a certain velocity value on a wall, but consider it also as adiabatic. We shall explicitly indicate in our examples how the initial and boundary conditions are prescribed, as already discussed in Section 2.4.3.

Now in order to reduce continuity requirements, integration by parts is usually performed in the diffusive terms, what in turn allows to introduce Neumann boundary conditions naturally. After the introduction of the following forms

$$\begin{aligned} \mathscr{B}(\mathbf{y}_\star;\mathbf{y},\mathbf{z}) &:= \int_\Omega \mathbf{z}^T \cdot \left(\mathscr{A}_j(\mathbf{y}_\star)\partial_j \mathbf{y} - \mathscr{S}(\mathbf{y}_\star)\mathbf{y}\right)\, \mathrm{d}\Omega \\ &+ \int_\Omega \partial_j \mathbf{z}^T \cdot \left(\mathscr{K}_{jk}(\mathbf{y}_\star)\partial_k \mathbf{y}\right)\, \mathrm{d}\Omega, \qquad (3.5a) \\ \ell(\mathbf{z}) &:= \int_\Omega \mathbf{z}^T \cdot \mathscr{F}\, \mathrm{d}\Omega, \qquad (3.5b) \end{aligned}$$

the weak form can be rewritten as:

Weak form of the general problem

Find the vector function $\mathbf{y} : (0, t_\mathrm{f}) \to \mathbb{Y}$ such that,

$$\langle \mathbf{z}, \mathscr{M}(\mathbf{y})\partial_t \mathbf{y}\rangle + \mathscr{B}(\mathbf{y};\mathbf{y},\mathbf{z}) = \ell(\mathbf{z}), \quad \forall\, \mathbf{z} \in \mathbb{Y}. \qquad (3.6)$$

From this continuous equation, discretization in space and in time can be performed with different techniques. We discuss next the time discretization.

3.4 Time discretization

In order to introduce the time discretizaion, let

$$0 \le t^0 \le t^1 \le \ldots \le t^N = t_\mathrm{f},$$

be a uniform partition of the time interval of analysis with time step size

$$\delta t = t^n - t^{n-1},\ n = 1, \ldots, N.$$

In this work, we suggest backward difference (BDF) schemes of order $\theta = 1, 2, \ldots$, which can be introduced upon the definition the following BDF operator

Definition 3.4.1 *BDF-operator*

$$D_\theta f^{n+1} := \frac{1}{\phi_\theta}\left(f^{n+1} - \sum_{i=0}^{\theta-1} \zeta_\theta^i f^{n-i}\right), \qquad (3.7)$$

being ϕ_θ and ζ_θ^i numerical parameters which depend on the order of the temporal approximation. In particular, for the first and second order schemes, it is found that

$$
\begin{aligned}
D_1 f^{n+1} &= \delta f^{n+1} := f^{n+1} - f^n, \\
D_2 f^{n+1} &= \frac{3}{2}\left(f^{n+1} - \frac{4}{3} f^n + \frac{1}{3} f^{n-1}\right).
\end{aligned}
$$

The first order one (BDF1) coincides with classical Backward Euler method. Both BDF1 and the second order scheme (BDF2) are known to be A-stable schemes. The concept of A-stability is based on the socalled *Dahlquist* or *stiff test* problem, formulated as:

$$
\begin{aligned}
&\frac{\mathrm{d}y}{\mathrm{d}t} = \lambda y, \\
&|y(t)| \leq |y(0)|, \ \forall\, t \geq 0, \ \text{if}\, \lambda \in \mathbb{C}^-,
\end{aligned}
$$

with,

$$
\mathbb{C}^- := \{z \in \mathbb{C} \mid \Re(z) \leq 0\},
$$

where $\Re$ stands for the real part of the complex number z.

Specifically in the context of BDF integrators, we need to consider the following test equation:

$$
\frac{D_\theta y^{n+1}}{\delta t} = \lambda y^{n+1},
$$

and A-stability states that $\left|y^{n+1}\right| \leq |y^n|$, *i. e.*, solutions do not grow uncontrollably in time.

However, a mathematical analysis of the previous statement does not hold for BDF methods of higher order than 2, a limitation referred to as the *second Dahlquist barrier* in the literature. See [113] for a detailed exposition of the whole family of BDF methods and the analysis of their stability properties.

[113]: Hundsdorfer et al. (2003), *Numerical Solution of Time-Dependent Advection-Diffusion-Reaction Equations*

For the design of fractional step schemes, it is particularly advantageous to make use of the backward extrapolation operators, which permit the explicit treatment in time of some terms of the equations in the design stage of an algorithm. These extrapolation operators are given as

$$
\widehat{f}_0^{n+1} = 0, \tag{3.8a}
$$

$$
\widehat{f}_1^{n+1} = f^n, \tag{3.8b}
$$

$$
\widehat{f}_2^{n+1} = 2f^n - f^{n-1}, \tag{3.8c}
$$

or, in general as

$$\hat{f}_{\theta}^{n+1} := f^{n+1} - \delta^{(\theta)} f^{n+1} = f^{n+1} + \mathcal{O}\left(\delta t^{\theta}\right), \quad \theta = 0, 1, 2 \ldots \quad (3.9)$$

where

$$\delta^{(i+1)} f^{n+1} = \delta^{(i)} f^{n+1} - \delta^{(i)} f^{n}, \quad \forall\, i = 1, 2, 3, \ldots .$$

When the BDF operator is applied to the continuous problem Equation 3.6, we obtain a time-discrete space-continous problem which reads: given the known $\mathbf{y}^{n-i}$ values from $i = 0$ to $\theta - 1$, compute the next time step unknown $\mathbf{y}^{n+1} \in \mathbb{Y}$ such that

$$\left\langle \mathbf{z}, \mathscr{M}(\mathbf{y}^{n+1}) \delta_t \mathbf{y}^{n+1} \right\rangle + \mathscr{B}(\mathbf{y}^{n+1}; \mathbf{y}^{n+1}, \mathbf{z}) = \ell(\mathbf{z}), \qquad (3.10)$$

for all $\mathbf{z} \in \mathbb{Y}$, where we have introduced the following notation for the discrete time derivative

$$\delta_t(\bullet) \equiv \frac{D_\theta(\bullet)}{\delta t}.$$

3.5 The VMS framework

In this section, we recast the basic theory of the Variational Multi-Scale framework, which is the base for all the developments contained in the next chapters.

3.5.1 Galerkin finite element discretization

Let us assume a polyhedral domain Ω for which we can consider a finite element partition, $\Omega^{(e)}$. It is understood that the subdomains $\Omega^{(e)}$ are open, non-overlapping and the union of their closures is the closure of Ω. In the following, the approximations we consider are conforming, *i. e.*, the finite element spaces will be chosen as finite dimensional subspaces of the functional ones where the problem is posed. To this end, let $\mathbb{Y}_h \subset \mathbb{Y}$ be the finite element approximating space for the problem in hand.

We then consider the discrete space

$$\mathbb{Y}_h := \left\{ \mathbf{y} \in \mathbb{Y} \mid \mathbf{y}(\cdot, t)\big|_{\Omega^{(\mathrm{e})}} \in \mathscr{P}_m\left(\Omega^{(\mathrm{e})}\right), t \in (0, t_{\mathrm{f}}) \right\} \subset \mathbb{Y}$$

where $\mathscr{P}_m$ stands for the set of complete polynomials of degree $\leq m$ in $\Omega^{(\mathrm{e})}$. In several spatial dimensions, different types of polynominals can be chose, *e.g.*, P_m, the set of polynomials of degree $\leq m$ defined over a reference triangle, Q_m, the set of polynomials of degree $\leq m$ in each variable defined over a reference square, or $S_m = P_m \oplus \mathrm{span}\{x^m y, xy^m\}$, also known as serendipity spaces over a reference square.

In order to make the discussion clearer, we shall depart from Equation 3.6 since time discretization is not relevant for this subsection. The raw Galerkin finite element approximation of the problem in hand is stated by approximating $\mathbf{y} \approx \mathbf{y}_h$ and then consists now in finding $\mathbf{y}_h : (0, t_\mathrm{f}) \to \mathbb{Y}_h$ such that

$$\langle \mathbf{z}_h, \mathscr{M}(\mathbf{y})\partial_t \mathbf{y}_h \rangle + \mathscr{B}(\mathbf{y}; \mathbf{y}_h, \mathbf{z}_h) = \ell(\mathbf{z}_h), \quad \forall\ \mathbf{z}_h \in \mathbb{Y}_h. \quad (3.11)$$

Denoting by $\Lambda = \{1, 2, \dots, N_\mathrm{tp}\}$ the set of global nodes in the finite element mesh, the approximation of the problem unknown is then stated as

$$\mathbf{y}(\mathbf{x}, t) \approx \mathbf{y}_h(\mathbf{x}, t) = \sum_{a\,\in\,\Lambda} \varphi^a(\mathbf{x})\mathbf{Y}^a(t)$$

where φ^a is the shape function associated with the node a and $\mathbf{Y}$ is the nodal unknown. Likewise, the arbitrary test functions are defined analogously in the Galerkin methodology.

In practice, the computations are performed over an individual element $\Omega^{(e)}$, being the shape functions φ^a, $a = 1, \dots, N_\mathrm{no}$ defined on a master element in normalized coordinates, *e.g.*, a square $(\xi, \eta) = [-1, 1] \times [1, 1]$. This leads to the commonly known as isoparametric approximation for an element. The integrals are then evaluated element by element in local coordinates using a numerical quadrature and later assembled into the global system what leads to the final matrix system (see a complete explanation in [6]).

3.5.2 Scale splitting

As we stated in the introduction of this chapter, it is well known that raw Galerkin formulations may suffer from different types of numerical instabilities, particularly when applied to flow problems. The main ones arise, precisely, from the non-elliptic nature of the equations and others come from compatibility restrictions between the approximations of the different components of the vector of unknowns. In any case, they all depend on the expression of the matrices that define the nonlinear convection-diffusion-reaction operator in Equation 3.2.

The cornerstone of the VMS approach is to split the space of the unknowns $\mathbb{Y}$ in the following manner

$$\mathbb{Y} = \mathbb{Y}_h \oplus \widetilde{\mathbb{Y}},$$

where $\mathbb{Y}_h$ is the finite element space (and hence finite dimensional) and $\widetilde{\mathbb{Y}}$ is any complementary space which completes $\mathbb{Y}_h$ in $\mathbb{Y}$, usually termed *subgrid scale space* and which is in principle infinite dimensional. Each VMS-type method will depend on the approximation introduced for the computation of $\widetilde{\mathbb{Y}}$. Therefore, distinct methodologies arise from different approximations of the subgrid scale space and this is precisely why we refer to VMS as a framework, rather than a single method.

The previous splitting of the space $\mathbb{Y}$ induces a scale separation of unknowns and test functions, in such a way that

$$\begin{aligned} &\mathrm{y} = \mathrm{y}_h + \tilde{\mathrm{y}}, && \mathrm{y}_h \in \mathbb{Y}_h, && \tilde{\mathrm{y}} \in \widetilde{\mathbb{Y}}, \\ &\mathrm{z} = \mathrm{z}_h + \tilde{\mathrm{z}}, && \mathrm{z}_h \in \mathbb{Y}_h, && \tilde{\mathrm{z}} \in \widetilde{\mathbb{Y}}. \end{aligned}$$

Taking this into account, it is readily checked that the continuous problem can be written as the following system of equations:

$$\langle \mathrm{z}_h, \mathscr{M}(\mathrm{y})\partial_t \mathrm{y}\rangle + \mathscr{B}(\mathrm{y}; \mathrm{y}, \mathrm{z}_h) = \ell(\mathrm{z}_h) \qquad \forall \mathrm{z}_h \in \mathbb{Y}_h, \qquad (3.12a)$$

$$\langle \tilde{\mathrm{z}}, \mathscr{M}(\mathrm{y})\partial_t \mathrm{y}\rangle + \mathscr{B}(\mathrm{y}; \mathrm{y}, \tilde{\mathrm{z}}) = \ell(\tilde{\mathrm{z}}) \qquad \forall \tilde{\mathrm{z}} \in \widetilde{\mathbb{Y}}, \qquad (3.12b)$$

where the first row Equation 3.12a is termed finite element scale equation (which is posed in the finite element space) and the second row Equation 3.12b is referred to as subgrid scale equation in the literature (it is posed in the subscale space)[6].

3.5.3 Approximation of the subgrid scales

In order to derive a computationally feasible methodology, some approximation needs to be introduced due to the fact

[6] Note that setting $\widetilde{\mathbb{Y}} = \{0\}$ would yield the original Galerkin method, but better options are expected to be found when that method is unstable.

that the subscale problem Equation 3.12b is posed in an infinite dimensional space. In this regard, the goal is to find an approximation of the subscales in order to end up with a problem which should depend just on the finite element scales, hence maintaining the original number of degrees of freedom. In other words, the goal is to find an explicit expression for the computation of $\tilde{\mathbf{y}}$ in Equation 3.12b which could then be plugged into Equation 3.12a.

Integration by parts within each element can be performed in Equation 3.12a, which avoids, precisely, the introduction of a model for the spatial derivatives of the subscale unknown $\tilde{\mathbf{y}}$. Hence, making use of the additivity property of the integral, it is easy to check that

$$\begin{aligned}\langle \mathbf{z}_h, \mathscr{M}(\mathbf{y})\partial_t \mathbf{y}_h\rangle + \mathscr{B}(\mathbf{y}; \mathbf{y}_h, \mathbf{z}_h)& \\ + \sum_{e=1}^{N_{\mathrm{el}}} \int_{\Omega^{(e)}} [\mathscr{L}^\star(\mathbf{y}; \mathbf{z}_h)]^T \cdot \tilde{\mathbf{y}} \, \mathrm{d}\Omega &= \ell(\mathbf{z}_h),\end{aligned} \tag{3.13}$$

where the boundary terms over the skeleton of the mesh are neglected by supposing that the subscales vanish at the element boundaries, though this assumption could be relaxed by including some strategy to account for the subscales on the element boundaries[7]. In [114, 115] this fact is extensively discussed, concluding that enhanced stability properties might be achieved under some conditions. The star superscript denotes the formal adjoint operator of $\mathscr{L}(\mathbf{y}; \mathbf{y})$ from Equation 3.2. Such adjoint operator satisfies, up to boundary terms, the following relation

$$\int_\Omega \mathbf{z}^T \cdot \mathscr{L}(\mathbf{y}; \mathbf{w}) \, \mathrm{d}\Omega = \int_\Omega [\mathscr{L}^\star(\mathbf{y}; \mathbf{z})]^T \cdot \mathbf{w} \, \mathrm{d}\Omega \quad \forall \, \mathbf{y}, \mathbf{w}, \mathbf{z},$$

and the outcome of this operator when it is applied to the test function vector is

$$\begin{aligned}\mathscr{L}^\star(\mathbf{y}; \mathbf{z}_h) := &- \partial_j \left(\mathscr{A}_j^T(\mathbf{y})\mathbf{z}_h\right) - \partial_k \left(\mathscr{K}_{jk}^T(\mathbf{y})\partial_j \mathbf{z}_h\right) \\ &- \mathscr{S}(\mathbf{y})^T \mathbf{z}_h.\end{aligned} \tag{3.14}$$

The finite element scale equation Equation 3.12a can be interpreted as the projection of the original problem onto $\mathbb{Y}_h$. Similarly, the subgrid scale equation Equation 3.12b can be understood as the projection of the equations onto the space of subscales $\widetilde{\mathbb{Y}}$, *i.e.*, by taking the test function in the space of subscales instead of taking it in the finite element space.

[7] In other words, the space $\widetilde{\mathbb{Y}}$ is taken as the space of bubble functions. This approximation makes the subscale problem decoupled into N_{el} independent subproblems. Otherwise, finding a solution for the subscale at the element boundaries would require to solve a global problem, precisely that of satisfying continuity of fluxes across element edges.

[114]: Codina et al. (2009), "Subscales on the element boundaries in the variational two-scale finite element method"

[115]: Codina et al. (2018), "Variational Multiscale Methods in Computational Fluid Dynamics"

Hence, if $\widetilde{\mathscr{P}}$ denotes the classical $L^2(\Omega)$-projection onto the space of subscales, Equation 3.12b can be equivalently rewritten as follows:

$$\widetilde{\mathscr{P}}\left[\mathscr{M}(\mathrm{y})\partial_t\tilde{\mathrm{y}} + \mathscr{L}(\mathrm{y};\tilde{\mathrm{y}})\right] = \widetilde{\mathscr{P}}\left[\mathscr{R}(\mathrm{y};\mathrm{y}_h)\right],$$

where $\mathscr{R}(\mathrm{y};\mathrm{y}_h)$ is the (strong) finite element residual, *i. e.*

$$\mathscr{R}(\mathrm{y};\mathrm{y}_h) \coloneqq \mathscr{F} - \mathscr{M}(\mathrm{y})\partial_t\mathrm{y}_h - \mathscr{L}(\mathrm{y};\mathrm{y}_h). \tag{3.15}$$

In principle, solving the fine scale problem for $\tilde{\mathrm{y}}$ would require to find a certain inverse operator $\mathscr{L}^{-1}(\mathrm{y};\tilde{\mathrm{y}})$. However, since such an inverse operator cannot be directly computed, an element by element approximation is performed by means of the socalled matrix of stabilization parameters, which we denote by $\boldsymbol{\tau}$ (generally nonlinear in y), and in such a way that

$$\mathscr{L}(\mathrm{y};\tilde{\mathrm{y}}) \approx \boldsymbol{\tau}^{-1}(\mathrm{y})\tilde{\mathrm{y}}.$$

Therefore, Equation 7 might be rewritten as

$$\mathscr{M}(\mathrm{y})\partial_t\tilde{\mathrm{y}} + \boldsymbol{\tau}^{-1}(\mathrm{y})\tilde{\mathrm{y}} = \widetilde{\mathscr{P}}\left[\mathscr{R}(\mathrm{y};\mathrm{y}_h)\right], \tag{3.16}$$

where we have assumed that the left-hand-side (LHS) of the equation already belongs to the space of subscales and hence its projection is precisely the same LHS.

The definition of the matrix of stabilization parameters $\boldsymbol{\tau}(\mathrm{y})$ is by no means a closed question. Up to our knowledge, there is no general rule to define it for systems of equations. It must be designed for each particular problem taking into account its stability deficiencies or even scaling requirements. In this regard, an approximate Fourier analysis of the subscale problem was performed in [116], where the dependence of the stabilization parameters on the equation coefficients and the mesh size was established. We shall keep the definition of the stabilization parameters aside, and come back to it in the following chapters as these are problem dependent, as previously stated.

[116]: Principe et al. (2010), “On the stabilization parameter in the subgrid scale approximation of scalar convection-diffusion-reaction equations on distorted meshes”

3.5.4 Algebraic vs orthogonal, quasi-static vs dynamic subscales

Depending on the choice of the projection operator $\widetilde{\mathscr{P}}$ (which implicitly involves the choice of $\widetilde{\mathbb{Y}}$), different approximation equations for the subscales can be defined. In particular, in

[115] two alternatives for formulating the subscale equations are described. The first one is named *Algebraic Subgrid Scales*, hereinafter ASGS. This is the most common approach and it is defined after setting the projection operator equal to the identity projector, that is to say

$$\widetilde{\mathscr{P}} = \mathscr{I}, \qquad \text{(ASGS)}$$

when applied to the finite element residual appearing in the right-hand-side of Equation 3.16. The second alternative corresponds to

$$\widetilde{\mathscr{P}} = \mathscr{P}_h^{\perp} := \mathscr{I} - \mathscr{P}_h, \qquad \text{(OSGS)}$$

being $\mathscr{P}_h$ the projector operator onto the finite element space. The resulting formulation is called *Orthogonal Subgrid Scales* (OSGS) because when the stabilization parameters $\boldsymbol{\tau}$ are the same for all elements in the mesh, this choice exactly corresponds to taking $\widetilde{\mathbb{Y}}$ as the orthogonal complement of $\mathbb{Y}_h$ in $\mathbb{Y}$.

Apart from this, and as the reader might have noticed, Equation 3.16 includes the time derivative of the subscale. Since the numerical instabilities of flow problems have essentially a spatial nature, the time dependency of the subscales is not considered as a standard choice [117–119]. In such scenario, the subscales are usually called *quasi-static* (QSS) due to the fact that although their time derivative is neglected, the subscales still vary in time since the residual does. Therefore, in such sceneario, the subscales are simply computed from

$$\tilde{\mathrm{y}} = \boldsymbol{\tau}(\mathrm{y})\widetilde{\mathscr{P}}\left[\mathscr{R}(\mathrm{y};\mathrm{y}_h)\right]. \qquad (3.17)$$

The subscale as a time dependent variable of the problem was novelly introduced in [99] and further analyzed in [104] and [120]. The inclusion of the time derivative of the subscales was shown to give rise to important properties such as the commutativity of space and time discretizations, the stability without restrictions on the time step size and, when they are additionally combined with orthogonal subscales, to enhanced stability and convergence properties in time as well as to improved accuracy (see Section 5 in [115]).

However, in order to deal with dynamic subscales one needs to integrate Equation 3.16 in time, *e.g.*, using for example a finite differences scheme although there is also the possibility to integrate the subscales in time analytically, as explained

[117]: Bazilevs et al. (2007), "Variational multiscale residual-based turbulence modeling for large eddy simulation of incompressible flows"

[118]: Hughes et al. (2000), "Large eddy simulation and the variational multiscale method."

[119]: Hughes et al. (2001), "Large eddy simulation of turbulent channel flows by the variational multiscale method."

[120]: Badia et al. (2009), "On a multiscale approach to the transient Stokes problem: Dynamic subscales and anisotropic space-time discretization"

in [105]. Moreover, the storage of the subscales at the integration points is needed, since at a certain time step the subscales of the previous one are required to advance the solution in time[8]. As it is clearly discussed in [104], the choice of the time integration scheme of the subscales equation can be less accurate than that of the general finite element equation without altering the time accuracy of the numerical scheme. Since in this thesis we will consider mainly second order integration schemes for the finite element equations, we select a simple backward Euler scheme for the subscales[9]. Following Section 3.4, it yields

$$\begin{aligned}\tilde{\mathrm{y}}^{n+1} = {} & \boldsymbol{\tau}_{\mathrm{d}}(\mathrm{y}^{n+1})\widetilde{\mathscr{P}}\left[\mathscr{R}(\mathrm{y}^{n+1};\mathrm{y}_h)\right] \\ & + \boldsymbol{\tau}_{\mathrm{d}}(\mathrm{y}^{n+1})\mathscr{M}(\mathrm{y}^{n+1})\frac{\tilde{\mathrm{y}}^{n}}{\delta t},\end{aligned} \tag{3.18}$$

where we have introduced an *effective* stabilization parameter which is defined as

$$\boldsymbol{\tau}_{\mathrm{d}}(\mathrm{y}^{n+1}) := \left[\frac{\mathscr{M}(\mathrm{y}^{n+1})}{\delta t} + \boldsymbol{\tau}^{-1}(\mathrm{y}^{n+1})\right]^{-1}. \tag{3.19}$$

Now that we have an explicit strategy to solve for the subscales, *i.e.* either Equation 3.17 or Equation 3.18 with the algebraic or orthogonal definition of $\widetilde{\mathscr{P}}$, we can take those expressions to the former finite element scales equation Equation 3.13 to finally get a problem which involves only the finite element subscales.

The final problem is stated in the following abstract form, considered as an extension of Equation 3.10 with the addition of the stabilization terms based on the VMS strategy. Then, it yields

$$\begin{aligned}\left\langle \mathrm{z}_h,\ \mathscr{M}(\mathrm{y}^{n+1})\delta_t \mathrm{y}_h^{n+1}\right\rangle + \mathscr{B}(\mathrm{y}^{n+1};\mathrm{y}_h^{n+1},\mathrm{z}_h) & \\ + \mathscr{B}_{\mathrm{stab}}(\mathrm{y}^{n+1};\mathrm{y}_h^{n+1},\mathrm{z}_h) = \ell(\mathrm{z}_h) + \ell_{\mathrm{stab}}(\mathrm{z}_h) &\end{aligned} \tag{3.20}$$

The definition of the stabilization forms for each specific case are provided in the following tables: Table 3.1 and Table 3.2 contain the definition of the LHS-form $\mathscr{B}_{\mathrm{stab}}(\mathrm{y}^{n+1};\mathrm{y}_h^{n+1},\mathrm{z}_h)$ for the ASGS and OSGS approaches, and Table 3.3 and Table 3.4 the definitions of the RHS-form $\ell_{\mathrm{stab}}(\mathrm{z}_h)$, respectively[10]. Taking into account the previously discussed features of the dynamic OSGS approach, we favor the implementation of this methodology.

[8] Hence, the subscales play the role of an internal variable as in computational solid mechanics problems.

[9] The rationale behind using such a dissipative scheme for the time integration of the the fine scales is precisely the assumption of bubble functions.

[10] The reader should note that formally the term $\mathscr{B}_{\mathrm{stab}}(\mathrm{y}^{n+1};\mathrm{y}_h^{n+1},\mathrm{z}_h)$ may contain the temporal derivative of the unknown y_h^{n+1}, and hence a contribution to the RHS of Equation 3.20 appears as a result of known information from previous time steps.

Table 3.1: Definition of the $\mathscr{B}_{\text{stab}}(\mathrm{y}^{n+1};\mathrm{y}_h^{n+1},\mathrm{z}_h)$ form for both dynamic (DYN) and quasi-static (QSS) algebraic subgrid scales.

DYN	$-\sum_{e=1}^{N_{\text{el}}}\left\langle\mathscr{M}(\mathrm{y}^{n+1})\delta_t\mathrm{y}_h^{n+1}+\mathscr{L}(\mathrm{y}^{n+1};\mathrm{y}_h^{n+1}),\boldsymbol{\tau}_{\mathrm{d}}(\mathrm{y}^{n+1})\mathscr{L}^{\star}(\mathrm{y}^{n+1};\mathrm{z}_h)\right\rangle$ $-\sum_{e=1}^{N_{\text{el}}}\left\langle\mathscr{M}(\mathrm{y}^{n+1})\delta_t\mathrm{y}_h^{n+1}+\mathscr{L}(\mathrm{y}^{n+1};\mathrm{y}_h^{n+1}),\left[\mathbf{I}-\boldsymbol{\tau}(\mathrm{y}^{n+1})^{-1}\boldsymbol{\tau}_{\mathrm{d}}(\mathrm{y}^{n+1})\right]\mathrm{z}_h\right\rangle$
QSS	$-\sum_{e=1}^{N_{\text{el}}}\left\langle\mathscr{M}(\mathrm{y}^{n+1})\delta_t\mathrm{y}_h^{n+1}+\mathscr{L}(\mathrm{y}^{n+1};\mathrm{y}_h^{n+1}),\boldsymbol{\tau}_{\mathrm{d}}(\mathrm{y}^{n+1})\mathscr{L}^{\star}(\mathrm{y}^{n+1};\mathrm{z}_h)\right\rangle$

Table 3.2: Definition of the form $\mathscr{B}_{\text{stab}}(\mathrm{y}^{n+1};\mathrm{y}_h^{n+1},\mathrm{z}_h)$ for both dynamic and quasi-static orthogonal subgrid scales.

DYN	$-\sum_{e=1}^{N_{\text{el}}}\left\langle\mathscr{P}_h^{\perp}\left[\mathscr{L}(\mathrm{y}^{n+1};\mathrm{y}_h^{n+1})\right],\boldsymbol{\tau}_{\mathrm{d}}(\mathrm{y}^{n+1})\mathscr{L}^{\star}(\mathrm{y}^{n+1};\mathrm{z}_h)\right\rangle$
QSS	$-\sum_{e=1}^{N_{\text{el}}}\left\langle\mathscr{P}_h^{\perp}\left[\mathscr{L}(\mathrm{y}^{n+1};\mathrm{y}_h^{n+1})\right],\boldsymbol{\tau}(\mathrm{y}^{n+1})\mathscr{L}^{\star}(\mathrm{y}^{n+1};\mathrm{z}_h)\right\rangle$

Remark 3.5.1 The treatment of the unknown nonlinear term $\mathbf{y}$ in the operators $\mathscr{M}(\mathbf{y},\bullet)$, $\mathscr{L}(\mathbf{y},\bullet)$ and the adjoint operator $\mathscr{L}^{\star}(\mathbf{y},\bullet)$ presents another dichotomy in the treatment of the subscales. Two different alternatives are devised, respectively labeled as linear subscales, where $\mathbf{y}\approx\mathbf{y}_h$, and nonlinear subscales, where $\mathbf{y}\approx\mathbf{y}_h+\tilde{\mathbf{y}}$. Here, the words linear and nonlinear just indicate whether the subscales appear only in the linear terms or also in the nonlinear ones. Since the improvements in the performance of the formulation with nonlinear subscales are limited, we restrict ourselves in this thesis to linear subscales. We refer to [99] and [121] for a detailed description of nonlinear subscales.

[121]: Colomes et al. (2015), "Assessment of variational multiscale models for the large eddy simulation of turbulent incompressible flows"

A note on the computation of the projection operations

When compared to the raw Galerkin method, the matrices emerging from the orthogonal projection of the unknowns show a wide stencil, introducing new couplings with the neighboring elements from subsequent levels. A practical strategy to get rid of this inconvenience is to solve for the projection onto the finite element space $\mathscr{P}_h$ and then directly use $\mathscr{P}_h^{\perp}=\mathscr{I}-\mathscr{P}_h$. Thus, if we denote by $\boldsymbol{\xi}_h$ the projection of $\mathscr{L}(\mathrm{y},\mathrm{y}_h)-\mathscr{F}$ onto the finite element space $\mathbb{Y}_h$, the proposed dynamic OSGS methodology consists in solving $\mathrm{y}_h^{n+1},\boldsymbol{\xi}_h^{n+1}\in\mathbb{Y}_h\times\mathbb{Y}_h$ such that

$$\left\langle\mathrm{z}_h,\mathscr{M}(\mathrm{y}^{n+1})\delta_t\mathrm{y}_h^{n+1}\right\rangle+\mathscr{B}(\mathrm{y}^{n+1};\mathrm{y}_h^{n+1},\mathrm{z}_h)$$

Table 3.3: Definition of the form $\ell_{\mathrm{stab}}(\mathrm{z}_h)$ for both dynamic and quasi-static algebraic subgrid scales.

DYN	$-\sum_{e=1}^{N_{\mathrm{el}}} \left\langle \mathscr{F}, \boldsymbol{\tau}_{\mathrm{d}}(\mathrm{y}^{n+1})\mathscr{L}^{\star}(\mathrm{y}^{n+1};\mathrm{z}_h) + \left[\mathbf{I} - \boldsymbol{\tau}(\mathrm{y}^{n+1})^{-1}\boldsymbol{\tau}_{\mathrm{d}}(\mathrm{y}^{n+1})\right]\mathrm{z}_h\right\rangle$ $-\sum_{e=1}^{N_{\mathrm{el}}} \left\langle \delta t^{-1}\mathscr{M}(\mathrm{y}^{n+1})\tilde{\mathrm{y}}^{n-1}, \boldsymbol{\tau}_{\mathrm{d}}(\mathrm{y}^{n+1})\mathscr{L}^{\star}(\mathrm{y}^{n+1};\mathrm{z}_h)\right\rangle$ $+\sum_{e=1}^{N_{\mathrm{el}}} \left\langle \delta t^{-1}\mathscr{M}(\mathrm{y}^{n+1})\tilde{\mathrm{y}}^{n-1}, \boldsymbol{\tau}(\mathrm{y}^{n+1})^{-1}\boldsymbol{\tau}_{\mathrm{d}}(\mathrm{y}^{n+1})\mathrm{z}_h\right\rangle$
QSS	$-\sum_{e=1}^{N_{\mathrm{el}}} \left\langle \mathscr{F}, \boldsymbol{\tau}_{\mathrm{d}}(\mathrm{y}^{n+1})\mathscr{L}^{\star}(\mathrm{y}^{n+1};\mathrm{z}_h)\right\rangle$

Table 3.4: Definition of the form $\ell_{\mathrm{stab}}(\mathrm{z}_h)$ for both dynamic and quasi-static orthogonal subgrid scales.

DYN	$-\sum_{e=1}^{N_{\mathrm{el}}} \left\langle \mathscr{P}_h^{\perp}\left[\mathscr{F}\right] + \delta t^{-1}\mathscr{M}(\mathrm{y}^{n+1})\tilde{\mathrm{y}}^{n-1}, \boldsymbol{\tau}_{\mathrm{d}}(\mathrm{y}^{n+1})\mathscr{L}^{\star}(\mathrm{y}^{n+1};\mathrm{z}_h)\right\rangle$
QSS	$-\sum_{e=1}^{N_{\mathrm{el}}} \left\langle \mathscr{P}_h^{\perp}\left[\mathscr{F}\right], \boldsymbol{\tau}_{\mathrm{d}}(\mathrm{y}^{n+1})\mathscr{L}^{\star}(\mathrm{y}^{n+1};\mathrm{z}_h)\right\rangle$

$$
\begin{aligned}
&-\sum_{e=1}^{N_{\mathrm{el}}} \left\langle \mathscr{L}(\mathrm{y}^{n+1};\mathrm{y}_h^{n+1}) - \boldsymbol{\xi}_h^{n+1}, \boldsymbol{\tau}_{\mathrm{d}}(\mathrm{y}^{n+1})\mathscr{L}^{\star}(\mathrm{y}^{n+1};\mathrm{z}_h)\right\rangle \\
&= \ell(\mathrm{z}_h) - \sum_{e=1}^{N_{\mathrm{el}}} \left\langle \mathscr{F}, \boldsymbol{\tau}_{\mathrm{d}}(\mathrm{y}^{n+1})\mathscr{L}^{\star}(\mathrm{y}^{n+1};\mathrm{z}_h)\right\rangle \\
&-\sum_{e=1}^{N_{\mathrm{el}}} \left\langle \delta t^{-1}\mathscr{M}(\mathrm{y}^{n+1})\tilde{\mathrm{y}}^{n}, \boldsymbol{\tau}_{\mathrm{d}}(\mathrm{y}^{n+1})\mathscr{L}^{\star}(\mathrm{y}^{n+1};\mathrm{z}_h)\right\rangle
\end{aligned} \tag{3.21a}
$$

$$
\left\langle \boldsymbol{\xi}_h^{n+1}, \boldsymbol{\pi}_h\right\rangle - \sum_{e=1}^{N_{\mathrm{el}}} \left\langle \mathscr{L}(\mathrm{y}^{n+1},\mathrm{y}_h^{n+1}) - \mathscr{F}, \boldsymbol{\pi}_h\right\rangle = 0 \tag{3.21b}
$$

which must hold for all $[\mathrm{z}_h, \boldsymbol{\pi}_h]$.

From this point, the solution of Equation 3.21a together with Equation 3.21b comprises the solution of an algebraic problem. If an iterative solver is to be used, it is computationally feasible to solve it in a direct monolithic way, with y_h^{n+1} and $\boldsymbol{\xi}_h^{n+1}$ as unknowns. See *e.g.*, [122, 123].

[122]: Codina (2008), "Analysis of a stabilized finite element approximation of the Oseen equations using orthogonal subscales"
[123]: Aguirre et al. (2021), "A variational multiscale stabilized finite element formulation for Reissner-Mindlin plates and Timoshenko beams"

However, the solution strategy can be even simplified by implementing a block iteration algorithm which segregates the calculation of $\boldsymbol{\xi}_h$ from that of y_h. This amounts to saying that at the i-th iteration of the n-th time step we may approximate the projection of any generic function g as

$$
\mathscr{P}_h^{\perp}\left(g^{n,(i)}\right) \approx g^{n,(i)} - \mathscr{P}_h\left(g^{n,(i-1)}\right)
$$

or even as

$$
\mathscr{P}_h^{\perp}\left(g^{n,(i)}\right) \approx g^{n,(i)} - \mathscr{P}_h\left(g^{n-1}\right).
$$

In other words, we perform the projection by means of known values from either the previous iteration or time step. Numerical tests reveal that both options are effective, and in this thesis we make use of these two alternatives.

The isentropic Navier-Stokes problem 4

4.1 Abstract

In this chapter we consider the approximation of the isentropic (weakly compressible) Navier-Stokes equations. The model we present is capable of taking into account acoustics and flow scales at once. After space and time discretizations have been chosen, it is very convenient from the computational point of view to design fractional step schemes in time so as to permit a segregated calculation of the problem unknowns. While these segregation schemes are well established for incompressible flows, much less is known in the case of isentropic flows. We discuss this issue in this chapter and, furthermore, we study the way to impose Dirichlet boundary conditions weakly via Nitsche's method. In order to avoid spurious reflections of the acoustic waves, Nitsche's method is combined with a non-reflecting boundary condition. Employing a purely algebraic approach to discuss the problem, some of the boundary contributions are treated explicitly and we explain how these are included in the different steps of the final algorithm. Numerical evidence shows that this explicit treatment does not have a significant impact on the convergence rate of the resulting time integration scheme. The equations of the formulation are solved using a subgrid scale technique based on a term-by-term stabilization, which we will introduce here as a particularization of the OSGS method from the previous chapter.

4.2 Introduction

Within the field of Computational Aeroacoustics (CAA), the solution of the complete set of Navier-Stokes equations, *i.e.*, the coupled problem involving mass, momentum and energy conservation equations, is referred to as Direct Noise Computation (DNC)[124]. This formulation represents a direct approach to consistently deal with aerodynamic and acoustic scales in an unified manner. The solution of this fully compressible problem via the Finite Element Method (see *e.g.* [28]) is known to be excessively demanding in terms

[124]: Bailly et al. (2010), “Progress in direct noise computation”

of computational power. Likewise, most of the compressible flow solvers derived in conservative variables found in the literature exhibit an inadequate performance in the low Mach number regime. This is mainly due to the fact that flow and acoustic scales start to considerably differ one from each other under the subsonic condition as the Mach number is progressively reduced. As a consequence, the algebraic systems arising from those formulations are commonly very ill-conditioned and difficult to solve in practice.

With the aim of overcoming such conditioning issues, several hybrid methods were developed. In this kind of techniques the computation of aerodynamic and acoustic fields is decoupled and hence they are solved independently. One of the early works in this area is the well known Lighthill's analogy [125], in which the acoustic field is obtained upon the derivation of a source term computed with the flow equations. It is also worth mentioning the socalled incompressible acoustic split method (see *e.g.* [126–128] and references therein) which consists in solving the incompressible Navier-Stokes equations followed by an inviscid acoustic part which accounts for the wave propagation. In [129], this approach is revised by also retaining the viscous terms in the acoustic set of equations. The advantage of these techniques with respect to the acoustic analogy is that the source term is directly obtained and it accounts for both sound generation and scattering. These type of hybrid methods allow a certain flexibility, as they permit to combine different models for flow and acoustic fields. However, since the incompressible problem is solved prior to the acoustic one, these methods do not account for any feedback from acoustics to the flow. Thus, their application is usually limited to problems with a light coupling between acoustic and flow scales.

[125]: Lighthill (1952), "On sound generated aerodynamically I. General theory"

[126]: Hardin et al. (1994), "An acoustic/viscous splitting technique for computational aeroacoustics"

[127]: Shen et al. (1999), "Aeroacoustic modelling of low-speed flows"

[128]: Shen et al. (2009), "Aeroacoustic Computations for Turbulent Airfoil Flows"

[129]: Shen et al. (2004), "A collocated grid finite volume method for aeroacoustic computations of low-speed flows"

The methodology we propose in this chapter aims at combining the simplicity of the aforementioned hybrid methods with the unified scale computation of DNC. Assuming a low Mach number flow, with neither shocks nor thermal sources, and entropy to remain constant, a simplified (weak) compressible Navier-Stokes problem involving only velocity and pressure fields as unknowns can be derived. This is the socalled *isentropic* flow problem (see a previous work in [130]). Solving in a monolithic (coupled) manner the algebraic system of equations that arises after the discretization via the finite element method of the continuous problem is the classical solution strategy. Despite of the several simplifications

[130]: Pont et al. (2018), "Unified solver for fluid dynamics and aeroacoustics in isentropic gas flows"

that can be introduced thanks to the constant entropy assumption, solving the resulting linear system of equations might still be computationally expensive, specially in 3D geometries. The unknowns are highly coupled and nonlinearities need to be treated with some strategy too. An alternative to that standard approach is to solve the problem by means of a fractional step method in time. This technique consists in segregating the calculation of the unknowns, so that they can be computed separately, probably with the addition of some correction steps. On the negative side, fractional step methods have an associated temporal error, frequently labeled as fractional or segregation error. It is indispensable to ensure that such error is at least of the order of the integration scheme used in time, with the purpose of maintaining the global temporal accuracy of the method.

Apart from a possible compatibility restriction between velocity and pressure interpolating spaces, the convective terms appearing in the governing equations may render the solution unstable when using a finite element formulation, showing spurious node-to-node oscillations. Though this fluctuating behavior could be avoided setting a specific mesh size (which commonly is not computationally affordable), stabilized formulations appear to circumvent this issue. In these formulations, the weak form of the problem obtained by the classical Galerkin method is modified upon the introduction of some mesh-dependent terms weighted by the residuals (or even part of them) of the differential equations. In this work we adopt the VMS framework. The key idea behind the VMS approach is to split the unknowns of the problem into two scales, namely, the scale that can be approximated by the finite element mesh and the subgrid scale, the unresolvable one. As we have already discussed previously, the general methodology consists in finding an approximation for the subgrid scale so as to yield a stable formulation involving only the finite element scales, hence maintaining the number of degrees of freedom of the starting Galerkin variational problem. There are different ways to model the subgrid scale, provided a definition of the functional space where it belongs. Here, we will define such space as the orthogonal one to the finite element space and, using this concept, we will state a term-by-term technique by neglecting the extra cross products which do not play any stability role in the formulation. As a result, this stabilized formulation is not residual based, and hence not consistent, being consistency understood in the classical finite element context. However, for the incompressible flow problem this term-by-term possibility provides a slightly improved pressure stability [99], and in [131, 132] it was applied to the viscoelastic flow problem resulting more robust and convenient than a classical residual-based formulation.

[131]: Castillo et al. (2014), "Stabilized stress-velocity-pressure finite element formulations of the Navier-Stokes problem for fluids with non-linear viscosity"

[132]: Castillo et al. (2017), "Finite element approximation of the viscoelastic flow problem: A non-residual based stabilized formulation"

Another important feature of nearly incompressible aeroacoustic flows in that external computational boundaries may produce deceptive wave reflections which pollute the solution. Ingoing waves can interfere with acoustic signals as well as originate numerical instabilities if the numerical technique is unable to introduce enough dissipation. This distinguishing issue has been widely studied and as a result, there are several numerical techniques which deal with the backscattering of waves in the aeroacoustics field. Among the most remarkable ones are: the damping of the compressible equations, the addition of an artificial counter signal, and the application of non-reflecting boundary conditions. Performing a damping of some terms of the compressible equations is a robust approach to face spurious reflections at the boundary (usually named in this case buffer zones). However, this technique brings an extra computational effort associated with the new terms that need to be included, and hence other approaches are often adopted. The literature on compressible boundary conditions is extensive, so we refer to the reviews in [133–135] and references therein. For the specific case of the isentropic problem, a novel method for the unified prescription of boundary conditions was introduced in [130] (see Section 3 in that publication). The particularity of this technique is that it combines a weak imposition of Dirichlet boundary conditions of the mean flow variables, plus a Sommerfeld non-reflecting boundary condition for the acoustic component of the pressure (similarly as in [136]).

[133]: Colonius et al. (1993), "Boundary conditions for direct computation of aerodynamic sound generation"

[134]: Fosso et al. (2012), "Comparison of outflow boundary conditions for subsonic aeroacoustic simulations"

[135]: Granet et al. (2010), "Comparison of nonreflecting outlet boundary conditions for compressible solver on unstructured grids"

[136]: Espinoza et al. (2014), "A Sommerfeld non-reflecting boundary condition for the wave equation in mixed form"

To sum up, in this chapter we will present an algebraic fractional step method in time which allows to solve the isentropic Navier-Stokes problem in a segregated manner. Our algorithm includes a stabilization within the VMS framework, making use of the orthogonal subscale concept to derive a term-by-term technique. In order to avoid any artificial reflection at the external boundaries, we incorporate the abovementioned unified prescription of boundary conditions for the isentropic problem, formulating here its segregated counterpart.

The set of equations to be discussed in the following can be understood as an extension of the incompressible case, since the final problem to be solved requires to compute only velocity and pressure fields, being the thermal problem mathematically uncoupled. This is possible due to the constant entropy assumption, which in turn allows to a establish a direct connection between density and pressure derivatives. As a result, the isentropic model presents two main advantages: first it takes into account any possible acoustic feedback on the flow scales and second, the validity of the acoustic field is not subject to the particular motion of the flow. On top of that, the computational cost of the present technique is reduced with respect to other methods. Apart from the fact that both acoustic and flow scales are solved altogether and that we get rid of the energy conservation equation, the final system is better conditioned (we refer to [130] for a detailed discussion on this).

The chapter is organized as follows: in Section 4.3 the isentropic compressible Navier-Stokes equations are introduced, as well as its variational formulation. The details of the compatible prescription of boundary conditions are reviewed in Section 4.4, whereas in Section 4.5 we present the monolithic time discretization of the problem with the boundary conditions described earlier. In Section 4.6 we design the fractional step scheme from an algebraic viewpoint, taking into account the modifications due to the application of boundary conditions. In Section 4.7, we state the stabilized finite element formulation we favor, together with the relevant adjustments that need to be considered. Numerical experiments are conducted in Section 4.8 and, finally, conclusions are drawn in Section 4.9.

4.3 Problem statement

4.3.1 Preliminaries

In this chapter we aim at solving the isentropic Navier-Stokes problem. Hence, we shall introduce some considerations in order to rewrite the general system formed by Equation 2.20a, Equation 2.20b and Equation 2.20c in a more convenient form. By definition of an isentropic (reversible and adiabatic) flow, the entropy remains constant, and hence pressure and density are related through Equation 2.18. Taking into account that density is just a function of pressure, Equation 2.20a shall be rewritten by expanding the derivatives as follows

$$\frac{1}{\rho a^2}\left[\partial_t p + (\mathbf{u}\cdot\nabla)p\right] + \nabla\cdot\mathbf{u} = 0,$$

where we recall that a stands for the speed of sound. Hence, in practice, the following relations hold

$$\partial_t p = a^2\,\partial_t\rho \tag{4.1a}$$

$$\nabla p = a^2\,\nabla\rho. \tag{4.1b}$$

The previous relations in Equation 4.1a and Equation 4.1b establish a connection between pressure and density variations in a straightforward manner and it helps to reduce the general complexity of the problem while making possible to capture the acoustic scales of the flow. This is in contrast to other non-isentropic formulations for low Mach flows (see *e.g.*, [137]) in which density variations might be related to temperature instead of pressure, and hence no acoustics are modeled.

[137]: Avila et al. (2011), "A finite element dynamical nonlinear subscale approximation for the low Mach number flow equations"

4.3.2 Initial and boundary value problem

The continuous problem finally consists in finding the fluid velocity $\mathbf{u} : \Omega\times(0,t_\mathrm{f}) \to \mathbb{R}^{N_\mathrm{sd}}$ and the pressure $p : \Omega\times(0,t_\mathrm{f}) \to \mathbb{R}$, which are solution of the following strong form of the isentropic compressible Navier-Stokes problem:

Note that in this case the energy equation is uncoupled from the mass and momentum equations.

Isentropic Navier-Stokes problem

$$\begin{aligned}\rho\left[\partial_t\mathbf{u} + (\mathbf{u}\cdot\nabla)\mathbf{u}\right] - 2\nabla\cdot\left[\mu\boldsymbol{\varepsilon}(\mathbf{u})\right] - \nabla\left[\lambda(\nabla\cdot\mathbf{u})\right]&\\ + \nabla p = \rho\mathbf{b}, &\quad \text{in } \Omega,\ t\in(0,t_\mathrm{f}) \quad (4.2\mathrm{a})\\ \epsilon^{-1}\left[\partial_t p + (\mathbf{u}\cdot\nabla)\,p\right] + \nabla\cdot\mathbf{u} = 0, &\quad \text{in } \Omega,\ t\in(0,t_\mathrm{f}) \quad (4.2\mathrm{b})\end{aligned}$$

together with the two closure equations

$$p = \mathscr{C}\rho^{\gamma}, \quad \mathscr{C} = \text{const.} \tag{4.3a}$$

$$a = \sqrt{\frac{\gamma p}{\rho}} = \sqrt{\frac{\epsilon}{\rho}} \tag{4.3b}$$

where ϵ is the bulk modulus of the fluid.

The previous problem can be rewritten in the compact manner as in Equation 3.1 after setting

$$\begin{aligned}
\mathbf{y} &= [\mathbf{u}, p]^T, \\
\mathscr{M}(\mathbf{y}) &= \operatorname{diag}\left(\rho, \epsilon^{-1}\right), \\
\mathscr{F} &= [\rho\mathbf{b}, 0]^T, \\
\mathscr{L}(\mathbf{y};\mathbf{y}) &= \begin{bmatrix} \rho(\mathbf{u}\cdot\nabla)\mathbf{u} - 2\nabla\cdot[\mu\boldsymbol{\varepsilon}(\mathbf{u})] - \nabla[\lambda(\nabla\cdot\mathbf{u})] + \nabla p \\ \epsilon^{-1}(\mathbf{u}\cdot\nabla)p + \nabla\cdot\mathbf{u} \end{bmatrix}.
\end{aligned}$$

The governing equations need to be complemented with a suitable set of both initial and boundary conditions to ensure the well-possedness of the problem[1].

Let us now set

$$\Gamma = \partial\Omega = \overline{\Gamma_{\mathrm{D},\mathbf{u}} \cup \Gamma_{\mathrm{N},\mathbf{u}}},$$

where subscript D refers to Dirichlet or essential boundary conditions, whereas N refers to Neumann or natural boundary conditions. The second subscript indicates the variable to which the condition is applied, in this case velocity. If $\mathbf{n}$ denotes the unit vector normal to Γ, $\mathbf{u}_{\mathrm{g}}$ the given velocity prescribed on $\Gamma_{\mathrm{D},\mathbf{u}}$ and $\bar{\mathbf{t}}$ the prescribed traction on $\Gamma_{\mathrm{N},\mathbf{u}}$, the boundary conditions to be considered for all time $t \in (0, t_{\mathrm{f}})$ are *initially* written as:

$$\mathbf{u} - \mathbf{u}_{\mathrm{g}} = \mathbf{0} \quad \text{on } \Gamma_{\mathrm{D},\mathbf{u}}, \tag{4.4a}$$

$$\mathbf{n}\cdot\boldsymbol{\sigma} - \bar{\mathbf{t}} = \mathbf{0} \quad \text{on } \Gamma_{\mathrm{N},\mathbf{u}}. \tag{4.4b}$$

The initial conditions for Equation 4.2a–Equation 4.2b are set for velocity and pressure, and shall be written in the form,

$$\mathbf{u}(\mathbf{x}, 0) = \mathbf{u}_0(\mathbf{x}) \quad \text{in } \Omega, \tag{4.5a}$$

$$p(\mathbf{x}, 0) = p_0(\mathbf{x}) \quad \text{in } \Omega. \tag{4.5b}$$

Remark 4.3.1 The reader might have noticed that although several simplifications were introduced, the governing equations still depend on both density and sound velocity fields. In order to resolve these additional nonlinearities, Equation 4.3a and Equation 4.3b are used to complete the formulation and help to solve the nonlinearities . Hence, one would need to solve only for velocity and pressure fields,

[1] Note that the problem defined by Equation 4.2a and Equation 4.2b can be seen as a direct extension of the incompressible Navier-Stokes case with the addition of the total time derivative (temporal plus convective) of the pressure. It is precisely this term the responsible for the wave propagation modeling.

as previously stated.

4.3.3 Variational form

In order to write the weak form of the problem from Equation 4.2a and Equation 4.2b together with the boundary conditions in Equation 4.4a and Equation 4.4b, let $\mathbf{v}$, q be the corresponding test functions for velocity and pressure, which are time-independent. Additionally $\mathbf{v}$ is assumed to vanish on $\Gamma_{\mathrm{D},\mathbf{u}}$.

Let now $V_{\mathbf{u}}$ and $\mathbb{V}_p$ be the proper functional spaces where each component of the velocity and the pressure are properly defined for each fixed time $t \in (0, t_{\mathrm{f}})$, with appropriate regularity. In addition, the functional spaces of trial solutions and test functions for the velocity are written as

$$\begin{aligned} \mathbb{V}_{\mathbf{u}} &= \left\{ \mathbf{u} \in [V_{\mathbf{u}}]^{N_{\mathrm{sd}}} \mid \mathbf{u}|_{\Gamma_{\mathrm{D},\mathbf{u}}} = \mathbf{u}_{\mathrm{g}} \right\}, \\ \mathbb{W}_{\mathbf{u}} &= \left\{ \mathbf{v} \in [V_{\mathbf{u}}]^{N_{\mathrm{sd}}} \mid \mathbf{v}|_{\Gamma_{\mathrm{D},\mathbf{u}}} = \mathbf{0} \right\}. \end{aligned}$$

Performing the integration over the computational domain Ω and using the intregration-by-parts formula on second order terms, the resulting variational form of the problem with the boundary conditions from Equation 4.4a-Equation 4.4b that we consider is given as follows: Find the pair $[\mathbf{u}, p] : (0, t_{\mathrm{f}}) \rightarrow \mathbb{V}_{\mathbf{u}} \times \mathbb{V}_p$ such that

$$\langle \mathbf{v}, \rho \partial_t \mathbf{u} \rangle + c(\rho, \mathbf{u}; \mathbf{u}, \mathbf{v}) + a(\mathbf{u}, \mathbf{v}) - b(p, \mathbf{v}) = \ell_{\mathbf{u}}(\rho; \mathbf{v}), \tag{4.6a}$$

$$\left\langle q, \epsilon^{-1} \partial_t p \right\rangle + d(\rho, \mathbf{u}; p, q) + b(q, \mathbf{u}) = 0, \tag{4.6b}$$

$$\langle \mathbf{u}(\mathbf{x}, 0), \mathbf{v} \rangle = \langle \mathbf{u}_0(\mathbf{x}), \mathbf{v} \rangle, \tag{4.6c}$$

$$\langle p(\mathbf{x}, 0), q \rangle = \langle p_0(\mathbf{x}), q \rangle, \tag{4.6d}$$

which must hold for all time $t \in (0, t_{\mathrm{f}})$ and for all test functions $[\mathbf{v}, q] \in \mathbb{W}_{\mathbf{u}} \times \mathbb{W}_p$ $\left(\mathbb{W}_p \equiv \mathbb{V}_p\right)$. The following forms where introduced:

$$c(\rho, \mathbf{u}_1; \mathbf{u}_2, \mathbf{v}) := \int_\Omega \rho \left[(\mathbf{u}_1 \cdot \nabla) \mathbf{u}_2 \right] \cdot \mathbf{v} \, \mathrm{d}\Omega, \tag{4.7a}$$

$$\begin{aligned} a(\mathbf{u}, \mathbf{v}) :=& 2 \int_\Omega \mu \boldsymbol{\varepsilon}(\mathbf{u}) : \boldsymbol{\varepsilon}(\mathbf{v}) \, \mathrm{d}\Omega \\ & - \frac{2}{3} \int_\Omega \mu (\nabla \cdot \mathbf{u})(\nabla \cdot \mathbf{v}) \, \mathrm{d}\Omega, \end{aligned} \tag{4.7b}$$

$$b(p, \mathbf{v}) := \int_\Omega p (\nabla \cdot \mathbf{v}) \, \mathrm{d}\Omega, \tag{4.7c}$$

$$d(\rho; \mathbf{u}, p, q) := \int_{\Omega} \epsilon^{-1} \left[(\mathbf{u} \cdot \nabla) p\right] q \, \mathrm{d}\Omega, \tag{4.7d}$$

$$\ell_{\mathbf{u}}(\rho; \mathbf{v}) := \int_{\Omega} \rho \mathbf{b} \cdot \mathbf{v} \, \mathrm{d}\Omega + \int_{\Gamma_{\mathrm{N},\mathbf{u}}} \bar{\mathbf{t}} \cdot \mathbf{v} \, \mathrm{d}\partial\Omega, \tag{4.7e}$$

The previous weak formulation is nothing but Equation 3.6 applied to the isentropic compressible Navier-Stokes problem, taking into account that now

$$\begin{aligned} \mathscr{B}(\mathbf{u}, \mathbf{y}, \mathbf{z}) &= c(\rho, \mathbf{u}; \mathbf{u}, \mathbf{v}) + a(\mathbf{u}, \mathbf{v}) - b(p, \mathbf{v}) \\ &\quad + d(\rho, \mathbf{u}; p, q) + b(q, \mathbf{u}) \\ \ell(\mathbf{z}) &= \ell_{\mathbf{u}}(\rho; \mathbf{v}) \end{aligned}$$

with the addition of the boundary term in momentum equation. In this regard, special care needs to be taken on the imposition of boundary conditions of the isentropic problem. This is to be treated next, so that the right hand side boundary term of Equation 4.6a and the right hand side of Equation 4.6b are modified in order to allow a compatible treatment of waves and flow velocity conditions.

4.4 Imposition of boundary conditions

Since the formulation we present aims at accounting for both flow and acoustic scales at once, there must be a compatibility requirement between the treatment of acoustic waves and the flow boundary conditions. In particular, a special type of condition must be imposed for the pressure field, whose main purpose is to allow the sound waves to leave the external boundaries of the computational domain smoothly. In this section we review the method proposed in [130] for the prescription of boundary conditions for the isentropic problem.

4.4.1 Unknown and boundary splitting

The starting idea of the method is the splitting of the two unknown fields of the problem, *i. e.*, velocity and pressure, into mean and oscillatory components[2]. For a given time instant $t \in (0, t_{\mathrm{f}})$ and a point in the spatial domain $\mathbf{x} \in \Omega$, we perform the following splitting

$$\mathbf{u}(\mathbf{x}, t) = \overline{\mathbf{u}}(\mathbf{x}, t) + \mathbf{u}'(\mathbf{x}, t), \tag{4.8a}$$

[2] The reader should note that the splitting of unknowns done in this section is a particularity of the technique to incorporate the boundary conditions and has nothing to do with the derivation of the fractional step method to be discussed later on.

$$p(\mathbf{x},t) = \overline{p}(\mathbf{x},t) + p'(\mathbf{x},t), \tag{4.8b}$$

where the mean variables are mathematically described as

$$\overline{\mathbf{u}}(\mathbf{x},t) := \frac{1}{T_w}\int_{t-T_w}^{t} \mathbf{u}(\mathbf{x},\xi)\,\mathrm{d}\xi, \tag{4.9a}$$

$$\overline{p}(\mathbf{x},t) := \frac{1}{T_w}\int_{t-T_w}^{t} p(\mathbf{x},\xi)\,\mathrm{d}\xi, \tag{4.9b}$$

being T_w an appropriate time window for the integration.

In the following, we will identify the oscillatory components with the acoustic fluctuations and the mean variables with the flow variables. The main idea is that T_w implicitly defines a filtering frequency for the acoustic waves, which must be chosen small enough to allow a damping of the acoustic waves while still reproducing the flow behavior with certainty.

Complementing the previous variable decomposition, we also divide the boundary where velocity conditions exist (either essential or natural) into internal and external contributions. Internal contributions are, for instance, those corresponding to solid walls in the interior of the domain. External contours correspond to inlet and outlet boundaries (artificial boundaries). The *external* boundary where velocity shall be prescribed $\Gamma^e_{\mathbf{u}}$ is divided into two different disjoint subsets, $\Gamma^e_{\mathrm{D},\mathbf{u}}$, $\Gamma^e_{\mathrm{N},\mathbf{u}}$. These subsets are such that

$$\overline{\Gamma^e_{\mathrm{D},\mathbf{u}} \cap \Gamma^e_{\mathrm{N},\mathbf{u}}} = \emptyset$$
$$\overline{\Gamma^e_{\mathrm{D},\mathbf{u}} \cup \Gamma^e_{\mathrm{N},\mathbf{u}}} = \Gamma^e_{\mathbf{u}}.$$

We remark that this boundary splitting is performed at the external artificial contours of the domain. Should the domain contain any interior wall with prescribed velocity, we shall expect sound waves to be reflected in such location and hence no particular boundary treatment is needed. On both $\Gamma^e_{\mathrm{D},\mathbf{u}}$ and $\Gamma^e_{\mathrm{N},\mathbf{u}}$, which are in the far field, it is assumed that the acoustic scales are dominant.

Remark 4.4.1 The key idea behind our boundary formulation is the introduction of the socalled Sommerfeld boundary condition. Such condition is derived from the wave equation written in mixed form, which represents a set of wave-like equations for $\mathbf{u}(\mathbf{x},t)$ and $p(\mathbf{x},t)$ [136].

4.4.2 Unified prescription of boundary conditions

In this subsection, we summarize the different conditions to be applied on each boundary. The two main mathematical ingredients of the methodology are the weak prescription of essential boundary conditions and the application of (zero order) Sommerfeld-like non-reflecting boundary conditions.

On the frontiers belonging to the truncation boundary $\Gamma^e_{\mathrm{D},\mathbf{u}}$, distinct conditions are enforced:

- The mean value of the velocity is prescribed to the flow given velocity
$$\overline{\mathbf{u}} - \mathbf{u}_{\mathrm{g}} = \mathbf{0} \quad \text{on} \quad \Gamma^e_{\mathrm{D},\mathbf{u}}, \tag{4.10}$$
and this will be done weakly via Nitsche's method.
- A Sommerfeld-like non-reflecting boundary condition is considered for the acoustic component of the velocity field. In the normal direction to the boundary we set
$$\mathbf{n} \cdot [\mathbf{n} \cdot \boldsymbol{\sigma}(\mathbf{u}', p')] = \rho a \mathbf{n} \cdot \mathbf{u}' \quad \text{on} \quad \Gamma^e_{\mathrm{D},\mathbf{u}}, \tag{4.11}$$
and for the tangential direction we directly write
$$\mathbf{t} \cdot [\mathbf{n} \cdot \boldsymbol{\sigma}(\mathbf{u}', p')] = 0 \quad \text{on} \quad \Gamma^e_{\mathrm{D},\mathbf{u}}, \tag{4.12}$$
for any vector $\mathbf{t}$ in the tangent direction to $\Gamma^e_{\mathrm{D},\mathbf{u}}$.

Finally, on the boundary $\Gamma^e_{\mathrm{N},\mathbf{u}}$, the following conditions are enforced:

- The mean value tractions are prescribed[3], *i.e.*
$$\mathbf{n} \cdot \boldsymbol{\sigma}(\overline{\mathbf{u}}, \overline{p}) = \overline{\mathbf{t}} \quad \text{on} \quad \Gamma^e_{\mathrm{N},\mathbf{u}}. \tag{4.13}$$
- The same approach as in $\Gamma^e_{\mathrm{D},\mathbf{u}}$ is used now for the fluctuating component. Therefore
$$\mathbf{n} \cdot [\mathbf{n} \cdot \boldsymbol{\sigma}(\mathbf{u}', p')] = \rho a \mathbf{n} \cdot \mathbf{u}' \quad \text{on} \quad \Gamma^e_{\mathrm{N},\mathbf{u}}, \tag{4.14a}$$
$$\mathbf{t} \cdot [\mathbf{n} \cdot \boldsymbol{\sigma}(\mathbf{u}', p')] = 0 \quad \text{on} \quad \Gamma^e_{\mathrm{N},\mathbf{u}}. \tag{4.14b}$$

Taking now into account these definitions, the prescription of the boundary conditions in the weak form of the problem can be done upon the modification of the boundary term in Equation 4.6a, which after the introduction of the symmetric

[3] Assuming that $\Gamma^e_{\mathrm{N},\mathbf{u}}$ is located sufficiently far away from a possible solid boundary, *i. e.*, in the far field-region, it is reasonable to set $\overline{p} \approx 0$ and $\nabla\,\overline{\mathbf{u}} \approx \mathbf{0}$ and hence the natural condition to be imposed is $\overline{\mathbf{t}} = \mathbf{0}$.

[138]: Juntunen et al. (2009), “Nitche’s method for general boundary conditions”

and the penalty terms for the imposition of $\overline{\mathbf{u}} = \mathbf{u}_\mathrm{g}$ using Nitsche’s method [138] reads:

$$\begin{aligned}
\int_{\Gamma^e_\mathbf{u}} [\mathbf{n}\cdot \boldsymbol{\sigma}(\mathbf{u}, p)] \cdot \mathbf{v} \,\mathrm{d}\partial\Omega = \int_{\Gamma^e_{\mathrm{D},\mathbf{u}}} &[\mathbf{n} \cdot \boldsymbol{\sigma}(\overline{\mathbf{u}}, \overline{p})] \cdot \mathbf{v} \,\mathrm{d}\partial\Omega \\
&- \int_{\Gamma^e_{\mathrm{D},\mathbf{u}}} \rho a(\mathbf{u}' \cdot \mathbf{n})(\mathbf{v} \cdot \mathbf{n}) \,\mathrm{d}\partial\Omega \\
&+ \int_{\Gamma^e_{\mathrm{D},\mathbf{u}}} (\overline{\mathbf{u}} - \mathbf{u}_\mathrm{g}) \cdot [\mathbf{n} \cdot \boldsymbol{\sigma}(\mathbf{v}, q)] \,\mathrm{d}\partial\Omega \\
&- \int_{\Gamma^e_{\mathrm{D},\mathbf{u}}} \psi(\overline{\mathbf{u}} - \mathbf{u}_\mathrm{g}) \cdot \mathbf{v} \,\mathrm{d}\partial\Omega \\
&- \int_{\Gamma^e_{\mathrm{N},\mathbf{u}}} \rho a(\mathbf{u}' \cdot \mathbf{n})(\mathbf{v} \cdot \mathbf{n}) \,\mathrm{d}\partial\Omega \\
&+ \int_{\Gamma^e_{\mathrm{N},\mathbf{u}}} \overline{\mathbf{t}} \cdot \mathbf{v} \,\mathrm{d}\partial\Omega,
\end{aligned} \tag{4.15}$$

where ψ denotes the numerical Nitche’s penalty parameter.

The reader should also note that there are several terms in Equation 4.15 which are known and therefore can be taken to the right hand side of the problem. Let us group those boundary terms introducing the following forms for the isentropic problem:

$$\begin{aligned}
c_\Gamma(\rho; \mathbf{u}, \mathbf{v}) := &\int_{\Gamma^e_\mathbf{u}} \rho a(\mathbf{u}' \cdot \mathbf{n})(\mathbf{v} \cdot \mathbf{n}) \,\mathrm{d}\partial\Omega \\
&+ \int_{\Gamma_{\mathrm{D},\mathbf{u}}} \psi\overline{\mathbf{u}} \cdot \mathbf{v} \,\mathrm{d}\partial\Omega \\
&- \int_{\Gamma^e_{\mathrm{D},\mathbf{u}}} 2\mu[\mathbf{n} \cdot \boldsymbol{\varepsilon}(\overline{\mathbf{u}})] \cdot \mathbf{v} \,\mathrm{d}\partial\Omega \\
&+ \int_{\Gamma^e_{\mathrm{D},\mathbf{u}}} \frac{2}{3}\mu\nabla \cdot \overline{\mathbf{u}}(\mathbf{n} \cdot \mathbf{v}) \,\mathrm{d}\partial\Omega \\
&- \int_{\Gamma^e_{\mathrm{D},\mathbf{u}}} 2\mu[\mathbf{n} \cdot \boldsymbol{\varepsilon}(\mathbf{v})] \cdot \overline{\mathbf{u}} \,\mathrm{d}\partial\Omega \\
&+ \int_{\Gamma^e_{\mathrm{D},\mathbf{u}}} \frac{2}{3}\mu\nabla \cdot \mathbf{v}(\mathbf{n} \cdot \overline{\mathbf{u}}) \,\mathrm{d}\partial\Omega,
\end{aligned} \tag{4.16a}$$

$$b_\Gamma(p, \mathbf{v}) := \int_{\Gamma^e_{\mathrm{D},\mathbf{u}}} \overline{p}(\mathbf{n} \cdot \mathbf{v}) \,\mathrm{d}\partial\Omega, \tag{4.16b}$$

$$\begin{aligned}
\ell_{\Gamma,\mathbf{u}}(\mathbf{v}) := &\int_{\Gamma^e_{\mathrm{D},\mathbf{u}}} \psi\mathbf{u}_\mathrm{g} \cdot \mathbf{v} \,\mathrm{d}\partial\Omega - \int_{\Gamma^e_{\mathrm{D},\mathbf{u}}} 2\mu[\mathbf{n} \cdot \boldsymbol{\varepsilon}(\mathbf{v})] \cdot \mathbf{u}_\mathrm{g} \,\mathrm{d}\partial\Omega \\
&+ \int_{\Gamma^e_{\mathrm{D},\mathbf{u}}} \frac{2}{3}\mu\nabla \cdot \mathbf{v}(\mathbf{n} \cdot \mathbf{u}_\mathrm{g}) \,\mathrm{d}\partial\Omega
\end{aligned}$$

$$+\int_{\Gamma^e_{\mathrm{N},\mathbf{u}}} \mathbf{v}\cdot\bar{\mathbf{t}}\,\mathrm{d}\partial\Omega, \tag{4.16c}$$

$$\ell_{\Gamma,p}(q) := \int_{\Gamma^e_{\mathrm{D},\mathbf{u}}} q(\mathbf{n}\cdot\mathbf{u}_{\mathrm{g}})\,\mathrm{d}\partial\Omega, \tag{4.16d}$$

which will go to the left and right hand side of the problem, respectively.

Finally, the variational formulation with the boundary conditions consists now in solving for velocity and pressure such that the following equations are satisfied

$$\begin{aligned}\langle \mathbf{v}, \rho\partial_t\mathbf{u}\rangle + c(\rho,\mathbf{u};\mathbf{u},\mathbf{v}) + a(\mathbf{u},\mathbf{v}) - b(p,\mathbf{v}) + c_\Gamma(\rho;\mathbf{u},\mathbf{v})&\\ + b_\Gamma(p,\mathbf{v}) = \ell_{\mathbf{u}}(\rho;\mathbf{v}) + \ell_{\Gamma,\mathbf{u}}(\mathbf{v})& \qquad (4.17a)\\ \left\langle q, \epsilon^{-1}\partial_t p\right\rangle + d(\rho,\mathbf{u};p,q) + b(q,\mathbf{u})&\\ + b_\Gamma(q,\mathbf{u}) = \ell_{\Gamma,p}(q)& \qquad (4.17b)\end{aligned}$$

for all test functions $[\mathbf{v}, q]$ and satisfying the initial conditions too.

4.5 Numerical approximation

4.5.1 Space and time discretization

Let now $\mathbb{V}_{\mathbf{u},h} \subset \mathbb{V}_{\mathbf{u}}$, $\mathbb{V}_{p,h} \subset \mathbb{V}_p$ be the velocity and pressure finite element spaces associated with the corresponding triangulation. Therefore, the raw Galerkin method applied to the problem stated in Equation 4.17a and Equation 4.17b reads: find the functions $\mathbf{u}_h$ and p_h such that,

$$\begin{aligned}\langle \mathbf{v}_h, \rho\partial_t\mathbf{u}_h\rangle + c(\rho,\mathbf{u}_h;\mathbf{u}_h,\mathbf{v}_h) + a(\mathbf{u}_h,\mathbf{v}_h) - b(p_h,\mathbf{v}_h)&\\ + c_\Gamma(\rho;\mathbf{u}_h,\mathbf{v}_h) + b_\Gamma(p_h,\mathbf{v}_h) = \ell_{\mathbf{u}}(\rho;\mathbf{v}_h)&\\ + \ell_{\Gamma,\mathbf{u}}(\mathbf{v}_h)& \qquad (4.18a)\\ \left\langle q_h, \epsilon^{-1}\partial_t p_h\right\rangle + d(\rho,\mathbf{u}_h;p_h,q_h) + b(q_h,\mathbf{u}_h)&\\ + b_\Gamma(q_h,\mathbf{u}_h) = \ell_{\Gamma,p}(q_h)& \qquad (4.18b)\end{aligned}$$

The time discretization of the problem in hand is performed by following the notation and statements already introduced in Section 3.4. Then, making use of the BDF operator in Equation 3.7, the fully discrete problem we need to solve is: for $n = 0, 1, \ldots, N-1$, solve for $\mathbf{u}_h^{n+1}, p_h^{n+1}$, given the values

$\mathbf{u}_h^{n-l}, p_h^{n-l}$ for $l = 0$ to $\theta - 1$, such that

$$\begin{aligned}\left\langle \mathbf{v}_h, \rho\delta_t \mathbf{u}_h^{n+1} \right\rangle &+ c(\rho, \mathbf{u}_h^{n+1}; \mathbf{u}_h^{n+1}, \mathbf{v}_h) + a(\mathbf{u}_h^{n+1}, \mathbf{v}_h) \\ &- b(p_h^{n+1}, \mathbf{v}_h) + c_\Gamma(\rho; \mathbf{u}_h^{n+1}, \mathbf{v}_h) \\ &+ b_\Gamma(p_h^{n+1}, \mathbf{v}_h) = \ell_{\mathbf{u}}(\rho; \mathbf{v}_h) + \ell_{\Gamma,\mathbf{u}}(\mathbf{v}_h) \qquad (4.19a) \\ \left\langle q_h, \epsilon^{-1}\partial_t p_h^{n+1} \right\rangle &+ d(\rho, \mathbf{u}_h^{n+1}; p_h^{n+1}, q_h) + b(q_h, \mathbf{u}_h^{n+1}) \\ &+ b_\Gamma(q_h, \mathbf{u}_h^{n+1}) = \ell_{\Gamma,p}(q_h) \qquad (4.19b)\end{aligned}$$

Remark 4.5.1 We want to remark that the unknowns of the problem are $\mathbf{u}_h^{n+1}$, and p_h^{n+1} and that ρ and a (and hence ϵ) shall be explicitly computed in the final algorithm by means of a linearization process. Their values are obtained from finite element quantities but not solved as unknowns for each time step and nonlinear iteration. In other words, ρ and a *do not* belong to the finite element spaces, and that is why we did not include neither the h subscript nor the superscript $n+1$ in the equations. It should be understood just as notation.

It remains to provide a discrete expression to compute the mean components of the unknowns. At the discrete level, the time window introduced in Equation 4.9a and Equation 4.9b is computed as $T_w = N_w\delta t$ being N_w a certain amount of time steps. It is proposed to use the trapezoidal rule for integration in order to compute the mean variables. The expression we use for the average values is then

$$\overline{\mathbf{u}}_h^{n+1} = \frac{\delta t}{T_w}\left(\frac{1}{2}\mathbf{u}_h^{n+1} + \sum_{j=n-N_w+2}^{n} \mathbf{u}_h^j + \frac{1}{2}\mathbf{u}_h^{n-N_w+1}\right), \qquad (4.20)$$

and equivalently for the pressure. This expression maintains the integration implicit and second order accurate, but several time steps need to be run prior to its application so as to obtain representative data for a reliable mean computation.

4.5.2 On the linearization of the problem

Prior to perform any implementation in our computer code `FEMUSS`, we shall select a linearization strategy to solve the previous nonlinear problem.

Apart from the classical nonlinearities appearing in the convective terms due to the advection velocity, there are others inherent to the nature of the isentropic equations. In particular, all the temporal terms in the problem are nonlinear due to the presence of the density ρ and the speed of sound a, computed in terms of the pressure (and the density).

Two different iterative strategies are usually considered for solving the nonlinearities in flow problems, namely, the Picard (fixed point) and the Newton-Raphson algorithms. Denoting by $\mathbf{u}^{n+1,(i)}$, $\rho^{n+1,(i)}$ and $p^{n+1,(i)}$ the known velocity, density and pressure at time step $n+1$ and iteration (i), the convective terms can be approximated by,

$$\begin{aligned}
&c(\rho^{n+1,(i+1)}, \mathbf{u}_h^{n+1,(i+1)}; \mathbf{u}_h^{n+1,(i+1)}, \mathbf{v}_h) \\
&\approx c(\rho^{n+1,(i)}, \mathbf{u}_h^{n+1,(i)}; \mathbf{u}_h^{n+1,(i+1)}, \mathbf{v}_h) \\
&+ \zeta c(\rho^{n+1,(i)}, \mathbf{u}_h^{n+1,(i+1)}; \mathbf{u}_h^{n+1,(i)}, \mathbf{v}_h) \\
&- \zeta c(\rho^{n+1,(i)}, \mathbf{u}_h^{n+1,(i)}; \mathbf{u}_h^{n+1,(i)}, \mathbf{v}_h)
\end{aligned}$$

$$\begin{aligned}
&d(\rho^{n+1,(i+1)}, \mathbf{u}_h^{n+1,(i+1)}; p_h^{n+1,(i+1)}, q_h) \\
&\approx d(\rho^{n+1,(i)}, \mathbf{u}_h^{n+1,(i)}; p_h^{n+1,(i+1)}, q_h) \\
&+ \zeta d(\rho^{n+1,(i)}, \mathbf{u}_h^{n+1,(i+1)}; p_h^{n+1,(i)}, q_h) \\
&- \zeta d(\rho^{n+1,(i)}, \mathbf{u}_h^{n+1,(i)}; p_h^{n+1,(i)}, q_h)
\end{aligned}$$

For $\zeta = 0$ the previous equations correspond to the Picard approximation of the convective terms whereas for $\zeta = 1$ it yields the Newton-Raphson strategy [4].

In this thesis, we are mainly interested in the development of fractional step schemes for compressible flow. For the implementation of this kind of techniques, numerical experience suggests that the time step of the computations δt cannot be taken very large for the method to be effective, for instance when it is compared to the critical time step of an explicit time integration scheme. This fact is of remarkable importance in the compressible regime, as the time step should be sufficiently small in order to reproduce the wide range of different scales of compressible flow problems. Thus, for a given solution at a particular nonlinear iteration, the next solution should be particularly close. Hence, only a few non-

[4] If fact we should refer to the case of $\zeta = 1$ as a ”pseudo” Newton-Raphson approach, since we should expand also the expression for the density, by using Equation 4.3a, what would introduce the pressure as an unknown in this term too.

linear iterations are required to converge and the fixed-point option is usually enough for the temporal and convective nonlinearities. Otherwise one should include an expansion by means of a Taylor series of the expressions for density and speed of sound. Although this may be appealing, it definitely introduces some burden in the formulation since the resulting terms involve rational expressions which are in general arduous to integrate numerically.

Remark 4.5.2 Concerning the way convergence is checked, we have used the following criterion,

$$\left\| \mathbf{y}_h^{n+1,(i+1)} - \mathbf{y}_h^{n+1,(i)} \right\|_{L^s} \leq \mathrm{TOL} \left\| \mathbf{y}_h^{n+1,(i)} \right\|_{L^s}$$

where TOL is the tolerance that we set and $\|\bullet\|_{L^s}$ denotes the discrete L^s norm. The choice of the parameter s controls the convergence, yet we select $s = 2$ as standard in the computations.

Remark 4.5.3 When running the calculations, the initial guess for each time step can be taken as the converged unknowns from the previous step, that is to say

$$\begin{aligned} \mathbf{u}_h^{n+1,0} &= \mathbf{u}_h^n, \\ p_h^{n+1,0} &= p_h^n. \end{aligned}$$

Another possibility is to make an extrapolation in time, depending on the order of the selected time integration scheme, using Equation 3.9 with known values from previous time steps.

4.5.3 Monolithic algebraic system

Once the finite element interpolation has been chosen, every element of the spaces of test functions and of trial solutions will be represented by a vector containing the nodal values of this element. This vector will be denoted by the boldface capital letter corresponding to the lower case function, *e.g.*, **V** will be the vector of nodal values of a generic velocity test function and **U** the vector of nodal values of the unknown velocity, and the same criteria is employed for pressure, respectively **Q** and **P**. As usual, superscripts will be used to indicate the time step and the iteration counter.

Matrix version	Term where it comes from
$\mathbf{V}^T\mathbf{M}_{\mathbf{u}}\mathbf{U}$	$\langle \mathbf{v}_h, \rho\partial_t \mathbf{u}_h\rangle$
$\mathbf{V}^T\mathbf{K}_{\mathbf{u}}\left(\mathbf{U}_1\right)\mathbf{U}_2$	$c(\rho, \mathbf{u}_{h,1}; \mathbf{u}_{h,2}, \mathbf{v}_h)$
$\mathbf{V}^T\mathbf{M}_{\Gamma}\mathbf{U}$	$\left\langle \psi\bar{\mathbf{u}}, \mathbf{v}_h\right\rangle_{\Gamma_{\mathrm{D},\mathbf{u}}}$
$\mathbf{V}^T\mathbf{K}_{\Gamma}\mathbf{U}$	$c_{\Gamma}(\rho; \mathbf{u}_h, \mathbf{v}_h) - \left\langle \psi\bar{\mathbf{u}}, \mathbf{v}_h\right\rangle_{\Gamma_{\mathrm{D},\mathbf{u}}}$
$\mathbf{V}^T\mathbf{G}\mathbf{P}$	$b(p_h, \mathbf{v}_h)$
$\mathbf{V}^T\mathbf{G}_{\Gamma}\mathbf{P}$	$b_{\Gamma}(p_h, \mathbf{v}_h)$
$\mathbf{V}^T\mathbf{F}$	$\ell_{\mathbf{u}}(\rho; \mathbf{v}_h)$
$\mathbf{V}^T\mathbf{F}_{\Gamma,\mathbf{u}}$	$\ell_{\Gamma,\mathbf{u}}(\mathbf{v}_h)$

Table 4.1: Matrix form of the isentropic terms corresponding to the momentum equation.

Matrix version	Term where it comes from
$\mathbf{Q}^T\mathbf{M}_p\mathbf{P}$	$\left\langle q_h, \epsilon^{-1}\partial_t p_h\right\rangle$
$\mathbf{Q}^T\mathbf{K}_p\left(\mathbf{U}\right)\mathbf{P}$	$d(\rho, \mathbf{u}_h; p_h, q_h)$
$\mathbf{Q}^T\mathbf{D}\mathbf{U}$	$b(q_h, \mathbf{u}_h)$
$\mathbf{Q}^T\mathbf{D}_{\Gamma}\mathbf{U}$	$b_{\Gamma}(q_h, \mathbf{u}_h)$
$\mathbf{Q}^T\mathbf{F}_{\Gamma,p}$	$\ell_{\Gamma,p}(q_h)$

Table 4.2: Matrix form of the isentropic terms corresponding to the mass equation.

The definitions of the arrays involved in this problem are collected in Table 4.1 and Table 4.2. The notation here is as follows: the subscripts $(\cdot)_{\mathbf{u}}$ and $(\cdot)_p$ refer to matrices of the momentum and continuity equation. In addition, $(\cdot)_{\Gamma}$ stands for terms arising from the special treatment of boundary conditions, with $\mathbf{M}_{\Gamma}$ containing the penalty term and $\mathbf{K}_{\Gamma}$, $\mathbf{G}_{\Gamma}$ and $\mathbf{D}_{\Gamma}$ the remaining Nitsche and Sommerfeld contributions.
Having introduced all these matrices and vectors, the resolution of the isentropic compressible flow problem via the FE method is stated now as: given the initial data and the corresponding values $\mathbf{U}^{n-l}$, $\mathbf{P}^{n-l}$ for $l = 0$ to $\theta - 1$, find $\mathbf{U}^{n+1}$ and $\mathbf{P}^{n+1}$, approximation to $\mathbf{U}(t^{n+1})$, $\mathbf{P}(t^{n+1})$, as the converged solutions of the following iterative procedure:

$$\begin{aligned}\mathbf{M}_{\mathbf{u},\rho^{(i)}}\frac{D_\theta}{\delta t}\mathbf{U}^{n+1,(i+1)} &+ \mathbf{K}_{\mathbf{u},\rho^{(i)}}\left(\mathbf{U}^{n+1,(i)}\right)\mathbf{U}^{n+1,(i+1)}\\ &+ \mathbf{M}_{\Gamma}\mathbf{U}^{n+1,(i+1)} + \mathbf{K}_{\Gamma,\rho^{(i)}}\mathbf{U}^{n+1,(i+1)}\\ &- \mathbf{G}\mathbf{P}^{n+1,(i+1)} + \mathbf{G}_{\Gamma}\mathbf{P}^{n+1,(i+1)} = \mathbf{F}^{n+1}_{\rho^{(i)}} + \mathbf{F}^{n+1}_{\Gamma,\mathbf{u}}, \qquad (4.21a)\end{aligned}$$

$$\mathbf{M}_{p,\rho^{(i)}}\frac{D_\theta}{\delta t}\mathbf{P}^{n+1,(i+1)} + \mathbf{K}_{p,\rho^{(i)}}(\mathbf{U}^{n+1,(i)})\mathbf{P}^{n+1,(i+1)} + \mathbf{D}\mathbf{U}^{n+1,(i+1)}$$

$$+\,\mathbf{D}_\Gamma \mathbf{U}^{n+1,(i+1)} = \mathbf{F}^{n+1}_{\Gamma,p}\,, \tag{4.21b}$$

where the dependence of matrices $\mathbf{K}_\mathbf{u}$ and $\mathbf{K}_p$ on the vector of velocity unknowns $\mathbf{U}$ has been explicitly displayed in order to remark the nonlinear character of the problem. Furthermore, we have included a subscript $\rho^{(i)}$ to indicate that those arrays are computed by taking a previously computed value of the density. This system, in a more compact manner for each iteration, can be rearranged for each iteration as follows:

$$\begin{bmatrix} \mathbf{A}_{\mathbf{uu}} & \mathbf{A}_{\mathbf{u}p} \\ \mathbf{A}_{p\mathbf{u}} & \mathbf{A}_{pp} \end{bmatrix} \cdot \begin{bmatrix} \mathbf{U}^{n+1} \\ \mathbf{P}^{n+1} \end{bmatrix} = \begin{bmatrix} \mathbf{F}^{n+1}_{\mathbf{U}} \\ \mathbf{F}^{n+1}_{\mathbf{P}} \end{bmatrix} \tag{4.22}$$

with the following definitions

$$\begin{aligned}
\mathbf{A}_{\mathbf{uu}} :=& \mathbf{M}_\mathbf{u}(\rho)\frac{D_\theta}{\delta t} + \mathbf{K}_\mathbf{u}\left(\rho, \mathbf{U}^{n+1}\right) + \mathbf{M}_\Gamma + \mathbf{K}_\Gamma(\rho) \\
\mathbf{A}_{\mathbf{u}p} :=& -\mathbf{G} + \mathbf{G}_\Gamma \\
\mathbf{A}_{p\mathbf{u}} :=& \mathbf{D} + \mathbf{D}_\Gamma \\
\mathbf{A}_{pp} :=& \mathbf{M}_p(\rho)\frac{D_\theta}{\delta t} + \mathbf{K}_p\left(\rho, \mathbf{U}^{n+1}\right) \\
\mathbf{F}^{n+1}_{\mathbf{U}} :=& \mathbf{F}^{n+1}_{\mathbf{u}}(\rho) + \mathbf{F}^{n+1}_{\Gamma,\mathbf{u}} \\
\mathbf{F}^{n+1}_{\mathbf{P}} :=& \mathbf{F}^{n+1}_{\Gamma,p}
\end{aligned}$$

The high non-linear character of the problem is made explicit in the system by including the dependence of the arrays on the variables in the parenthesis.

4.6 Design of the fractional step methodology

The method we propose in this section is directly linked to the classical pressure-correction scheme applied to the incompressible Navier-Stokes flow problem [50], in which a velocity guess is first computed and then corrected once the pressure is calculated. Another possibility would be to calculate first a pressure guess, what would provide a velocity-correction-like algorithm (see *e.g.*., [139]). We will not discuss them here, yet the ideas presented next could be also used to design velocity-correction schemes.

[139]: Owen et al. (2012), "A third-order velocity correction scheme obtained at the discrete level"

4.6.1 Pressure-correction algorithm

In order to simplify the exposition and the notation, let us drop the iteration counter (i) in this section. For the purpose of the derivation of the method, let us start by writing system Equation 4.21a-Equation 4.21b in the following *equivalent* manner:

$$\begin{aligned}
&\mathbf{M_u}(\rho)\frac{D_\theta}{\delta t}\widetilde{\mathbf{U}}^{n+1} + \mathbf{K_u}(\rho, \widetilde{\mathbf{U}}^{n+1})\widetilde{\mathbf{U}}^{n+1} + \mathbf{M}_\Gamma\widetilde{\mathbf{U}}^{n+1} + \mathbf{K}_\Gamma(\rho)\widetilde{\mathbf{U}}^{n+1} \\
&\qquad - (\mathbf{G} - \mathbf{G}_\Gamma)\hat{\mathbf{P}}^{n+1}_{\theta'} = \mathbf{F}^{n+1}(\rho) + \mathbf{F}^{n+1}_{\Gamma,\mathbf{u}}, && (4.23a)\\
&\mathbf{M_u}(\rho)\frac{1}{\phi_\theta\delta t}(\mathbf{U}^{n+1} - \widetilde{\mathbf{U}}^{n+1}) + \mathbf{N}^{n+1}_\mathbf{u} + \mathbf{N}^{n+1}_\psi + \mathbf{N}^{n+1}_\Gamma \\
&\qquad - (\mathbf{G} - \mathbf{G}_\Gamma)(\mathbf{P}^{n+1} - \hat{\mathbf{P}}^{n+1}_{\theta'}) = 0, && (4.23b)\\
&\mathbf{M}_p(\rho)\frac{D_\theta}{\delta t}\mathbf{P}^{n+1} + \mathbf{K}_p(\rho, \mathbf{U}^{n+1})\mathbf{P}^{n+1} - \phi_\theta\delta t(\mathbf{D} + \mathbf{D}_\Gamma)\mathbf{M}_\mathbf{u}^{-1}\mathbf{N}^{n+1}_\mathbf{u} \\
&\qquad - \phi_\theta\delta t(\mathbf{D} + \mathbf{D}_\Gamma)\mathbf{M}_\mathbf{u}^{-1}\mathbf{N}^{n+1}_\psi - \phi_\theta\delta t(\mathbf{D} + \mathbf{D}_\Gamma)\mathbf{M}_\mathbf{u}^{-1}\mathbf{N}^{n+1}_\Gamma \\
&\qquad + \phi_\theta\delta t(\mathbf{D} + \mathbf{D}_\Gamma)\mathbf{M}_\mathbf{u}^{-1}(\mathbf{G} + \mathbf{G}_\Gamma)(\mathbf{P}^{n+1} - \hat{\mathbf{P}}^{n+1}_{\theta'}) \\
&\qquad + (\mathbf{D} + \mathbf{D}_\Gamma)\widetilde{\mathbf{U}}^{n+1} = \mathbf{F}^{n+1}_{\Gamma,p}, && (4.23c)
\end{aligned}$$

where we have introduced the following arrays,

$$\begin{aligned}
\mathbf{N}^{n+1}_\mathbf{u} &= \mathbf{K_u}(\mathbf{U}^{n+1})\mathbf{U}^{n+1} - \mathbf{K_u}(\widetilde{\mathbf{U}}^{n+1})\widetilde{\mathbf{U}}^{n+1}, && (4.24a)\\
\mathbf{N}^{n+1}_\psi &= \mathbf{M}_\Gamma\mathbf{U}^{n+1} - \mathbf{M}_\Gamma\widetilde{\mathbf{U}}^{n+1}, && (4.24b)\\
\mathbf{N}^{n+1}_\Gamma &= \mathbf{K}_\Gamma\mathbf{U}^{n+1} - \mathbf{K}_\Gamma\widetilde{\mathbf{U}}^{n+1}. && (4.24c)
\end{aligned}$$

In these equations, $\widetilde{\mathbf{U}}^{n+1}$ is an auxiliary variable to which we shall refer to as *intermediate velocity* and $\hat{\mathbf{P}}^{n+1}_{\theta'}$ is an extrapolation of the pressure of order θ' at time step t^{n+1}. See Equation 3.9 for details. The main idea of the previous splitting is that adding up Equation 4.23a and Equation 4.23b we recover Equation 4.21a. Likewise, Equation 4.23c is derived upon substitution into Equation 4.21b of the relation between $\mathbf{U}^{n+1}$ and $\widetilde{\mathbf{U}}^{n+1}$ obtained from Equation 4.23b, and this relation is

$$\begin{aligned}
\mathbf{U}^{n+1} &= \widetilde{\mathbf{U}}^{n+1} + \phi_\theta\delta t\mathbf{M}_\mathbf{u}^{-1}\left[(\mathbf{G} + \mathbf{G}_\Gamma)\left(\mathbf{P}^{n+1} - \hat{\mathbf{P}}^{n+1}_{\theta'}\right)\right] \\
&\quad - \phi_\theta\delta t\mathbf{M}_\mathbf{u}^{-1}\left[\mathbf{N}^{n+1}_\mathbf{u} + \mathbf{N}^{n+1}_\psi + \mathbf{N}^{n+1}_\Gamma\right]. \qquad (4.25)
\end{aligned}$$

Generally speaking, the fractional step approach to solve the isentropic Navier-Stokes problem has three main steps: first compute the intermediate velocity from Equation 4.23a, then obtain the pressure from Equation 4.23c, and finally correct the velocity result using Equation 4.23b.

Although this scheme will make possible to segregate the calculation of the unknowns of the problem and provides an algorithm of pressure-correction type, some extra information is needed since equations Equation 4.23b and Equation 4.23c still couple the calculation of $\mathbf{U}^{n+1}$ and $\mathbf{P}^{n+1}$. At this point, it is very convenient to make the following remarks:

Remark 4.6.1 One should notice that the resulting matrix from $\mathbf{D}\mathbf{M}_{\mathbf{u}}^{-1}\mathbf{G}$ Equation 4.23c can be viewed as an approximation to the discrete version of the Laplacian operator $\Delta(\bullet)$ as it is discussed in [140] and [50]. In order to avoid dealing with that matrix, which has a wide stencil and might be computationally feasible only if $\mathbf{M}_{\mathbf{u}}$ is approximated by a diagonal matrix, we can work with

$$\mathbf{D}\mathbf{M}_{\mathbf{u}}^{-1}\mathbf{G} \approx \mathbf{L}$$

where $\mathbf{L}$ is a Laplacian matrix obtained from the assembly of an elemental matrix computed using the gradient of the standard shape functions. If i and j run from 1 to the number of elemental nodes, the matrix is computed as

$$[\mathbf{L}^{(e)}]^{ij} = \int_{\Omega^{(e)}} \frac{1}{\rho} \nabla\varphi^i \cdot \nabla\varphi^j \, \mathrm{d}\Omega$$
$$\mathbf{L} = \mathbb{A}^{(e)}\mathbf{L}^{(e)}$$

where $\mathbb{A}^{(e)}$ is the assembly operator (addition plus injection) acting on the local element matrix.

[140]: Codina et al. (2004), "A stabilized finite element predictor–corrector scheme for the incompressible Navier–Stokes equations using a nodal–based implementation"

Remark 4.6.2 If we wanted to compute the pressure from Equation 4.23c, we would still have to face the difficulty of computing terms such as $\mathbf{D}_\Gamma\mathbf{M}_{\mathbf{u}}^{-1}\mathbf{G}$, $\mathbf{D}\mathbf{M}_{\mathbf{u}}^{-1}\mathbf{G}_\Gamma$ and $\mathbf{D}_\Gamma\mathbf{M}_{\mathbf{u}}^{-1}\mathbf{G}_\Gamma$. Such computations can be really time consuming and burdensome. Note that an approximation similar to the one just commented above is not possible due to the character of the boundary matrices $\mathbf{D}_\Gamma$ and $\mathbf{G}_\Gamma$. A possible strategy to get rid of those calculation is to introduce an explicit treatment of some on the terms involved in the calculations.

Remark 4.6.3 Note that from the definition of the extrapolation operators in Section 3.4, the difference between the pressure and the extrapolated pressure is of the following order,

$$\left\|\mathbf{P}^{n+1} - \hat{\mathbf{P}}^{n+1}_{\theta-1}\right\| \sim \mathcal{O}(\delta t^{\theta-1}).$$

Therefore, it is easy to see from Equation 4.25 that,

$$\mathcal{O}\left(\left\|\mathbf{U}^{n+1} - \widetilde{\mathbf{U}}^{n+1}\right\|\right) = \mathcal{O}(\delta t^{\theta})$$

and thus, the intermediate velocity could be used as an approximation to the actual velocity without affecting the global accuracy of the temporal integrator.

4.6.2 Explicit treatment of boundary terms and final fractional step scheme

Having the previous information in mind, the novel idea we propose in this work is to modify Equation 4.23a and Equation 4.23c in such a way that both boundary terms $\mathbf{G}_\Gamma\mathbf{P}^{n+1}$ and $\mathbf{D}_\Gamma\mathbf{U}^{n+1}$ are treated explicitly, *by means of an extrapolation of the same order of the time integration scheme, θ.* This implies that system in Equation 4.23a and Equation 4.23c would now read as

$$\begin{aligned}
&\mathbf{M_u}(\rho)\frac{D_\theta}{\delta t}\widetilde{\mathbf{U}}^{n+1} + \mathbf{K_u}(\rho,\widetilde{\mathbf{U}}^{n+1})\widetilde{\mathbf{U}}^{n+1} + \mathbf{M}_\Gamma\widetilde{\mathbf{U}}^{n+1} + \mathbf{K}_\Gamma(\rho)\widetilde{\mathbf{U}}^{n+1}\\
&\qquad - \mathbf{G}\hat{\mathbf{P}}^{n+1}_{\theta'} + \mathbf{G}_\Gamma\hat{\mathbf{P}}^{n+1}_{\theta} = \mathbf{F}^{n+1}(\rho) + \mathbf{F}^{n+1}_{\Gamma,\mathbf{u}}, \qquad (4.26a)\\
&\mathbf{M_u}(\rho)\frac{1}{\phi_\theta\delta t}(\mathbf{U}^{n+1} - \widetilde{\mathbf{U}}^{n+1}) + \mathbf{N}^{n+1}_{\mathbf{u}} + \mathbf{N}^{n+1}_{\psi} + \mathbf{N}^{n+1}_{\Gamma}\\
&\qquad - \mathbf{G}(\mathbf{P}^{n+1} - \hat{\mathbf{P}}^{n+1}_{\theta'}) = 0, \qquad (4.26b)\\
&\mathbf{M}_p(\rho)\frac{D_\theta}{\delta t}\mathbf{P}^{n+1} + \mathbf{K}_p(\rho,\mathbf{U}^{n+1})\mathbf{P}^{n+1} - \phi_\theta\delta t(\mathbf{D}+\mathbf{D}_\Gamma)\mathbf{M}_{\mathbf{u}}^{-1}\mathbf{N}^{n+1}_{\mathbf{u}}\\
&\qquad - \phi_\theta\delta t(\mathbf{D}+\mathbf{D}_\Gamma)\mathbf{M}_{\mathbf{u}}^{-1}\mathbf{N}^{n+1}_{\psi} - \phi_\theta\delta t(\mathbf{D}+\mathbf{D}_\Gamma)\mathbf{M}_{\mathbf{u}}^{-1}\mathbf{N}^{n+1}_{\Gamma}\\
&\qquad + \phi_\theta\delta t\mathbf{D}\mathbf{M}_{\mathbf{u}}^{-1}\mathbf{G}(\mathbf{P}^{n+1} - \hat{\mathbf{P}}^{n+1}_{\theta'}) + \mathbf{D}\widetilde{\mathbf{U}}^{n+1}\\
&\qquad + \mathbf{D}_\Gamma\widehat{\mathbf{U}}^{n+1}_{\theta} = \mathbf{F}^{n+1}_{\Gamma,p}. \qquad (4.26c)
\end{aligned}$$

Note that now the products $\mathbf{D}_\Gamma\mathbf{M}_{\mathbf{u}}^{-1}\mathbf{G}$, $\mathbf{D}\mathbf{M}_{\mathbf{u}}^{-1}\mathbf{G}_\Gamma$ and $\mathbf{D}_\Gamma\mathbf{M}_{\mathbf{u}}^{-1}\mathbf{G}_\Gamma$ do not appear in the formulation and that we treat some terms on the boundary explicitly via extrapolations in $\mathbf{G}_\Gamma\hat{\mathbf{P}}^{n+1}_{\theta}$ and $\mathbf{D}_\Gamma\widehat{\mathbf{U}}^{n+1}_{\theta}$.

Formally, the fractional step algorithm of order θ can be stated by taking $\theta' = \theta - 1$ and it entails the following steps:

1. Compute an intermediate velocity $\widetilde{\mathbf{U}}^{n+1}$ by solving Equation 4.26a.
2. Compute an approximation to the pressure $\mathbf{P}^{n+1}$ after solving Equation 4.26c neglecting $\mathbf{N}_{\mathbf{u}}^{n+1}$, $\mathbf{N}_{\psi}^{n+1}$ $\mathbf{N}_{\Gamma}^{n+1}$ and substituting $\mathbf{U}^{n+1}$ by $\widetilde{\mathbf{U}}^{n+1}$ in the term $\mathbf{K}_p(\mathbf{U}^{n+1})\mathbf{P}^{n+1}$. As we have already pointed out this perturbation is of order $\mathcal{O}(\delta t^{\theta})$ and it is the key point that permits to uncouple the calculation of $\mathbf{U}^{n+1}$ and $\mathbf{P}^{n+1}$.
3. Perform the correction and compute the end-of-step velocity $\mathbf{U}^{n+1}$ from Equation 4.26b neglecting $\mathbf{N}_{\mathbf{u}}^{n+1}$, $\mathbf{N}_{\Gamma}^{n+1}$ but taking into account $\mathbf{N}_{\psi}^{n+1}$. This can be seen as a sort of Yosida factorization for the imposition of boundary conditions (see [50] and references inside).

It is well known that the extrapolation of second order of the term $\mathbf{G}\hat{\mathbf{P}}_{\theta'}^{n+1}$, *i. e.*, taking $\theta' = 2$, is unstable. Hence the resulting scheme is known to be stable up to $\theta = 2$. In fact, this issue motivated the study of velocity correction algorithms, which allow to design fractional step schemes of third order in time. However, we did not observe any erratic behaviour of the term $\mathbf{G}_{\Gamma}\hat{\mathbf{P}}_{\theta}^{n+1}$ for the extrapolation of second order. The final algorithm in its matrix form is included down below for $\theta = 1, 2$.

First and second order fractional step scheme for the isentropic problem

- Set/read the initial conditions for $\mathbf{U}^0$ and $\mathbf{P}^0$.
- WHILE $n < N$ DO
    - Set $\mathbf{U}^{n,0} = \mathbf{U}^{n-1}$ and $\mathbf{P}^{n,0} = \mathbf{P}^{n-1}$
    - WHILE (not converged) DO
        - Compute intermediate velocity $\widetilde{\mathbf{U}}^{n+1}$

$$\begin{aligned}\mathbf{M}_{\mathbf{u},\rho^n}\frac{D_\theta}{\delta t}\widetilde{\mathbf{U}}^{n+1,(i+1)} &+ \mathbf{K}_{\mathbf{u},\rho^n}\left(\widetilde{\mathbf{U}}^{n+1,(i)}\right)\widetilde{\mathbf{U}}^{n+1,(i+1)}\\ &+ \mathbf{M}_{\Gamma}\widetilde{\mathbf{U}}^{n+1,(i+1)} + \mathbf{K}_{\Gamma,\rho^n}\widetilde{\mathbf{U}}^{n+1,(i+1)}\\ &- \mathbf{G}\hat{\mathbf{P}}_{\theta'}^{n+1} + \mathbf{G}_{\Gamma}\hat{\mathbf{P}}_{\theta}^{n+1} = \mathbf{F}_{\rho^{(i)}}^{n+1} + \mathbf{F}_{\Gamma,\mathbf{u}}^{n+1}\end{aligned}$$

        - Check convergence
    - END while (not converged)
    - Compute the pressure $\mathbf{P}^{n+1}$ using the interme-

diate velocity from the previous step

$$\begin{aligned}\mathbf{M}_{p,\rho^n}\frac{D_\theta}{\delta t}\mathbf{P}^{n+1} &+ \mathbf{K}_{p,\rho^n}\left(\widetilde{\mathbf{U}}^{n+1}\right)\mathbf{P}^{n+1}\\ &+ \phi_\theta \delta t \mathbf{L}_{\rho^n}\left(\mathbf{P}^{n+1} - \hat{\mathbf{P}}^{n+1}_{\theta'}\right) + \mathbf{D}\widetilde{\mathbf{U}}^{n+1}\\ &+ \mathbf{D}_\Gamma \widehat{\mathbf{U}}^{n+1}_\theta = \mathbf{F}^{n+1}_{\Gamma,p}\end{aligned}$$

- Velocity correction to obtain the end-of-step velocity $\mathbf{U}^{n+1}$

$$\begin{aligned}\mathbf{M}_{\mathbf{u},\rho^{n+1}}\frac{1}{\phi_\theta \delta t}\left(\mathbf{U}^{n+1} - \widetilde{\mathbf{U}}^{n+1}\right) &+ \mathbf{N}^{n+1}_\psi\\ &- \mathbf{G}\left(\mathbf{P}^{n+1} - \hat{\mathbf{P}}^{n+1}_{\theta'}\right) = 0\end{aligned}$$

▸ END while $n < N$ (non-stationary)

The equation to solve for the pressure is in principle nonlinear since we need the pressure to compute the density through the isentropic law. One option is to perform a loop in the implementation, iterating for instance by means of a Picard's approach, so that we compute the density with the pressure values from the previous iteration. Another possibility could be just to compute the density with the pressure values already available from the previous time steps, for instance performing an extrapolation in time. Since the implementation of the isentropic problem is coded over an already-existing implementation of the classical incompressible Navier-Stokes solver, we favor the latter option.

Remark 4.6.4 The inclusion of the penalization correction $\mathbf{N}^{n+1}_\psi$ in the last step of the algorithm aids to properly impose the boundary conditions of the problem avoiding possible instabilities. It seems reasonable to take it into account, bearing in mind that the splitting in Equation 4.26a-Equation 4.26c needs to be done taking into account boundary conditions, similarly to the standard case in which the boundary conditions are enforced strongly.

Remark 4.6.5 It is also important to note that $\mathbf{M}_\Gamma$ displays a structure of mass matrix but for boundary contributions, what in turn would allow to solve directly the system for $\mathbf{U}^{n+1}$ if a lumping technique is used. Moreover, the correction of the convective term $\mathbf{N}^{n+1}_{\mathbf{u}}$ could also be taken into consideration in this last step, yielding a complete Yosida scheme. This would permit to derive a high order method in time (see [50], Section 4.3).

Remark 4.6.6 Another possibility for the extrapolation of the velocity boundary term could be argued. Since $\widetilde{\mathbf{U}}^{n+1}$ is an approximation of $\mathcal{O}(\delta t^{\theta})$ to $\mathbf{U}^{n+1}$, and the intermediate velocity is already computed when the term $\mathbf{D}_{\Gamma}\mathbf{U}^{n+1}$ needs to be treated explicitly, one could even consider to compute $\mathbf{D}_{\Gamma}\widetilde{\mathbf{U}}^{n+1}$ instead of $\mathbf{D}_{\Gamma}\widehat{\mathbf{U}}_{\theta}^{n+1}$. Numerical experiments show that both options provide basically equivalent results.

4.7 VMS stabilized formulation

This section is devoted to the discussion of the application of the Variational Multiscale method to the isentropic problem. The general procedure was already described in Chapter 3. Hence, the stabilized version of the isentropic compressible problem is nothing but Equation 3.20 with the pertinent definitions of the stabilization terms (and up to boundary terms).

4.7.1 Stabilized formulation applied to the isentropic Navier-Stokes problem

For reasons already discussed, we will consider the OSGS technique, as stated in Section 3.5.4. Taking into account the information there presented, the finite element discrete residuals of the momentum and mass equations can be written as in Equation 3.15, excluding the viscous terms as

$$\mathscr{R}(\mathbf{y};\mathbf{y}_h) = -\begin{bmatrix} \rho(\mathbf{u}_h^{n+1}\cdot\nabla)\mathbf{u}_h^{n+1} + \nabla p_h^{n+1} \\ \frac{1}{\epsilon}(\mathbf{u}_h^{n+1}\cdot\nabla)p_h^{n+1} + \nabla\cdot\mathbf{u}_h^{n+1} \end{bmatrix}. \tag{4.27}$$

Similarly, the adjoint operator of the problem as in Equation 3.14 is then identified as

$$\mathscr{L}^{\star}(\mathbf{y};\mathbf{z}_h) = -\begin{bmatrix} \nabla\cdot\left(\rho\mathbf{u}_h^{n+1}\otimes\mathbf{v}_h\right) + \nabla q_h \\ \nabla\cdot\left(\epsilon^{-1}\mathbf{u}_h^{n+1}q\right) + \nabla\cdot\mathbf{v}_h \end{bmatrix}. \tag{4.28}$$

Furthermore, the subscales are time tracked in time by solving Equation 3.18 which for the problem in hand reads:

$$\begin{aligned}\tilde{\mathbf{u}}^{n+1} &= -\tau_{\mathbf{u},\mathrm{d}}\mathscr{P}_h^{\perp}\left[\rho(\mathbf{u}_h^{n+1}\cdot\nabla)\mathbf{u}_h^{n+1}+\nabla p_h^{n+1}\right]\\ &\quad+\tau_{\mathbf{u},\mathrm{d}}\rho\frac{\tilde{\mathbf{u}}^n}{\delta t}, \qquad (4.29a)\\ \tilde{p}^{n+1} &= -\tau_{p,\mathrm{d}}\mathscr{P}_h^{\perp}\left[\epsilon^{-1}(\mathbf{u}_h^{n+1}\cdot\nabla)p_h^{n+1}+\nabla\cdot\mathbf{u}_h^{n+1}\right]\\ &\quad+\tau_{p,\mathrm{d}}\frac{\tilde{p}^n}{\epsilon\delta t}. \qquad (4.29b)\end{aligned}$$

Remark 4.7.1 It is assumed that the orthogonal projections of the residual temporal terms cancel, *i. e.*

$$\mathscr{P}_h^{\perp}\left[\rho\partial_t\mathbf{u}_h\right]\approx 0 \quad\text{and}\quad \mathscr{P}_h^{\perp}\left[\frac{1}{\epsilon}\partial_t p_h\right]\approx 0.$$

These terms would be exactly zero if both ρ and ϵ were equal to a constant, which is not the case for the isentropic problem. However, we consider as true that both variables are such that $\rho\partial_t\mathbf{u}_h$ and $\epsilon^{-1}\partial_t p_h$ already belong to the finite element spaces and hence its orthogonal projection vanishes. Additionally, we assume

$$\mathscr{P}_h^{\perp}[\rho\mathbf{b}]\approx 0,$$

which yields a weakly consistent method.

4.7.2 On the stabilization parameters

The stabilization parameters $\tau_{\mathbf{u},\mathrm{d}}$ and $\tau_{p,\mathrm{d}}$ defined over each element $\Omega^{(e)}$ of the partition contribute to provide the stabilization for the weak forms of the momentum and mass conservation equations. Up to our knowledge, there is no general rule to define it for systems of equations. It must be designed for each particular problem taking into account its stability deficiencies or even scaling requirements. For the problem in hand, we will take a simple diagonal expression. Hence, we define

$$\boldsymbol{\tau}(\mathbf{y}^{n+1})=\mathrm{diag}(\tau_{\mathbf{u},\mathrm{d}}\mathbf{I}_{N_{\mathrm{sd}}},\tau_{p,\mathrm{d}}). \qquad (4.30)$$

Following Equation 3.19, we can now write

$$\tau_{\mathbf{u},\mathrm{d}} = \left[\frac{\rho}{\delta t} + \tau_{\mathbf{u}}^{-1}(\mathbf{y}^{n+1})\right]^{-1}, \tag{4.31a}$$

$$\tau_{p,\mathrm{d}} = \left[\frac{\epsilon^{-1}}{\delta t} + \tau_{p}^{-1}(\mathbf{y}^{n+1})\right]^{-1}. \tag{4.31b}$$

The definition of both $\tau_{\mathbf{u}}$ and τ_p is based on a Fourier analysis, which we will not discuss here (see the developments in [99]). We compute them as

$$\tau_{\mathbf{u}} = \left[c_1\frac{\mu}{h^2} + c_2\rho\frac{\|\mathbf{u}_h\|}{h}\right]^{-1}, \tag{4.32a}$$

$$\tau_p = \frac{h^2}{c_1\tau_{\mathbf{u}}}, \tag{4.32b}$$

where $\|\mathbf{u}_h\|$ is the mean Euclidean norm of the velocity in each element and h is the element size. Note that their values are needed at each integration point. The algorithmic constants c_1 and c_2 depend on the polynomial order of the interpolation. For linear elements, the values $c_1 = 4$ and $c_2 = 2$ are commonly set.

4.7.3 Term-by-term stabilization

From the point of view of stability, not all the terms of the finite element residual aid to enhance the stability of the formulation. Therefore, some of them could be even neglected and a less costly method emerges. Precisely, it is this last idea the one that motivates the socalled term-by-term stabilization methods (see *e.g.* [132] and [141]).

[141]: Rebollo (1998), "A term by term stabilization algorithm for finite element solution of incompressible flow problems"

The stabilized formulation we favor in this work is a term-by-term OSGS approach, also referred to as split OSGS. Although this scheme is not completely residual-based, it has been concluded that it has an optimal consistency error (see [122] for a formal discussion and numerical analysis on the Oseen equations). The key idea behind this method resides in *neglecting the extra cross products among operators applied on both test and trial functions*, which arise from the classical orthogonal stabilization.

Let us rewrite Equation 4.29a–Equation 4.29b as follows

$$\tilde{\mathbf{u}}^{n+1} = -\tau_{\mathbf{u},\mathrm{d}}\mathscr{P}_h^{\perp}\left[\rho(\mathbf{u}_h^{n+1}\cdot\nabla)\mathbf{u}_h^{n+1}\right] - \tau_{\mathbf{u},\mathrm{d}}\mathscr{P}_h^{\perp}\left[\nabla p_h^{n+1}\right]$$

$$+ \tau_{\mathbf{u},\mathrm{d}} \rho \frac{\tilde{\mathbf{u}}^n}{\delta t}, \tag{4.33a}$$

$$\begin{aligned} \tilde{p}^{n+1} &= -\tau_{p,\mathrm{d}} \mathscr{P}_h^{\perp} \left[\epsilon^{-1} (\mathbf{u}_h^{n+1} \cdot \nabla) p_h^{n+1} \right] - \tau_{p,\mathrm{d}} \mathscr{P}_h^{\perp} \left[\nabla \cdot \mathbf{u}_h^{n+1} \right] \\ &+ \tau_{p,\mathrm{d}} \frac{\tilde{p}^n}{\epsilon \delta t}. \end{aligned} \tag{4.33b}$$

It is clear that omitting any of the projections in the previous system would have a remarkable effect on the stability of the final formulation, yet this does not affect the general accuracy of the scheme. In order to provide stability and convergence on both convective terms, the contributions

$$\mathscr{P}_h^{\perp} \left[\rho \mathbf{u}_h \cdot \nabla \mathbf{u}_h \right] \quad \text{and} \quad \mathscr{P}_h^{\perp} \left[\epsilon^{-1} \mathbf{u}_h \cdot \nabla p_h \right]$$

are essential. In addition, control is also needed over the pressure gradient

$$\mathscr{P}_h^{\perp} \left[\nabla p_h \right].$$

We shall consider now that both velocity and pressure subscales can be split in the form $\tilde{\mathbf{u}} = \tilde{\mathbf{u}}_1 + \tilde{\mathbf{u}}_2$ and $\tilde{p} = \tilde{p}_1 + \tilde{p}_2$, each component corresponding to the first and second terms in the right hand side of Equation 4.33a and Equation 4.33b, so that the stabilization terms are independent (see [142]). This amounts to saying that the subscales are computed in practice by solving:

[142]: Castillo et al. (2019), "Dynamic term-by-term stabilized finite element formulation using orthogonal subgrid-scales for the incompressible Navier-Stokes problem"

$$\tilde{\mathbf{u}}_1^{n+1} = - \tau_{\mathbf{u},\mathrm{d}} \mathscr{P}_h^{\perp} \left[\rho (\mathbf{u}_h^{n+1} \cdot \nabla) \mathbf{u}_h^{n+1} \right] + \tau_{\mathbf{u},\mathrm{d}} \rho \frac{\tilde{\mathbf{u}}_1^n}{\delta t}, \tag{4.34a}$$

$$\tilde{\mathbf{u}}_2^{n+1} = - \tau_{\mathbf{u},\mathrm{d}} \mathscr{P}_h^{\perp} \left[\nabla p_h^{n+1} \right] + \tau_{\mathbf{u},\mathrm{d}} \rho \frac{\tilde{\mathbf{u}}_2^n}{\delta t}, \tag{4.34b}$$

$$\tilde{p}_1^{n+1} = - \tau_{p,\mathrm{d}} \mathscr{P}_h^{\perp} \left[\epsilon^{-1} (\mathbf{u}_h^{n+1} \cdot \nabla) p_h^{n+1} \right] + \tau_{p,\mathrm{d}} \frac{\tilde{p}_1^n}{\epsilon \delta t}, \tag{4.34c}$$

$$\tilde{p}_2^{n+1} = - \tau_{p,\mathrm{d}} \mathscr{P}_h^{\perp} \left[\nabla \cdot \mathbf{u}_h^{n+1} \right] + \tau_{p,\mathrm{d}} \frac{\tilde{p}_2^n}{\epsilon \delta t}. \tag{4.34d}$$

and taking into account that the extra cross products among operators are neglected, the final formulation reads: for $n = 0, 1, \ldots, N-1$, solve for $\mathbf{u}_h^{n+1}$, p_h^{n+1}, given the values $\mathbf{u}_h^{n-l}$, p_h^{n-l} for $l = 0$ to $\theta - 1$, such that

$$\begin{aligned} \left\langle \mathbf{v}_h, \rho \delta_t \mathbf{u}_h^{n+1} \right\rangle &+ c(\rho, \mathbf{u}_h^{n+1}; \mathbf{u}_h^{n+1}, \mathbf{v}_h) + a(\mathbf{u}_h^{n+1}, \mathbf{v}_h) \\ &- b(p_h^{n+1}, \mathbf{v}_h) + c_\Gamma(\rho; \mathbf{u}_h^{n+1}, \mathbf{v}_h) \\ &+ b_\Gamma(p_h^{n+1}, \mathbf{v}_h) + \mathscr{B}^{\perp}_{\mathbf{u},\mathrm{stab}}(\rho, \mathbf{u}_h^{n+1}; \mathbf{u}_h^{n+1}, \mathbf{v}_h) \\ &= \ell_{\mathbf{u}}(\rho; \mathbf{v}_h) + \ell_{\Gamma,\mathbf{u}}(\mathbf{v}_h) + \ell_{\mathbf{u},\mathrm{stab}}(\rho; \mathbf{v}_h) \end{aligned} \tag{4.35a}$$

$$
\begin{aligned}
\left\langle q_h, \frac{1}{\epsilon}\partial_t p_h^{n+1}\right\rangle &+ d(\rho, \mathbf{u}_h^{n+1}; p_h^{n+1}, q_h) + b(q_h, \mathbf{u}_h^{n+1}) \\
&+ b_\Gamma(q_h, \mathbf{u}_h^{n+1}) + \mathscr{B}^\perp_{p,\mathrm{stab}}(\rho, \mathbf{u}_h^{n+1}; p_h^{n+1}, q_h) \\
&= \ell_{\Gamma,p}(q_h) + \ell_{p,\mathrm{stab}}(\rho; q_h) \qquad (4.35\mathrm{b})
\end{aligned}
$$

where the following forms were introduced

$$
\begin{aligned}
&\mathscr{B}^\perp_{\mathbf{u},\mathrm{stab}}(\rho, \mathbf{u}_h; \mathbf{u}_h, \mathbf{v}_h) := \sum_{e=1}^{N_{\mathrm{el}}} \left\langle \nabla\cdot\mathbf{v}_h, \tau_{p,\mathrm{d}} \mathscr{P}_h^\perp\left[\nabla\cdot\mathbf{u}_h\right]\right\rangle_{\Omega^{(e)}} \\
&+ \sum_{e=1}^{N_{\mathrm{el}}} \left\langle \rho(\mathbf{u}_h\cdot\nabla)\mathbf{v}_h, \tau_{\mathbf{u},\mathrm{d}} \mathscr{P}_h^\perp\left[\rho(\mathbf{u}_h\cdot\nabla)\mathbf{u}_h\right]\right\rangle_{\Omega^{(e)}}, \qquad (4.36\mathrm{a}) \\
&\ell_{\mathbf{u},\mathrm{stab}}(\rho; \mathbf{v}_h) := \sum_{e=1}^{N_{\mathrm{el}}} \left\langle \rho(\mathbf{u}_h\cdot\nabla)\mathbf{v}_h, \tau_{\mathbf{u},\mathrm{d}}\rho\frac{\tilde{\mathbf{u}}^n}{\delta t}\right\rangle_{\Omega^{(e)}} \\
&+ \sum_{e=1}^{N_{\mathrm{el}}} \left\langle \nabla\cdot\mathbf{v}_h, \tau_{p,\mathrm{d}}\frac{\tilde{p}^n}{\epsilon\delta t}\right\rangle_{\Omega^{(e)}} \qquad (4.36\mathrm{b}) \\
&\mathscr{B}^\perp_{p,\mathrm{stab}}(\rho, \mathbf{u}_h; p_h, q_h) := \sum_{e=1}^{N_{\mathrm{el}}} \left\langle \nabla q_h, \tau_{\mathbf{u},\mathrm{d}} \mathscr{P}_h^\perp\left[\nabla p_h\right]\right\rangle_{\Omega^{(e)}} \\
&+ \sum_{e=1}^{N_{\mathrm{el}}} \left\langle \epsilon^{-1}(\mathbf{u}_h\cdot\nabla)q_h, \tau_{p,\mathrm{d}} \mathscr{P}_h^\perp\left[\epsilon^{-1}(\mathbf{u}_h\cdot\nabla)p_h\right]\right\rangle_{\Omega^{(e)}} \qquad (4.36\mathrm{c}) \\
&\ell_{p,\mathrm{stab}}(\rho; q_h) := \sum_{e=1}^{N_{\mathrm{el}}} \left\langle \epsilon^{-1}(\mathbf{u}_h\cdot\nabla)q_h, \tau_{p,\mathrm{d}}\frac{\tilde{p}^n}{\epsilon\delta t}\right\rangle_{\Omega^{(e)}} \\
&+ \sum_{e=1}^{N_{\mathrm{el}}} \left\langle \nabla q_h, \tau_{\mathbf{u},\mathrm{d}}\rho\frac{\tilde{\mathbf{u}}^n}{\delta t}\right\rangle_{\Omega^{(e)}}. \qquad (4.36\mathrm{d})
\end{aligned}
$$

The terms inside the previous forms modify, respectively, the weak forms of the momentum and continuity equations providing a stabilized formulation which adds the numerical diffusion in an efficient manner by means of completely symmetric terms.

4.7.4 Algebraic formulation and stabilized fractional step algorithm

The final variational formulation of the isentropic compressible problem was stated in Equation 4.35a–Equation 4.35b. From there, the derivation of the matrix version is straightforward and the matrix system that needs to be solved at each

Matrix version	Term where it comes from
$\mathbf{V}^T\mathbf{S}_{\mathbf{u}}(\mathbf{U})\mathbf{U}$	$\mathscr{B}^{\perp}_{\mathbf{u},\mathrm{stab}}(\rho, \mathbf{u}_h; \mathbf{u}_h, \mathbf{v}_h)$
$\mathbf{V}^T\mathbf{F}_{\mathbf{u},\mathrm{stab}}$	$\ell_{\mathbf{u},\mathrm{stab}}(\rho; \mathbf{v}_h)$
$\mathbf{Q}^T\mathbf{S}_p\left(\mathbf{U}\right)\mathbf{P}$	$\mathscr{B}^{\perp}_{p,\mathrm{stab}}(\rho, \mathbf{u}_h; p_h, q_h)$
$\mathbf{Q}^T\mathbf{F}_{p,\mathrm{stab}}$	$\ell_{p,\mathrm{stab}}(\rho; q_h)$

Table 4.3: Matrix form of the stabilization terms.

time step has the same algebraic structure as Equation 4.21a–Equation 4.21b with the addition of the corresponding stabilization arrays, as we show in Table 4.3.

With these observations in mind, the general procedure described in Section 4.6 is facilely extended to the stabilized algorithm. Down below we include the final scheme in its matrix form.

First and second order stabilized fractional step scheme for the isentropic problem

- Set/read the initial conditions for $\mathbf{U}^0$ and $\mathbf{P}^0$.
- WHILE $n < N$ DO
  - Set $\mathbf{U}^{n,0} = \mathbf{U}^{n-1}$ and $\mathbf{P}^{n,0} = \mathbf{P}^{n-1}$
  - WHILE (not converged) DO
    - Compute intermediate velocity $\widetilde{\mathbf{U}}^{n+1}$

$$\begin{aligned}\mathbf{M}_{\mathbf{u},\rho^n}\frac{D_\theta}{\delta t}\widetilde{\mathbf{U}}^{n+1,(i+1)} &+ \mathbf{K}_{\mathbf{u},\rho^n}\left(\widetilde{\mathbf{U}}^{n+1,(i)}\right)\widetilde{\mathbf{U}}^{n+1,(i+1)}\\ &+ \mathbf{M}_\Gamma\widetilde{\mathbf{U}}^{n+1,(i+1)} + \mathbf{K}_{\Gamma,\rho^n}\widetilde{\mathbf{U}}^{n+1,(i+1)}\\ &+ \mathbf{S}_{\mathbf{u},\rho^n}\left(\mathbf{U}^{n+1,(i)}\right)\mathbf{U}^{n+1,(i+1)} - \mathbf{G}\hat{\mathbf{P}}^{n+1}_{\theta'}\\ &+ \mathbf{G}_\Gamma\hat{\mathbf{P}}^{n+1}_{\theta} = \mathbf{F}^{n+1}_{\rho^n} + \mathbf{F}^{n+1}_{\Gamma,\mathbf{u}} + \mathbf{F}^{n+1}_{\mathbf{u},\rho^n,\mathrm{stab}}\end{aligned}$$

    - Check convergence
  - END while (not converged)
  - Compute the pressure $\mathbf{P}^{n+1}$ using the intermediate velocity from the previous step

$$\begin{aligned}\mathbf{M}_{p,\rho^n}\frac{D_\theta}{\delta t}\mathbf{P}^{n+1} &+ \mathbf{K}_{p,\rho^n}\left(\widetilde{\mathbf{U}}^{n+1}\right)\mathbf{P}^{n+1}\\ &+ \phi_\theta\delta t\mathbf{L}_{\rho^n}\left(\mathbf{P}^{n+1} - \hat{\mathbf{P}}^{n+1}_{\theta'}\right) + \mathbf{D}\widetilde{\mathbf{U}}^{n+1}\\ &+ \mathbf{D}_\Gamma\widehat{\mathbf{U}}^{n+1}_\theta + \mathbf{S}_{p,\rho^n}\left(\widetilde{\mathbf{U}}^{n+1}\right)\mathbf{P}^{n+1} = \mathbf{F}^{n+1}_{\Gamma,p}\\ &+ \mathbf{F}^{n+1}_{p,\rho^n,\mathrm{stab}}\end{aligned}$$

- Velocity correction to obtain the end-of-step velocity $\mathbf{U}^{n+1}$

$$\mathbf{M}_{\mathbf{u},\rho^{n+1}} \frac{1}{\phi_\theta \delta t} \left(\mathbf{U}^{n+1} - \widetilde{\mathbf{U}}^{n+1} \right) + \mathbf{N}_{\psi}^{n+1} - \mathbf{G} \left(\mathbf{P}^{n+1} - \hat{\mathbf{P}}_{\theta'}^{n+1} \right) = 0$$

▸ END while $n < N$ (non-stationary)

Note that the additional stabilization term in the system for the pressure, $\mathbf{S}_p(\widetilde{\mathbf{U}}^{n+1})\mathbf{P}^{n+1}$, does not need to be linearized since $\widetilde{\mathbf{U}}^{n+1}$ is already known by the time that $\mathbf{P}^{n+1}$ needs to be computed.

4.8 Numerical results

In this section, some numerical examples are presented to show the performance of the proposed formulation. The first case we consider is a test with a manufactured solution in order to analyze the time discretization errors of the fractional step technique. After that, a 2D low-speed viscous flow over a cylinder at Ma = 0.0583 is calculated. Later, the noise radiated by the flow over a cavity at Ma=0.7 is discussed.

For all the numerical examples, we consider

$$\gamma = 1.4, \quad \text{and} \quad a_0 = \sqrt{\frac{\gamma p_0}{\rho_0}} = 343 \text{ m/s}.$$

In addition to this, the boundary formulation with the weak imposition of Dirichlet boundary conditions plus the NRBC is used, as explained in Section 4.4. Hence, a penalty parameter needs to be set to perform the simulation, ψ. In the case, this parameter behaves as

$$\psi = \psi_0 \left(\frac{\mu}{h} + \rho \|\mathbf{u}_h\| \right),$$

for some constant ψ_0 and mesh size h, which will be fixed for each example.

As previously discussed, the nonlinearities in the problem are solved via Picard's scheme. This leads to a monotonically decreasing relative error among consecutive iterations, ensuring the convergence of the method. A maximum of 10 iterations is set, and the numerical tolerance for the L^2 norm is 1×10^{-6}.

In order to solve the underlying systems of linear equations, we use the Biconjugate Gradients solver, `BiCGstab` [143], which is already implemented in the `PETSc` parallel solver library [61]. All variables in the upcoming plots are in SI units.

[143]: Vorst (1992), "Bi-CGSTAB: A fast and smoothly converging variant of Bi-CG for the solution of nonsymmetric linear systems"

4.8.1 A test with analytical solution

Let us first perform a simple test whose main objective is to numerically check the time convergence of the fractional step schemes defined above. For this purpose we use the so-called method of manufactured solutions. In this procedure, an exact analytical solution is defined a priori and later substituted into the continuum equations in order to obtain the associated forcing terms. Continuedly, these forcing terms are introduced as perturbations in the finite element computation. The time-dependent manufactured solutions are composed of smooth functions with no physical meaning. Dirichlet boundary conditions are prescribed weakly over the boundaries upon evaluation of the velocity analytical solution and the initial conditions arise from the prescribed functions evaluated at $t = 0$ over the whole computational domain.

The region we consider is the unit square, *i. e.*

$$\overline{\Omega} = [0, 1] \times [0, 1],$$

and we assume the following manufactured fields:

$$\begin{aligned} \mathbf{u}(x_1, x_2, t) &= g(t) \left[-\cos(x_1)\sin(x_2), \sin(x_1)\cos(x_2) \right]^T \\ p(x_1, x_2, t) &= -\frac{1}{4} g^2(t) \left(\cos(2x_1) + \cos(2x_2) \right) \end{aligned}$$

with $g(t) = \sin(2t)$.

A structured mesh of size $h = 0.05$ with bilinear elements has been employed to discretize the computational domain. Finally a constant $\psi_0 = 1000$ has been chosen to ensure a proper prescription of boundary conditions, thus avoiding excessive boundary errors.

The normalized error has been computed in different norms: $\ell^\infty(L^2(\Omega))$ (maximum of the time sequence of spatial L^2-norms

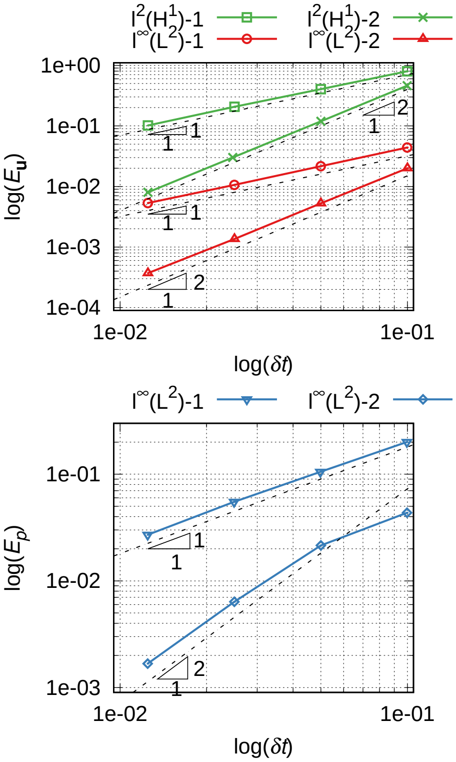

Figure 4.1: Convergence test results for the proposed fractional step algorithm for the isentropic Navier-Stokes problem: (top) velocity error, (bottom) pressure error. The number after the dash in the plot stands for first or second order results.

of the solution) and $\ell^2(H^1(\Omega))$ (ℓ^2-norm of the time sequence of spatial H^1-norms of the solution) for velocity, and $\ell^\infty(L^2(\Omega))$ for pressure.

Figure 4.1 shows the convergence plot for the fractional step algorithm using the BDF1 and BDF2 schemes in time for velocity and pressure fields, respectively. The reader can note that the schemes proposed in previous sections show the desired rate of convergence, and hence the extrapolations of the boundary terms explained in Section 4.6 do maintain the general temporal accuracy of the method. From the convergence plots it is also observed that the spatial error is not significant for the mesh size used.

4.8.2 Aeolian tones of low Mach viscous flow

The second numerical example we have considered to assess the proposed formulation is a benchmark consisting in the aerodynamic sound radiated by an uniform flow past a cylinder, what is commonly referred to as aeolian tones problem in the literaure (see *e.g.* [144, 145] for further details). In

[144]: Guasch et al. (2009), "Computational aeroacoustics of viscous low speed flows using subgrid scale finite element methods"
[145]: Guasch et al. (2007), "An algebraic subgrid scale finite element method for the convected Helmholtz equation in two dimensions with applications in aeroacoustics."

this example, the cylinder undergoes lift fluctuations in response to the vortex shedding generated at the lee of the cylinder, and such fluctuations generate the sound pressure pulses. The emitted sound is named aeolian tone and a typical example of this phenomenon is the wire whistle that can be heard when wind impacts power transmission lines.

The problem domain is

$$\overline{\Omega} = [0, L] \times [0, L] \setminus \mathfrak{C},$$

with $L = 200$ m, being $\mathfrak{C}$ the cylinder region of diameter $D = 0.3$ m and located at the center point of the square. The domain is big enough to describe the far field conditions far away from the cylinder.

The prescription of boundary conditions is as follows: the flow is injected from the left boundary with constant horizontal velocity $u_\infty = 20$ m/s. Over both upper and lower walls the vertical component of the velocity is imposed to zero. These prescriptions are done weakly, using $\psi_0 = 10$. We have taken a dynamic viscosity coefficient of $\mu = 0.006$ kg/(m s) and density of $\rho = 1$ kg/m^3 to initiate the computation. All this information leads to the following Reynolds and Mach numbers

$$\mathrm{Re} = 1,000, \quad \text{and} \quad \mathrm{Ma} = 0.0583,$$

used by the benchmark solution.

The unstructured mesh for the simulation is composed of $N_{\mathrm{el}} \sim 500,000$ $P1$ elements using equal interpolation for velocity and pressure thanks to the stabilized formulation above discussed. The mesh near the cylinder wall is progressively refined, so as to capture the expected high gradients in that region. The time step size selected for the computation is $\delta t = 1 \times 10^{-3}$ s. It is important to note that the time step has to be small enough in order to be able to reproduce the aeroacoustic signal in an adequate manner. The second order BDF2 scheme has been used for the large scales time evolution, while a first order scheme has been used for the tracking of subscales. In order to complete the simulation, we set a filtering frequency of 50 Hz to avoid reflections at the external boundaries. We recall here the necessity of letting the code run for several time steps prior to the application of the boundary formulation, in order to accumulate representative data for the computations. The initial condition for the simulation is provided by several time steps of an incompressible segregated solver.

In Figure 4.2a and Figure 4.2b we present the flow pressure contours for a certain time step of the vortex shedding cycle, qualitatively comparing the proposed fractional step scheme with its monolithic version (for the same mesh and time step size), being the latter already validated in [130]. It can be observed that the pressure pulses evolve radially from the cylinder area with time, yet they do not propagate normally to the flow direction since this case is based on an uniform flow.

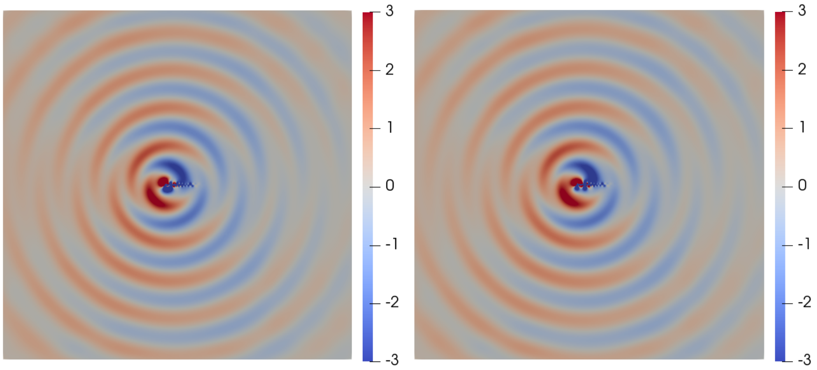

(a) Pressure contours of the segregated scheme

(b) Pressure contours of the monolithic solution

Figure 4.2: Aeolian tones isentropic problem: (a) flow pressure contour for the fractional step scheme, (b) pressure contour for the monolithic counterpart.

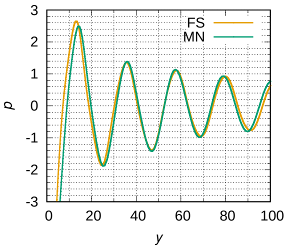

Figure 4.3: Aeolian tones isentropic problem: comparison of the wave propagation along the y direction. Here and it what follows, `MN` stands for monolithic results and `FS` for fractional step results.

Figure 4.3 displays the pressure pulse along the positive y axis for both formulations for the same time instant. The reader can notice that the acoustic wave propagation obtained with the segregation algorithm manages to reasonably reproduce the amplitude and frequency of the wave obtained with the monolithic reference scheme. Although some minor discrepancies might be noticed, the overall results are equivalent in a reasonable manner. The differences should come from the errors introduced by the fractional step approach and the approximate boundary condition.

As pointed out previously, the behavior of pressure waves once they reach the external artificial boundaries is a controversial situation in compressible solvers. The raw isentropic formulation would lead to the reflection of waves into the computational domain, but the compatible prescription for flow and acoustic variables adopted in this work allows the pressure pulses to abandon the domain in a smooth fashion.

This fact demonstrates the satisfactory performance of the weak imposition of Dirichlet boundary conditions combined with a segregation technique and, similarly, it exposes the ability of the non-reflecting boundary conditions to attenuate the propagated sound waves.

In order to further asses the suitability of the fractional step approach so as to replace its monolithic counterpart (taken as reference), we perform a comparison on both lift C_l and drag C_d non-dimensional coefficients of the cylinder. These are defined as:

$$C_d := \frac{\mathrm{f}_x}{\frac{1}{2}\rho_\infty u_\infty^2 D}, \tag{4.38a}$$

$$C_l := \frac{\mathrm{f}_y}{\frac{1}{2}\rho_\infty u_\infty^2 D}, \tag{4.38b}$$

and computed from the exerted force of the fluid over the cylinder

$$\mathbf{f} = -\int_{\partial\Omega_{\text{Cylinder}}} \boldsymbol{\sigma} \cdot \mathbf{n} \, \mathrm{d}\partial\Omega. \tag{4.39}$$

In addition, the Strouhal number is

$$\mathrm{St} = \frac{\omega D}{u_\infty},$$

being here ω the vortex shedding frequency.

A part of the time histories of these coefficients are included in Figure 4.4. Both exhibit the expected sinusoidal behavior, with minimal deviation between the two formulations, as a result of the segregation error.

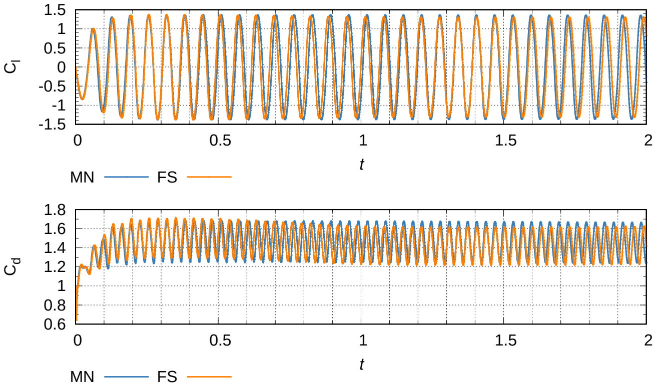

Figure 4.4: Aeolian tones isentropic problem: (top) time evolution of non-dimensional lift coefficient, (bottom) time evolution of non-dimensional drag coefficient.

We also take these historical values to the frequency domain via a Fourier transform algorithm, and the results are shown in Figure 4.5a and Figure 4.5b. For the case of the lift coefficient and the monolithic scheme, it has an amplitude of 1.363 and oscillates at the vortex shedding frequency of 15.625 Hz (St= 0.234). These values have a remarkable agreement with the ones reported in [145], where the problem is solved using a convected Helmholtz equation (see Section 4.2 in that publication). When the solution is obtained with the segregated approach, C_l has an amplitude of 1.335 and shows a frequency of 15.435 Hz (St= 0.231). In addition to this, the drag coefficient displays an amplitude of 0.181 for the monolithic solution and 0.169 for the fractional counterpart. In terms of frequency, C_d oscillates at 31.251 Hz for the monolithic (which is precisely twice the vortex shedding frequency) and at 31.105 Hz for the segregated algorithm, what translates into a relative error of ∼ 0.5 % with respect to the reference solution. These values are collected in Table 4.4 down below.

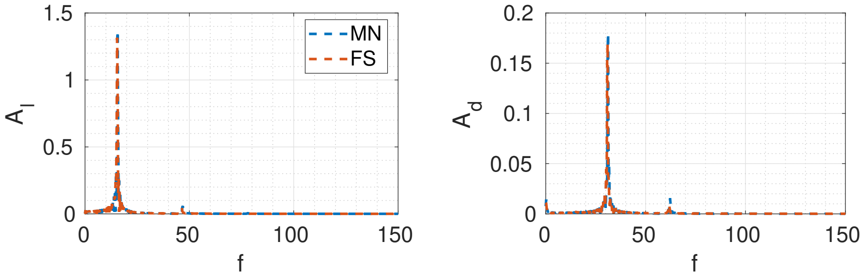

(a) C_l spectrum

(b) C_d spectrum

Figure 4.5: Aeolian tones isentropic problem: non-dimensional lift and drag spectrums. In this figure, A_l and A_d stand for the lift and drag amplitudes, and f is the frequency.

Table 4.4: Comparison of frequency and amplitude values for the non-dimensional lift and drag coefficients when the solution of the problem is computed with the monolithic or fractional step algorithms.

	Monolithic		Fractional step	
	Amplitude [-]	Frequency [Hz]	Amplitude [-]	Frequency [Hz]
C_l	1.363	15.625	1.335	15.435
C_d	0.181	31.265	0.169	31.105

The computational savings that segregation techniques offer when compared to monolithic schemes are undoubted. The linear systems to be solved in fractional step methods are smaller and better conditioned, and usually each unknown requires a distinct number of iterations to solve its corresponding linear system. Although in this example we have used the same solver for all subsystems arising in the segregation method, specific solving techniques could be exploited in order to improve the performance of fractional step schemes even further. For the problem in hand, it was obtained that the CPU time of the fractional step algorithm over the CPU time of the monolithic case was 0.39. In other words, the computational savings go up to 60 %.

In view of the information provided by previous quantitative comparisons, we can conclude that the fractional step approach is an effective alternative to the classical monolithic technique.

4.8.3 Noise radiated by the flow past an open cavity

As a final numerical example, the simulation of the noise radiated by a 2D flow past an open cavity is performed in order to further investigate the aeroacoustic feedback of the formulation.

The problem setting consists in an infinitely long rectangular cavity of aspect ratio 2, with depth $D = 0.00254$ m and length $L = 2D$. The accurate simulation of the acoustic radiation from the cavity relies on an adequate definition of the boundaries. Hence, the computational domain extends over $H = 25D$ vertically and $W = 50D$ horizontally, meaning that both upstream and downstream walls are sufficiently far away from the cavity itself in order to avoid any possible self-forcing and to allow a proper impinging of the propagated sound waves, see Figure 4.6.

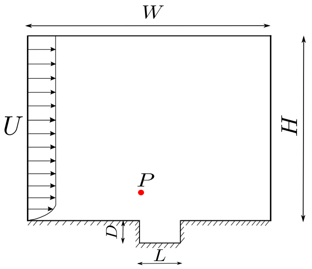

Figure 4.6: Flow past a cavity. Description of the domain.

This is a challenging problem, where acoustics and flow dynamics are highly coupled. Essentially, periodic vortices start to develop just downstream the leading edge of the cavity, and when they impinge the trailing edge, pressure pulses are generated which start propagating upstream.

Non slip boundary conditions are prescribed on the cavity walls and the flow is injected at the left-most side with uniform velocity $u_\infty = 245$ m/s. The right-most side is left free and over the higher wall the vertical component of the velocity is prescribed to zero. Additional parameters for the simulation are chosen as follows: $\rho = 1.16$ kg/m^3, $\mu = 1.76 \times 10^{-5}$ kg/(m s), $\psi_0 = 25$, $\delta t = 5 \times 10^{-6}$, and the filtering frequency is $5,000$ Hz. Hence, we obtain, based on the cavity depth

$$\mathrm{Re} = 41,000, \quad \text{and} \quad \mathrm{Ma} = 0.7,$$

conditions that have been studied by several authors in the literature [146–148]. An unstructured mesh with nearly $N_{\mathrm{el}} \sim 275,000$ triangular elements is used for the computations. The point P is used to monitor the pressure, whose coordinates are $x_1 = -0.04D$ and $x_2 = 2D$. It is located at the beginning at the acoustic region outside the cavity.

[146]: Rowley et al. (2002), "On self-sustained oscillations in two-dimensional compressible flow over rectangular cavities"
[147]: Bres et al. (2008), "Three–dimensional instabilities in compressible flow over open cavities"
[148]: Gloerfelt et al. (2003), "Direct computation of the noise radiated by a subsonic cavity flow and application of integral methods"

The sound pressure level (SPL) or acoustic pressure level is a (logarithmic) measure of the sound pressure with respect to reference sound pressure. Mathematically, it is computed as

$$\mathrm{SPL} = 20\log_{10}\left(\frac{p}{p_{\mathrm{ref}}}\right) \quad [\mathrm{dB}]$$

where p_{ref} is the reference pressure. A value usually taken as reference is 20 μPa, the threshold of human hearing. Figure 4.7 shows the corresponding sound pressure level spectrum versus the Strouhal number for this case. The principal peak is located at St = 0.64 whereas in [148], where a DNS of the compressible flow equations is performed and taken as reference here, it is located at St = 0.66. A maximum of 158 dB was obtained, which agrees with the values shown in that publication. Furthermore, the slope of the cascade that appears at higher Strouhal numbers is comparable.

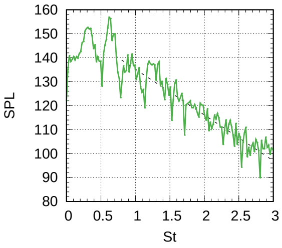

Figure 4.7: Flow past a cavity. Sound pressure level spectrum

Likewise, the propagation of acoustic waves can be visualized and compared in Figure 4.8a and Figure 4.8b. Pressure contours obtained in the present simulation, in contrast to the ones from [148] are depicted. Visual comparisons of the radiated pressure field coincide reasonably. The reader should also note that the computational domain used for the simulation does not affect the solution as it allows to damp completely the reflection of the sound waves at the artificial walls. The aforementioned agreement cannot be achieved without the use of non-reflecting conditions (or any similar damping technique).

Regarding the near field results, Figure 4.9 and Figure 4.10 show respectively the vorticity and pressure fields for a given time instant once the fluctuating mechanism is established. In Figure 4.9 one can observe different vortical structures. One of them inside the cavity, as the interaction between flow and acoustics causes a highly chaotic behavior in this region. Another vortex can be seen just above the trailing

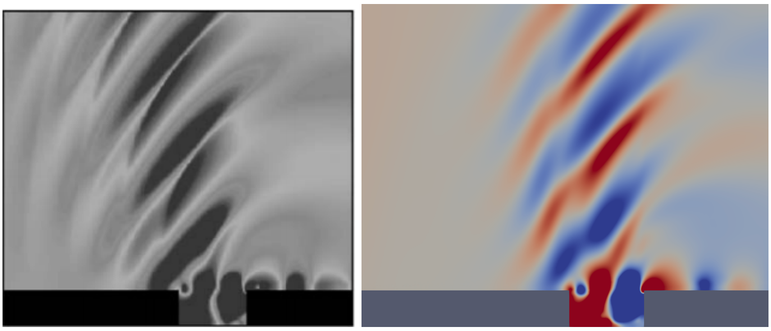

(a) Pressure solution from [148].

(b) Fractional step pressure solution

Figure 4.8: Flow past a cavity: (a) DNS reference pressure field (b) calculated pressure field using the second order fractional step scheme. (scale between ∓3000 Pa)

edge. As the vortex first hits this edge, it spills over the corner and, eventually, it is convected downstream, increasing the thickness of the reattached boundary layer. Figure 4.10 is the corresponding pressure field. A recirculation zone is located in the second half of the cavity, which is mainly associated with the low pressure region in the plot (in blue). In addition, a subsequent high-low pressure structure outside the cavity can be observed, which is propagating towards the far field. This sequence can be directly compared to the ones presented in [148] (see Section 2 in that publication), so we conclude that the present implementation manages to reproduce the same flow patterns (same scaling is used for the comparison).

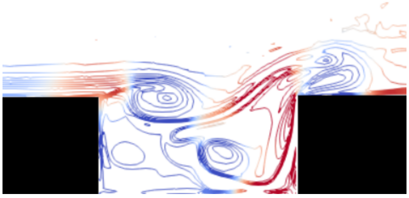

Figure 4.9: Flow past a cavity: vorticity contours for a given time instant within the main oscillation. Fifteen contours between $\omega_{x_3} D/U = -10.5$ and 1.35 were used.

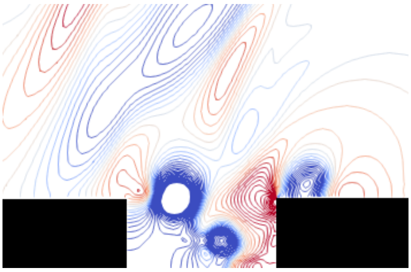

Figure 4.10: Flow past a cavity: pressure isocontours for a given time instant within the main oscillation. Twenty five contours between ∓10000 Pa were used.

4.9 Conclusions

In this chapter, a methodology up to second order in time to solve the isentropic compressible Navier-Stokes equations in a segregated manner has been presented. The formulation is constructed using the extrapolation concept at the pure algebraic level. From the numerical point of view, the fractional step approach has been combined with other ingredients, such as the split-orthogonal and dynamic definition of subscales, the weak imposition of Dirichlet boundary conditions via extrapolations of boundary terms and the application of non-reflecting boundary conditions, a major issue in compressible solvers.

The accuracy of the resulting schemes has been tested numerically using the method of manufactured solutions, obtaining optimal convergence rates for smooth enough solutions. Additionally, the implementation managed to reproduce the aeolian tones radiated by a flow past a cylinder and the problem of flow past a cavity at Ma=0.7. All these examples cover the subsonic range and highlight the satisfactory performance of the proposed prescription of boundary conditions, combining Nitche's method and a Sommerfeld-like non-reflecting condition in a segregated approach. The inclusion of the latter is crucial in this problem, in which reflections at the boundaries develop oscillations and instabilities that end up affecting the simulation results if a standard methodology is used. In addition to this, an important reduction in the CPU time with respect to the monolithic case has been verified.

The low implementation requirements when departing from a Navier-Stokes (incompressible) solver, added to the computational savings of the segregated approach, make this algorithm appealing for aeroacoustic problems within the subsonic regime, where shocks and heat transfer can be neglected.

The Navier-Stokes problem: primitive formulation 5

5.1 Abstract

In this part we address the compressible Navier-Stokes equations written in the socalled primitive formulation. The proposed methodology is a finite-element solver based on a fractional step scheme in time, which allows to uncouple the calculation of the problem unknowns providing important savings in computational cost. In addition, we include a stabilization technique within the Variational Multi-Scale framework and, in particular, we consider orthogonal and dynamic definitions for the subscales. In order to overcome any wave reflections which may arise in aeroacoustic simulations at the low compressibility regime, we present a method for enforcing boundary conditions based on a combination of a zero order non-reflecting condition plus the weak imposition of Dirichlet boundary conditions over the external contours. Several representative benchmark flow simulations are performed, which demonstrate the suitability of the proposed algorithm for the subsonic regime.

5.2 Introduction

The socalled compressible Navier-Stokes equations are commonly used to model flow problems where compressibility effects become relevant, *e.g.* in aerodynamic and aeroacoustic research areas, with applications ranging from classical turbo-machinery design [149] to modern speech therapy simulations [150]. The general mathematical setting consists of the momentum, mass and energy conservation equations. This set of partial differential equations describes a wide range of scales, and hence reliable computational methods are required. In general, in order to compute an accurate solution of this problem one could proceed either by choosing small mesh and time step sizes or by using high precision schemes. Regardless of the selected approach, obtaining a representative solution of the problem is particularly demanding from the computational point of view and this still remains as one of the main limitations in compressible flow simulations in

[149]: Bazilevs et al. (2021), “Gas turbine computational flow and structure analysis with isogeometric discretization and a complex-geometry mesh generation method”

[150]: Lu et al. (2021), “Numerical investigation of effects of incisor angle on production of sibilant /s/”

spite of the increasing amount of computing facilities available for the scientific and engineering communities.

The development of numerical approximations for the compressible Navier-Stokes equations which perform adequately at low compressibility regimes is one of the major concerns related to compressible flow simulations. However, the classical compressible flow solvers found in the literature display a deterioration in the solution when the free stream Mach number is reduced. According to [151], the rationale behind this misbehavior is a possible mismatch between numerical and continuous fluxes, a fact principally attributed to the broad difference in length and time scales of the solution. In this regard, a widespread alternative for performing wave-propagation simulations is to solve the classical incompressible Navier-Stokes equations supplemented with an aeroacoustic model, commonly referred in the literature to as hybrid methods (see *e.g.* [126–128]). Nonetheless, this common approach generally involves a sequential calculation of aerodynamics and aeroacoustics, what directly leads to discard any feedback related to the sound waves into the flow. Apart from this, and although they are not suitable for wave-like problems, there exist the socalled unified methods, a completely different family of techniques which are intended to be suitable for either compressible and incompressible flows [152].

[151]: Wong et al. (2001), "The solution of the compressible Euler equations at low Mach numbers using a stabilized finite element algorithm"

[152]: Pesch et al. (2008), "A discontinuous Galerking finite element discretization of the Euler equations for compressible and incompressible fluids"

Probably the main reason for developing a compressible formulation which could be properly applied to low Mach flows is the fact that very low Mach number zones can coexist with regions where the flow compressibility becomes significant. In addition to this, several applications traditionally solved with incompressible formulations could be successfully handled by appropriate compressible solution techniques. The general trend in the literature is to make use of the conservative variables (namely density, momentum, and total energy) for the compressible formulation, whereas primitive variables (pressure, velocity, and temperature) are preferred for the incompressible equations. However, including density as a variable in the compressible problem (like in the conservative formulation), might yield singularities for problems within the low Mach number limit. Hence, primitive and even entropic unknowns remain as the two main possibilities in order to solve compressible problems posed in low compressibility conditions. Particularly, the entropy variable formulation ensures a global entropy stability condition, but it is subject to the definition of the entropy function [153]. For a general review on the different set of variables for solving compressible and incompressible flow problems we refer to [95].

[153]: Hughes et al. (1986), "A new finite element formulation for computations fluid dynamics. I. Symmetric forms of the compressible Euler and Navier-Stokes equations and the second law of thermodynamics"

[95]: Hauke et al. (1998), "A comparative study of different sets of variables for solving compressible and incompressible flows"

As we discussed in the previous chapter, another particular feature of nearly incompressible aeroacoustic flows is that external computational boundaries may produce artificial wave reflections related to the ingoing part of the sound waves and which can completely pollute the solution of the problem. Ingoing waves may not only interfere with the acoustic signal, but they can also produce numerical instabilities if the numerical method is not able to provide enough dissipation. Among the most remarkable numerical techniques which deal with the backscattering of waves in the acoustic field we would like to highlight the damping of the compressible equations and the application of non-reflecting boundary conditions. Even though performing a damping of some terms of the compressible equations is a robust approach to face spurious reflections at the boundary (usually referred to as buffer or sponge zones), this technique brings an extra computational effort related to the new terms that need to be included over an augmented computational domain. Therefore, other approaches are often adopted, being one of the main alternatives the inclusion of non-reflecting boundary conditions, an approach that we favor in this work. The backscattering issue represents a traditional research topic in aeroacoustics and thus the literature on compressible boundary conditions is really extensive. Nevertheless, we refer to the early work in [133] and to the more recent reviews in [134, 135] and [154] for a deeper understanding on this topic.

[154]: Colonious (2004), "Modeling artificial boundary conditions for compressible flow"

The principal objective of the present chapter is to discuss the development of pressure segregation methods for the transient compressible Navier-Stokes equations written in primitive variables and using a finite element approximation for the space discretization. As a reference in the comparisons, we will take the solution of the socalled monolithic problem, that is to say, the standard coupled calculation involving all the problem unknowns. Clearly, the fully discrete and linearized monolithic scheme leads to an algebraic system the structure of which can be exploited so as to solve independently for the velocity, the pressure and the temperature degrees of freedom.

Referring to the time integration, on the following we will concentrate on first and second order implicit finite difference schemes. The backward Euler method will be used for the former, whereas for second order methods we will stick to backward differentiation (or Gear) schemes, yet our developments are not restricted and, in principle, any other discretization methods might be used to advance the solution in time.

The technique we will discuss here corresponds to the classical fractional step algorithms. Our approach in this work is to present the splitting of the equations at the pure algebraic level once the equations have already been discretized in space and in time (see *e.g.* [53, 55, 155] for algebraic approaches on the incompressible, viscoelastic and isentropic flow equations). This way to face the problem emerged after the identification in [47] of the classical pressure segregation method as an inexact factorization of the final algebraic system. In this chapter we favor such algebraic viewpoint since it is generally simpler and, although a particular treatment of boundary conditions will be discussed to avoid the reflection of sound waves, it makes possible to obviate a discussion on specific boundary conditions for the different steps of the fractional step scheme [46, 50].

The outline of the present chapter is as follows: in Section 5.3 we introduce the compressible Navier-Stokes problem written in primitive variables, as well as its variational formulation. In Section 5.4 we discuss the imposition of boundary conditions in order to avoid the spurious wave reflections at the external boundaries of the computational domain, whereas in Section 5.5 we present the standard finite element approximation and the monolithic time discretization. Section 5.6 is devoted to the design of pressure-correction algorithms, taking into account the modifications due to the application of boundary conditions. In Section 5.7, we introduce the VMS stabilized finite element formulation. Numerical experiments are conducted in Section 5.8, and, finally, we close the chapter with some concluding statements in Section 5.9.

5.3 Problem statement

5.3.1 Preliminaries

In this chapter we aim at solving the compressible Navier-Stokes problem for the socalled primitive variables, namely, velocity $\mathbf{u}(\mathbf{x}, t)$, pressure $p(\mathbf{x}, t)$ and temperature $\vartheta(\mathbf{x}, t)$[1]. For this purpose, we shall introduce some considerations in order to rewrite the system formed by Equation 2.20a, Equation 2.20b and Equation 2.20c in a more convenient form.

Henceforth, we will make use of the most frequently encountered form of the thermal equation of state, *i. e.* the ideal-gas law Equation 2.15. Taking into account that density is then a function of pressure and temperature, Equation 2.20a shall be rewritten by expanding the derivatives as follows

$$\beta \left[\partial_t p + (\mathbf{u} \cdot \nabla) p\right] - \alpha \left[\partial_t \vartheta + (\mathbf{u} \cdot \nabla)\vartheta\right] + \nabla \cdot \mathbf{u} = 0.$$

In this equation, two new physical variables are introduced, which relate temperature, pressure and density derivatives. These are the socalled *volume expansivity* and *isothermal compressibility* coefficients, denoted respectively as α and β hereafter. Their definitions are

$$\alpha := -\frac{1}{\rho}\left(\frac{\partial \rho}{\partial \theta}\right)_p, \tag{5.1a}$$

$$\beta := \frac{1}{\rho}\left(\frac{\partial \rho}{\partial p}\right)_\theta, \tag{5.1b}$$

where $(\cdot)_\theta$ and $(\cdot)_p$ stand for a constant temperature and pressure constrain. Since the ideal gas law is considered, it is readily checked that the previous expressions simply reduce to

$$\beta = p^{-1} \quad \text{and} \quad \alpha = \theta^{-1}.$$

If we consider a calorically perfect gas, then the internal energy is a sole function of the temperature as stated in Section 2.3.2. By using Equation 2.13 into Equation 2.20c, the energy conservation equation takes the form

$$\rho c_v \left[\partial_t \vartheta + (\mathbf{u} \cdot \nabla)\vartheta\right] - \nabla \cdot (\kappa \nabla \vartheta) + p(\nabla \cdot \mathbf{u}) - \Phi(\mathbf{u}) = \rho r,$$

where we recall that $\Phi(\mathbf{u})$ is the dissipation function from Section 2.3.4.

[1] There are some authors in the literature who also consider velocity $\mathbf{u}(\mathbf{x}, t)$, density $\rho(\mathbf{x}, t)$ and temperature $\vartheta(\mathbf{x}, t)$ as primitive variables. Hence, the triplet $[\mathbf{u}(\mathbf{x}, t), p(\mathbf{x}, t), \vartheta(\mathbf{x}, t)]$ is usually named *pressure primitive variables.* However, in the context of this thesis, we shall just use primitive variables to denote the set formed by velocity, pressure and temperature.

5.3.2 Initial and boundary value problem

Let Ω be an open, bounded and polyhedral domain of $\mathbb{R}^{N_{\mathrm{sd}}}$ and $[0, t_{\mathrm{f}}]$ the time interval of analysis. The unknowns of the problem are the *primitive* variables, *i. e.* the fluid velocity $\mathbf{u}(\mathbf{x}, t) : \Omega \times (0, t_{\mathrm{f}}) \to \mathbb{R}^{N_{\mathrm{sd}}}$, the thermodynamic pressure $p(\mathbf{x}, t) : \Omega \times (0, t_{\mathrm{f}}) \to \mathbb{R}$, and the temperature $\vartheta(\mathbf{x}, t) : \Omega \times (0, t_{\mathrm{f}}) \to \mathbb{R}$ which are the solution of the following system of partial differential equations:

Primitive Navier-Stokes problem

$$\begin{aligned} \rho \frac{\mathrm{d}\mathbf{u}}{\mathrm{d}t} - 2\nabla \cdot (\mu \boldsymbol{\varepsilon}) + \frac{2}{3}\nabla(\mu \nabla \cdot \mathbf{u}) & \\ + \nabla p = \rho \mathbf{b} & \qquad \text{in } \Omega \times (0, t_{\mathrm{f}}), \quad (5.2a) \\ \beta \frac{\mathrm{d}p}{\mathrm{d}t} - \alpha \frac{\mathrm{d}\vartheta}{\mathrm{d}t} + \nabla \cdot \mathbf{u} = 0 & \qquad \text{in } \Omega \times (0, t_{\mathrm{f}}), \quad (5.2b) \\ \rho c_v \frac{\mathrm{d}\vartheta}{\mathrm{d}t} - \nabla \cdot (\kappa \nabla \vartheta) + p(\nabla \cdot \mathbf{u}) = Q & \qquad \text{in } \Omega \times (0, t_{\mathrm{f}}), \quad (5.2c) \end{aligned}$$

where Q stands for the energy source terms, which accounts for mechanical dissipation into heat, chemical reactions or even electromagnetic effects. Therefore,

$$Q := \rho r + \Phi(\mathbf{u}) = \rho r + 2\mu \boldsymbol{\varepsilon}(\mathbf{u}) : \boldsymbol{\varepsilon}(\mathbf{u}) - \frac{2}{3}\mu(\nabla \cdot \mathbf{u})^2. \qquad (5.3)$$

Here and in what follows in this chapter, μ, κ and c_v are assumed to be constant to ease the discussion. The reader should note that the coupling among all the variables in the primitive problem defined by Equation 5.2a–Equation 5.2c is remarkably relevant, mostly through nonlinear relations.

The previous problem can be rewritten in the compact manner as in Equation 3.1 after setting

$$\begin{aligned} \mathbf{y} &= [\mathbf{u}, p, \vartheta]^T, \\ \mathscr{M}(\mathbf{y}) &= \begin{bmatrix} \rho & 0 & 0 \\ 0 & \beta & -\alpha \\ 0 & 0 & \rho c_v \end{bmatrix}, \\ \mathscr{F} &= [\rho \mathbf{b}, 0, Q]^T, \\ \mathscr{L}(\mathbf{y}; \mathbf{y}) &= \begin{bmatrix} \rho(\mathbf{u} \cdot \nabla)\mathbf{u} - 2\nabla \cdot [\mu \boldsymbol{\varepsilon}(\mathbf{u})] - \nabla [\lambda(\nabla \cdot \mathbf{u})] + \nabla p \\ \beta(\mathbf{u} \cdot \nabla)p - \alpha(\mathbf{u} \cdot \nabla)\vartheta + \nabla \cdot \mathbf{u} \\ \rho c_v(\mathbf{u} \cdot \nabla)\vartheta - \nabla \cdot (\kappa \nabla \vartheta) + p(\nabla \cdot \mathbf{u}) \end{bmatrix}. \end{aligned}$$

Boundary conditions need to be appended to the previous problem. Let us consider the following disjoint splittings

$$\Gamma = \partial\Omega = \overline{\Gamma_{\mathrm{D},\mathbf{u}} \cup \Gamma_{\mathrm{N},\mathbf{u}}} = \overline{\Gamma_{\mathrm{D},\vartheta} \cup \Gamma_{\mathrm{N},\vartheta}}.$$

Subscript D refers to Dirichlet boundary conditions, whereas N refers to Neumann or natural boundary conditions. The second subscript indicates the variable to which the condition is applied. Note that boundaries for velocity and temperature may overlap. Let $\mathbf{n}$ be the unit vector normal to Γ, $\mathbf{u}_{\mathrm{g}}$ the given velocity prescribed on $\Gamma_{\mathrm{D},\mathbf{u}}$, $\bar{\mathbf{t}}$ the prescribed traction on $\Gamma_{\mathrm{N},\mathbf{u}}$, ϑ_{g} the given temperature on $\Gamma_{\mathrm{D},\vartheta}$ and $\overline{\varphi}$ the prescribed heat flux on $\Gamma_{\mathrm{N},\vartheta}$. The boundary conditions to be considered for all time $t \in (0, t_{\mathrm{f}}]$ are *initially* written as:

$$\mathbf{u} - \mathbf{u}_{\mathrm{g}} = \mathbf{0} \qquad \text{on } \Gamma_{\mathrm{D},\mathbf{u}}, \tag{5.4a}$$

$$\mathbf{n} \cdot \boldsymbol{\sigma} = \bar{\mathbf{t}} \qquad \text{on } \Gamma_{\mathrm{N},\mathbf{u}}, \tag{5.4b}$$

$$\vartheta - \vartheta_{\mathrm{g}} = 0 \qquad \text{on } \Gamma_{\mathrm{D},\vartheta}, \tag{5.4c}$$

$$-\kappa\mathbf{n} \cdot \nabla\vartheta = \overline{\varphi} \qquad \text{on } \Gamma_{\mathrm{N},\vartheta}. \tag{5.4d}$$

Sometimes, the Neumann-type prescription for the temperature has to be generalized to a Robbin boundary condition to include the surface heat convection, although this is immaterial for what follows. To complete the definition of the problem we need to add initial conditions of the form

$$\begin{aligned} \mathbf{u}(\mathbf{x}, 0) &= \mathbf{u}_0(\mathbf{x}), \\ p(\mathbf{x}, 0) &= p_0(\mathbf{x}), \\ \vartheta(\mathbf{x}, 0) &= \vartheta_0(\mathbf{x}). \end{aligned}$$

Remark 5.3.1 For ideal gases at the low Mach number limit, the fluid usually presents very large values of pressure and temperature, specially if the international system is used. Therefore, both volume expansivity and isothermal compressibility coefficients tend to zero, and the system from Equation 5.2a–Equation 5.2c recovers the classical incompressible form with almost constant density.

5.3.3 Variational formulation

In order to write the weak form of Equation 5.2a–Equation 5.2c together with the boundary conditions in Equation 5.4a – Equation 5.4d let $\mathbf{v}$, q, and η be the test functions for $\mathbf{u}$, p and ϑ, respectively. We consider them time-independent, and additionally $\mathbf{v}$ and η are assumed to vanish separately on $\Gamma_{\mathrm{D},\mathbf{u}}$ and $\Gamma_{\mathrm{D},\vartheta}$, respectively.

Let now $V_{\mathbf{u}}$, $\mathbb{V}_p$ and V_ϑ be, respectively, the proper functional spaces where each component of the velocity, the pressure and the temperature are well defined for each fixed time $t \in (0, t_{\mathrm{f}})$, with appropriate regularity. In addition, let us further introduce the following functional spaces of trial solutions and test functions

$$\begin{aligned}
\mathbb{V}_{\mathbf{u}} &= \left\{ \mathbf{u} \in [V_{\mathbf{u}}]^{N_{\mathrm{sd}}} \;\mid\; \mathbf{u}|_{\Gamma_{\mathrm{D},\mathbf{u}}} = \mathbf{u}_{\mathrm{g}} \right\}, \\
\mathbb{W}_{\mathbf{u}} &= \left\{ \mathbf{v} \in [V_{\mathbf{u}}]^{N_{\mathrm{sd}}} \;\mid\; \mathbf{v}|_{\Gamma_{\mathrm{D},\mathbf{u}}} = \mathbf{0} \right\}, \\
\mathbb{V}_\vartheta &= \left\{ \vartheta \in V_\vartheta \mid \vartheta|_{\Gamma_{\mathrm{D},\vartheta}} = \vartheta_{\mathrm{g}} \right\}, \\
\mathbb{W}_\vartheta &= \left\{ \eta \in V_\vartheta \mid \eta|_{\Gamma_{\mathrm{D},\vartheta}} = 0 \right\}.
\end{aligned}$$

Once Equation 5.2a–Equation 5.2c are multiplied by the corresponding test functions, integrated over the computational domain Ω, second order terms integrated by parts, and the boundary conditions are also taken into account, the resulting variational form of the problem that we consider is given as follows: Find the triplet $[\mathbf{u}, p, \vartheta] : (0, t_{\mathrm{f}}) \rightarrow \mathbb{V}_{\mathbf{u}} \times \mathbb{V}_p \times \mathbb{V}_\vartheta$ such that

$$\langle \rho \partial_t \mathbf{u}, \mathbf{v} \rangle + c(\rho, \mathbf{u}; \mathbf{u}, \mathbf{v}) + a(\mathbf{u}, \mathbf{v}) - b(p, \mathbf{v}) = \ell_{\mathbf{u}}(\rho; \mathbf{v}), \tag{5.6a}$$

$$\begin{aligned}\langle \beta \partial_t p, q \rangle - \langle \alpha \partial_t \vartheta, q \rangle + d(\beta, \mathbf{u}; p, q) - d(\alpha, \mathbf{u}; \vartheta, q) \\ + b(q, \mathbf{u}) = 0,\end{aligned} \tag{5.6b}$$

$$\begin{aligned}\langle \rho c_v \partial_t \vartheta, \eta \rangle + f(\rho, \mathbf{u}; \vartheta, \eta) + e(\vartheta, \eta) \\ + g(\mathbf{u}; p, \eta) = \ell_\vartheta(\rho, \mathbf{u}; \eta),\end{aligned} \tag{5.6c}$$

$$\langle \mathbf{u}(\mathbf{x}, 0), \mathbf{v} \rangle = \langle \mathbf{u}_0(\mathbf{x}), \mathbf{v} \rangle, \tag{5.6d}$$

$$\langle p(\mathbf{x}, 0), q \rangle = \langle p_0(\mathbf{x}), q \rangle, \tag{5.6e}$$

$$\langle \vartheta(\mathbf{x}, 0), \eta \rangle = \langle \vartheta_0(\mathbf{x}), \eta \rangle, \tag{5.6f}$$

which must hold for all test functions $\mathbf{v} \in \mathbb{W}_{\mathbf{u}}$, $q \in \mathbb{W}_p \equiv \mathbb{V}_p$ and $\eta \in \mathbb{W}_\vartheta$ and for all $t \in (0, t_{\mathrm{f}})$. Following the notation used in the previous chapter, the different forms appearing in the previous weak equation are defined as [2]:

[2] Some forms were already introduced for the weak form of the isentropic problem, but they are included here again for the sake of completeness.

$$c(\rho, \mathbf{u}_1; \mathbf{u}_2, \mathbf{v}) := \int_\Omega \rho \left[(\mathbf{u}_1 \cdot \nabla)\mathbf{u}_2\right] \cdot \mathbf{v} \, \mathrm{d}\Omega \tag{5.7a}$$

$$\begin{aligned} a(\mathbf{u}, \mathbf{v}) := & \int_\Omega 2\mu \boldsymbol{\varepsilon}(\mathbf{u}) : \boldsymbol{\varepsilon}(\mathbf{v}) \, \mathrm{d}\Omega \\ & - \int_\Omega \frac{2}{3}\mu(\nabla \cdot \mathbf{u})(\nabla \cdot \mathbf{v}) \, \mathrm{d}\Omega, \end{aligned} \tag{5.7b}$$

$$b(p, \mathbf{v}) := \int_\Omega p(\nabla \cdot \mathbf{v}) \, \mathrm{d}\Omega, \tag{5.7c}$$

$$d(\beta, \mathbf{u}; p, q) := \int_\Omega \beta[(\mathbf{u} \cdot \nabla)p]q \, \mathrm{d}\Omega, \tag{5.7d}$$

$$f(\rho, \mathbf{u}; \vartheta, \eta) := \int_\Omega \rho c_v[(\mathbf{u} \cdot \nabla)\vartheta]\eta \, \mathrm{d}\Omega \tag{5.7e}$$

$$e(\vartheta, \eta) := \int_\Omega \kappa \nabla\vartheta \cdot \nabla\eta \, \mathrm{d}\Omega, \tag{5.7f}$$

$$g(\mathbf{u}; p, \eta) := \int_\Omega p(\nabla \cdot \mathbf{u})\eta \, \mathrm{d}\Omega, \tag{5.7g}$$

$$\ell_{\mathbf{u}}(\rho; \mathbf{v}) := \int_\Omega \rho \mathbf{b} \cdot \mathbf{v} \, \mathrm{d}\Omega + \int_{\Gamma_{\mathrm{N},\mathbf{u}}} \bar{\mathbf{t}} \cdot \mathbf{v} \, \mathrm{d}\Gamma, \tag{5.7h}$$

$$\ell_\vartheta(\rho, \mathbf{u}; \eta) := \int_\Omega Q\eta \, \mathrm{d}\Omega + \int_{\Gamma_{\mathrm{N},\vartheta}} \bar{\varphi}\eta \, \mathrm{d}\Gamma. \tag{5.7i}$$

The previous weak form in Equation 5.6a–Equation 5.6f is nothing but Equation 3.6 applied to the compressible Navier-Stokes problem in primitive variables considering the following definitions:

$$\begin{aligned} \mathscr{B}(\mathbf{y}; \mathbf{y}, \mathbf{z}) &= c(\rho, \mathbf{u}; \mathbf{u}, \mathbf{v}) + a(\mathbf{u}, \mathbf{v}) - b(p, \mathbf{v}) \\ &\quad + d(\beta, \mathbf{u}; p, q) - d(\alpha, \mathbf{u}; \vartheta, q) + b(q, \mathbf{u}) \\ &\quad + f(\rho, \mathbf{u}; \vartheta, \eta) + e(\vartheta, \eta) + g(\mathbf{u}, p, \eta) \\ \ell(\mathbf{z}) &= \ell_{\mathbf{u}}(\rho; \mathbf{v}) + \ell_\vartheta(\rho, \mathbf{u}; \eta) \end{aligned}$$

with the addition of the corresponding boundary terms. In this regard, special care needs to be taken on the imposition of boundary conditions. We discuss this issue in the upcoming section.

5.4 Non reflecting boundary conditions

The compressible Navier-Stokes equations represent a direct path to consistently deal with both aerodynamic and acoustic scales at once. As a consequence, acoustic waves and the flow boundary conditions must be treated consistently and a certain compatibility requirement should be introduced. In this section we review the boundary setting described originally in [130] and also in Section 4.4. This technique is basically the same as in the previous chapter, but we pretend to extend its application for the compressible problem in primitive variables accounting for the corresponding modifications. We recall that the main ingredients of the methodology are the weak prescription of essential boundary conditions together with the application of a zero-order non-reflecting boundary condition.

5.4.1 Unknown and boundary splitting

For the sake of completeness, let us start again by considering a splitting of the velocity and pressure fields, respectively into mean and oscillatory components. For a given time instant $t \in (0, t_\text{f})$, we have

$$\mathbf{u}(\mathbf{x}, t) = \overline{\mathbf{u}}(\mathbf{x}, t) + \mathbf{u}'(\mathbf{x}, t), \tag{5.8a}$$

$$p(\mathbf{x}, t) = \overline{p}(\mathbf{x}, t) + p'(\mathbf{x}, t), \tag{5.8b}$$

where the time-average variables are mathematically defined as

$$\overline{\mathbf{u}}(\mathbf{x}, t) \doteq \frac{1}{T_\text{w}} \int_{t-T_w}^{t} \mathbf{u}(\mathbf{x}, \xi)\, \mathrm{d}\xi, \tag{5.9a}$$

$$\overline{p}(\mathbf{x}, t) \doteq \frac{1}{T_\text{w}} \int_{t-T_w}^{t} p(\mathbf{x}, \xi)\, \mathrm{d}\xi, \tag{5.9b}$$

Hereafter, the oscillatory components correspond to the acoustic fluctuations and the mean components to the flow variables. In this definition, T_w represents an appropriate time window and thus it implicitly defines a filtering frequency for the acoustic waves, which must be chosen small enough to allow a damping of the acoustic perturbations without damaging the flow evolution.

The boundary where velocity conditions exist (either essential or natural) is divided into internal and external contributions. Internal contributions are *e.g.* those corresponding to solid walls in the interior of the domain. External (artificial) boundaries correspond to inlet and outlet boundaries. The *external* boundary where velocity shall be prescribed $\Gamma^e_{\mathbf{u}}$ is divided into two different disjoint subsets,

$$\overline{\Gamma^e_{\text{D},\mathbf{u}} \cap \Gamma^e_{\text{N},\mathbf{u}}} = \emptyset$$

$$\overline{\Gamma^e_{\mathrm{D},\mathbf{u}} \cup \Gamma^e_{\mathrm{N},\mathbf{u}}} = \Gamma^e_{\mathbf{u}}.$$

We remark that this boundary splitting is performed at the external artificial contours of the domain. Should the domain contain any interior wall with prescribed velocity, we should expect sound waves to be reflected in such location and no particular boundary treatment is needed. The key idea behind our boundary formulation is the introduction of the so-called Sommerfeld boundary condition. Such condition is derived from the wave equation written in mixed form, which represents a set of wave-like equations for $\mathbf{u}(\mathbf{x}, t)$ and $p(\mathbf{x}, t)$ [136].

Remark 5.4.1 Some might argue that there exits a wave-like equation for heat. However, following the ideas in [156], it is easily shown that although temperature oscillations may have the mathematical expression of a wave, they are not real travelling waves as there is no actual transport of energy, and hence they show neither wave fronts nor reflection/refraction phenomena. As a result, there is no need to introduce any splitting for the temperature into mean and oscillatory components and the only contribution to the weak form from the imposition of boundary conditions in the temperature equation would be Equation 5.4d.

[156]: Salazar (2006), "Energy propagation of thermal waves"

5.4.2 Unified prescription of boundary conditions

In this subsection, we summarize the different conditions to be applied on each boundary.

On the frontiers belonging to the truncation boundary $\Gamma^e_{\mathrm{D},\mathbf{u}}$, distinct conditions are enforced:

- The mean value of the velocity is prescribed to a given velocity value

$$\bar{\mathbf{u}} = \mathbf{u}_{\mathrm{g}} \quad \text{on} \quad \Gamma^e_{\mathrm{D},\mathbf{u}}, \tag{5.10}$$

  and this will be done weakly via Nitsche's method.
- A Sommerfeld-like non-reflecting boundary condition is enforced for the acoustic component of the velocity

field. In the normal direction to the boundary we set

$$\mathbf{n} \cdot [\mathbf{n} \cdot \boldsymbol{\sigma}(\mathbf{u}', p')] = -\sqrt{\frac{\rho}{\beta}} \mathbf{n} \cdot \mathbf{u}' \quad \text{on} \quad \Gamma^e_{\mathrm{D},\mathbf{u}}, \tag{5.11}$$

and for the tangential direction we directly write

$$\mathbf{t} \cdot [\mathbf{n} \cdot \boldsymbol{\sigma}(\mathbf{u}', p')] = 0 \quad \text{on} \quad \Gamma^e_{\mathrm{D},\mathbf{u}}, \tag{5.12}$$

for any vector $\mathbf{t}$ in the tangent direction to $\Gamma^e_{\mathrm{D},\mathbf{u}}$.

Finally, on the boundary $\Gamma^e_{\mathrm{N},\mathbf{u}}$, the following conditions are enforced:

- The mean value tractions are prescribed, *i. e.*

$$\mathbf{n} \cdot \boldsymbol{\sigma}(\overline{\mathbf{u}}, \overline{p}) = \bar{\mathbf{t}} \quad \text{on} \quad \Gamma^e_{\mathrm{N},\mathbf{u}}. \tag{5.13}$$

- The same approach as in $\Gamma^e_{\mathrm{D},\mathbf{u}}$ is used now for the fluctuating component. Therefore

$$\mathbf{n} \cdot [\mathbf{n} \cdot \boldsymbol{\sigma}(\mathbf{u}', p')] = -\sqrt{\frac{\rho}{\beta}} \mathbf{n} \cdot \mathbf{u}' \quad \text{on} \quad \Gamma^e_{\mathrm{N},\mathbf{u}}, \tag{5.14a}$$

$$\mathbf{t} \cdot [\mathbf{n} \cdot \boldsymbol{\sigma}(\mathbf{u}', p')] = 0 \quad \text{on} \quad \Gamma^e_{\mathrm{N},\mathbf{u}}. \tag{5.14b}$$

Taking now into account these definitions, the prescription of boundary conditions in the weak form of the problem can be done upon the modification of the boundary term on the right-hand-side of the momentum equation Equation 5.6a, which after the introduction of the symmetric and the penalty terms for the imposition of $\bar{\mathbf{u}} = \mathbf{u}_{\mathrm{g}}$ using Nitsche's method reads:

$$\begin{aligned}
\int_{\Gamma^e_{\mathbf{u}}} [\mathbf{n} \cdot \boldsymbol{\sigma}(\mathbf{u}, p)] \cdot \mathbf{v} \, \mathrm{d}\partial\Omega = & \int_{\Gamma^e_{\mathrm{D},\mathbf{u}}} [\mathbf{n} \cdot \boldsymbol{\sigma}(\overline{\mathbf{u}}, \overline{p})] \cdot \mathbf{v} \, \mathrm{d}\partial\Omega \\
& - \int_{\Gamma^e_{\mathrm{D},\mathbf{u}}} \sqrt{\frac{\rho}{\beta}} (\mathbf{u}' \cdot \mathbf{n})(\mathbf{v} \cdot \mathbf{n}) \, \mathrm{d}\partial\Omega \\
& + \int_{\Gamma^e_{\mathrm{D},\mathbf{u}}} (\bar{\mathbf{u}} - \mathbf{u}_{\mathrm{g}}) \cdot [\mathbf{n} \cdot \boldsymbol{\sigma}(\mathbf{v}, q)] \, \mathrm{d}\partial\Omega \\
& - \int_{\Gamma^e_{\mathrm{D},\mathbf{u}}} \psi (\bar{\mathbf{u}} - \mathbf{u}_{\mathrm{g}}) \cdot \mathbf{v} \, \mathrm{d}\partial\Omega \\
& - \int_{\Gamma^e_{\mathrm{N},\mathbf{u}}} \sqrt{\frac{\rho}{\beta}} (\mathbf{u}' \cdot \mathbf{n})(\mathbf{v} \cdot \mathbf{n}) \, \mathrm{d}\partial\Omega \\
& + \int_{\Gamma^e_{\mathrm{N},\mathbf{u}}} \bar{\mathbf{t}} \cdot \mathbf{v} \, \mathrm{d}\partial\Omega,
\end{aligned} \tag{5.15}$$

where again ψ stands for the numerical penalty parameter. If we now group these boundary terms in the following forms:

$$
\begin{aligned}
c_\Gamma(\rho,\beta;\mathbf{u},\mathbf{v}) :=& \int_{\Gamma^e_{\mathbf{u}}} \sqrt{\frac{\rho}{\beta}}(\mathbf{u}'\cdot\mathbf{n})(\mathbf{v}\cdot\mathbf{n})\,\mathrm{d}\partial\Omega \\
&+\int_{\Gamma_{\mathrm{D},\mathbf{u}}} \psi\overline{\mathbf{u}}\cdot\mathbf{v}\,\mathrm{d}\partial\Omega \\
&-\int_{\Gamma^e_{\mathrm{D},\mathbf{u}}} 2\mu[\mathbf{n}\cdot\boldsymbol{\varepsilon}(\overline{\mathbf{u}})]\cdot\mathbf{v}\,\mathrm{d}\partial\Omega \\
&+\int_{\Gamma^e_{\mathrm{D},\mathbf{u}}} \frac{2}{3}\mu\nabla\cdot\overline{\mathbf{u}}(\mathbf{n}\cdot\mathbf{v})\,\mathrm{d}\partial\Omega \\
&-\int_{\Gamma^e_{\mathrm{D},\mathbf{u}}} 2\mu[\mathbf{n}\cdot\boldsymbol{\varepsilon}(\mathbf{v})]\cdot\overline{\mathbf{u}}\,\mathrm{d}\partial\Omega \\
&+\int_{\Gamma^e_{\mathrm{D},\mathbf{u}}} \frac{2}{3}\mu\nabla\cdot\mathbf{v}(\mathbf{n}\cdot\bar{\mathbf{u}})\,\mathrm{d}\partial\Omega, && (5.16a) \\
b_\Gamma(p,\mathbf{v}) :=& \int_{\Gamma^e_{\mathrm{D},\mathbf{u}}} \overline{p}(\mathbf{n}\cdot\mathbf{v})\,\mathrm{d}\partial\Omega, && (5.16b) \\
\ell_{\Gamma,\mathbf{u}}(\mathbf{v}) :=& \int_{\Gamma^e_{\mathrm{D},\mathbf{u}}} \psi\mathbf{u}_{\mathrm{g}}\cdot\mathbf{v}\,\mathrm{d}\partial\Omega \\
&-\int_{\Gamma^e_{\mathrm{D},\mathbf{u}}} 2\mu[\mathbf{n}\cdot\boldsymbol{\varepsilon}(\mathbf{v})]\cdot\mathbf{u}_{\mathrm{g}}\,\mathrm{d}\partial\Omega \\
&+\int_{\Gamma^e_{\mathrm{D},\mathbf{u}}} \frac{2}{3}\mu\nabla\cdot\mathbf{v}(\mathbf{n}\cdot\mathbf{u}_{\mathrm{g}})\,\mathrm{d}\partial\Omega \\
&+\int_{\Gamma^e_{\mathrm{N},\mathbf{u}}} \mathbf{v}\cdot\bar{\mathbf{t}}\,\mathrm{d}\partial\Omega, && (5.16c) \\
\ell_{\Gamma,p}(q) :=& \int_{\Gamma^e_{\mathrm{D},\mathbf{u}}} q(\mathbf{n}\cdot\mathbf{u}_{\mathrm{g}})\,\mathrm{d}\partial\Omega, && (5.16d)
\end{aligned}
$$

the weak formulation of the Navier-Stokes compressible primitive problem would now consist in seeking the velocity, the pressure and the temperature satisfying

$$
\begin{aligned}
&\langle\rho\partial_t\mathbf{u},\mathbf{v}\rangle + c(\rho,\mathbf{u};\mathbf{u},\mathbf{v}) + a(\mathbf{u},\mathbf{v}) - b(p,\mathbf{v}) + c_\Gamma(\rho,\beta;\mathbf{u},\mathbf{v}) \\
&\qquad + b_\Gamma(p,\mathbf{v}) = \ell_{\mathbf{u}}(\rho;\mathbf{v}) + \ell^\Gamma_{\mathbf{u}}(\mathbf{v}), && (5.17a) \\
&\langle\beta\partial_t p,q\rangle - \langle\alpha\partial_t\vartheta,q\rangle + d(\beta,\mathbf{u};p,q) - d(\alpha,\mathbf{u};\vartheta,q) \\
&\qquad + b(q,\mathbf{u}) + b_\Gamma(q,\mathbf{u}) = \ell^\Gamma_p(q), && (5.17b) \\
&\langle\rho c_v\partial_t\vartheta,\eta\rangle + f(\rho,\mathbf{u};\vartheta,\eta) + e(\vartheta,\eta) \\
&\qquad + g(\mathbf{u},p,\eta) = \ell_\vartheta(\rho,\mathbf{u};\eta), && (5.17c)
\end{aligned}
$$

for all test functions and for all $t \in (0,t_{\mathrm{f}})$, and fulfilling weakly the initial conditions at $t = 0$.

5.5 Numerical approximation

5.5.1 Finite element discretization

Let now $\mathbb{V}_{\mathbf{u},h} \subset \mathbb{V}_{\mathbf{u}}$, $\mathbb{V}_{p,h} \subset \mathbb{V}_p$ and $\mathbb{V}_{\vartheta,h} \subset \mathbb{V}_\vartheta$ be the velocity, pressure and temperature finite element spaces associated with the chosen triangulation.

The discrete problem is obtained by approximating $\mathbf{u}$, p and ϑ. The raw Galerkin method applied to the problem stated in Equation 5.17a– Equation 5.17c reads: find the functions $\mathbf{u}_h$, p_h and ϑ_h such that

$$\begin{aligned}
\langle \rho \partial_t \mathbf{u}_h, \mathbf{v}_h \rangle &+ c(\rho, \mathbf{u}_h; \mathbf{u}_h, \mathbf{v}_h) + a(\mathbf{u}_h, \mathbf{v}_h) - b(p_h, \mathbf{v}_h) \\
&+ c_\Gamma(\rho, \beta; \mathbf{u}_h, \mathbf{v}_h) + b_\Gamma(p_h, \mathbf{v}_h) = \ell_{\mathbf{u}}(\rho; \mathbf{v}_h) \\
&+ \ell_{\Gamma,\mathbf{u}}(\mathbf{v}_h), \qquad (5.18a) \\
\langle \beta \partial_t p_h, q_h \rangle &- \langle \alpha \partial_t \vartheta_h, q_h \rangle + d(\beta, \mathbf{u}_h; p_h, q_h) - d(\alpha, \mathbf{u}_h; \vartheta_h, q_h) \\
&+ b(q_h, \mathbf{u}_h) + b_\Gamma(q_h, \mathbf{u}_h) = \ell_{\Gamma,p}(q), \qquad (5.18b) \\
\langle \rho c_v \partial_t \vartheta_h, \eta_h \rangle &+ f(\rho, \mathbf{u}_h; \vartheta_h, \eta_h) + e(\vartheta_h, \eta_h) \\
&+ g(\mathbf{u}_h, p_h, \eta_h) = \ell_\vartheta(\rho, \mathbf{u}_h; \eta_h). \qquad (5.18c)
\end{aligned}$$

The time discretization of the problem is performed by following the notation and statements already introduced in Section 3.4. Then, making use of the BDF operator in Equation 3.7, the fully discrete problem we need to solve is: for $n = 0, 1, \dots, N-1$, solve for $\mathbf{u}_h^{n+1}$, p_h^{n+1} and ϑ_h^{n+1} given the values $\mathbf{u}_h^{n-l}$, p_h^{n-l}, ϑ_h^{n-l} for $l = 0$ to $\theta - 1$, such that

$$\begin{aligned}
\left\langle \rho \delta_t \mathbf{u}_h^{n+1}, \mathbf{v}_h \right\rangle &+ c(\rho, \mathbf{u}_h^{n+1}; \mathbf{u}_h^{n+1}, \mathbf{v}_h) + a(\mathbf{u}_h^{n+1}, \mathbf{v}_h) - b(p_h^{n+1}, \mathbf{v}_h) \\
&+ c_\Gamma(\rho, \beta; \mathbf{u}_h^{n+1}, \mathbf{v}_h) + b_\Gamma(p_h^{n+1}, \mathbf{v}_h) = \ell_{\mathbf{u}}(\rho; \mathbf{v}_h) \\
&+ \ell_{\Gamma,\mathbf{u}}(\mathbf{v}_h), \qquad (5.19a) \\
\left\langle \beta \delta_t p_h^{n+1}, q_h \right\rangle &- \left\langle \alpha \delta_t \vartheta_h^{n+1}, q_h \right\rangle + d(\beta, \mathbf{u}_h^{n+1}; p_h^{n+1}, q_h) \\
&- d(\alpha, \mathbf{u}_h^{n+1}; \vartheta_h^{n+1}, q_h) + b(q_h, \mathbf{u}_h^{n+1}) \\
&+ b_\Gamma(q_h, \mathbf{u}_h^{n+1}) = \ell_{\Gamma,p}(q), \qquad (5.19b) \\
\left\langle \rho c_v \delta_t \vartheta_h^{n+1}, \eta_h \right\rangle &+ f(\rho, \mathbf{u}_h^{n+1}; \vartheta_h^{n+1}, \eta_h) + e(\vartheta_h^{n+1}, \eta_h) \\
&+ g(\mathbf{u}_h^{n+1}, p_h^{n+1}, \eta_h) = \ell_\vartheta(\rho, \mathbf{u}_h^{n+1}; \eta_h). \qquad (5.19c)
\end{aligned}$$

In order to compute the mean components of the unknowns, we use the same expression as in the isentropic problem in the previous chapter, *i. e.*, Equation 4.20.

Remark 5.5.1 In the case of the primitive compressible problem, the unknowns are $\mathbf{u}_h^{n+1}$, p_h^{n+1}, ϑ_h^{n+1}. Then ρ, α and β shall be explicitly computed in the final algorithm by means of a linearization process. Hence their values are obtained from finite element quantities but not solved as unknowns for each time step and non-linear iteration. In other words, they *do not* belong to the finite element spaces, and that is why we did not include neither the h subscript nor the superscript $n + 1$ in the equations. It should be understood just as notation. In particular, we follow the ideas explained in Section 4.5.2 for the linearization of the problem.

5.5.2 Monolithic algebraic system

We assume that $\mathbf{u}_h^{n+1}$, p_h^{n+1}, and ϑ_h^{n+1} are constructed using the standard finite element interpolation from the nodal values, which we denote hereafter as $\mathbf{U}^{n+1}$, $\mathbf{P}^{n+1}$ and $\mathbf{\Theta}^{n+1}$, respectively. These are computed as the solution of a nonlinear algebraic system, which is derived from Equation 5.17a–Equation 5.17c. The definitions of the arrays involved in this problem are collected in Table 5.1, Table 5.2 and Table 5.3. The reader should note that the terms containing temporal derivatives of the unknowns in the table actually contribute to both LHS and RHS of the final equation after introducing the chosen temporal discretization.

The first subscript on the arrays refers to the momentum ($\mathbf{u}$), energy (ϑ) and continuity (p) equation, and the second stands for the unknown to which the term refers to. The symbol $\mathbf{M}$ stands for the mass matrices and, in addition, the subscript Γ stands for the terms arising from the special treatment of boundary conditions, as described in Section 5.4. Having introduced all these matrices and vectors, the resolution of the compressible flow problem via the FE method is stated now as: given the initial data and the corresponding values $\mathbf{U}^{n-l}$, $\mathbf{P}^{n-l}$, $\mathbf{\Theta}^{n-l}$ for $l = 0$ to $\theta - 1$, find $\mathbf{U}^{n+1}$, $\mathbf{P}^{n+1}$, $\mathbf{\Theta}^{n+1}$ approximation to $\mathbf{U}(t^{n+1})$, $\mathbf{P}(t^{n+1})$, $\mathbf{\Theta}(t^{n+1})$ as the converged solutions of

Table 5.1: Matrix form of the terms corresponding to the momentum equation.

Matrix version	Term where it comes from
$\mathbf{V}^T\mathbf{M}_{\mathbf{uu}}\mathbf{U}$	$\langle \mathbf{v}_h, \rho\partial_t\mathbf{u}_h\rangle$
$\mathbf{V}^T\mathbf{K}_{\mathbf{uu}}\left(\mathbf{U}_1\right)\mathbf{U}_2$	$c(\rho, \mathbf{u}_{h,1}; \mathbf{u}_{h,2}, \mathbf{v}_h) + a(\mathbf{u}_{h,2}, \mathbf{v}_h)$
$\mathbf{V}^T\mathbf{M}_{\Gamma,\mathbf{uu}}\mathbf{U}$	$\left\langle \psi\overline{\mathbf{u}}, \mathbf{v}_h\right\rangle_{\Gamma_{\mathrm{D},\mathbf{u}}}$
$\mathbf{V}^T\mathbf{K}_{\Gamma,\mathbf{uu}}\mathbf{U}$	$c_\Gamma(\rho, \beta; \mathbf{u}_h, \mathbf{v}_h) - \left\langle \psi\overline{\mathbf{u}}, \mathbf{v}_h\right\rangle_{\Gamma_{\mathrm{D},\mathbf{u}}}$
$\mathbf{V}^T\mathbf{G}\mathbf{P}$	$b(p_h, \mathbf{v}_h)$
$\mathbf{V}^T\mathbf{G}_\Gamma\mathbf{P}$	$b_\Gamma(p_h, \mathbf{v}_h)$
$\mathbf{V}^T\mathbf{F}_{\mathbf{u}}$	$\ell_{\mathbf{u}}(\rho; \mathbf{v}_h)$
$\mathbf{V}^T\mathbf{F}_{\Gamma,\mathbf{u}}$	$\ell_{\Gamma,\mathbf{u}}(\mathbf{v}_h)$

Table 5.2: Matrix form of the terms corresponding to the mass equation.

Matrix version	Term where it comes from
$\mathbf{Q}^T\mathbf{M}_{pp}\mathbf{P}$	$\langle q_h, \beta\partial_t p_h\rangle$
$\mathbf{Q}^T\mathbf{K}_{pp}\left(\mathbf{U}\right)\mathbf{P}$	$d(\rho, \mathbf{u}_h; p_h, q_h)$
$\mathbf{Q}^T\mathbf{M}_{p\vartheta}\mathbf{P}$	$\langle q_h, \alpha\partial_t\vartheta_h\rangle$
$\mathbf{Q}^T\mathbf{K}_{p\vartheta}\left(\mathbf{U}\right)\mathbf{P}$	$d(\rho, \mathbf{u}_h; \vartheta_h, q_h)$
$\mathbf{Q}^T\mathbf{D}\mathbf{U}$	$b(q_h, \mathbf{u}_h)$
$\mathbf{Q}^T\mathbf{D}_\Gamma\mathbf{U}$	$b_\Gamma(q_h, \mathbf{u}_h)$
$\mathbf{Q}^T\mathbf{F}_{\Gamma,p}$	$\ell_{\Gamma,p}(q_h)$

the following iterative problem:

$$\begin{aligned}
\mathbf{M}_{\mathbf{uu},\rho^{(i)}}\frac{D_\theta}{\delta t}\mathbf{U}^{n+1,(i+1)} &+ \mathbf{K}_{\mathbf{uu},\rho^{(i)}}\left(\mathbf{U}^{n+1,(i)}\right)\mathbf{U}^{n+1,(i+1)} \\
&+ \mathbf{M}_{\Gamma,\mathbf{uu}}\mathbf{U}^{n+1,(i+1)} + \mathbf{K}_{\Gamma,\mathbf{uu},\rho^{(i)}\beta^{(i)}}\mathbf{U}^{n+1,(i+1)} \\
&+ \mathbf{G}\mathbf{P}^{n+1,(i+1)} + \mathbf{G}_\Gamma\mathbf{P}^{n+1,(i+1)} = \mathbf{F}^{n+1}_{\mathbf{u},\rho^{(i)}} + \mathbf{F}^{n+1}_{\Gamma,\mathbf{u}}, \qquad (5.20\text{a})
\end{aligned}$$

$$\begin{aligned}
\mathbf{M}_{pp,\beta^{(i)}}\frac{D_\theta}{\delta t}\mathbf{P}^{n+1,(i+1)} &+ \mathbf{K}_{pp,\beta^{(i)}}(\mathbf{U}^{n+1,(i)})\mathbf{P}^{n+1,(i+1)} \\
&- \mathbf{M}_{p\vartheta,\alpha^{(i)}}\frac{D_\theta}{\delta t}\mathbf{\Theta}^{n+1,(i+1)} - \mathbf{K}_{p\vartheta,\alpha^{(i)}}(\mathbf{U}^{n+1,(i)})\mathbf{\Theta}^{n+1,(i+1)} \\
&+ \mathbf{D}\mathbf{U}^{n+1,(i+1)} + \mathbf{D}_\Gamma\mathbf{U}^{n+1,(i+1)} = \mathbf{F}^{n+1}_{\Gamma,p}, \qquad (5.20\text{b})
\end{aligned}$$

$$\begin{aligned}
\mathbf{M}_{\vartheta\vartheta,\rho^{(i)}}\frac{D_\theta}{\delta t}\mathbf{\Theta}^{n+1,(i+1)} &+ \mathbf{K}_{\vartheta\vartheta,\rho^{(i)}}\left(\mathbf{U}^{n+1,(i)}\right)\mathbf{\Theta}^{n+1,(i+1)} \\
&+ \mathbf{K}_{\vartheta p}\left(\mathbf{U}^{n+1,(i)}\right)\mathbf{P}^{n+1,(i+1)} = \mathbf{F}^{n+1}_{\vartheta,\rho^{(i)}\mathbf{u}^{(i)}}, \qquad (5.20\text{c})
\end{aligned}$$

where we have included a subscript $\rho^{(i)}$, $\alpha^{(i)}$, $\beta^{(i)}$ so as to indicate that those arrays are computed by taking a previously

Matrix version	Term where it comes from
$\mathbf{H}^T\mathbf{M}_{\vartheta\vartheta}\boldsymbol{\Theta}$	$\langle \eta_h, \rho c_v \partial_t \vartheta_h \rangle$
$\mathbf{H}^T\mathbf{K}_{\vartheta\vartheta}(\mathbf{U})\boldsymbol{\Theta}$	$f(\rho, \mathbf{u}_h; \vartheta_h, \eta_h) + e(\vartheta_h, \eta_h)$
$\mathbf{H}^T\mathbf{K}_{\vartheta p}(\mathbf{U})\mathbf{P}$	$g(\mathbf{u}_h, p_h, \eta_h)$
$\mathbf{H}^T\mathbf{F}_{\vartheta}$	$\ell_{\vartheta}(\rho, \mathbf{u}_h; \eta_h)$

Table 5.3: Matrix form of the terms corresponding to the energy equation.

computed value of density, volume expansivity and isothermal compressibility coefficients. This system, in a more compact manner for each iteration, can be rearranged as

$$\begin{bmatrix} \mathbf{A}_{\mathbf{uu}} & \mathbf{A}_{\mathbf{u}p} & \mathbf{0} \\ \mathbf{A}_{p\mathbf{u}} & \mathbf{A}_{pp} & \mathbf{A}_{p\vartheta} \\ \mathbf{0} & \mathbf{A}_{\vartheta p} & \mathbf{A}_{\vartheta\vartheta} \end{bmatrix} \cdot \begin{bmatrix} \mathbf{U}^{n+1} \\ \mathbf{P}^{n+1} \\ \boldsymbol{\Theta}^{n+1} \end{bmatrix} = \begin{bmatrix} \mathbf{F}^{n+1}_{\mathbf{U}} \\ \mathbf{F}^{n+1}_{\mathbf{P}} \\ \mathbf{F}^{n+1}_{\boldsymbol{\Theta}} \end{bmatrix} \tag{5.21}$$

with the following matrices:

$$\begin{aligned}
\mathbf{A}_{\mathbf{uu}} :=& \mathbf{M}_{\mathbf{uu}}(\rho)\frac{D_\theta}{\delta t} + \mathbf{K}_{\mathbf{uu}}\left(\rho, \mathbf{U}^{n+1}\right) + \mathbf{M}_{\Gamma,\mathbf{uu}} + \mathbf{K}_{\Gamma,\mathbf{uu}}(\rho, \beta) \\
\mathbf{A}_{\mathbf{u}p} :=& \mathbf{G} + \mathbf{G}_{\Gamma} \\
\mathbf{A}_{p\mathbf{u}} :=& \mathbf{D} + \mathbf{D}_{\Gamma} \\
\mathbf{A}_{pp} :=& \mathbf{M}_{pp}(\beta)\frac{D_\theta}{\delta t} + \mathbf{K}_{pp}\left(\beta, \mathbf{U}^{n+1}\right) \\
\mathbf{A}_{p\vartheta} :=& -\mathbf{M}_{p\vartheta}(\alpha)\frac{D_\theta}{\delta t} - \mathbf{K}_{p\vartheta}\left(\alpha, \mathbf{U}^{n+1}\right) \\
\mathbf{A}_{\vartheta p} :=& \mathbf{K}_{\vartheta p}\left(\mathbf{U}^{n+1}\right) \\
\mathbf{A}_{\vartheta\vartheta} :=& \mathbf{M}_{\vartheta\vartheta}(\rho)\frac{D_\theta}{\delta t} + \mathbf{K}_{\vartheta\vartheta}\left(\rho, \mathbf{U}^{n+1}\right) \\
\mathbf{F}^{n+1}_{\mathbf{U}} :=& \mathbf{F}^{n+1}_{\mathbf{u}}(\rho) + \mathbf{F}^{n+1}_{\Gamma,\mathbf{u}} \\
\mathbf{F}^{n+1}_{\mathbf{P}} :=& \mathbf{F}^{n+1}_{\Gamma,p} \\
\mathbf{F}^{n+1}_{\boldsymbol{\Theta}} :=& \mathbf{F}^{n+1}_{\vartheta}\left(\rho, \mathbf{U}^{n+1}\right)
\end{aligned}$$

The high non-linear character of the problem is made explicit in the system by including the dependency of the arrays on the variables in the parenthesis.

5.6 Design of the fractional step method

In this section we develop the algebraic fractional step methods for the compressible Navier-Stokes problem written in primitive variables. The algorithm here proposed could be viewed as a natural extension of pressure-segregation schemes previously developed for viscoelastic flows [55] or incompressible flows [50].

The basic procedure entails a calculation of an intermediate velocity with a guess of the pressure, as we already discussed for the isentropic case in the previous chapter, yet we will broaden here the original technique by computing also an intermediate temperature. After computing the pressure, we will finally correct the velocity and temperature intermediate values, so as to ensure that the global time accuracy of the method is maintained. We will not discuss here different segregation techniques such as velocity-correction methods [139] (based on the opposite procedure, a velocity guess is assumed to solve for the pressure) or predictor-multicorrector techniques [56].

5.6.1 The algebraic viewpoint. Extrapolation.

In order to simplify the exposition and the notation, let us drop the iteration counter (i) in this section. For the purpose of the derivation of the method, let us start by writing the previous system Equation 5.21 in the following *equivalent* manner:

$$\begin{aligned}
&\mathbf{M}_{\mathbf{uu}}(\rho)\frac{D_\theta}{\delta t}\widetilde{\mathbf{U}}^{n+1} + \mathbf{K}_{\mathbf{uu}}(\rho, \mathbf{U}^{n+1})\mathbf{U}^{n+1} - \mathbf{K}_{\mathbf{u}p}\hat{\mathbf{P}}^{n+1}_{\theta-1} \\
&\qquad + \mathbf{M}_{\Gamma,\mathbf{uu}}\mathbf{U}^{n+1} + \mathbf{K}_{\Gamma,\mathbf{uu}}(\rho, \beta)\mathbf{U}^{n+1} \\
&\qquad + \mathbf{K}_{\Gamma,\mathbf{u}p}\mathbf{P}^{n+1} = \mathbf{F}^{n+1}_{\mathbf{U}}, \qquad (5.22\text{a})
\end{aligned}$$

$$\mathbf{M}_{\mathbf{uu}}(\rho)\frac{1}{\phi_\theta \delta t}(\mathbf{U}^{n+1} - \widetilde{\mathbf{U}}^{n+1}) - \mathbf{K}_{\mathbf{u}p}(\mathbf{P}^{n+1} - \hat{\mathbf{P}}^{n+1}_{\theta-1}) = \mathbf{0}, \quad (5.22\text{b})$$

$$\begin{aligned}
&\mathbf{M}_{\vartheta\vartheta}(\rho)\frac{D_\theta}{\delta t}\widetilde{\mathbf{\Theta}}^{n+1} + \mathbf{K}_{\vartheta\vartheta}(\rho, \mathbf{U}^{n+1})\mathbf{\Theta}^{n+1} \\
&\qquad + \mathbf{K}_{\vartheta p}(\mathbf{U}^{n+1})\hat{\mathbf{P}}^{n+1}_{\theta-1} = \mathbf{F}^{n+1}_{\mathbf{\Theta}}, \qquad (5.22\text{c})
\end{aligned}$$

$$\mathbf{M}_{\vartheta\vartheta}(\rho)\frac{1}{\phi_\theta \delta t}(\mathbf{\Theta}^{n+1} - \widetilde{\mathbf{\Theta}}^{n+1}) + \mathbf{K}_{\vartheta p}(\mathbf{U}^{n+1})(\mathbf{P}^{n+1} - \hat{\mathbf{P}}^{n+1}_{\theta-1}) = \mathbf{0}, \qquad (5.22\text{d})$$

$$\begin{aligned}
&\mathbf{M}_{pp}(\beta)\frac{D_\theta}{\delta t}\mathbf{P}^{n+1} + \mathbf{K}_{pp}(\beta, \mathbf{U}^{n+1})\mathbf{P}^{n+1} - \mathbf{M}_{p\vartheta}(\alpha)\frac{D_\theta}{\delta t}\mathbf{\Theta}^{n+1} \\
&\qquad - \mathbf{K}_{p\vartheta}(\alpha, \mathbf{U}^{n+1})\mathbf{\Theta}^{n+1} + \mathbf{K}_{p\mathbf{u}}\mathbf{U}^{n+1} \\
&\qquad + \mathbf{K}_{\Gamma,p\mathbf{u}}\mathbf{U}^{n+1} = \mathbf{F}^{n+1}_{\mathbf{P}}, \qquad (5.22\text{e})
\end{aligned}$$

where $D_\theta \tilde{f}^{n+1}$ is computed as $D_\theta f^{n+1}$ but replacing f^{n+1} by a yet undetermined function $\tilde{f}^{n+1}$, for $f = \mathbf{U}$ and $f = \mathbf{\Theta}$. The chosen ordering of the equations is consistent with the steps of the fractional step algorithm proposed below.

The reader should note that adding up Equation 5.22a and Equation 5.22b we obtain the former momentum equation, *i. e.*, the first row of the system in Equation 5.21. Adding up Equation 5.22c and Equation 5.22d we recover the original energy equation, *i. e.*, the last row in Equation 5.21. We shall refer to Equation 5.22a and Equation 5.22c as *intermediate momentum* and *intermediate energy* equations, respectively and to Equation 5.22b–Equation 5.22d as *momentum correction* and *energy correction* equations. Similarly, the auxiliary variables $\widetilde{\mathbf{U}}^{n+1}$ and $\widetilde{\mathbf{\Theta}}^{n+1}$ are the socalled intermediate velocity and intermediate temperature. Likewise, $\hat{\mathbf{P}}^{n+1}_{\theta-1}$ is an extrapolation of the pressure of order $\theta - 1$ at time step $n + 1$. Note that we introduce a pressure extrapolation of one order less than the general time integration scheme, but we re-include this extrapolated term in the correction equations. This is essential for the scheme to be formally of order θ.

Let us now proceed as follows: if we multiply Equation 5.22b by the matrix $\mathbf{K}_{p\mathbf{u}}\mathbf{M}^{-1}_{\mathbf{uu}}$, we get

$$\mathbf{K}_{p\mathbf{u}}\mathbf{U}^{n+1} = \mathbf{K}_{p\mathbf{u}}\widetilde{\mathbf{U}}^{n+1} + \phi_\theta \delta t \mathbf{K}_{p\mathbf{u}}\mathbf{M}^{-1}_{\mathbf{uu}}\mathbf{K}_{\mathbf{u}p}(\mathbf{P}^{n+1} - \hat{\mathbf{P}}^{n+1}_{\theta-1}),$$

and multiplying Equation 5.22d by $\mathbf{K}_{p\vartheta}\mathbf{M}^{-1}_{\theta\theta}$, we obtain

$$\mathbf{K}_{p\vartheta}\mathbf{\Theta}^{n+1} = \mathbf{K}_{p\vartheta}\widetilde{\mathbf{\Theta}}^{n+1} - \phi_\theta \delta t \mathbf{K}_{p\vartheta}\mathbf{M}^{-1}_{\vartheta\vartheta}\mathbf{K}_{\vartheta p}(\mathbf{P}^{n+1} - \hat{\mathbf{P}}^{n+1}_{\theta-1}),$$

and both expressions can be used in the equation for the pressure Equation 5.22e and this yields

$$\begin{aligned}
\mathbf{M}_{pp}(\beta)\frac{D_\theta}{\delta t}\mathbf{P}^{n+1} &+ \mathbf{K}_{pp}(\beta, \mathbf{U}^{n+1})\mathbf{P}^{n+1} - \mathbf{M}_{p\vartheta}(\alpha)\frac{D_\theta}{\delta t}\mathbf{\Theta}^{n+1} \\
&- \mathbf{K}_{p\vartheta}(\alpha, \mathbf{U}^{n+1})\widetilde{\mathbf{\Theta}}^{n+1} + \mathbf{K}_{p\mathbf{u}}\widetilde{\mathbf{U}}^{n+1} \\
&+ \phi_\theta \delta t \mathbf{K}_{p\vartheta}\mathbf{M}^{-1}_{\vartheta\vartheta}\mathbf{K}_{\vartheta p}(\mathbf{P}^{n+1} - \hat{\mathbf{P}}^{n+1}_{\theta-1}) \\
&+ \phi_\theta \delta t \mathbf{K}_{p\mathbf{u}}\mathbf{M}^{-1}_{\mathbf{uu}}\mathbf{K}_{\mathbf{u}p}(\mathbf{P}^{n+1} - \hat{\mathbf{P}}^{n+1}_{\theta-1}) \\
&+ \mathbf{K}_{\Gamma,p\mathbf{u}}\mathbf{U}^{n+1} = \mathbf{F}^{n+1}_{\mathbf{P}}.
\end{aligned}$$

At this point, several remarks are in order, since we have to note that we have modified the original matrix version of the continuity equation by introducing some burden related to appearance of the inverse of the mass matrices $\mathbf{M}_{\vartheta\vartheta}$ and $\mathbf{M}_{\mathbf{uu}}$.

Remark 5.6.1 Similarly as in the case of the isentropic problem, one should notice that the resulting matrix from $\mathbf{K}_{p\mathbf{u}}\mathbf{M}_{\mathbf{uu}}^{-1}\mathbf{K}_{\mathbf{u}p}$ can be viewed as an approximation to the discrete version of a Laplacian operator, [140]. Hence, Remark 4.6.1 also applies here and we can simply use matrix $\mathbf{L}$ as an approximation to $\mathbf{K}_{p\mathbf{u}}\mathbf{M}_{\mathbf{uu}}^{-1}\mathbf{K}_{\mathbf{u}p}$. The reader should note that $\mathbf{K}_{p\mathbf{u}} = \mathbf{D}$ and $\mathbf{K}_{\mathbf{u}p} = \mathbf{G}$.

Remark 5.6.2 The case of $\mathbf{K}_{p\vartheta}\mathbf{M}_{\theta\theta}^{-1}\mathbf{K}_{\vartheta p}$ deserves an special comment. We need to take into account that, of course, we want to avoid computing inverse of matrices by all means. We approximate *the effect* of this term by

$$\mathbf{K}_{p\vartheta}\mathbf{M}_{\theta\theta}^{-1}\mathbf{K}_{\vartheta p} \approx \mathbf{Q},$$

which we compute in each element as

$$[\mathbf{Q}^{(e)}]^{ab} = \int_{\Omega^{(e)}} \frac{\alpha}{\rho c_v} (\mathbf{u}_h \cdot \nabla)\, \varphi^a (\nabla \cdot \mathbf{u}_h) \varphi^b \, \mathrm{d}\Omega,$$
$$\mathbf{Q} = \mathbb{A}^{(e)}\mathbf{Q}^{(e)},$$

for a, b running from 1 to the number of elemental nodes and where the first factor in the integral is introduced to keep the proper scaling.

Remark 5.6.3 Note from the definition of the extrapolation operators, Equation 3.9, that the difference

$$\left\| \mathbf{P}^{n+1} - \hat{\mathbf{P}}^{n+1}_{\theta-1} \right\| \sim \mathcal{O}(\delta t^{\theta-1})$$

is of order $\mathcal{O}(\delta t^{\theta-1})$. Therefore, it is easy to see from Equation 5.22b and Equation 5.22d that

$$\mathcal{O}(\|\mathbf{U}^{n+1} - \widetilde{\mathbf{U}}^{n+1}\|) = \mathcal{O}(\delta t^{\theta})$$
$$\mathcal{O}(\|\boldsymbol{\Theta}^{n+1} - \widetilde{\boldsymbol{\Theta}}^{n+1}\|) = \mathcal{O}(\delta t^{\theta})$$

and thus, the global accuracy of the temporal integrator is formally maintained.

5.6.2 Pressure-correction scheme

Generally speaking, the fractional step approach that we favor to solve the fully compressible Navier-Stokes problem in primitive variables has five main steps:

(i) Compute an intermediate velocity from Equation 5.22a.
(ii) Compute an intermediate temperature from Equation 5.22c.
(iii) Compute an approximation to the end-of-step pressure by using Equation 5.22e.
(iv) Update the end-of-step velocity with Equation 5.22b.
(v) Solve for the end-of-step temperature by using Equation 5.22d.

This procedure will make possible to segregate the calculation of the unknowns of the problem and provides a pressure-correction-like algorithm.

However, in Equation 5.22a to Equation 5.22e there are still some terms which involve some coupling of the unknowns and hence some extra information is still needed in order to complete the algorithm. One of the key approximations we introduce to decouple the calculation of the problem unknowns is to substitute $\mathbf{U}^{n+1}$ by $\widetilde{\mathbf{U}}^{n+1}$ and $\mathbf{\Theta}^{n+1}$ by $\widetilde{\mathbf{\Theta}}^{n+1}$ in the rest of the terms in the intermediate momentum and energy equations, respectively Equation 5.22a and Equation 5.22c. This approximation is supported by Remark 5.6.3. In addition to this, the boundary pressure term in Equation 5.22a is made explicit by considering an extrapolation of order θ following Equation 3.9. This is the same strategy as we explained in Section 4.6.2 for the isentropic case. Hence this term is not accounted for in any correction step.

The remaining terms which could still couple the problem variables can be evaluated with $\widetilde{\mathbf{U}}^{n+1}$ or $\widetilde{\mathbf{\Theta}}^{n+1}$ (Remark 4.6.6 also applies here) and the possible additional nonlinearities are solved by taking the known values of the unknowns from the previous iteration, time step or from the intermediate equations. Taking all this information into account, the final algorithmic procedure is included down below.

First and second order fractional step scheme for the primitive Navier-Stokes problem

- Set/read the initial conditions for $\mathbf{U}^0$, $\mathbf{P}^0$ and $\mathbf{\Theta}^0$.

```
▸ WHILE $n < N$ DO
    • Set $\mathbf{U}^{n,0} = \mathbf{U}^{n-1}$, $\mathbf{P}^{n,0} = \mathbf{P}^{n-1}$ and $\mathbf{\Theta}^{n,0} = \mathbf{\Theta}^{n-1}$
    • WHILE (not converged) DO
        ⋆ Compute intermediate velocity $\widetilde{\mathbf{U}}^{n+1}$:

          $\mathbf{M}_{\mathbf{uu},\rho^n} \frac{D_\theta}{\delta t} \widetilde{\mathbf{U}}^{n+1,(i+1)} + \mathbf{K}_{\mathbf{uu},\rho^n} \left(\widetilde{\mathbf{U}}^{n+1,(i)}\right) \widetilde{\mathbf{U}}^{n+1,(i+1)}$
              $+ \mathbf{M}_{\Gamma,\mathbf{uu}} \widetilde{\mathbf{U}}^{n+1,(i+1)} + \mathbf{K}_{\Gamma,\mathbf{uu}_{,\rho^n \beta^n}} \widetilde{\mathbf{U}}^{n+1,(i+1)}$
              $= \mathbf{F}_{\mathbf{U}}^{n+1} + \mathbf{K}_{\mathbf{u}p} \hat{\mathbf{P}}_{\theta-1}^{n+1} - \mathbf{K}_{\Gamma,\mathbf{u}p} \hat{\mathbf{P}}_{\theta}^{n+1}$

        ⋆ Check convergence
    • END while (not converged)
    • WHILE (not converged) DO
        ⋆ Compute the intermediate temperature $\widetilde{\mathbf{\Theta}}^{n+1}$
          after solving:

          $\mathbf{M}_{\vartheta\vartheta,\rho^{(i)}} \frac{D_\theta}{\delta t} \widetilde{\mathbf{\Theta}}^{n+1,(i+1)} + \mathbf{K}_{\vartheta\vartheta,\rho^{(i)}} \left(\widetilde{\mathbf{U}}^{n+1}\right) \widetilde{\mathbf{\Theta}}^{n+1,(i+1)}$
              $= \mathbf{F}_{\mathbf{\Theta}}^{n+1} - \mathbf{K}_{\vartheta p} \left(\widetilde{\mathbf{U}}^{n+1}\right) \hat{\mathbf{P}}_{\theta-1}^{n+1}$

        ⋆ Check convergence
    • END while (not converged)
    • WHILE (not converged) DO
        ⋆ Compute the pressure $\mathbf{P}^{n+1}$ using the intermediate velocity and temperature:

          $\mathbf{M}_{pp,\beta^{(i)}} \frac{D_\theta}{\delta t} \mathbf{P}^{n+1,(i+1)} + \mathbf{K}_{pp,\beta^{(i)}} \left(\widetilde{\mathbf{U}}^{n+1}\right) \mathbf{P}^{n+1,(i+1)}$
              $+ \phi_\theta \delta t \mathbf{Q}_{\rho^{(i)}\alpha^{(i)}} \left(\mathbf{P}^{n+1,(i+1)} - \hat{\mathbf{P}}_{\theta-1}^{n+1}\right)$
              $+ \phi_\theta \delta t \mathbf{L}_{\rho^{(i)}} \left(\mathbf{P}^{n+1,(i+1)} - \hat{\mathbf{P}}_{\theta-1}^{n+1}\right) = \mathbf{F}_{\mathbf{P}}^{n+1}$
              $- \mathbf{K}_{p\mathbf{u}} \widetilde{\mathbf{U}}^{n+1} + \mathbf{K}_{p\vartheta_{,\alpha^{(i)}}} \left(\widetilde{\mathbf{U}}^{n+1}\right) \widetilde{\mathbf{\Theta}}^{n+1}$
              $+ \mathbf{M}_{p\vartheta_{,\alpha^{(i)}}} \frac{D_\theta}{\delta t} \widetilde{\mathbf{\Theta}}^{n+1}$
              $- \mathbf{K}_{\Gamma,p\mathbf{u}} \widetilde{\mathbf{U}}^{n+1}$

        ⋆ Check convergence
    • END while (not converged)
    • Velocity correction to obtain the end-of-step velocity $\mathbf{U}^{n+1}$:

      $\mathbf{M}_{\mathbf{uu},\rho^{n+1}} \frac{1}{\phi_\theta \delta t} \mathbf{U}^{n+1} + \mathbf{M}_{\Gamma,\mathbf{uu}} \mathbf{U}^{n+1} = \mathbf{M}_{\mathbf{uu},\rho^{n+1}} \frac{1}{\phi_\theta \delta t} \widetilde{\mathbf{U}}^{n+1}$
```

$$+ \mathbf{M}_{\Gamma,\mathbf{uu}}\widetilde{\mathbf{U}}^{n+1} + \mathbf{K}_{\mathbf{u}p}\left(\mathbf{P}^{n+1} - \hat{\mathbf{P}}^{n+1}_{\theta-1}\right)$$

- Temperature correction to obtain the end-of-step temperature $\boldsymbol{\Theta}^{n+1}$:

$$\mathbf{M}_{\vartheta\vartheta,\rho^{n+1}}\frac{1}{\phi_\theta \delta t}\left(\boldsymbol{\Theta}^{n+1} - \widetilde{\boldsymbol{\Theta}}^{n+1}\right) = -\mathbf{K}_{\vartheta p}\left(\mathbf{U}^{n+1}\right)\left(\mathbf{P}^{n+1} - \hat{\mathbf{P}}^{n+1}_{\theta-1}\right)$$

- END while $n < N$ (non-stationary)

It is well known that the extrapolation of second order of the term $\mathbf{K}_{\mathbf{u}p}\mathbf{P}^{n+1}$ is unstable. In fact, this issue motivated the study of other methods to upgrade the temporal order of the fractional step scheme, such as the Yosida regularization technique (see *e.g.* [50]). On the contrary, we did not observe any erratic behavior of the term $\mathbf{K}_{\Gamma,\mathbf{u}p}\hat{\mathbf{P}}^{n+1}_{\theta}$ when $\theta = 2$ is chosen. Both Remark 4.6.4 and Remark 4.6.5 do apply here as well.

5.7 Variational Multiscale stabilized formulation

In this section, we discuss the application of the Variational Multiscale method to the Navier-Stokes problem formulated in primitive variables. The general procedure was already described in Chapter 3. Hence, the stabilized version of the primitive compressible problem is nothing but Equation 3.20 with the pertinent definitions of the stabilization terms (and up to boundary terms), which we discuss next.

5.7.1 Stabilized formulation applied to the compressible Navier-Stokes problem written in primitive variables

For reasons already discussed, we make use the OSGS technique, as stated in Section 3.5.4. The OSGS method allows certain type of simplifications [99]:

- The orthogonal projection of the external forces might be neglected. External loads are assumed to belong to the finite element spaces or are approximated by an element of the corresponding space. Hence

$$\begin{aligned}\mathscr{P}_h^{\perp}(\rho r) &\approx 0,\\ \mathscr{P}_h^{\perp}(\rho \mathbf{b}) &\approx 0.\end{aligned}$$

- The orthogonal projection of terms involving temporal derivatives might be also neglected. Their orthogonal projection would be exactly zero if ρ, β and α were constant. However we consider as true that those parameters are such the temporal terms already belong to the finite element space. This simplification is key in order to solve the problem by means of a fractional step method in time. This amounts to saying that

$$\begin{aligned}\mathscr{P}_h^{\perp}(\rho \partial_t \mathbf{u}_h) &\approx 0,\\ \mathscr{P}_h^{\perp}(\beta \partial_t p_h) &\approx 0,\\ \mathscr{P}_h^{\perp}(\alpha \partial_t \vartheta_h) &\approx 0,\\ \mathscr{P}_h^{\perp}(\rho c_v \partial_t \vartheta_h) &\approx 0.\end{aligned}$$

  All this statements are similar as collected in Remark 4.7.1 for the isentropic problem.
- The evaluation of second derivatives in the stabilization terms is a costly and cumbersome process in finite element implementations which can be avoided using orthogonal subgrid scales. Second order derivatives are exactly zero for linear elements and for higher order interpolation, disregarding them leads to a weakly consistent formulation in the context of finite elements, that is to say, the stabilization terms do not cancel for the exact solution but vanish as the mesh size goes to zero.

Taking into account all this information, the finite element discrete residuals can be written as in Equation 3.15, excluding viscous and external forcing terms as

$$\mathscr{R}(\mathbf{y}^{n+1};\mathbf{y}_h^{n+1}) = -\begin{bmatrix}\mathscr{R}_{\mathbf{u}}(\mathbf{y}^{n+1};\mathbf{y}_h^{n+1})\\ \mathscr{R}_p(\mathbf{y}^{n+1};\mathbf{y}_h^{n+1})\\ \mathscr{R}_\vartheta(\mathbf{y}^{n+1};\mathbf{y}_h^{n+1})\end{bmatrix}, \tag{5.23}$$

where the corresponding residuals of the momentum, mass and energy conservation equations are defined as follows:

$$\mathscr{R}_{\mathbf{u}}(\mathbf{y}^{n+1};\mathbf{y}_h^{n+1}) := \rho^{n+1}(\mathbf{a}^{n+1}\cdot\nabla)\mathbf{u}_h^{n+1} + \nabla p_h^{n+1}, \tag{5.24a}$$

$$\begin{aligned}\mathscr{R}_p(\mathbf{y}^{n+1};\mathbf{y}_h^{n+1}) :=& \beta^{n+1}(\mathbf{a}^{n+1}\cdot\nabla)p_h^{n+1} - \alpha^{n+1}(\mathbf{a}^{n+1}\cdot\nabla)\vartheta_h^{n+1}\\ &+\nabla\cdot\mathbf{u}_h^{n+1}, \qquad (5.24b)\\ \mathscr{R}_\vartheta(\mathbf{y}^{n+1};\mathbf{y}_h^{n+1}) :=& \rho^{n+1}c_v(\mathbf{a}^{n+1}\cdot\nabla)\vartheta_h^{n+1}\\ &+(\nabla\cdot\mathbf{u}_h^{n+1})p_h^{n+1}, \qquad (5.24c)\end{aligned}$$

and with $\mathbf{a}^{n+1} = \mathbf{u}_h^{n+1}$ or $\mathbf{a}^{n+1} = \mathbf{u}_h^{n+1} + \breve{\mathbf{u}}^{n+1}$ if the nonlinear character of the subscales was to be accounted for.

In addition, the adjoint operator is formally defined as

$$\mathscr{L}^*(\mathbf{y}^{n+1};\mathbf{z}_h) = -\begin{bmatrix}\mathscr{L}^*_{\mathbf{u}}(\mathbf{y}^{n+1};\mathbf{z}_h)\\ \mathscr{L}^*_p(\mathbf{y}^{n+1};\mathbf{z}_h)\\ \mathscr{L}^*_\vartheta(\mathbf{y}^{n+1};\mathbf{z}_h)\end{bmatrix}, \qquad (5.25)$$

and where the definition of the adjoint operators corresponding to the momentum, mass and energy equations are[3]

$$\begin{aligned}\mathscr{L}^*_{\mathbf{u}}(\mathbf{y}^{n+1};\mathbf{z}_h) :=& \nabla\cdot\left(\rho^{n+1}\mathbf{a}^{n+1}\otimes\mathbf{v}_h\right) + \nabla q_h, \qquad (5.26a)\\ \mathscr{L}^*_p(\mathbf{y}^{n+1};\mathbf{z}_h) :=& \nabla\cdot\mathbf{v}_h + \nabla\cdot\left(\beta^{n+1}\mathbf{a}^{n+1}q_h\right), \qquad (5.26b)\\ \mathscr{L}^*_\vartheta(\mathbf{y}^{n+1};\mathbf{z}_h) :=& -\nabla\cdot\left(\alpha^{n+1}\mathbf{a}^{n+1}q_h\right)\\ &+ c_v\nabla\cdot\left(\rho^{n+1}\mathbf{a}^{n+1}\eta_h\right). \qquad (5.26c)\end{aligned}$$

Furthermore, the subscales are time tracked in time by solving Equation 3.18 which for the problem in hand reads as follows

$$\begin{aligned}\tilde{\mathbf{u}}^{n+1} =& -\tau_{\mathbf{u},\mathrm{d}}\mathscr{P}_h^\perp\left[\rho(\mathbf{u}^{n+1}\cdot\nabla)\mathbf{u}_h^{n+1} + \nabla p_h^{n+1}\right]\\ &+ \tau_{\mathbf{u}}\rho\frac{\tilde{\mathbf{u}}^n}{\delta t}, \qquad (5.27a)\\ \tilde{p}^{n+1} =& -\tau_{p,\mathrm{d}}\mathscr{P}_h^\perp\left[\beta(\mathbf{u}^{n+1}\cdot\nabla)p_h^{n+1} - \alpha(\mathbf{u}^{n+1}\cdot\nabla)\vartheta_h^{n+1} + \nabla\cdot\mathbf{u}_h^{n+1}\right]\\ &+ \tau_p\beta\frac{\tilde{p}^n}{\delta t}, \qquad (5.27b)\\ \tilde{\vartheta}^{n+1} =& -\tau_{\vartheta,\mathrm{d}}\mathscr{P}_h^\perp\Big[\rho c_v(\mathbf{u}^{n+1}\cdot\nabla)\vartheta_h^{n+1} + (\nabla\cdot\mathbf{u}_h^{n+1})p_h\\ &-2\mu\boldsymbol{\varepsilon}(\mathbf{u}_h^{n+1}) : \boldsymbol{\varepsilon}(\mathbf{u}_h^{n+1}) + \frac{2}{3}\mu(\nabla\cdot\mathbf{u}_h^{n+1})^2\Big]\\ &+ \tau_\vartheta\rho c_v\frac{\tilde{\vartheta}^n}{\delta t}. \qquad (5.27c)\end{aligned}$$

5.7.2 On the stabilization parameters

Although the application of the VMS method to the compressible Navier-Stokes problem has already been discussed,

[3] Note that we have not included in the adjoint operator of the temperature equation the terms corresponding to the compression work and the dissipation function. The hope is that their influence on the stability of the scheme is small. The formulation is then weakly consistent, as already stated above, and it is designed by taking the subscales in the orthogonal space to the finite-dimensional resolved space.

the stabilization technique is not completed until one introduces a definition to compute the matrix of stabilization parameters $\boldsymbol{\tau}(\mathbf{y}^{n+1})$ (generally nonlinear). This is what we do next.

Up to our knowledge, there is no general rule to define it for systems of equations. It must be designed for each particular problem taking into account its stability deficiencies or even scaling requirements. For the problem in hand, we will take a simple diagonal expression. In the most general scenario we define

$$\boldsymbol{\tau}(\mathbf{y}^{n+1}) = \mathrm{diag}(\tau_{\mathbf{u}}\mathbf{I}_{N_{\mathrm{sd}}}, \tau_p, \tau_\vartheta). \tag{5.28}$$

and following Equation 3.19, we can now write

$$\tau_{\mathbf{u},\mathrm{d}} = \left[\frac{\rho}{\delta t} + \tau_{\mathbf{u}}^{-1}(\mathbf{y}^{n+1})\right]^{-1}, \tag{5.29a}$$

$$\tau_{p,\mathrm{d}} = \left[\frac{\beta}{\delta t} + \tau_{p}^{-1}(\mathbf{y}^{n+1})\right]^{-1}, \tag{5.29b}$$

$$\tau_{\vartheta,\mathrm{d}} = \left[\frac{\rho c_v}{\delta t} + \tau_{\vartheta}^{-1}(\mathbf{y}^{n+1})\right]^{-1}. \tag{5.29c}$$

The usual definition of the compressible stabilization parameters include a local sound velocity that arises from a linearization of the characteristic compressible flow problem (see [28] for a Fourier analysis). At the low Mach number limit the sound speed tends to infinity, and therefore such stabilization parameters are not suitable for the computations. In this work, we consider the following definition [29]:

$$\tau_{\mathbf{u}}^{-1} = c_1\frac{\mu}{h^2} + c_2\frac{\rho\xi}{h}, \tag{5.30a}$$

$$\tau_{p}^{-1} = \frac{\tau_{\mathbf{u}}}{h^2}, \tag{5.30b}$$

$$\tau_{\vartheta}^{-1} = c_1\frac{\kappa}{h^2} + c_2\frac{\rho c_v\xi}{h}. \tag{5.30c}$$

where we recall that h stands for the mesh size. It is understood that these expressions are evaluated element by element. The numerical constants c_1 and c_2 are independent of the physical parameters of the problem. In the numerical calculations we take them as,

$$c_1 = 15\omega^4,$$
$$c_2 = 2,$$

where ω stands for the order of the finite element interpolation. In the case of the largest characteristic velocity in the convective contribution, which theoretically should correspond to ($\|\mathbf{u}\| + a$), we introduce a modified velocity ξ, that we take as the harmonic mean value of $\|\mathbf{u}_h\|$ and a, that is to say

$$\xi = \frac{1}{\frac{1}{\|\mathbf{u}_h\|} + \frac{1}{a}}.$$

This definition for the characteristic velocity accounts for the effect of the sound speed, and ensures the proper definition at the zero Mach limit ($a \to \infty$).

5.7.3 Final stabilized problem

We shall start this part by specifically writing the stabilized version of the problem in hand. As stated before, the general equation is Equation 3.20, but now taking into account the definitions of the residuals and adjoint operators from the previous subsection. The final stabilized formulation is then nothing but an extension of the problem in Equation 5.19a–Equation 5.19c with the addition of the corresponding stabilization terms.

The final problem reads as follows: for $n = 0, 1, \dots, N-1$, solve for $\mathbf{u}_h^{n+1}$, p_h^{n+1} and ϑ_h^{n+1} given the values $\mathbf{u}_h^{n-l}$, p_h^{n-l}, ϑ_h^{n-l} for $l = 0$ to $\theta - 1$, such that

$$\begin{aligned}
&\langle \rho \ \delta_t \mathbf{u}_h^{n+1}, \mathbf{v}_h \rangle + c(\rho, \mathbf{u}_h^{n+1}; \mathbf{u}_h^{n+1}, \mathbf{v}_h) + a(\mathbf{u}_h^{n+1}, \mathbf{v}_h) - b(p_h^{n+1}, \mathbf{v}_h) \\
&\quad + c_\Gamma(\rho, \beta; \mathbf{u}_h^{n+1}, \mathbf{v}_h) + b_\Gamma(p_h^{n+1}, \mathbf{v}_h) \\
&\quad + \mathscr{B}^\perp_{\mathbf{uu},\mathrm{stab}}(\rho, \mathbf{u}_h^{n+1}; \mathbf{u}_h^{n+1}, \mathbf{v}_h) + \mathscr{B}^\perp_{\mathbf{u}p,\mathrm{stab}}(\rho, \mathbf{u}_h^{n+1}; p_h^{n+1}, \mathbf{v}_h) \\
&\quad + \mathscr{B}^\perp_{\mathbf{u}\vartheta,\mathrm{stab}}(\alpha, \mathbf{u}_h^{n+1}; \vartheta_h^{n+1}, \mathbf{v}_h) = \ell_{\mathbf{u}}(\rho; \mathbf{v}_h) + \ell_{\Gamma,\mathbf{u}}(\mathbf{v}_h) \\
&\quad + \ell_{\mathbf{u},\mathrm{stab}}(\rho; \mathbf{v}_h), && (5.31a) \\
&\langle \beta \ \delta_t p_h^{n+1}, q_h \rangle - \langle \alpha \delta_t \vartheta_h^{n+1}, q_h \rangle + d(\beta, \mathbf{u}_h^{n+1}; p_h^{n+1}, q_h) \\
&\quad - d(\alpha, \mathbf{u}_h^{n+1}; \vartheta_h^{n+1}, q_h) + b(q_h, \mathbf{u}_h^{n+1}) + b_\Gamma(q_h, \mathbf{u}_h^{n+1}) \\
&\quad + \mathscr{B}^\perp_{pp,\mathrm{stab}}(\alpha, \beta, \mathbf{u}_h^{n+1}; p_h^{n+1}, q_h) + \mathscr{B}^\perp_{p\mathbf{u},\mathrm{stab}}(\rho, \beta, \mathbf{u}_h^{n+1}; \mathbf{u}_h^{n+1}, q_h) \\
&\quad + \mathscr{B}^\perp_{p\vartheta,\mathrm{stab}}(\rho, \alpha, \beta, \mathbf{u}_h^{n+1}; \vartheta_h^{n+1}, q_h) = \ell_{\Gamma,p}(q_h) \\
&\quad + \ell_{p,\mathrm{stab}}(\rho, \alpha, \beta; q_h), && (5.31b) \\
&\langle \rho \ c_v \delta_t \vartheta_h^{n+1}, \eta_h \rangle + f(\rho, \mathbf{u}_h^{n+1}; \vartheta_h^{n+1}, \eta_h) + g(\mathbf{u}_h^{n+1}, p_h^{n+1}, \eta_h) \\
&\quad + e(\vartheta_h^{n+1}, \eta_h) + \mathscr{B}^\perp_{\vartheta\vartheta,\mathrm{stab}}(\rho, \mathbf{u}_h; \vartheta_h, \eta_h) = \ell_\vartheta(\rho, \mathbf{u}_h^{n+1}; \eta_h) \\
&\quad + \ell_{\vartheta,\mathrm{stab}}(\rho; \eta_h). && (5.31c)
\end{aligned}$$

where the following forms were introduced (dropping the superscript $n+1$ in order to simplify the notation),

$$\mathscr{B}^{\perp}_{\mathbf{uu},\mathrm{stab}}(\rho, \mathbf{u}_h; \mathbf{u}_h, \mathbf{v}_h) := \sum_{e=1}^{N_{\mathrm{el}}} \left\langle \nabla \cdot \mathbf{v}_h, \tau_{p,\mathrm{d}} \mathscr{P}_h^{\perp} \left[\nabla \cdot \mathbf{u}_h \right] \right\rangle$$

$$+ \sum_{e=1}^{N_{\mathrm{el}}} \left\langle \nabla \cdot (\rho \mathbf{u}_h \otimes \mathbf{v}_h), \tau_{\mathbf{u},\mathrm{d}} \mathscr{P}_h^{\perp} \left[\rho (\mathbf{u}_h \cdot \nabla) \mathbf{u}_h \right] \right\rangle, \tag{5.32a}$$

$$\mathscr{B}^{\perp}_{\mathbf{u}p,\mathrm{stab}}(\rho, \mathbf{u}_h; p_h, \mathbf{v}_h) := \sum_{e=1}^{N_{\mathrm{el}}} \left\langle \nabla \cdot (\rho \mathbf{u}_h \otimes \mathbf{v}_h), \tau_{\mathbf{u},\mathrm{d}} \mathscr{P}_h^{\perp} \left[\nabla p_h \right] \right\rangle$$

$$+ \sum_{e=1}^{N_{\mathrm{el}}} \left\langle \nabla \cdot \mathbf{v}_h, \tau_{p,\mathrm{d}} \mathscr{P}_h^{\perp} \left[\beta (\mathbf{u}_h \cdot \nabla) p_h \right] \right\rangle, \tag{5.32b}$$

$$\mathscr{B}^{\perp}_{\mathbf{u}\vartheta,\mathrm{stab}}(\alpha, \mathbf{u}_h; \vartheta_h, \mathbf{v}_h) := \sum_{e=1}^{N_{\mathrm{el}}} \left\langle \nabla \cdot \mathbf{v}_h, \tau_{p,\mathrm{d}} \mathscr{P}_h^{\perp} \left[-\alpha (\mathbf{u}_h \cdot \nabla) \vartheta_h \right] \right\rangle, \tag{5.32c}$$

$$\mathscr{B}^{\perp}_{pp,\mathrm{stab}}(\alpha, \beta, \mathbf{u}_h; p_h, q_h) := \sum_{e=1}^{N_{\mathrm{el}}} \left\langle \nabla \cdot q_h, \tau_{\mathbf{u},\mathrm{d}} \mathscr{P}_h^{\perp} \left[\nabla p_h \right] \right\rangle$$

$$+ \sum_{e=1}^{N_{\mathrm{el}}} \left\langle \nabla \cdot (\beta \mathbf{u}_h q_h), \tau_{p,\mathrm{d}} \mathscr{P}_h^{\perp} \left[\beta (\mathbf{u}_h \cdot \nabla) p_h \right] \right\rangle$$

$$- \sum_{e=1}^{N_{\mathrm{el}}} \left\langle \nabla \cdot (\alpha \mathbf{u}_h q_h), \tau_{\vartheta,\mathrm{d}} \mathscr{P}_h^{\perp} \left[(\nabla \cdot \mathbf{u}_h) p_h \right] \right\rangle \tag{5.32d}$$

$$\mathscr{B}^{\perp}_{p\mathbf{u},\mathrm{stab}}(\rho, \beta, \mathbf{u}_h; \mathbf{u}_h, q_h) := \sum_{e=1}^{N_{\mathrm{el}}} \left\langle \nabla \cdot (\beta \mathbf{u}_h q_h), \tau_{p,\mathrm{d}} \mathscr{P}_h^{\perp} \left[\nabla \cdot \mathbf{u}_h \right] \right\rangle$$

$$+ \sum_{e=1}^{N_{\mathrm{el}}} \left\langle \nabla q_h, \tau_{\mathbf{u},\mathrm{d}} \mathscr{P}_h^{\perp} \left[\rho (\mathbf{u}_h \cdot \nabla) \mathbf{u}_h \right] \right\rangle \tag{5.32e}$$

$$\mathscr{B}^{\perp}_{p\vartheta,\mathrm{stab}}(\rho, \alpha, \beta, \mathbf{u}_h; \vartheta_h, q_h) := \sum_{e=1}^{N_{\mathrm{el}}} \left\langle \nabla \cdot (\beta \mathbf{u}_h q_h), \tau_{p,\mathrm{d}} \mathscr{P}_h^{\perp} \left[-\alpha (\mathbf{u}_h \cdot \nabla) \vartheta_h \right] \right\rangle$$

$$- \sum_{e=1}^{N_{\mathrm{el}}} \left\langle \nabla \cdot (\alpha \mathbf{u}_h q_h), \tau_{\vartheta,\mathrm{d}} \mathscr{P}_h^{\perp} \left[\rho c_v (\mathbf{u}_h \cdot \nabla) \vartheta_h \right] \right\rangle \tag{5.32f}$$

$$\mathscr{B}^{\perp}_{\vartheta\vartheta,\mathrm{stab}}(\rho, \mathbf{u}_h; \vartheta_h, \eta_h) := \sum_{e=1}^{N_{\mathrm{el}}} \left\langle \nabla \cdot (\rho c_v \mathbf{u}_h \eta_h), \tau_{\vartheta,\mathrm{d}} \mathscr{P}_h^{\perp} \left[\rho c_v (\mathbf{u}_h \cdot \nabla) \vartheta_h \right] \right\rangle \tag{5.32g}$$

$$\ell_{\mathbf{u},\mathrm{stab}}(\rho, \beta; \mathbf{v}_h) := \sum_{e=1}^{N_{\mathrm{el}}} \left\langle \nabla \cdot (\rho \mathbf{u}_h \otimes \mathbf{v}_h), \tau_{\mathbf{u},\mathrm{d}} \rho \frac{\tilde{\mathbf{u}}^n}{\delta t} \right\rangle$$

$$+\left\langle \nabla\cdot\mathbf{v}_h, \tau_{p,\mathrm{d}}\beta\frac{\tilde{p}^n}{\delta t}\right\rangle \tag{5.32h}$$

$$\ell_{p,\mathrm{stab}}(\rho,\alpha,\beta;q_h) := \sum_{e=1}^{N_{\mathrm{el}}}\left\langle \nabla\cdot(\beta\mathbf{u}_h q_h), \tau_{p,\mathrm{d}}\beta\frac{\tilde{p}^n}{\delta t}\right\rangle$$

$$+\left\langle \nabla q_h, \tau_{\mathbf{u},\mathrm{d}}\rho\frac{\tilde{\mathbf{u}}^n}{\delta t}\right\rangle - \left\langle \nabla\cdot(\alpha\mathbf{u}_h q_h), \tau_{\vartheta,\mathrm{d}}\rho c_v\frac{\tilde{\vartheta}^n}{\delta t}\right\rangle \tag{5.32i}$$

$$\ell_{\vartheta,\mathrm{stab}}(\rho;\eta_h) := \left\langle \nabla\cdot(\rho c_v\mathbf{u}_h\eta_h), \tau_{\vartheta,\mathrm{d}}\rho c_v\frac{\tilde{\vartheta}^n}{\delta t}\right\rangle \tag{5.32j}$$

and all the integrals evaluated over $\Omega^{(e)}$.

5.7.4 Stabilized fractional step algorithm

The final variational formulation of the compressible problem was stated in Equation 5.19a–Equation 5.19c. From there, the derivation of the matrix version is straightforward and the matrix system that needs to be solved at each time step has the same algebraic structure as Equation 5.21 with the addition of the corresponding stabilization arrays, as we show in Table 5.4. From this point, the derivation of the fractional step procedure can be facilely extended to account for the stabilization arrays and follows the same steps as done before. In addition, the unknown projections for a given equation can be computed with the values at the previous time

Matrix version	Term where it comes from
$\mathbf{V}^T\mathbf{S}_{\mathbf{uu}}(\mathbf{U})\,\mathbf{U}$	$\mathscr{B}^{\perp}_{\mathbf{uu},\mathrm{stab}}(\rho,\mathbf{u}_h;\mathbf{u}_h,\mathbf{v}_h)$
$\mathbf{V}^T\mathbf{S}_{\mathbf{u}p}(\mathbf{U})\,\mathbf{P}$	$\mathscr{B}^{\perp}_{\mathbf{u}p,\mathrm{stab}}(\rho,\mathbf{u}_h;p_h,\mathbf{v}_h)$
$\mathbf{V}^T\mathbf{S}_{\mathbf{u}\vartheta}(\mathbf{U})\,\boldsymbol{\Theta}$	$\mathscr{B}^{\perp}_{\mathbf{u}\vartheta,\mathrm{stab}}(\alpha,\mathbf{u}_h;\vartheta_h,\mathbf{v}_h)$
$\mathbf{V}^T\mathbf{F}_{\mathbf{u},\mathrm{stab}}$	$\ell_{\mathbf{u},\mathrm{stab}}(\rho,\beta,\mathbf{v}_h)$
$\mathbf{Q}^T\mathbf{S}_{pp}(\mathbf{U})\,\mathbf{P}$	$\mathscr{B}^{\perp}_{pp,\mathrm{stab}}(\alpha,\beta,\mathbf{u}_h;p_h,q_h)$
$\mathbf{Q}^T\mathbf{S}_{p\mathbf{u}}(\mathbf{U})\,\mathbf{U}$	$\mathscr{B}^{\perp}_{p\mathbf{u},\mathrm{stab}}(\rho,\beta,\mathbf{u}_h;\mathbf{u}_h,q_h)$
$\mathbf{Q}^T\mathbf{S}_{p\vartheta}(\mathbf{U})\,\boldsymbol{\Theta}$	$\mathscr{B}^{\perp}_{p\vartheta,\mathrm{stab}}(\rho,\alpha,\beta,\mathbf{u}_h;\vartheta_h,q_h)$
$\mathbf{Q}^T\mathbf{F}_{p,\mathrm{stab}}$	$\ell_{p,\mathrm{stab}}(\rho,\alpha,\beta;q_h)$
$\mathbf{H}^T\mathbf{S}_{\vartheta\vartheta}(\mathbf{U})\,\boldsymbol{\Theta}$	$\mathscr{B}^{\perp}_{\vartheta\vartheta,\mathrm{stab}}(\rho,\mathbf{u}_h;\vartheta_h,\eta_h)$
$\mathbf{H}^T\mathbf{F}_{\vartheta,\mathrm{stab}}$	$\ell_{\vartheta,\mathrm{stab}}(\rho;q_h)$

Table 5.4: Matrix form of the stabilization terms.

step or iteration. The final algorithm is included down below.

First and second order stabilized fractional step scheme for the primitive Navier-Stokes problem

```
▸ Set/read the initial conditions for $\mathbf{U}^0$, $\mathbf{P}^0$ and $\boldsymbol{\Theta}^0$.
▸ WHILE $n < N$ DO
    • Set $\mathbf{U}^{n,0} = \mathbf{U}^{n-1}$, $\mathbf{P}^{n,0} = \mathbf{P}^{n-1}$ and $\boldsymbol{\Theta}^{n,0} = \boldsymbol{\Theta}^{n-1}$
    • WHILE (not converged) DO
        ⋆ Compute intermediate velocity $\widetilde{\mathbf{U}}^{n+1}$:

          $\mathbf{M}_{\mathbf{uu},\rho^n} \frac{D_\theta}{\delta t} \widetilde{\mathbf{U}}^{n+1,(i+1)} + \mathbf{K}_{\mathbf{uu},\rho^n} \left( \widetilde{\mathbf{U}}^{n+1,(i)} \right) \widetilde{\mathbf{U}}^{n+1,(i+1)}$
              $+ \mathbf{M}_{\Gamma,\mathbf{uu}} \widetilde{\mathbf{U}}^{n+1,(i+1)} + \mathbf{K}_{\Gamma,\mathbf{uu}_{,\rho^n \beta^n}} \widetilde{\mathbf{U}}^{n+1,(i+1)}$
              $+ \mathbf{S}_{\mathbf{uu},\rho^n} \left( \widetilde{\mathbf{U}}^{n+1,(i)} \right) \widetilde{\mathbf{U}}^{n+1,(i+1)} = \mathbf{F}_{\mathbf{U}}^{n+1}$
              $+ \mathbf{K}_{\mathbf{u}p} \hat{\mathbf{P}}_{\theta-1}^{n+1} - \mathbf{K}_{\Gamma,\mathbf{u}p} \hat{\mathbf{P}}_{\theta}^{n+1}$
              $- \mathbf{S}_{\mathbf{u}p,\rho^n \beta^n} \left( \widetilde{\mathbf{U}}^{n+1,(i)} \right) \mathbf{P}^n$
              $- \mathbf{S}_{\mathbf{u}\vartheta,\alpha^n} \left( \widetilde{\mathbf{U}}^{n+1,(i)} \right) \boldsymbol{\Theta}^n$
              $+ \mathbf{F}_{\mathbf{u},\rho^n,\text{stab}} \left( \widetilde{\mathbf{U}}^{n+1,(i)} \right)$

        ⋆ Check convergence
    • END while (not converged)
    • WHILE (not converged) DO
        ⋆ Compute the intermediate temperature $\widetilde{\boldsymbol{\Theta}}^{n+1}$
          after solving:

          $\mathbf{M}_{\vartheta\vartheta,\rho^{(i)}} \frac{D_\theta}{\delta t} \widetilde{\boldsymbol{\Theta}}^{n+1,(i+1)} + \mathbf{K}_{\vartheta\vartheta,\rho^{(i)}} \left( \widetilde{\mathbf{U}}^{n+1} \right) \widetilde{\boldsymbol{\Theta}}^{n+1,(i+1)}$
              $+ \mathbf{S}_{\vartheta\vartheta,\rho^{(i)}} \left( \widetilde{\mathbf{U}}^{n+1} \right) \widetilde{\boldsymbol{\Theta}}^{n+1,(i+1)} = \mathbf{F}_{\boldsymbol{\Theta}}^{n+1}$
              $- \mathbf{K}_{\vartheta p} \left( \widetilde{\mathbf{U}}^{n+1} \right) \hat{\mathbf{P}}_{\theta-1}^{n+1} + \mathbf{F}_{\vartheta,\rho^{(i)},\text{stab}}$

        ⋆ Check convergence
    • END while (not converged)
    • WHILE (not converged) DO
        ⋆ Compute the pressure $\mathbf{P}^{n+1}$ using the intermediate velocity and temperature:

          $\mathbf{M}_{pp,\beta^{(i)}} \frac{D_\theta}{\delta t} \mathbf{P}^{n+1,(i+1)} + \mathbf{K}_{pp,\beta^{(i)}} \left( \widetilde{\mathbf{U}}^{n+1} \right) \mathbf{P}^{n+1,(i+1)}$
```

$$\begin{aligned}
&+ \phi_\theta \delta t \mathbf{Q}_{\rho^{(i)}\alpha^{(i)}} \left(\mathbf{P}^{n+1,(i+1)} - \hat{\mathbf{P}}^{n+1}_{\theta-1}\right)\\
&+ \phi_\theta \delta t \mathbf{L}_{\rho^{(i)}} \left(\mathbf{P}^{n+1,(i+1)} - \hat{\mathbf{P}}^{n+1}_{\theta-1}\right)\\
&+ \mathbf{S}_{pp,\alpha^n,\beta^{(i)}} \left(\widetilde{\mathbf{U}}^{n+1}\right) \mathbf{P}^{n+1,(i+1)} = \mathbf{F}^{n+1}_{\mathbf{P}}\\
&- \mathbf{K}_{p\mathbf{u}} \widetilde{\mathbf{U}}^{n+1} + \mathbf{K}_{p\vartheta\,,\alpha^{(i)}} \left(\widetilde{\mathbf{U}}^{n+1}\right) \widetilde{\boldsymbol{\Theta}}^{n+1}\\
&+ \mathbf{M}_{p\vartheta\,,\alpha^{(i)}} \frac{D_\theta}{\delta t} \widetilde{\boldsymbol{\Theta}}^{n+1} - \mathbf{K}_{\Gamma,p\mathbf{u}} \widetilde{\mathbf{U}}^{n+1}\\
&- \mathbf{S}_{p\mathbf{u},\rho^{(i)}\beta^{(i)}} \left(\widetilde{\mathbf{U}}^{n+1}\right) \widetilde{\mathbf{U}}^{n+1}\\
&- \mathbf{S}_{p\vartheta,\rho^{(i)}\alpha^n\beta^{(i)}} \left(\widetilde{\mathbf{U}}^{n+1}\right) \widetilde{\boldsymbol{\Theta}}^{n+1}\\
&+ \mathbf{F}_{p,\rho^{(i)}\alpha^n\beta^{(i)},\mathrm{stab}}
\end{aligned}$$

    * Check convergence

  - END while (not converged)
  - Velocity correction to obtain the end-of-step velocity $\mathbf{U}^{n+1}$:

$$\begin{aligned}
\mathbf{M}_{\mathbf{uu},\rho^{n+1}} \frac{1}{\phi_\theta \delta t} \mathbf{U}^{n+1} + \mathbf{M}_{\Gamma,\mathbf{uu}} \mathbf{U}^{n+1} &= \mathbf{M}_{\mathbf{uu},\rho^{n+1}} \frac{1}{\phi_\theta \delta t} \widetilde{\mathbf{U}}^{n+1}\\
&+ \mathbf{M}_{\Gamma,\mathbf{uu}} \widetilde{\mathbf{U}}^{n+1} + \mathbf{K}_{\mathbf{u}p} \left(\mathbf{P}^{n+1} - \hat{\mathbf{P}}^{n+1}_{\theta-1}\right)
\end{aligned}$$

  - Temperature correction to obtain the end-of-step temperature $\boldsymbol{\Theta}^{n+1}$:

$$\begin{aligned}
&\mathbf{M}_{\vartheta\vartheta,\rho^{n+1}} \frac{1}{\phi_\theta \delta t} \left(\boldsymbol{\Theta}^{n+1} - \widetilde{\boldsymbol{\Theta}}^{n+1}\right)\\
&\qquad = -\mathbf{K}_{\vartheta p} \left(\mathbf{U}^{n+1}\right) \left(\mathbf{P}^{n+1} - \hat{\mathbf{P}}^{n+1}_{\theta-1}\right)
\end{aligned}$$

▸ END while $n < N$ (non-stationary)

5.7.5 A final note on implementation

As stated before in this work, the primitive formulation for ideal gases in the low Mach number limit results in very large quantities in the continuity and energy equations, specially if the international system of units is to be used. When an implicit numerical scheme is used, the resulting linear system of equations which needs to be solved at each time step commonly contains very large values for these two equations, making it very inefficient to solve by using iterative methods. In order to overcome this difficulty, we perform a decomposition of the primitive (absolute) variables into a relative (or *gauge*) part and a reference (or *atmospheric*) part. Thus, we set

$$p = p^* + p_{\text{atm}} \quad , \quad \mathbf{u} = \mathbf{u}^* \quad \text{and} \quad \vartheta = \vartheta^* + \theta_{\text{atm}},$$

assuming the atmospheric values to be constant. Taking this into account, we may write the initial system of equations using the relative part of the unknowns, but taking special care of the non-linear terms, where the complete contribution is needed to obtain reliable results. Furthermore, initial and boundary conditions must be set for the primitive problem written using relative unknowns.

5.8 Numerical Experiments

In this section we include some numerical examples in order to demonstrate, on the one hand, the performance of the proposed stabilized fractional scheme and, on the other hand, the suitability of the developed method to replace a standard monolithic strategy.

First, we perform a test with analytical solution in order to numerically check the convergence rate in time. Next, we include a classical benchmark in the field of aeroacoustics, which consists in simulating the sound generated by the flow past a cylinder, also known as the aeolian tones problem. The last example is based on simulating the differentially heated flow inside a cavity, which is a well-known benchmark for thermal problems.

As stated in the introduction, all the implementations have been carried out into our in-house code `FEMUSS` after the development from scratch of a specific solver module for compressible flow simulations. In order to solve the final underlying systems of linear equations, if nothing else is stated, we make use of an iterative algorithm based on the stabilized version of the BiConjugate Gradient method `BiCGstab` [143], which is already included in the `PETSc` parallel solver library [61]. In order to solve the nonlinearities , we set a maximum of 10 iterations, and the relative numerical tolerance for the L^2-norm is 1×10^{-5}. For all the upcoming numerical simulations, we consider an ideal gas with $\gamma = 1.4$ ($\mathrm{R_g} = 287$ J/(kg K)) and $c_p = 1004.5$ J/(kg K). All the plots are in SI units.

5.8.1 Convergence test

The first example is a convergence test where we analyze the time errors of the fractional step scheme, similar to the one from [38]. Here we make use of the method of manufactured solutions, which has been traditionally used to quantify the numerical error of partial differential equations solvers. In this example, an exact solution for pressure, velocity and temperature is specified in the computational domain, which are composed of smooth functions, yet they have no physical meaning. We solve the Navier-Stokes problem over the unit square $\overline{\Omega} = [0,1]^2$ and the force term is set so that the exact solution of the problem is:

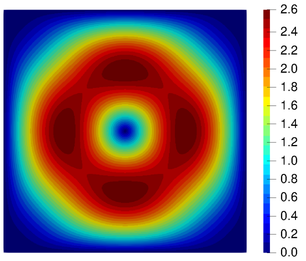

Figure 5.1: Convergence test: contour plot of the exact velocity magnitude $\|\mathbf{u}(\mathbf{x},t)\|$ at $t = 1$ s.

$$p^*(x_1,x_2,t) = \cos(\pi x_1)\sin(\pi x_2)\sin(t), \tag{5.33a}$$

$$u(x_1,x_2,t) = \pi\sin(2\pi x_2)\sin^2(\pi x_1)\sin(t), \tag{5.33b}$$

$$v(x,y,t) = -\pi\sin(2\pi x_1)\sin^2(\pi x_2)\sin(t), \tag{5.33c}$$

$$\vartheta^*(x_1,x_2,t) = u(x_1,x_2,t). \tag{5.33d}$$

The contour plots of these fields are presented for completeness in Figure 5.1–Figure 5.4. The finite element partition is structured and uniform and contains $Q_2/Q_2/Q_2$ finite elements of size $h = 1/200$. Both the boundary and initial conditions are evaluated from the previous equations, and particularized for each of the sides of the square at each time step and for $t = 0$, respectively. We use a range of time step sizes from 0.1 s to 0.003125 s and the problem is solved until $t_f = 1$ s. In addition, we set $\mu = 0.001$ kg/(m s), $\kappa = 1$ W/(m K), $p_{\text{atm}} = 1 \times 10^5$ Pa and $\vartheta_{\text{atm}} = 300$ K and we make use of a sparse direct solver from the MUMPS library [157, 158].

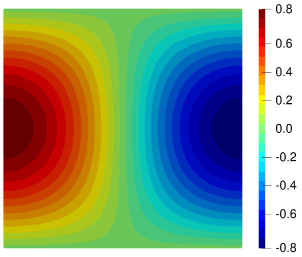

Figure 5.2: Convergence test: contour plot of the exact pressure function $p^*(\mathbf{x},t)$ at $t = 1$ s.

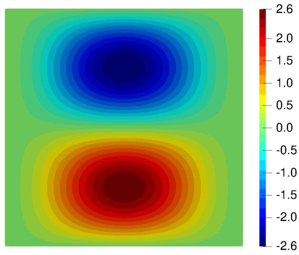

Figure 5.3: Convergence test: contour plot of the exact temperature function $\vartheta^*(\mathbf{x},t)$ at $t = 1$ s.

The error between the exact solution of the Navier-Stokes equations and the numerical one is measured in the ℓ^2-norm of the sequence of spatial L^2-norms of the solutions, *i.e.*

$$E_f := \left(\delta t \sum_{n=1}^{N} \frac{\|f_h^n - f(t^n)\|_{L^2}^2}{\|f(t^n)\|_{L^2}^2}\right)^{1/2},$$

for $f = \mathbf{u}$, p or ϑ, respectively.

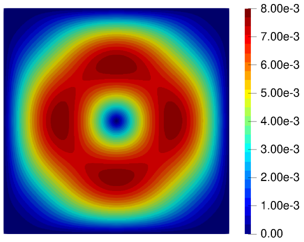

Figure 5.4: Convergence test: contour plot of the associated Mach number distribution Ma at $t = 1$ s.

In Figure 5.5 we compare the convergence results of the standard monolithic solution with the ones obtained with the fractional step algorithm for both first and second order time integration schemes. The monolithic results can be used as a reference against which the results obtained with the fractional step can be compared because they have no splitting error. The expected convergence rate can be clearly seen for both temporal approximations and for all the time step sizes, yet the splitting errors of the fractional step approach become more noticeable for the BDF2 scheme. From the convergence plots it is also observed that the spatial error is not significant for the mesh size used.

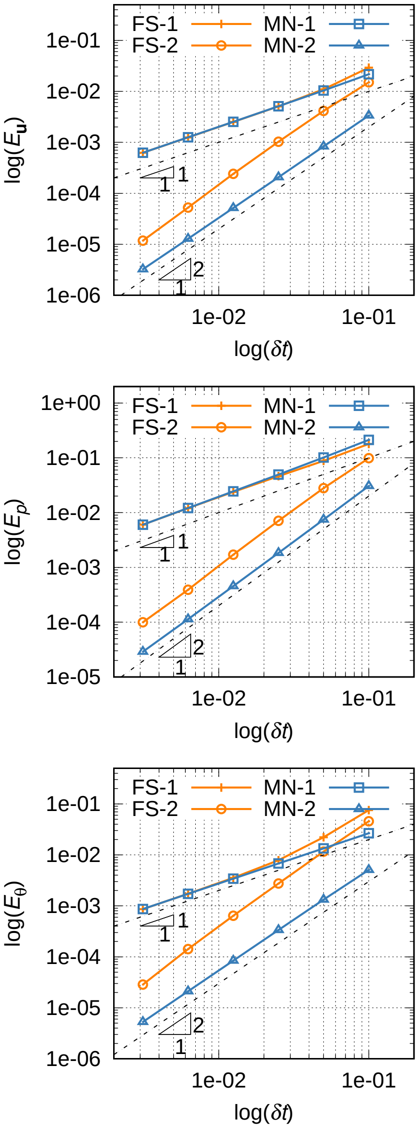

Figure 5.5: Convergence test: time convergence of the relative errors of velocity (top), pressure (middle) and temperature (bottom) measured in the $\ell^2(0, t_f, L^2(\Omega))$-norm. Here and in what follows, `FS` stands for fractional step results and `MN` for monolithic results. The number after the dash symbol stands for first (1) or second (2) order scheme in time.

5.8.2 Aeolian tones: flow past a cylinder

The next example consists in a two-dimensional circular cylinder embedded in a flow with free stream. We use this example to evaluate the performance of the VMS formulation in unsteady flows and to test the proposed non-reflecting boundary conditions.

In this problem, a sequence of vortices are generated at the lee of the cylinder which are transported downstream. As a reaction to this fact, the cylinder undergoes lift fluctuations that lead to the emission of sound, with a wave frequency established at the fixed value of the wake fluctuation. The emitted noise is commonly referred to as an aeolian tone.

The computational domain for this simulation is

$$\overline{\Omega} = [0,0] \times [50,50] \setminus \mathfrak{C}$$

being $\mathfrak{C}$ the cylinder region of diameter $D = 0.1$ m which is placed at point $O(20,25)$. The domain is big enough to describe the far field conditions far away from the cylinder. A free stream enters from the left-most boundary with the following data:

$$\begin{aligned} u_\infty &= 70 \text{ m/s}, \\ v_\infty &= 0 \text{ m/s}, \\ p_\infty &= p_{\text{atm}} = 101325 \text{ Pa}, \\ \vartheta_\infty &= \vartheta_{\text{atm}} = 300 \text{ K}, \end{aligned}$$

which allow to match the tested flow conditions

$$\text{Re}_\infty = 150, \quad \text{and} \quad \text{Ma}_\infty = 0.2,$$

for which meaningful 2D calculations can be performed. The Prandtl number is $\text{Pr} = 0.75$.

No slip-adiabatic boundary conditions are prescribed on the cylinder surface and the free stream values are used as initial condition. We solve the compressible Navier-Stokes equations on an unstructured mesh of linear triangular elements, progressively refined on the cylinder surface, accounting for a total of $N_{\text{el}} \sim 225{,}000$ elements. The time step size used in the computation is constant and equal to $\delta t = 0.0001$ s. The second order BDF2 scheme has been used for the large scales time evolution, while a first-order scheme has been used for the tracking of the subscales. In order to overcome all the burden related to any possible wave reflections at the external walls, we use the boundary formulation described in Section 5.4 and for this purpose we set a filtering frequency of 200 Hz.

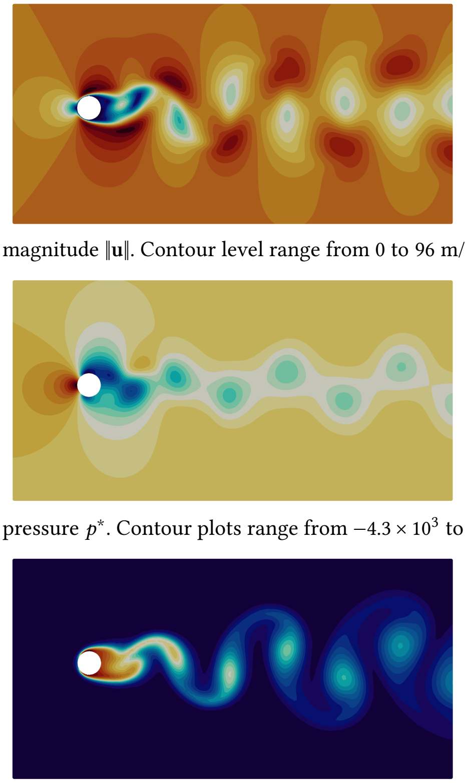

(a) Velocity magnitude $\|\mathbf{u}\|$. Contour level range from 0 to 96 m/s.

(b) Relative pressure p^*. Contour plots range from -4.3×10^3 to 3.1×10^3 Pa.

(c) Relative temperature ϑ^*. Contour plots range from 0 to 6 K.

Figure 5.6: 2D flow past a cylinder: near-field contours, (a) velocity magnitude $\|\mathbf{u}\|$, (b) relative pressure p^* and (c) relative temperature ϑ^* obtained with the fractional step scheme.

In Figure 5.6 we present a depiction of the near-field developed flow, including the instantaneous contours of velocity (magnitude), pressure and temperature obtained with the fractional step algorithm. As we can see, they display the classical oscillating wake after the cylinder surface. Since no notable differences were observed between the results of both the monolithic and fractional step counterpart, we provide a quantitative comparison by computing some aerodynamic integral values of the flow. In particular, we calculate the lift and drag non-dimensional coefficients using Equation 4.38a and Equation 4.38b.

Several studies on flow past bluff bodies, *e.g.*, [159, 160] discuss that time varying fluctuating loads over the surface of

[159]: Liow et al. (2006), "Sound generated in laminar flow past a two-dimensional rectangular cylinder"

[160]: Mahato et al. (2018), "Direct simulation of sound generation by a two-dimensional flow past a wedge"

the studied body (fluctuations in lift and drag coefficients) are the main mechanism for generation and propagation of sound waves. Here we evaluate the fluctuations in the lift and drag coefficients (which we denote hereafter as C_l' and C_d', respectively) as the difference between their instantaneous and mean values, respectively.

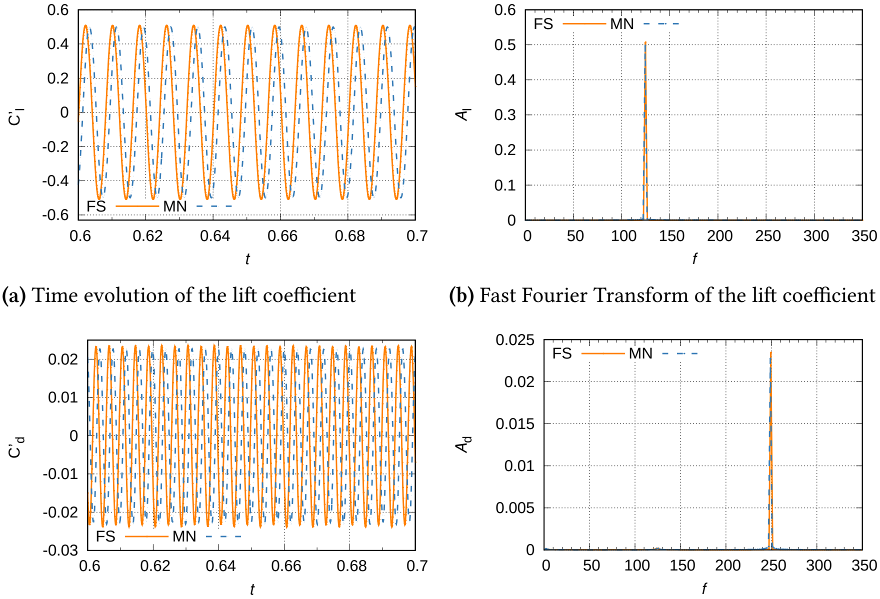

(a) Time evolution of the lift coefficient

(b) Fast Fourier Transform of the lift coefficient

(c) Time evolution of the draf coefficient

(d) Fast Fourier Transform of the dradg coeffcient

Figure 5.7: 2D flow past a cylinder: part of the time history of the fluctuating non-dimensional lift (a) and drag (c) coefficients, together with FFTs obtained for time varying fluctuations in lift (b) and drag (d).

A part of the time history of the lift and drag fluctuations is presented in Figure 5.7a and Figure 5.7c for both monolithic and fractional step schemes. The Fast Fourier Transform (FFT) of these time varying signals has been obtained, and the plots of the corresponding Fourier amplitudes (A_l and A_d) as a function of the Fourier frequency are presented in Figure 5.7b and Figure 5.7d.

Both monolithic and segregated methods basically provide the same frequencies of oscillation for lift and drag. The lift coefficient oscillates at a frequency of 124.673 Hz (St = 0.178), and the drag coefficient at 249.341 Hz (twice of the vortex shedding one). Additional statistic results are collected in Table 5.5, together with some reference values reported in the literature and which cover a different variety of numerical methods [161–164]. An overall agreement can be ob-

[161]: Margnat (2015), "Hybrid prediction of the aerodynamic noise radiated by a rectangular cylinder at incidence"

[162]: Inoue et al. (2002), "Sound generation by a two-dimensional circular cylinder in a uniform flow"

[163]: Laffite et al. (2009), "Investigation of the Noise Generated by Cylinder Flows Using a Direct Lattice-Boltzmann Approach"

[164]: Ganta et al. (2019), "Analysis of sound generation by flow past a circular cylinder performing rotary oscillations using direct simulation approach"

served.

Regarding the propagation of acoustic waves, Figure 5.8 contains the far field pressure contours at two certain time steps obtained with the fractional step algorithm, one before the acoustic waves reach the external boundaries and another one on the long term once the waves hit the artificial contours. The vortices located at the wake of the cylinder perturb the pressure field, which is propagated in the form of sound waves. These pressure pulses evolve radially from the cylinder area with time, yet they do not propagate normally to the flow direction since this case is based on an uniform flow. The inclusion of non-reflecting boundary conditions (or any other dumping technique) is essential for the adequate reproduction of the pressure waves, due to the fact that reflections may occur at the external boundary and hence local numerical oscillations may end up polluting the solution.

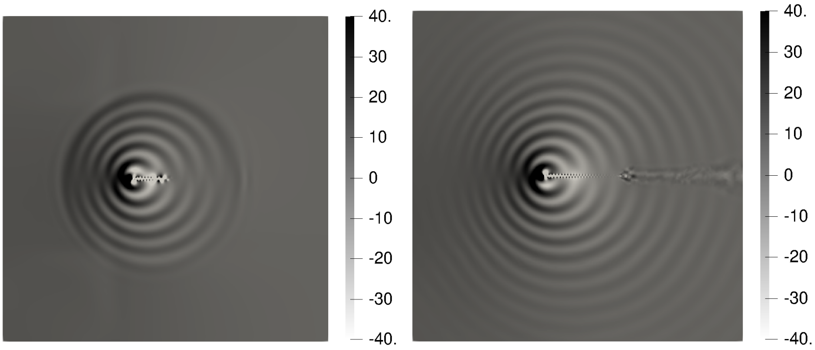

(a) Relative pressure p^* at $t = 0.05$ s.

(b) Relative pressure p^* at $t = 0.5$ s.

Figure 5.8: 2D flow past a cylinder: relative pressure p^* contours showing the propagation of sound waves towards the far field at two different time instants. Monolithic contour plots are omitted since they are remarkably similar.

In addition to this, a plot concerning the pressure wave along the positive y direction is included in Figure 5.9. We observe that our fractional step scheme is able to agreeably replicate the dissipation of the radiated sound wave of the monolithic scheme (which serves as reference here, [29]), yet minor discrepancies might be noticed. These minor differences should come from the splitting error introduced by the segregated approach as well as from the approximate boundary condition.

Table 5.5: 2D flow past a cylinder: aerodynamic statistics for $\mathrm{Re}_\infty = 150$ and $\mathrm{Ma}_\infty = 0.2$. IBM: Immersed boundary method, FD-DNC: Finite difference Direct Numerical Simulation, LBM: Lattice Boltzmann method, FE: Finite Element.

Ref.	Method	$\overline{C_\mathrm{d}}$	A_d	A_l	St
Margnat [161]	Hybrid IBM	1.35	0.026	0.52	0.189
Inoue & Hatakeyama [162]	FD-DNC	1.32	0.026	0.52	0.183
Laffite & Pérot [163]	LBM	1.39	0.028	0.56	0.183
Ganta *etal* [164]	FD-DNC	1.34	0.026	0.53	0.183
Present	FE-MN	1.328	0.023	0.499	0.178
Present	FE-FS	1.334	0.022	0.508	0.178

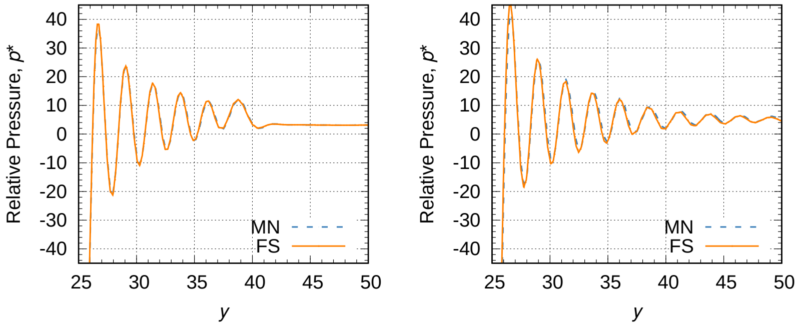

(a) Time $t = 0.05$ s.

(b) Time $t = 0.5$ s.

Figure 5.9: 2D flow past a cylinder: instantaneous pressure along the positive y direction from the center of the cylinder.

5.8.3 Differentially heated flow inside a cavity

In this numerical simulation, we model the flow in a differentially heated cavity both in 2D and 3D configurations (see *e.g.* [165]). This is a natural convection flow problem in which the fluid is driven both by a large temperature gradient between two walls and by a gravity force, which plays a significant role in the development of the buoyancy flow patterns.

[165]: Christon et al. (2002), "Computational predictability of time-dependent natural convection flows in enclosures (including a benchmark solution)"

The purpose of this example is twofold. First, we use this example to evaluate the applicability of the developed compressible formulation in the low Mach number limit and to investigate its behavior in unsteady chaotic flows. Second, we will perform some simple tests in order to provide some insights on the actual computational savings that the fractional step implementation offers with respect to the standard monolithic solver.

2D flow in a differentially heated cavity with aspect ratio 8: Pr $= 0.71$, Ra $= 1 \times 10^6$

Let us start by solving a 2D configuration. The computational domain is given by a rectangular cavity

$$\overline{\Omega} = [0, L] \times [0, H]$$

with $H/L = 8$ and $L = 1$ m.

The prescription of boundary conditions is as follows: the temperatures on the left and right boundaries, respectively hot and cold walls, are fixed to $\vartheta_{\mathrm{g,hot}} = 600$ K and $\vartheta_{\mathrm{g,cold}} = 300$ K, while adiabatic boundary conditions are prescribed on the upper and lower walls. No slip conditions are set for the velocity over all the boundaries. No pressure boundary conditions are prescribed for this example, yet we include an iterative penalization term of the form

$$\left\langle \psi \left(p_h^{n+1,(i+1)} - p_h^{n+1,(i)} \right), q_h \right\rangle$$

to the mass conservation equation at the ith iteration. This aims to overcome the mechanical pressure resolution for transient and confined flows, where small local oscillations of pressure might generate overall distortions on the global pressure levels. The factor ψ needs to be defined in such a way that it does not detriment neither the algebraic solver nor the convergence of the iterative procedure. For this simulation, we take $\psi = 1 \times 10^{-6}/\mu$, definition which renders this new term dimensionally consistent.

The initial conditions to start the computations are prescribed all over the whole domain as:

$$\begin{aligned} \mathbf{u}_0 &= \mathbf{0} \text{ m/s}, \\ p_0 &= p_{\mathrm{atm}} = 152525 \text{ Pa}, \\ \vartheta_0 &= \vartheta_{\mathrm{atm}} = 450 \text{ K}. \end{aligned}$$

The gravity acceleration is specified with a modulus $\|\mathbf{g}\| = 9.81$ m/s^2, acting on the negative y direction (downwards). For this problem we consider

$$\mathrm{Pr} = 0.71, \quad \text{and} \quad \mathrm{Ra} = 1 \times 10^6,$$

conditions which are reported in the literature as chaotic. The Rayleigh number is computed as expresssed in Equation 2.21d where the dimensionless temperature ratio $\Delta\vartheta$ is defined as

$$\Delta\vartheta := 2\frac{\vartheta_{\mathrm{g,hot}} - \vartheta_{\mathrm{g,cold}}}{\vartheta_{\mathrm{g,hot}} + \vartheta_{\mathrm{g,cold}}}.$$

The remaining parameters for the simulation are $\mu = 2.5 \times 10^{-3}$ kg/(m s) and $\kappa = 3.55$ W/(m K). The results down below are obtained from an structured mesh of $N_{\mathrm{tp}} = 20,451$ nodal points containing $N_{\mathrm{el}} = 20{,}000$ bilinear quadrilateral elements. The time step size chosen for the computations is $\delta t = 0.005$ s.

In this problem, a cyclic flow is established around the cavity due to the combination of both hot and cold shear layers. In order to analyze the dynamical response, in Figure 5.10 we have plotted the temperature evolution at a control point in the horizontal middle plane of the cavity, as well as the pressure-temperature cycle. The temperature evolution is completely smooth and the pressure-temperature cycle shows the capability of the fractional step scheme to reproduce, without oscillations, the randomness associated with chaotic flows. Should the flow be non-chaotic the pressure-temperature plot would be a completely closed curve [78].

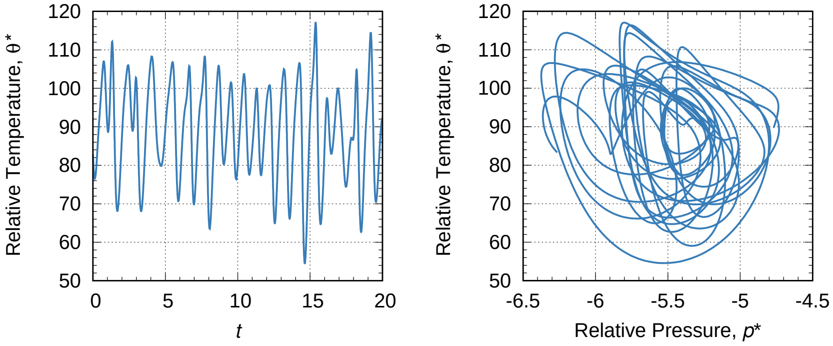

(a) Time history of relative temperature, ϑ^* **(b)** Phase diagram

Figure 5.10: 2D differentially heated cavity: (a) temperature evolution over time and (b) phase diagram pressure-temperature with values from the chosen control point (0.05,4).

In Figure 5.11 snapshots of temperature and velocity contours at a certain time step and for the BDF2 version of the fractional step algorithm are shown. The flow patterns replicated in these images agree with instant contours of fields previously presented in the literature for the same Rayleigh number and cavity ratio (see *e.g.* results in [78]).

In order to further assess the transient behavior of the flow

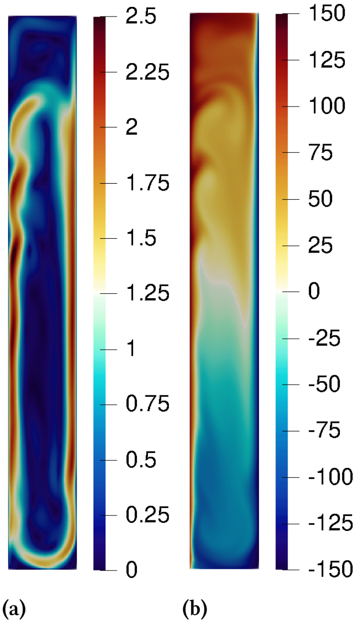

Figure 5.11: 2D differentially heated cavity: (a) velocity magnitude $\|\mathbf{u}\|$ and (b) relative temperature ϑ^* contours of the fractional step scheme. Monolithic contour plots are omitted since they are remarkably similar.

field and quantitatively compare the performance of the algorithms, we present the calculations of the non-dimensional Nusselt number, which we compute here in the cold and hot walls as:

$$\mathrm{Nu}(\mathbf{x},t) := \frac{L}{\vartheta_{\mathrm{g,hot}} - \vartheta_{\mathrm{g,cold}}} \int_{\partial\Omega} \mathbf{n} \cdot \nabla\vartheta(\mathbf{x},t)\, \mathrm{d}\partial\Omega,$$

for any point $\mathbf{x} \in \partial\Omega, t > 0$.

We can observe the unsteady character of the Nusselt number in Figure 5.12 for both hot and cold walls, where we also compare the values obtained with both monolithic and fractional step schemes. The computed average Nusselt numbers are, respectively

$$\begin{aligned}\overline{\mathrm{Nu}}_{\mathrm{FS,hot}} &= 41.8162,\\ \overline{\mathrm{Nu}}_{\mathrm{MN,hot}} &= 41.8908,\\ \overline{\mathrm{Nu}}_{\mathrm{FS,cold}} &= -46.2698,\\ \overline{\mathrm{Nu}}_{\mathrm{MN,cold}} &= -46.2418.\end{aligned}$$

We observe that the predicted values of the segregated computation show an agreement with the ones from the monolithic counterpart. However, there exist some differences which should come, precisely, from the temporal error associated to the fractional step scheme, as already stated.

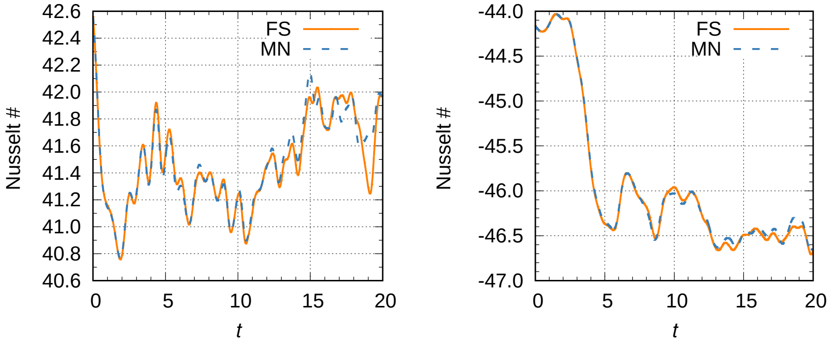

(a) Hot wall **(b)** Cold wall

Figure 5.12: 2D differentially heated cavity: Nusselt number evolution on (a) hot wall, (b) cold wall computed with both fractional step and monolithic second order schemes.

Now that we have checked that the solutions from both monolithic and fractional step schemes are significantly comparable (up to the splitting error, which was shown to maintain the temporal accuracy in time), we now include a comparison on the actual performance of the monolithic time integrator against the fractional step version, with an emphasis on the CPU time savings. We include the quotient between the CPU time of the fractional step scheme over the CPU time of the corresponding monolithic counterpart. A simple sequential implementation over a series of time steps has been used in all cases, so that to avoid any bias in the data resulting from a parallel computation. To this end, the results are presented in Table 5.6 and there we distinguish between the total CPU time needed by the algorithm and the time needed by the PETSC solver to obtain the solution of the final algebraic system (the remaining time is spent on assembling the different element contributions, updating variables, allocation and deallocation processes, etc.). As one can observe, the obtained savings in CPU time are remarkable, with a reduction of roughly 78 % of the total time and around 95 % in the solver time for the performed tests.

This result is directly related with the information in Table 5.7, where the number of iterations needed by the solver to obtain the solution of the system of equations and the number of nonlinear iterations used to obtain converged results are collected. The number of iterations needed by the monolithic

Table 5.6: 2D differentially heated cavity: ratio of CPU time of the fractional step schemes over the monolithic formulations in the 2D chaotic case (second order schemes).

Case	Total time ratio	Solver time ratio
Pr = 0.71, Ra = 1×10^6	0.2263	0.054

Table 5.7: 2D differentially heated cavity: number of iterations of the monolithic and fractional step algorithms (second order schemes). Here, $\overline{\text{nni}}$ is the average number of nonlinear iterations to achieve convergence and $\overline{\text{nsi}}$ stands for the average number of iterations needed by the iterative algebraic solver.

	Monolithic	Fractional step		
Case	$\overline{\text{nni}}/\overline{\text{nsi}}$	$\overline{\text{nni}}_{\mathbf{u}}/\overline{\text{nsi}}_{\mathbf{u}}$	$\overline{\text{nni}}_{\vartheta}/\overline{\text{nsi}}_{\vartheta}$	$\overline{\text{nni}}_{p}/\overline{\text{nsi}}_{p}$
Pr = 0.71, Ra = 1×10^6	8/105	3/3	3/2	2/146

method is greater both for the linear solver and for the nonlinear algorithm. The subsystems for the different steps of the segregated algorithm are smaller, and in general better conditioned what translates into a substantial diminution on the number of iterations and hence in the time of the computations, as already mentioned. It is observed that the pressure represents the bottleneck in the computations, as it shows the greatest number of solver iterations, and this is in fact the reason why the monolithic case delays the convergence of the total system. Likewise, the greater number of nonlinear iterations needed by the monolithic method confirms the better treatment of the nonlinearities when the problem is solved in a decoupled manner.

3D flow in a differentially heated cubic cavity: Pr = 0.71, Ra = 3.5×10^5

We will now consider a 3D version of the previous cavity problem. The computational domain is defined now as the unit cube $\overline{\Omega} = [0, L]^3$ with $L = 1$ m. The prescription of boundary conditions is similar as in the previous example: the temperatures on the boundaries perpendicular to the x-coordinate (horizontal) are fixed to $\vartheta_{\text{g,hot}} = 960$ K (most left boundary) and $\vartheta_{\text{g,cold}} = 240$ K (most right boundary), while adiabatic boundary conditions are prescribed on the remaining walls. No slip conditions are set for the velocity over all the walls. Furthermore, the initial conditions we consider now are:

$$\mathbf{u}_0 = \mathbf{0} \text{ m/s},$$
$$p_0 = p_{\text{atm}} = 101325 \text{ Pa},$$

$$\vartheta_0 = \vartheta_{\text{atm}} = 600 \text{ K}.$$

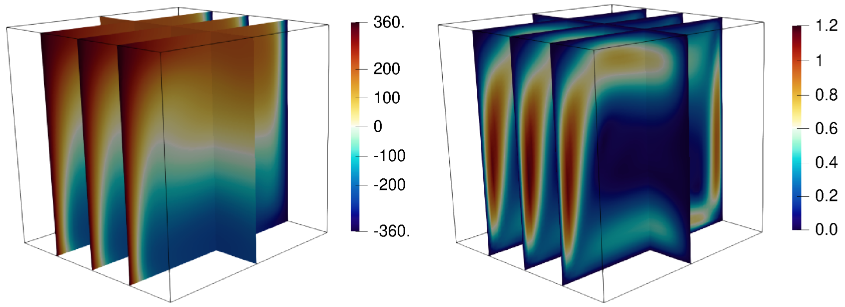

(a) Temperature, ϑ

(b) Velocity magnitude, $\|\mathbf{u}\|$

Figure 5.13: 3D differentially heated cavity: contour plots of (a) relative temperature ϑ^* and (b) velocity magnitude $\|\mathbf{u}\|$ at the final time step of the simulation using the BDF2 fractional step scheme.

The gravity acceleration is specified to be acting in the negative y-coordinate direction (vertical) with a modulus $\|\mathbf{g}\| = 9.81 \text{ m/s}^2$. For this problem we consider

$$\text{Pr} = 0.71, \quad \text{and} \quad \text{Ra} = 3.5 \times 10^5,$$

which is a non-chaotic problem. In this case $\Delta\vartheta = 1.2$. The remaining parameters are set so that to match the desired flow conditions. We perform the simulation using an uniform structured mesh composed of 64,000 hexahedron elements and we use a constant time step of $\delta t = 0.02$ s.

In Figure 5.13 some graphical results for this 3D cavity using the second order integrator (both the BDF1 fractional step scheme and the monolithic case provide practically identical contour plots and they are not included for the sake of conciseness).

We will again compare the CPU times for the different algorithms selected for this problem as well the number of iterations needed by the solver and the non-linear iterative scheme. All these results are included in Table 5.8 and Table 5.9, respectively. For the monolithic formulation, the total number of iterations of the linear system solver is really affected by the pressure. This seems to be a general trend for systems with primitive variables, as also discussed in [55] for the non-Newtonian incompressible case. This fact is one of the main downsides when compared to a fractional step algorithm, in which each step requires a different number of iterations to solve the corresponding linear system. Finally, although in these examples we have used the same solver for all subsystems arising in the segregation method, specific solving techniques could be exploited in order to improve the performance of fractional step schemes even further.

Table 5.8: 3D differentially heated cavity: ratio of CPU times of the fractional step schemes over the monolithic formulation for the 3D cavity (BDF1 results were equivalent).

Case	Total time ratio	Solver time ratio
Pr = 0.71, Ra = 3.5×10^5	0.3410	0.1016

Table 5.9: 3D differentially heated cavity: number of iterations of the monolithic and fractional step algorithm in the 3D cavity for the BDF2 scheme (BDF1 results were equivalent).

	Monolithic	Fractional step		
Case	$\overline{\text{nni}}/\overline{\text{nsi}}$	$\overline{\text{nni}}_{\mathbf{u}}/\overline{\text{nsi}}_{\mathbf{u}}$	$\overline{\text{nni}}_{\vartheta}/\overline{\text{nsi}}_{\vartheta}$	$\overline{\text{nni}}_{p}/\overline{\text{nsi}}_{p}$
Pr = 0.71, Ra = 3.5×10^5	8/32	3/6	3/2	2/63

5.9 Conclusions

In this chapter, we have introduced a pressure-segregation technique to solve the compressible Navier-Stokes equations using primitive variables. The development of this new technique, which is up to second order in time, has been designed at the pure algebraic level, considering as starting point the fully discretized monolithic problem both in space and in time and by using the extrapolation concept.

From the numerical viewpoint, the herein proposed fractional step compressible model is based on a stabilized VMS method and an implicit scheme to advance the solution in time. In addition, other ingredients were appended, such as the orthogonal and dynamic definition of subscales, the weak imposition of Dirichlet boundary conditions, the application of non-reflecting boundary conditions (a major issue in low Mach compressible solvers) and the decomposition of the pressure and temperature unknowns into relative plus atmospheric part in order to solve nearly incompressible cases.

We have shown that the fractional step method introduces an splitting error which maintains the general temporal accuracy of the time integration scheme. Furthermore, the differentially heated cavity problem has been used to test the performance of the algorithm in dynamic and chaotic cases and the possibility of directly computing acoustic pressure waves has been verified with the simulation of the aeolian tones problem, for which the dumping of acoustic perturbations at the external computational boundaries was also evaluated. Likewise, the fractional step formulation has been shown to be efficient since an important reduction in the CPU time has been obtained with respect to the monolithic counterpart for the tests performed, which have a relatively small number of degrees of freedom; much more important savings should be expected in large scale problems.

The Navier-Stokes problem: conservative formulation 6

6.1 Abstract

In this chapter we address the compressible Navier-Stokes equations written in the socalled conservative formulation. In particular, we focus on the possibility of uncoupling the computation of the problem unknowns, namely, density, linear momentum and total energy, a technique usually labeled as fractional step method, which allows to reduce the associated computational cost. The proposed methodology is a finite-element solver supplemented with a stabilization technique within the Variational Multi-Scale framework. In this regard, we consider orthogonal and dynamic definitions for the subscales. This discretization in space shows an adequate stability, permitting in particular the use of equal interpolation for all variables in play. However, we complement it with a shock-capturing operator in order to solve problems involving shocks. Several representative benchmark flow simulations are performed, which demonstrate the suitability of the proposed algorithm for a vast range of regimes.

6.2 Introduction

The socalled compressible Navier-Stokes equations are commonly used to model flow problems where compressibility effects become relevant with applications ranging from classical turbo-machinery design to modern speech therapy simulations. The general mathematical setting consists of the momentum, mass and energy conservation equations together with thermodynamic properties, constitutive relations and proper initial and boundary conditions, which are appended to close the mathematical description ensuring the well posedness of the problem. Such a set of partial differential equations describes a wide range of scales and, in general, computing its solution is a challenge in itself. One could proceed either by choosing small mesh and time step sizes or by using high precision numerical schemes. Regardless of the selected approach, obtaining a representative solution is particularly demanding from the computational viewpoint. This fact still remains as one of the main limitations in compressible flow simulations in spite of the increasing amount of computing facilities available for the scientific and engineering communities. In this chapter, we focus on the finite element approximation of the Navier-Stokes compressible flow problem written in the conservation form. Particularly, we aim at solving it in a segregated manner, that is to say, by uncoupling the calculation of the problem unknowns. These are the well-known conservative variables, *i. e.*, density, momentum, and total energy.

Although global stability is ensured by a VMS-based stabilized formulation, some localized oscillations may arise from sharp gradients in the solution, particularly at supersonic regimes. This effect is innate to compressible flows involving shocks (discontinuities). Hence, stabilized formulations usually need to be complemented with a local shock-capturing methodology. A possible approach to model shocks is the residual-based shock-capturing technique, first introduced in [166] and later tested in [167] for a SUPG compressible flow formulation. Another popular option is the socalled ”YZβ” method from [168]. In contrast to the previous formulations, our strategy is to introduce the numerical diffusion in a “physical manner”, that is to say, we shall modify the diffusion of the momentum and energy equations, but we avoid introducing artificial diffusion into the mass equation.

[166]: Hughes et al. (1986), “A new finite element formulation for computational fluid dynamics: III. The generalized streamline operator for multidimensional advective-diffusive systems”

[167]: Beau et al. (1991), “Finite element computation of compressible flows with the SUPG formulation”

[168]: Tezduyar et al. (2006), “Stabilization and shock-capturing parameters in SUPG formulation of compressible flows”

Nevertheless, in this work our main goal is the development of segregation methods for the transient compressible Navier-Stokes equations using a finite element approximation for the space discretization. As a reference in the comparisons, we shall take the solution of the monolithic problem, *i. e.*, the standard coupled calculation involving all the problem unknowns. The fully discrete and linearized monolithic scheme leads to an algebraic system, whose structure may be exploited in order to solve independently for the density, momentum and energy degrees of freedom.

The technique we will discuss here corresponds to the classical fractional step algorithms, which might be seen as an alternative methodology to solve transient problems. Our approach in this work is to present a splitting of the equations at the algebraic level once the equations have already been discretized in space and in time, simiarly as we did previously in Chapter 4 and Chapter 5. As we have discussed, this algebraic viewpoint is generally simpler and it makes possible to obviate a discussion on specific boundary conditions for the different stages of the fractional step scheme. Furthermore, it has been extensively and effectively applied to a wide range of different test cases in computational physics, including incompressible [50, 53], viscoelasticy [55], isentropic [155] and compressible (primitive variables) [169] problems.

This chapter is structured as follows: in Section 6.3 we introduce the compressible Navier-Stokes problem together with its variational formulation. In Section Section 6.4 we discuss differente numerical aspects which need to be taken into consideration for the problem in hand. Section 6.5 is devoted to the design of the fractional step scheme. Numerical experiments are conducted in Section 6.6, and, finally, we close the chapter with some concluding statements in Section 6.7.

6.3 Preliminaries

In this chapter we focus on the solution of the compressible Navier-Stokes problem for the socalled conservative variables, namely, density $\rho(\mathbf{x},t)$, momentum $\mathbf{m}(\mathbf{x},t)$ and total energy $E(\mathbf{x},t)$. Hence, we shall introduce some considerations in order to rewrite the system formed by Equation 2.20a, Equation 2.20b and Equation 2.20c in a more convenient form. The linear momentum and total energy variables are respectively defined as

$$\begin{aligned} \mathbf{m} &:= \rho \mathbf{u} \\ E = \rho e &:= \rho\left(\iota + \frac{1}{2}\|\mathbf{u}\|^2\right) = \rho\left(c_v\vartheta + \frac{1}{2}\|\mathbf{u}\|^2\right) \end{aligned}$$

where e is the specific energy or energy per unit of mass.

Taking into account the definition of the viscous part of the Newtonian stress tensor in Equation 2.9, that tensor can be directly calculated using the conservative variables as

$$\begin{aligned} \sigma_{ij}^{\mathrm{d}} = \nu\left(\frac{\partial m_i}{\partial x_j} + \frac{\partial m_j}{\partial x_i}\right) - \frac{2\nu}{3}\left(\frac{\partial m_k}{\partial x_k}\right)\delta_{ij} - \frac{\nu}{\rho}\left(m_i\frac{\partial \rho}{\partial x_j} + m_j\frac{\partial \rho}{\partial x_i}\right) \\ + \frac{2\nu}{3\rho}\left(m_l\frac{\partial \rho}{\partial x_l}\right)\delta_{ij} \quad i,j,k = 1,\dots,N_{\mathrm{sd}}. \qquad (6.1) \end{aligned}$$

In this equation, δ_{ij} is the Kronecker delta (*i. e.*, $\delta_{ij} = 1$ if $i = j$ and $\delta_{ij} = 0$ if $i \neq j$) and ν is the kinematic viscosity.

In order to calculate the pressure and the speed of sound in terms of conservative variables, the caloric equation of state Equation 2.13 and the ideal gas state equation Equation 2.15 are used. It is then found that the pressure and the speed of sound can be written respectively as

$$p = (\gamma - 1)\left((\rho e) - \frac{\mathbf{m}\cdot\mathbf{m}}{2\rho}\right), \tag{6.2}$$

$$a = \sqrt{\gamma(\gamma - 1)\left(\frac{(\rho e)}{\rho} - \frac{\mathbf{m}\cdot\mathbf{m}}{2\rho^2}\right)}. \tag{6.3}$$

In a similar fashion, applying the caloric and state equations to expand Equation 2.19, the heat flux vector can be computed as

$$\begin{aligned} q_i = &\left[\frac{\kappa(\rho e)}{c_v\rho^2} - \frac{\kappa(\mathbf{m}\cdot\mathbf{m})}{c_v\rho^3}\right]\frac{\partial\rho}{\partial x_i} + \frac{\kappa m_j}{c_v\rho^2}\frac{\partial m_j}{\partial x_i} \\ &- \frac{\kappa}{\rho c_v}\frac{\partial(\rho e)}{\partial x_i} \quad i = 1, \dots, N_{\mathrm{sd}}. \end{aligned} \tag{6.4}$$

6.3.1 Compact and quasi-linear form of the problem

The Navier-Stokes equations of compressible flow can be compactly written as

$$\partial_t \mathbf{y} + \nabla\cdot\left(\mathscr{F}^{\mathrm{c}}(\mathbf{y}) + \mathscr{F}^{\mathrm{d}}(\mathbf{y}, \nabla\mathbf{y})\right) = \mathscr{F}(\mathbf{y}) \quad \text{in } \Omega\times(0, t_{\mathrm{f}}), \tag{6.5}$$

where $\mathbf{y} \in \mathbb{R}^{N_{\mathrm{sd}}+2}$ is here the vector of conservative variables, $\mathscr{F}^{\mathrm{c}}(\mathbf{y})$ and $\mathscr{F}^{\mathrm{d}}(\mathbf{y}, \nabla\mathbf{y}) \in \mathbb{R}^{(N_{\mathrm{sd}}+2)\times N_{\mathrm{sd}}}$ are the convective and diffusion flux tensors, and $\mathscr{F}(\mathbf{y}) \in \mathbb{R}^{N_{\mathrm{sd}}+2}$ is the vector of external forcing terms, all of them respectively given by

$$\mathbf{y} = \begin{bmatrix} \rho \\ \rho\mathbf{u} \\ \rho e \end{bmatrix},$$

$$\mathscr{F}^{\mathrm{c}}(\mathbf{y}) = \begin{bmatrix} \rho\mathbf{u}^T \\ \rho\mathbf{u}\otimes\mathbf{u} + p\mathbf{I}_{N_{\mathrm{sd}}} \\ (\rho e + p)\mathbf{u}^T \end{bmatrix},$$

$$\mathscr{F}^{\mathrm{d}}(\mathbf{y}, \nabla\mathbf{y}) = \begin{bmatrix} \mathbf{0} \\ -\boldsymbol{\sigma}^{\mathrm{d}} \\ \left(\mathbf{q} - \boldsymbol{\sigma}^{\mathrm{d}}\mathbf{u}\right)^T \end{bmatrix},$$

$$\mathscr{F}(\mathbf{y}) = \begin{bmatrix} \mathbf{0} \\ \rho\mathbf{b} \\ \rho(r + \mathbf{b}^T \cdot \mathbf{u}) \end{bmatrix}.$$

where $p, \boldsymbol{\sigma}^{\mathrm{d}}$ and $\mathbf{q}$ are in this case given by Equation 6.2, Equation 6.1 and Equation 6.4, respectively.

However, the divergence of the convective and diffusive flux tensors from the original system in Equation 6.5, can be written in a more convenient manner upon the definition of the socalled Euler Jacobian and diffusion matrices. Making use of index notation, those are related to the convective and diffusive flux tensors as follows:

$$\mathscr{A}_j(\mathbf{y}) := \frac{\partial \mathscr{F}_j^{\mathrm{c}}(\mathbf{y})}{\partial \mathbf{y}} \qquad j = 1, \dots, N_{\mathrm{sd}}, \tag{6.6a}$$

$$\frac{\partial \mathscr{F}_j^{\mathrm{d}}(\mathbf{y})}{\partial x_j} := -\frac{\partial}{\partial x_k}\left(\mathscr{K}_{kj}(\mathbf{y})\frac{\partial \mathbf{y}}{\partial x_j}\right) \qquad j, k = 1, \dots, N_{\mathrm{sd}}. \tag{6.6b}$$

The last term in Equation 6.5, the vector of sources, can also be rewritten by means of a reactive-like term of the form

$$\mathscr{F}(\mathbf{y}) := \mathscr{S}\mathbf{y}. \tag{6.7}$$

Therefore, taking all this information into account, the original compressible Navier-Stokes system can be now stated as: find the set of conservative unknowns $\mathbf{y}$ such that the following is satisfied,

$$\partial_t \mathbf{y} + \mathscr{L}(\mathbf{y}; \mathbf{y}) = 0 \quad \text{in } \Omega \times (0, t_{\mathrm{f}}), \tag{6.8}$$

which is nothing but Equation 3.1 taking into account that now $\mathscr{M} = \mathbf{I}_{N_{\mathrm{sd}}}$. The second-order nonlinear operator $\mathscr{L}(\mathbf{y}; \mathbf{y})$ is given precisely by Equation 3.2.

The Euler matrix $\mathscr{A}_j(\mathbf{y})$ is developed using the spatial derivatives of the pressure using Equation 6.2 and hence we obtain

$$\mathscr{A}_j(\mathbf{y}) = \begin{bmatrix} 0 & \mathbf{e}_j^T & 0 \\ \frac{\mathbf{m}m_j}{\rho^2} + A_1\mathbf{e}_j & \mathbf{I}_{N_{\mathrm{sd}}}\frac{m_j}{\rho} + \frac{\mathbf{m}}{\rho} \otimes \mathbf{e}_j - (\gamma - 1)(\mathbf{e}_j \otimes \mathbf{e}_j)\frac{\mathbf{m}^T}{\rho} & (\gamma - 1)(\mathbf{e}_j \otimes \mathbf{e}_j) \\ (A_1 - A_2)\,\frac{m_j}{\rho} & -(\gamma - 1)\frac{\mathbf{m}^T m_j}{\rho^2} + A_2\mathbf{e}_j^{\boxtimes} & \gamma\frac{m_j}{\rho} \end{bmatrix}, \tag{6.9}$$

for $j = 1, \dots, N_{\mathrm{sd}}$, and where $\mathbf{e}_j$ stands for the unit vector in the

j-th direction. In the previous definition, the thermodynamic relations A_1 and A_2 stand for,

$$A_1 = \frac{1}{2}(\gamma - 1)|\mathbf{u}|^2,$$
$$A_2 = \frac{(\rho e) + p}{\rho}.$$

Let us now denote by $\mathbf{0}$ the vector of $\mathbb{R}^{N_{\text{sd}}}$ with null components. Using the viscous stress tensor and heat flux vector definitions based on conservative variables *i. e.*, Equation 6.1 – Equation 6.4 and the ideal gas law, each component in the diffusive matrix can be respectively computed as

$$\mathscr{K}_{jj}(\mathbf{y}) = \begin{bmatrix} 0 & \mathbf{0}^T & 0 \\ -\nu\frac{\mathbf{m}}{\rho} & \nu\mathbf{I}_{N_{\text{sd}}} & \mathbf{0} \\ \frac{(K-\nu)}{\rho^2}\|\mathbf{m}\|^2 - \frac{K}{\rho}E & (\nu - K)\frac{\mathbf{m}^T}{\rho} & K \end{bmatrix}, \tag{6.10}$$

with $j = 1, \dots, N_{\text{sd}}$ and

$$\mathscr{K}_{kj}(\mathbf{y}) = \begin{bmatrix} 0 & \mathbf{0}^T & 0 \\ -\nu\frac{m_k}{\rho}\mathbf{e}_j + \frac{2}{3}\nu\frac{m_j}{\rho}\mathbf{e}_k & \nu(\mathbf{e}_j \otimes \mathbf{e}_k) - \frac{2}{3}\nu(\mathbf{e}_k \otimes \mathbf{e}_j) & \mathbf{0} \\ -\frac{1}{3}\nu\frac{m_k m_j}{\rho^2} & \nu\frac{m_j}{\rho}\mathbf{e}_k^T - \frac{2}{3}\nu\frac{m_k}{\rho}\mathbf{e}_j^T & 0 \end{bmatrix}, \tag{6.11}$$

with $j, k = 1, \dots, N_{\text{sd}}$, and $k \neq j$. We recall that the symbol K represents throughout this chapter the thermal diffusivity Equation 2.22.

Finally, the reactive matrix can be written in terms of the external sources as

$$\mathscr{S} = \begin{bmatrix} 0 & 0 & 0 \\ \mathbf{b} & 0 & 0 \\ r & \mathbf{b}^T & 0 \end{bmatrix}. \tag{6.12}$$

Having defined the expressions for the Euler, diffusive and reactive matrices, the derivation of the solution procedure follows exactly what has been explained Chapter 3. Equation 3.6 is then the weak form of the problem and the application of the VMS framework to this problem yields nothing but Equation 3.20 taking into account the previous definitions.

6.4 Numerical aspects

6.4.1 Discontinuity capturing technique

Although the VMS stabilized finite element formulation yields a globally stable solution, *i. e.*, norms of the unknowns over the whole domain Ω are bounded, local stability is not guaranteed in the vicinity of shocks or regions with sharp gradients. In order to mitigate these possible local oscillations, an artificial shock-capturing (SC) term is added to the numerical approximation of the problem. The main idea of a shock capturing technique is to increase the amount of numerical dissipation in the proximity of sharp gradients. Many different approaches can be adopted to introduce artificial dissipation. Here, two different alternatives are presented, which introduce numerical diffusion only in the momentum and energy equations.

The first nonlinear method that we implement is a classical residual-based technique, which is consistent, that is to say, when it is applied to the exact solution, the added diffusion is zero. For this technique we calculate the artificial kinematic viscosity as

$$\nu_{\mathrm{sc}} = \frac{C_{\mathrm{sc}}h}{2}\frac{|\mathscr{R}_{\mathbf{m}}(\mathbf{y};\mathbf{y}_h)|}{|\nabla\mathbf{m}_h|}, \quad \text{if } |\nabla\mathbf{m}_h| \neq 0, \tag{6.13a}$$

$$\nu_{\mathrm{sc}} = 0, \quad \text{otherwise}, \tag{6.13b}$$

where C_{sc} is an algorithmic constant to be set before the simulation, h is the characteristic length that gives dimensional consistency to the expression, and $|\nabla\mathbf{m}_h|$ is the Frobenius norm of the gradient of the momentum finite element solution. In a similar manner, for the energy equation we introduce an artificial thermal diffusivity computed as

$$K_{\mathrm{sc}} = \frac{C_{\mathrm{sc}}h}{2}\frac{|\mathscr{R}_{E}(\mathbf{y},\mathbf{y}_h)|}{\|\nabla E_h\|}, \quad \text{if } \|\nabla E_h\| \neq 0, \tag{6.14a}$$

$$K_{\mathrm{sc}} = 0, \quad \text{otherwise}, \tag{6.14b}$$

where $\|\nabla E_h\|$ is the norm of the gradient of the total energy finite element solution.

An alternative to introduce the numerical diffusion is the weakly consistent orthogonal projection technique from [170]. It is based on the orthogonal projection onto the finite element space of the gradient of the unknown, instead of the

[170]: Codina (2011), "Finite Element Approximation of the Convection-Diffusion Equation: Subgrid-Scale Spaces, Local Instabilities and Anisotropic Space-Time Discretizations"

common residual approach. Mathematically speaking, we take the artificial viscosity as follows:

$$\nu_{\text{sc}} = \frac{C_{\text{sc}} h \|\mathbf{u}_h\|}{2} \frac{\left|\mathscr{P}_h^{\perp}\left[\nabla \mathbf{m}_h\right]\right|}{|\nabla \mathbf{m}_h|}, \quad \text{if } |\nabla \mathbf{m}_h| \neq 0, \tag{6.15a}$$

$$\nu_{\text{sc}} = 0, \quad \text{otherwise}, \tag{6.15b}$$

and the thermal diffusivity as

$$K_{\text{sc}} = \frac{C_{\text{sc}} h \|\mathbf{u}_h\|}{2} \frac{\left\|\mathscr{P}_h^{\perp}(\nabla E_h)\right\|}{\|\nabla E_h\|}, \quad \text{if } \|\nabla E_h\| \neq 0, \tag{6.16a}$$

$$K_{\text{sc}} = 0, \quad \text{otherwise}, \tag{6.16b}$$

where the norm of the velocity gives dimensional consistency.

In practice, the added numerical diffusion is introduced into the diffusive Galerkin term by computing a modified viscous stress tensor $\tilde{\boldsymbol{\sigma}}^d$ and heat flux $\tilde{\mathbf{q}}$ vector in the following isotropic manner

$$\tilde{\sigma}_{ij}^{\text{d}} = \left(1 + \frac{\rho \nu_{\text{sc}}}{\mu}\right) \sigma_{ij}^{\text{d}} \qquad \forall\, i,j = 1,\dots,N_{\text{sd}}, \tag{6.17a}$$

$$\tilde{q}_i = \left(1 + \frac{\rho c_v K_{\text{sc}}}{\kappa}\right) q_i \qquad \forall\, i = 1,\dots,N_{\text{sd}}. \tag{6.17b}$$

6.4.2 On the stabilization parameters

Although the application of the VMS method to the compressible Navier-Stokes problem should be now clear, the stabilization technique is not completed until one introduces a definition to compute the matrix of stabilization parameters.

The usual definition of the compressible stabilization parameters include a local sound velocity that arises from a linearization of the characteristic compressible flow problem. In this chapter we follow our previous findings published in [28] (see section 3.3 from that paper for a complete and detailed exposition) which are based on a Fourier analysis of the nonlinear operator of the problem.

Therefore, the stabilization matrix for the 3D case is computed here as

$$\boldsymbol{\tau}^{-1} = \begin{bmatrix} \tau_\rho^{-1} & \mathbf{0}^T & 0 \\ \mathbf{0} & \boldsymbol{\tau}_{\mathbf{m}}^{-1}\mathbf{I}_{N_{\rm sd}} & \mathbf{0} \\ 0 & \mathbf{0}^T & \tau_E^{-1} \end{bmatrix}, \tag{6.18}$$

with the following non-zero entries

$$\tau_\rho^{-1} = c_2 \frac{(\|\mathbf{u}\| + a)}{h} + c_3 \tau_{\rm aux}^{-1}, \tag{6.19a}$$

$$\tau_{\rho\mathbf{u}}^{-1} = c_1 \frac{4\nu}{3h^2} + c_2 \frac{(\|\mathbf{u}\| + a)}{h} + c_3 \tau_{\rm aux}^{-1}, \tag{6.19b}$$

$$\tau_E^{-1} = c_1 \frac{K}{h^2} + c_2 \frac{(\|\mathbf{u}\| + a)}{h} + c_3 \tau_{\rm aux}^{-1}. \tag{6.19c}$$

and where

$$\tau_{\rm aux}^{-1} := \left(\frac{r^2 + 2\|\mathbf{b}\|^2 a^2 + \sqrt{r^4 + 4a^2\|\mathbf{b}\|^2 r^2}}{2a^4} \right)^{1/2} .$$

It is understood that these expressions are evaluated element by element. The numerical constants c_1 and c_2 are independent of the physical parameters of the problem. In the numerical calculations we take them as $c_1 = 12\omega^4$, $c_2 = 2\omega$, $c_3 = 1$, ω being the order of the finite element interpolation.

6.5 Fractional step methods

Instead of solving the classical monolithic system, an alternative is to use a fractional step method in time, in which various equations need to be solved for the different variables in an uncoupled way, probably with the addition of some correction steps. The splitting of the equations introduced in fractional step methods has an additional temporal error, which has to be *at least* of the order of the time integration scheme used to approximate time derivatives. Otherwise, time accuracy is broken.

In this section we develop a novel algebraic fractional step method for the compressible Navier-Stokes problem. The basic procedure entails a calculation of an intermediate momentum with a guess of the density and total energy. After solving for density and energy (in that order), we will finally correct the intermediate momentum calculation, so as to ensure that the global time accuracy of the method is maintained.

6.5.1 Algebraic problem

We assume that ρ_h^{n+1}, $\mathbf{m}_h^{n+1}$ and E_h^{n+1} are constructed using the standard finite element interpolation from the nodal values, which we denote in this chapter as $\boldsymbol{\varrho}^{n+1}$, $\mathbf{U}^{n+1}$ and $\mathbf{E}^{n+1}$ respectively. These are computed as the solution of a nonlinear algebraic problem, which is obtained directly from Equation 3.11 after discretization in time. We shall skip the stabilization terms for the sake of conciseness. Their addition is straightforward once the fractional step method is developed, similarly as we did in previous chapters.

The structure of the final system can be written in a compact manner, for each iteration as

$$\begin{bmatrix} \mathbf{A}_{\rho\rho} & \mathbf{A}_{\rho\mathbf{m}} & \mathbf{0} \\ \mathbf{A}_{\mathbf{m}\rho} & \mathbf{A}_{\mathbf{mm}} & \mathbf{A}_{\mathbf{m}E} \\ \mathbf{A}_{E\rho} & \mathbf{A}_{E\mathbf{m}} & \mathbf{A}_{EE} \end{bmatrix} \cdot \begin{bmatrix} \boldsymbol{\varrho}^{n+1} \\ \mathbf{U}^{n+1} \\ \mathbf{E}^{n+1} \end{bmatrix} = \begin{bmatrix} \mathbf{F}_{\boldsymbol{\varrho}}^{n+1} \\ \mathbf{F}_{\mathbf{U}}^{n+1} \\ \mathbf{F}_{\mathbf{E}}^{n+1} \end{bmatrix} \tag{6.20}$$

with the following matrices

$$\begin{aligned}
\mathbf{A}_{\rho\rho} &:= \mathbf{M}_{\rho\rho}\frac{D_\theta}{\delta t} \\
\mathbf{A}_{\rho\mathbf{m}} &:= \mathbf{C}_{\rho\mathbf{m}} \\
\mathbf{A}_{\mathbf{m}\rho} &:= \mathbf{C}_{\mathbf{m}\rho}(\boldsymbol{\varrho}^{n+1}, \mathbf{U}^{n+1}) + \mathbf{D}_{\mathbf{m}\rho}(\boldsymbol{\varrho}^{n+1}, \mathbf{U}^{n+1}) \\
\mathbf{A}_{\mathbf{mm}} &:= \mathbf{M}_{\mathbf{mm}}\frac{D_\theta}{\delta t} + \mathbf{C}_{\mathbf{mm}}\left(\boldsymbol{\varrho}^{n+1}, \mathbf{U}^{n+1}\right) + \mathbf{D}_{\mathbf{mm}}\left(\boldsymbol{\varrho}^{n+1}\right) \\
\mathbf{A}_{\mathbf{m}E} &:= \mathbf{C}_{\mathbf{m}E} \\
\mathbf{A}_{E\rho} &:= \mathbf{C}_{E\rho}\left(\boldsymbol{\varrho}^{n+1}, \mathbf{U}^{n+1}, \mathbf{E}^{n+1}\right) + \mathbf{D}_{E\rho}\left(\boldsymbol{\varrho}^{n+1}, \mathbf{U}^{n+1}, \mathbf{E}^{n+1}\right) \\
\mathbf{A}_{E\mathbf{m}} &:= \mathbf{C}_{E\mathbf{m}}\left(\boldsymbol{\varrho}^{n+1}, \mathbf{U}^{n+1}, \mathbf{E}^{n+1}\right) + \mathbf{D}_{E\rho}\left(\boldsymbol{\varrho}^{n+1}, \mathbf{U}^{n+1}\right) \\
\mathbf{A}_{EE} &:= \mathbf{C}_{EE}\left(\boldsymbol{\varrho}^{n+1}, \mathbf{U}^{n+1}\right) + \mathbf{D}_{EE}\left(\boldsymbol{\varrho}^{n+1}\right)
\end{aligned}$$

The high nonlinear character of the problem is made explicit in the system by including the dependence of the arrays on the variables in the parenthesis, which are all evaluated at time step $n + 1$.

The first subscript on the arrays refers to the momentum ($\mathbf{m}$), energy (E) and continuity (ρ) equation, and the second stands for the unknown to which the term refers to. Mass matrices are labeled with the symbol $\mathbf{M}$, convective-like matrices with

$\mathbf{C}$ and diffusive-like matrices with the symbol $\mathbf{D}$. The latter comes from the discretization of the terms inside $\mathscr{K}_{kj}$ and the convective matrices from those in $\mathscr{A}_j$ (see Section 6.3.1). All the arrays in the system are computed from the local assembly of the elemental contributions. Furthermore, the right hand side terms in $\mathbf{F}$ might contain known terms such as external forces, yet we assume here the external forces to be zero in order to ease the discussion.

Matrix version	Term where it comes from
$\mathbf{Z}^T\mathbf{M}\mathbf{Y}$	$\langle \mathbf{z}_h, \partial_t \mathbf{y}_h \rangle$
$\mathbf{Z}^T\mathbf{C}(\mathbf{y})\mathbf{Y}$	$\left\langle \mathbf{z}_h, \mathscr{A}_j(\mathbf{y})\partial_j \mathbf{y}_h \right\rangle$
$\mathbf{Z}^T\mathbf{D}\,(\mathbf{y})\,\mathbf{Y}$	$\left\langle \partial_j \mathbf{z}_h, \mathscr{K}_{jk}(\mathbf{y})\partial_k \mathbf{y}_h \right\rangle$

Table 6.1: Matrix form of the conservative terms. Subscripts are appended depending on the equations and unknowns.

6.5.2 Design of the fractional step method

In order to derive the fractional step method, let us proceed as follows: if $\widetilde{\mathbf{U}}^{n+1}$ denotes an intermediate momentum variable, $\hat{\boldsymbol{\varrho}}^{n+1}_{\theta-1}$ and $\widehat{\mathbf{E}}^{n+1}_{\theta-1}$ are respectively density and energy extrapolated values of order $\theta-1$ according to Equation 3.9 and we split the former momentum equation into two parts, the previous system can be rewritten in the following *equivalent* form:

$$\begin{aligned}
\mathbf{M}_{\mathbf{mm}}\frac{D_\theta}{\delta t}\widetilde{\mathbf{U}}^{n+1} &+ \mathbf{C}_{\mathbf{mm}}(\boldsymbol{\varrho}^{n+1},\widetilde{\mathbf{U}}^{n+1})\widetilde{\mathbf{U}}^{n+1} + \mathbf{D}_{\mathbf{mm}}(\boldsymbol{\varrho}^{n+1})\widetilde{\mathbf{U}}^{n+1}\\
&+ \mathbf{C}_{\mathbf{m}\rho}(\boldsymbol{\varrho}^{n+1},\mathbf{U}^{n+1})\hat{\boldsymbol{\varrho}}^{n+1}_{\theta-1} + \mathbf{D}_{\mathbf{m}\rho}(\boldsymbol{\varrho}^{n+1},\mathbf{U}^{n+1})\hat{\boldsymbol{\varrho}}^{n+1}_{\theta-1}\\
&+ \mathbf{C}_{\mathbf{m}E}\widehat{\mathbf{E}}^{n+1}_{\theta-1} = \mathbf{0}, \qquad (6.21a)\\
\mathbf{M}_{\mathbf{mm}}\frac{1}{\phi_\theta \delta t}&\left(\mathbf{U}^{n+1} - \widetilde{\mathbf{U}}^{n+1}\right) + \mathbf{N}^{n+1}_{\mathbf{m}} + \mathbf{N}^{n+1}_{\rho}\\
&+ \mathbf{N}^{n+1}_{E} = \mathbf{0}, \qquad (6.21b)\\
\mathbf{M}_{\rho\rho}\frac{D_\theta}{\delta t}\boldsymbol{\varrho}^{n+1} &+ \mathbf{C}_{\rho\mathbf{m}}\mathbf{U}^{n+1} = 0, \qquad (6.21c)\\
\mathbf{M}_{EE}\frac{D_\theta}{\delta t}\mathbf{E}^{n+1} &+ \mathbf{C}_{EE}(\boldsymbol{\varrho}^{n+1},\mathbf{U}^{n+1})\mathbf{E}^{n+1} + \mathbf{D}_{EE}(\boldsymbol{\varrho}^{n+1})\mathbf{E}^{n+1}\\
&+ \mathbf{C}_{E\rho}(\boldsymbol{\varrho}^{n+1},\mathbf{U}^{n+1},\mathbf{E}^{n+1})\boldsymbol{\varrho}^{n+1}\\
&+ \mathbf{D}_{E\rho}(\boldsymbol{\varrho}^{n+1},\mathbf{U}^{n+1},\mathbf{E}^{n+1})\boldsymbol{\varrho}^{n+1}\\
&+ \mathbf{C}_{E\mathbf{m}}(\boldsymbol{\varrho}^{n+1},\mathbf{U}^{n+1},\mathbf{E}^{n+1})\mathbf{U}^{n+1}\\
&+ \mathbf{D}_{E\mathbf{m}}(\boldsymbol{\varrho}^{n+1},\mathbf{U}^{n+1})\mathbf{U}^{n+1} = 0, \qquad (6.21d)
\end{aligned}$$

with the following definitions

$$
\begin{aligned}
\mathbf{N}_{\mathbf{m}}^{n+1} &:= \left[\mathbf{C}_{\mathbf{mm}}(\boldsymbol{\varrho}^{n+1}, \mathbf{U}^{n+1}) + \mathbf{D}_{\mathbf{mm}}(\boldsymbol{\varrho}^{n+1})\right] \mathbf{U}^{n+1} \\
&\quad - \left[\mathbf{C}_{\mathbf{mm}}(\boldsymbol{\varrho}^{n+1}, \widetilde{\mathbf{U}}^{n+1}) + \mathbf{D}_{\mathbf{mm}}(\boldsymbol{\varrho}^{n+1})\right] \widetilde{\mathbf{U}}^{n+1}, \qquad (6.22a) \\
\mathbf{N}_{\rho}^{n+1} &:= \left[\mathbf{C}_{\mathbf{m}\rho}(\boldsymbol{\varrho}^{n+1}, \mathbf{U}^{n+1}) + \mathbf{D}_{\mathbf{m}\rho}(\boldsymbol{\varrho}^{n+1}, \mathbf{U}^{n+1})\right] \left(\boldsymbol{\varrho}^{n+1} - \hat{\boldsymbol{\varrho}}_{\theta-1}^{n+1}\right), \\
&\qquad (6.22b) \\
\mathbf{N}_{E}^{n+1} &:= \mathbf{C}_{\mathbf{m}E}\left(\mathbf{E}^{n+1} - \widehat{\mathbf{E}}_{\theta-1}^{n+1}\right), \qquad (6.22c)
\end{aligned}
$$

and where $D_\theta \widetilde{\mathbf{U}}^{n+1}$ is computed as $D_\theta \mathbf{U}^{n+1}$ but replacing $\mathbf{U}^{n+1}$ by a yet undetermined function $\widetilde{\mathbf{U}}^{n+1}$ (intermediate momentum). The reader should note that adding up Equation 6.21a and Equation 6.21b with the definitions in Equation 6.22a–Equation 6.22c, we obtain the former momentum equation, *i. e.*, the second row of the original system. We shall refer to Equation 6.21a as the *intermediate momentum equation* and Equation 6.21b as the *momentum correction equation*. The purpose of the latter is precisely to ensure that the global time accuracy is not broken.

If we denote the node indexes with superscripts a, b, and the standard shape function of node a by φ^a, the components of the matrix $\mathbf{C}_{\rho\mathbf{m}}$ are the following:

$$
\left[\mathbf{C}_{\rho\mathbf{m}}\right]_j^{ab} = \overset{N_{\mathrm{el}}}{\underset{e=1}{\mathbb{A}}} \int_{\partial\Omega^{(e)}} \varphi^a \partial_j \varphi^b \, \mathrm{d}\Omega \qquad \forall\, j = 1, \dots, N_{\mathrm{sd}}, \qquad (6.23)
$$

where, as usual, $\mathbb{A}$ symbolizes the assembly of the local contributions (addition plus injection) to the global equation.

Let us now proceed as follows: first, integration by parts over that term in the mass equation would momentarily yield

$$
\mathbf{M}_{\rho\rho} \frac{D_\theta}{\delta t} \boldsymbol{\varrho}^{n+1} - \check{\mathbf{C}}_{\rho\mathbf{m}} \mathbf{U}^{n+1} = -\check{\mathbf{F}}_{\rho}^{n+1}, \qquad (6.24)
$$

where

$$
\begin{aligned}
\left[\check{\mathbf{C}}_{\rho\mathbf{m}}\right]_j^{ab} &= \overset{N_{\mathrm{el}}}{\underset{e=1}{\mathbb{A}}} \int_{\Omega^{(e)}} \partial_j \varphi^a \varphi^b \, \mathrm{d}\Omega \quad \forall\, j = 1, \dots, N_{\mathrm{sd}}, \qquad (6.25a) \\
\left[\check{\mathbf{F}}_{\rho}^{n+1}\right]^a &= \overset{N_{\mathrm{el}}}{\underset{e=1}{\mathbb{A}}} \int_{\partial\Omega^{(e)}} \varphi^a (\mathbf{n} \cdot \mathbf{U}^{n+1}) \, \mathrm{d}\partial\Omega. \qquad (6.25b)
\end{aligned}
$$

Now, solving for $\mathbf{U}^{n+1}$ from Equation 6.21b and multiplying by $\check{\mathbf{C}}_{\rho\mathbf{m}}$ it gives,

$$
\check{\mathbf{C}}_{\rho\mathbf{m}} \mathbf{U}^{n+1} = -\phi_\theta \delta t \check{\mathbf{C}}_{\rho\mathbf{m}} \left[\mathbf{M}_{\mathbf{mm}}\right]^{-1} \left[\mathbf{N}_{\rho}^{n+1} + \mathbf{N}_{\mathbf{m}}^{n+1} + \mathbf{N}_{E}^{n+1}\right]
$$

$$+\check{\mathbf{C}}_{\rho\mathbf{m}}\widetilde{\mathbf{U}}^{n+1}. \tag{6.26}$$

This new expression can be now used in Equation 6.24. Therefore

$$\mathbf{M}_{\rho\rho}\frac{D_\theta}{\delta t}\varrho^{n+1}+\phi_\theta\delta t\check{\mathbf{C}}_{\rho\mathbf{m}}\left[\mathbf{M}_{\mathbf{mm}}\right]^{-1}\left[\mathbf{N}_\rho^{n+1}+\mathbf{N}_{\mathbf{m}}^{n+1}+\mathbf{N}_E^{n+1}\right]=-\check{\mathbf{F}}_\rho^{n+1}$$
$$+\check{\mathbf{C}}_{\rho\mathbf{m}}\widetilde{\mathbf{U}}^{n+1}. \tag{6.27}$$

At this point, we have modified the original mass equation by introducing some burden that we need to solve. We discuss this issue in the upcoming remarks.

Remark 6.5.1 One should notice that the resulting matrix from $\check{\mathbf{C}}_{\rho\mathbf{m}}\left[\mathbf{M}_{\mathbf{mm}}\right]^{-1}\mathbf{C}_{\mathbf{m}\rho}$ can be viewed as an approximation to the discrete version of a Laplacian-like operator, [140]. In order to avoid dealing with this matrix, which is in general dense and might still be expensive to compute even when $\mathbf{M}_{\mathbf{mm}}$ is lumped, we use the approximation $\check{\mathbf{C}}_{\rho\mathbf{m}}\left[\mathbf{M}_{\mathbf{mm}}\right]^{-1}\mathbf{C}_{\mathbf{m}\rho}\approx\mathbf{L}$ where $\mathbf{L}$ is a Laplacian matrix computed using the gradient of the standard shape functions. If a and b range from 0 to the number of elemental nodes and j from 1 to N_{sd}, the matrix is calculated as

$$[\mathbf{L}^{(e)}]^{ab}=\int_{\Omega^{(e)}}0.5(\mathbf{u}\cdot\mathbf{u})(\gamma-1)\partial_j\varphi^a\partial_j\varphi^b\,\mathrm{d}\Omega,$$
$$\mathbf{L}=\mathbb{A}^{(e)}\mathbf{L}^{(e)},$$

where the first factors in the integrand are introduced to keep the proper scaling. Being able to perform this approximation is what led us to obtain matrix $\check{\mathbf{C}}_{\rho\mathbf{m}}$ instead of working directly with $\mathbf{C}_{\rho\mathbf{m}}$.

Remark 6.5.2 Recalling the definition of the extrapolation operators, Equation 3.9, note that

$$\left\|\varrho^{n+1}-\hat{\varrho}_{\theta-1}^{n+1}\right\|\sim\mathcal{O}(\delta t^{\theta-1}),$$
$$\left\|\mathbf{E}^{n+1}-\widehat{\mathbf{E}}_{\theta-1}^{n+1}\right\|\sim\mathcal{O}(\delta t^{\theta-1}).$$

Therefore, it is easy to see from Equation 6.21b that,

$$\mathcal{O}(\left\|\mathbf{U}^{n+1}-\widetilde{\mathbf{U}}^{n+1}\right\|)=\mathcal{O}(\delta t^{\theta}),$$

and thus, the global accuracy of the temporal integrator is formally maintained for the intermediate momentum variable.

Remark 6.5.3 Note that if we substitute $\mathbf{U}^{n+1}$ by $\widetilde{\mathbf{U}}^{n+1}$ in the definition of $\check{\mathbf{F}}_{\rho}^{n+1}$, which is supported by the previous remark, the last two terms in Equation 6.24 can be grouped as $-\mathbf{C}_{\rho\mathbf{m}}\widetilde{\mathbf{U}}^{n+1}$ (integration by parts).

Remark 6.5.4 Up to our knowledge, there is not a possible approximation for the rest of the products involved in

$$\check{\mathbf{C}}_{\rho\mathbf{m}}\left[\mathbf{M}_{\mathbf{mm}}\right]^{-1}\left[\mathbf{N}_{\rho}^{n+1}+\mathbf{N}_{\mathbf{m}}^{n+1}+\mathbf{N}_{E}^{n+1}\right].$$

However, the presence of such extra products involving density and energy could be avoided by performing an extrapolation of the same order of that used to approximate time derivatives in the intermediate momentum equation. Then, we shall use $\mathbf{D}_{\mathbf{m}\rho}\hat{\boldsymbol{\varrho}}_{\theta}^{n+1}$ instead of $\mathbf{D}_{\mathbf{m}\rho}\hat{\boldsymbol{\varrho}}_{\theta-1}^{n+1}$ and $\mathbf{C}_{\mathbf{m}E}\widehat{\mathbf{E}}_{\theta}^{n+1}$ instead of $\mathbf{C}_{\mathbf{m}E}\widehat{\mathbf{E}}_{\theta-1}^{n+1}$ in Equation 6.21a. Therefore, there is no need to include such terms in the correction equation Equation 6.21b since $\left\|\boldsymbol{\varrho}^{n+1}-\hat{\boldsymbol{\varrho}}_{\theta}^{n+1}\right\|$ and $\left\|\mathbf{E}^{n+1}-\widehat{\mathbf{E}}_{\theta}^{n+1}\right\|$ are already of order $\mathcal{O}\left(\delta t^{\theta}\right)$.

Remark 6.5.5 Using directly $\mathbf{D}_{\mathbf{m}\rho}\hat{\boldsymbol{\varrho}}_{\theta}^{n+1}$ and $\mathbf{C}_{\mathbf{m}E}\widehat{\mathbf{E}}_{\theta}^{n+1}$ involves an explicit treatment of density and energy in the momentum equation that could imply the introduction of a critical time step to ensure stability. However, in practice we have not observed such time step limitation.

6.5.3 Fractional step algorithm

Taking all the previous information into account, the fractional step approach that we favor to solve the fully compressible Navier-Stokes problem in conservative variables is composed of four main steps:

i. Compute an intermediate momentum from Equation 6.21a making use of $\hat{\boldsymbol{\varrho}}_{\theta}^{n+1}$ and $\widehat{\mathbf{E}}_{\theta}^{n+1}$.
ii. Compute an approximation to the density from Equation 6.21c, neglecting $\mathbf{N}_{\mathbf{m}}^{n+1}$, replacing $\mathbf{U}^{n+1}$ by $\widetilde{\mathbf{U}}^{n+1}$ and

taking into account the previous Laplacian approximation.

$$\left[\mathbf{M}_{\rho\rho}\frac{D_\theta}{\delta t} + \phi_\theta \delta t \mathbf{L}\right]\boldsymbol{\varrho}^{n+1} = -\mathbf{C}_{\rho\mathbf{m}}\widetilde{\mathbf{U}}^{n+1} + \phi_\theta \delta t \mathbf{L}\hat{\boldsymbol{\varrho}}^{n+1}_{\theta-1}. \tag{6.28}$$

iii. Compute an approximation to the total energy from Equation 6.21d, replacing $\mathbf{U}^{n+1}$ by $\widetilde{\mathbf{U}}^{n+1}$ (already known as a result of the first step).

iv. Update the end-of-step momentum with Equation 6.21b neglecting $\mathbf{N}^{n+1}_{\mathbf{m}}$.

This procedure will make possible to segregate the calculation of the unknowns of the problem and we shall refer to it as density/energy-correction algorithm, using a similar nomenclature as it is usually done for incompressible/low Mach algorithms.

First and second order fractional step scheme for the conservative Navier-Stokes problem

```
▸ Set/read the initial conditions for $\boldsymbol{\varrho}^0$, $\mathbf{U}^0$ and $\mathbf{E}^0$.
▸ WHILE $n < N$ DO
    • Set $\mathbf{U}^{n,0} = \mathbf{U}^{n-1}$, $\mathbf{P}^{n,0} = \mathbf{P}^{n-1}$ and $\boldsymbol{\Theta}^{n,0} = \boldsymbol{\Theta}^{n-1}$
    • WHILE (not converged) DO
        * Compute intermediate momentum $\widetilde{\mathbf{U}}^{n+1}$:
          $\mathbf{M}_{\mathbf{mm}}\frac{D_\theta}{\delta t}\widetilde{\mathbf{U}}^{n+1,(i+1)} + \mathbf{C}_{\mathbf{mm}}\left(\hat{\boldsymbol{\varrho}}^{n+1}_\theta, \widetilde{\mathbf{U}}^{n+1,(i)}\right)\widetilde{\mathbf{U}}^{n+1,(i+1)}$
          $\quad + \mathbf{D}_{\mathbf{mm}}(\hat{\boldsymbol{\varrho}}^{n+1}_\theta)\widetilde{\mathbf{U}}^{n+1,(i+1)} = -\mathbf{C}_{\mathbf{m}\rho}(\hat{\boldsymbol{\varrho}}^{n+1}_\theta, \widetilde{\mathbf{U}}^{n+1,(i)})\boldsymbol{\varrho}^{n+1}_{\theta-1}$
          $\quad - \mathbf{D}_{\mathbf{m}\rho}(\hat{\boldsymbol{\varrho}}^{n+1}_\theta, \widetilde{\mathbf{U}}^{n+1,(i)})\hat{\boldsymbol{\varrho}}^{n+1}_\theta - \mathbf{C}_{\mathbf{m}E}\widehat{\mathbf{E}}^{n+1}_\theta$
        * Check convergence
    • END while (not converged)
    • Compute density using the previous intermediate momentum values:
      $\mathbf{M}_{\rho\rho}\frac{D_\theta}{\delta t}\boldsymbol{\varrho}^{n+1} + \phi_\theta \delta t \mathbf{L}\boldsymbol{\varrho}^{n+1} = -\mathbf{C}_{\rho\mathbf{m}}\widetilde{\mathbf{U}}^{n+1} + \phi_\theta \delta t \mathbf{L}\hat{\boldsymbol{\varrho}}^{n+1}_{\theta-1}$
    • Compute energy using intermediate momentum and density solutions:
      $\mathbf{M}_{EE}\frac{D_\theta}{\delta t}\mathbf{E}^{n+1} + \mathbf{C}_{EE}\left(\boldsymbol{\varrho}^{n+1}, \widetilde{\mathbf{U}}^{n+1}\right)\mathbf{E}^{n+1}$
```

$$
\begin{aligned}
&+ \mathbf{D}_{EE}(\boldsymbol{\varrho}^{n+1})\mathbf{E}^{n+1} = -\mathbf{C}_{E\rho}(\boldsymbol{\varrho}^{n+1}, \widetilde{\mathbf{U}}^{n+1}, \widehat{\mathbf{E}}_{\theta}^{n+1})\boldsymbol{\varrho}^{n+1} \\
&- \mathbf{D}_{E\rho}(\boldsymbol{\varrho}^{n+1}, \widetilde{\mathbf{U}}^{n+1}, \widehat{\mathbf{E}}_{\theta}^{n+1})\boldsymbol{\varrho}^{n+1} \\
&- \mathbf{C}_{E\mathbf{m}}(\boldsymbol{\varrho}^{n+1}, \widetilde{\mathbf{U}}^{n+1}, \widehat{\mathbf{E}}_{\theta}^{n+1})\widetilde{\mathbf{U}}^{n+1} \\
&- \mathbf{D}_{E\mathbf{m}}(\boldsymbol{\varrho}^{n+1}, \widetilde{\mathbf{U}}^{n+1})\widetilde{\mathbf{U}}^{n+1}
\end{aligned}
$$

- Momentum correction, *i. e.*, end-of-step momentum calculation:

$$
\mathbf{M}_{\mathbf{mm}}\frac{\mathbf{U}^{n+1}}{\phi_\theta \delta t} = \mathbf{M}_{\mathbf{mm}}\frac{\widetilde{\mathbf{U}}^{n+1}}{\phi_\theta \delta t} - \mathbf{C}_{\mathbf{m}\rho}(\boldsymbol{\varrho}^{n+1} - \boldsymbol{\varrho}_{\theta-1}^{n+1})
$$

▸ END while $n < N$ (non-stationary)

Once we introduce the VMS-based stabilization terms, new coupling terms involving the three unknown conservative variables appear. Hence, some extra information is required in order to achieve the complete uncoupling process. When needed, we may replace $\mathbf{U}^{n+1}$ by $\widetilde{\mathbf{U}}^{n+1}$, $\boldsymbol{\varrho}^{n+1}$ by $\hat{\boldsymbol{\varrho}}_{\theta}^{n+1}$ and $\mathbf{E}^{n+1}$ by $\widehat{\mathbf{E}}_{\theta}^{n+1}$. These approximations are supported by Remark 6.5.2.

The remaining terms which could still couple the problem variables can be evaluated by taking the known values of the unknowns from the previous iteration, time step or from the intermediate equations. In particular, note that density and energy equations become coupled, an important fact for the development of the whole methodology. The coupling blocks are taken to the right-hand side and treated in an explicit manner, generally with the most up-to-date known values. However, when evaluating the residuals and the projections, we have found of critical importance to perform the computations with all the terms evaluated at the same time instant. Otherwise, convergence problems may appear which we associate with the strong coupling between thermodynamic variables.

Remark 6.5.6 In the design of fractional step methods for incompressible flows there are two equations in play taking velocity and pressure as main variables. The classic and well-established pressure-correction procedure [50, 55] allows to split the calculation of the unknowns after performing some extrapolation in the momentum equation, prior to solving the continuity one. A similar design was carried out in [155] for isentropic flows. However, for the case of compressible flows, as the problem includes also the energy equation, there are more possibilities to perform the splitting and hence to design the algorithm. Our intention in this chapter was to follow the same pattern of previous developments in our group as in [46, 50, 53, 55] or the previous chapters, where the first equation to be solved is the intermediate momentum equation. Nevertheless, other approaches should be explored and compared.

6.6 Numerical examples

In this section, a set of numerical examples is presented to show the capabilities of the proposed fractional step method for the simulation of compressible flows at different regimes.

In order to solve the final underlying systems of linear equations, and if nothing else is stated, we make use of an iterative algorithm based on the stabilized version of the BiConjugate Gradient method `BiCGstab` [143], which is already included as a part of the parallel solver library `PETSc` [61], which has been coupled with `FEMUSS`.

We consider an ideal gas with $\gamma = 1.4$ ($R_\mathrm{g} = 287$ J/(kg K)) and $c_p = 1004.5$ J/(kg K) and $\mathrm{Pr} = 0.72$. A maximum of 10 iterations is set to solve each nonlinear problem, and the relative numerical tolerance for the L^2-norm is 1×10^{-5}. All the plots are in SI units.

6.6.1 Convergence test

In this first example we consider a simple convergence test whose goal is to check numerically the time rate of convergence for the proposed fractional step algorithm. We recall that as time integration scheme we use backward differences, of the same order as the fractional step to be tested.

As we did in previous chapters, we make use again of the manufactured solutions method and, in particular, exact solutions for density, momentum and energy are specified. The compressible Navier-Stokes problem is solved over the unit square $\overline{\Omega} = [0, 1] \times [0, 1]$ and the force term is set so that the exact solution of the problem is:

$$\begin{aligned} \rho(x, y, t) &\coloneqq \pi + x\cos(\sin t) + y\sin(\sin t), && (6.29a)\\ \rho u(x, y, t) &\coloneqq -y\cos(t), && (6.29b)\\ \rho v(x, y, t) &\coloneqq x\cos(t), && (6.29c)\\ \rho e(x, y, t) &\coloneqq 4\pi + x\cos(\sin(t)) + y\sin(\sin(t)). && (6.29d) \end{aligned}$$

The finite element partition is structured and uniform and it contains $Q_1/Q_1/Q_1$ finite elements of size $h = 1/100$. Both the boundary and initial conditions are evaluated from the previous equations, and particularized for each of the sides of the square at each time step and for $t = 0$, respectively. We select a range of time step sizes and, in addition, we set $\mu = 1 \times 10^{-5}$ kg/(m s), $\kappa = 0.0015$ W/(m K), and we make use of a sparse direct solver from the `MUMPS` library [157, 158].

The error between the exact solution and the numerical one is measured in the ℓ^2-norm of the sequence of spatial L^2-norms of the solutions, *i. e.*,

$$E_f \coloneqq \left(\delta t \sum_{n=1}^{N} \frac{\|f_h^n - f(t^n)\|_{L^2}^2}{\|f(t^n)\|_{L^2}^2} \right)^{1/2},$$

for $f = \rho$, $\rho\mathbf{u}$ or ρe, respectively.

Figure 6.1 shows the convergence results obtained with the fractional step algorithm for both first and second order time integration schemes. The expected convergence rate can be clearly seen for both temporal approximations and for all the time step sizes.

6.6.2 Supersonic viscous flow over a flat plate

Carter's flat plate problem is a simple and classical benchmark to examine the performance of the solver in a problem involving shock waves, boundary layers and the interaction between them. This example is based on a 2D viscous supersonic flow over a flat plate with conditions:

$$\mathrm{Re}_\infty = 1,000, \quad \text{and} \quad \mathrm{Ma}_\infty = 3.0.$$

Figure 6.2 shows the problem setup. If the coordinate origin is placed and the tip of the plate, the computational domain is

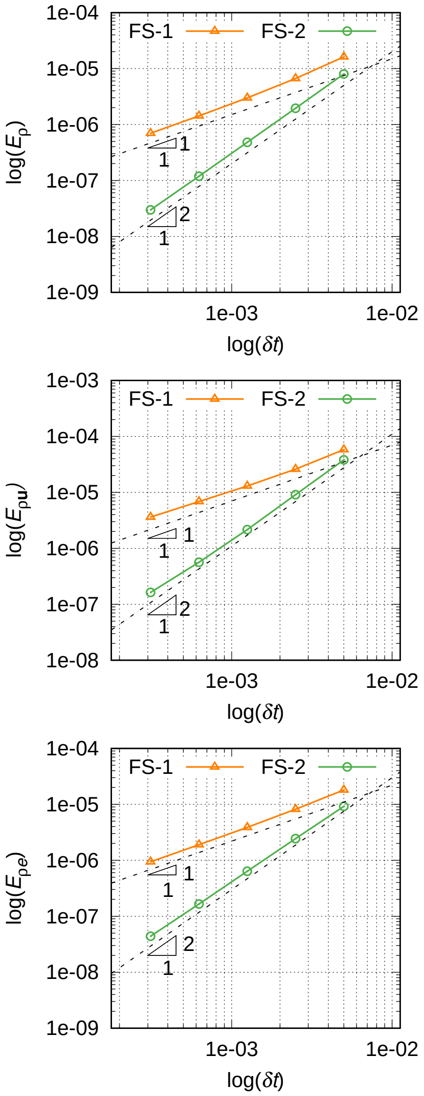

Figure 6.1: Convergence test: time convergence of the relative errors of density (top), momentum (middle) and energy (bottom) measured in the $\ell^2(0, t_f, L^2(\Omega))$-norm: The number after the dash symbol stands for first (1) or second (2) order scheme in time.

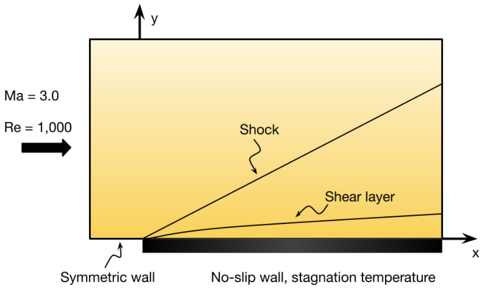

Figure 6.2: Supersonic flow over a flat plate. Problem setup and boundary conditions.

the rectangle covering from $-0.25\ \mathrm{m} \le x \le 1.2\ \mathrm{m}$ and $0 \le y \le 0.8\ \mathrm{m}$. Density, velocity and temperature are set at the left and top boundaries of the domain. These prescribed values are, respectively, $\rho_\infty = 1$ kg/m^3, $u_\infty = 1$ m/s, $v_\infty = 0$ m/s and $\vartheta_\infty = 2.769 \times 10^{-4}$ K. The no-slip boundary condition $\mathbf{u} = \mathbf{0}$ m/s is enforced at the plate wall, together with the stagnation temperature, which is computed as

$$\vartheta_{\text{stag}} = \vartheta_\infty \left(1 + \frac{\gamma - 1}{2}\text{Ma}_\infty^2\right).$$

On the "symmetric wall", *i. e.*, the boundary prior to the plate, normal velocity, tangential traction, and heat flux are all set to zero. No prescriptions are made at the outflow, and the computations are initialized with the free-stream values for each degree of freedom in the entire domain. The temperature dependent viscosity is computed according to the Sutherland's law in Equation 2.10, with $S = 0.0001406$, and $C_1 = 0.0906$.

The simulation was carried out using a time step corresponding to a CFL of 4. Here, we estimate the critical time step for the explicit scheme as the minimum of the stabilization parameters, *i. e.*, $\delta t = \min(\tau_\rho, \boldsymbol{\tau}_\mathbf{m}, \tau_E)$. In addition, we discretize the domain with a structured mesh of square elements of size $h = 0.01$.

Figure 6.3 displays the obtained contours of density, velocity and temperature. The results are in general agreement with the literature, *e. g.*, [56] and [171–174]. The solution is computed with the gradient-based shock capturing operator. Several values for the operator constant C_{sc} were tested, $C_{\text{sc}} = \{0.25, 0.5, 0.75\}$ although the results were all really similar. We shall use $C_{\text{sc}} = 0.25$ in the upcoming examples.

[171]: Zienkiewicz et al. (1995), "A general algorithm for the compressible and incompressible flows. Part I: The split, characteristic-based scheme"
[172]: Kouhi et al. (2015), "An implicit stabilized finite element method for the compressible Navier–Stokes equations using finite calculus"
[173]: Xu et al. (2017), "Compressible flows on moving domains: Stabilized methods, weakly enforced essential boundary conditions, sliding interfaces, and application to gas-turbine modeling"
[174]: Carter (1972), *Numerical solutions of the Navier–Stokes equations for the supersonic laminar flow over a two-dimensional compression corner*

In Figure 6.4, we plot the normalized density and temperature profiles along the line $x = 1.2$ for the stationary solution, in order to further compare our solutions with the literature. Although the obtained peak point values are not coincident with the reference ones, an overall good agreement with the reference results can be observed.

Since the solution is stationary, this example serves to demonstrate that the approximations in the matrices introduced in the design of the fractional step scheme maintain the accuracy and the ability to model shocks of the monolithic formulation.

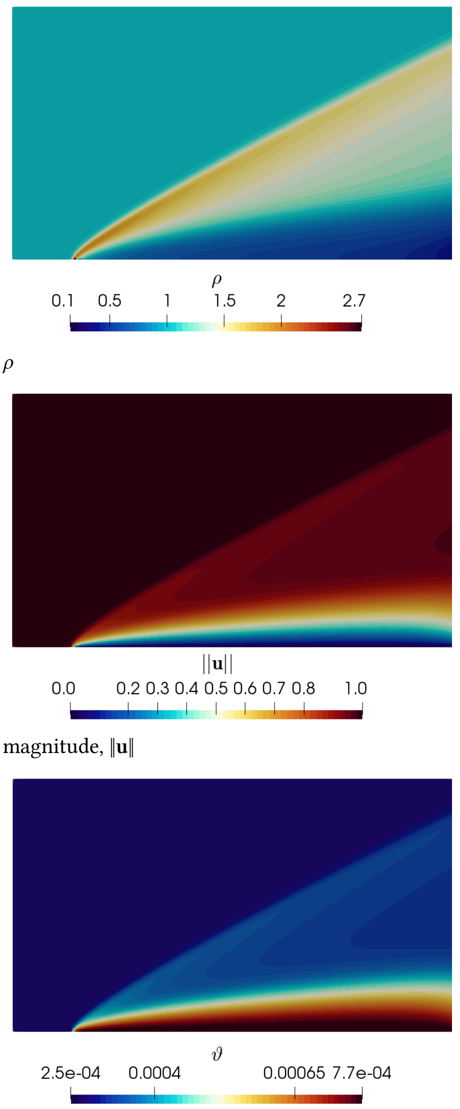

(a) Density, ρ

(b) Velocity magnitude, $\|\mathbf{u}\|$

(c) Temperature, ϑ

Figure 6.3: Carter's flow problem: (a) density, (b) velocity magnitude and (c) temperature contours computed with the monolithic algorithm. Fractional step results are basically the same and hence omitted.

6.6.3 Supersonic viscous flow over a cylinder

Another classical example in compressible flows is the supersonic viscous flow over a cylinder, as sketched in Figure 6.5, with free stream conditions

$$\mathrm{Re}_\infty = 2,000 \quad \text{and} \quad \mathrm{Ma}_\infty = 2.$$

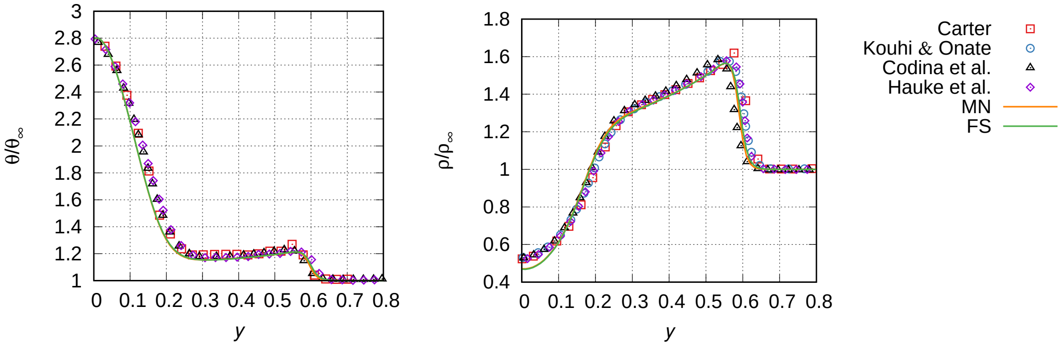

(a) Normalized temperature $\vartheta/\vartheta_\infty$ **(b)** Normalized temperature ρ/ρ_∞

Figure 6.4: Carter's flow problem: Comparison of the obtained (a) normalized temperature and (b) normalized density along the line $x = 1.2$ m with results reported in the literature [56, 171, 172, 174]. Hereinafter, MN stands for monolithic results and FS for fractional step results.

The specification of boundary conditions is as follows: all variables are specified on the upstream boundary matching those conditions. The cylinder wall is assumed to be adiabatic, no-slip condition is specified for the velocity on its surface, and at the downstream boundary, no conditions are imposed. The computations are initialized with the free-stream values for each degree of freedom in the entire domain. Likewise, we set $\mu = 0.001$ kg/(m s) and $\kappa = 1.39514$ W/(m K). The finite element mesh is unstructured and it is made of 31,288 linear triangular elements. Smaller elements are used near the wall cylinder, whereas the mesh is coarser in the rest of the domain. The mesh size was fixed to $h = 0.005$ m in the finer region near the cylinder wall. Comparing the solution obtained with monolithic and fractional step formulations, the field contours are almost identical, what shows, as in the previous example, that the space accuracy is not affected by the design of the fractional step scheme. Density, pressure, Mach number and temperature distributions are shown in Figure 6.6. A supersonic expansion develops from the cylinder surface, while in the wake the flow pattern is characterized by a recirculation zone and a weak tail shock. The presented contours for the steady state solution are in accordance with the ones presented in [111] and [175], although neither Sutherland law nor power law were used for viscosity in this example.

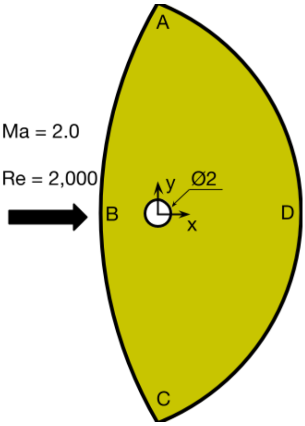

Figure 6.5: Supersonic flow over a cylinder: domain specification. The computational domain is defined as the area enclosed within two arcs passing, respectively, through points A(0,15), B(-4,0), C(0,-15), and A, D(10,0) and C. The cylinder is placed at the origin of coordinates with diameter equal to 2 m.

[175]: Mittal (1998), "Finite element computation of unsteady viscous compressible flows"

Since no noticeable qualitative differences were observed in our results, some aerodynamic integral values of the flow

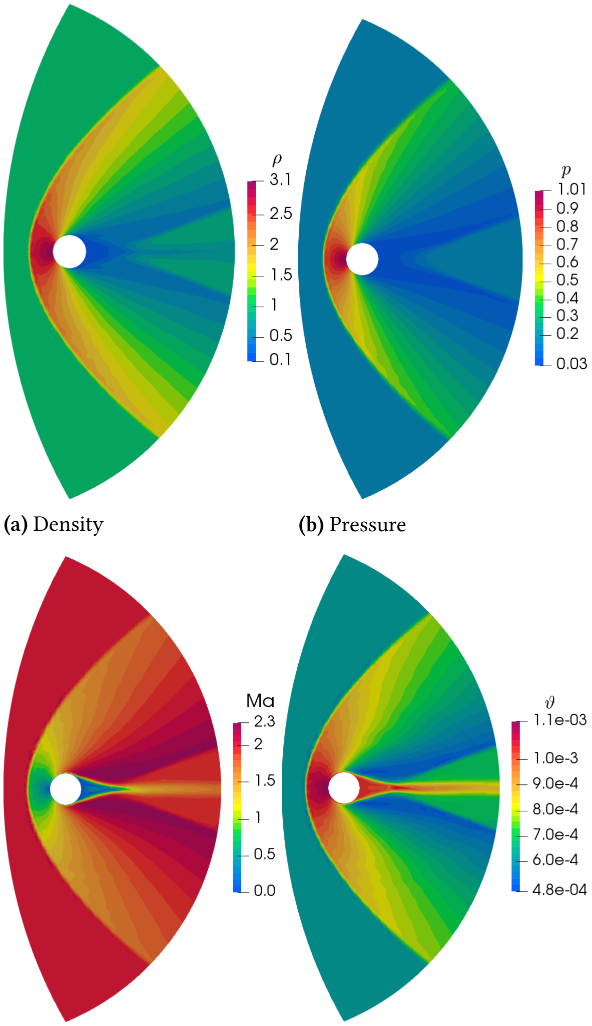

(a) Density

(b) Pressure

(c) Mach number

(d) Temperature

Figure 6.6: Supersonic flow over a cylinder: (a) density, (b) pressure, (c) Mach number and (d) temperature contours. The solution is obtained using the fractional step formulation together with the isotropic gradient-based shock capturing method.

were computed. In particular, we calculate the lift and drag non-dimensional coefficients, following Equation 4.38a, Equation 4.38b and Equation 4.39. The results are $C_d = 1.439$ for the monolithic case and $C_d = 1.442$ for the fractional step counterpart, which have an accuracy comparable to that reported in [175], $C_d = 1.44$.

6.6.4 NACA0012 airfoil

In this section we consider the well-known geometry of the NACA0012 airfoil with chord length $c = 1$ m and a sharp trailing edge. The objective now is to test our methodology in a wider range of regimes. For this purpose, we consider two cases with angle of attack AoA = 0°: first a subsonic case with

$$\mathrm{Re}_\infty = 5,000, \quad \text{and} \quad \mathrm{Ma}_\infty = 0.5,$$

and later a transonic problem with

$$\mathrm{Re}_\infty = 10,000, \quad \text{and} \quad \mathrm{Ma}_\infty = 0.85.$$

In order to perform the simulation, we define a circular O-type domain with the mid-chord point of the airfoil located at the coordinate origin. The far-field boundary is placed at 15 chord lengths from the airfoil. In the inflow part of the boundary, velocity and temperature are fixed according to the selected Reynolds and Mach numbers, whereas in the outflow part only density is prescribed. A no slip adiabatic wall condition is imposed at the airfoil surface and the computations are initialized with free-stream conditions in the entire domain. Furthermore, we use an unstructured mesh of triangular elements, including non-uniform refinement towards the airfoil surface. Figure 6.7 reports the details of the mesh, which features 254,186 elements. The problem is solved with a time step corresponding to a CFL of 12.

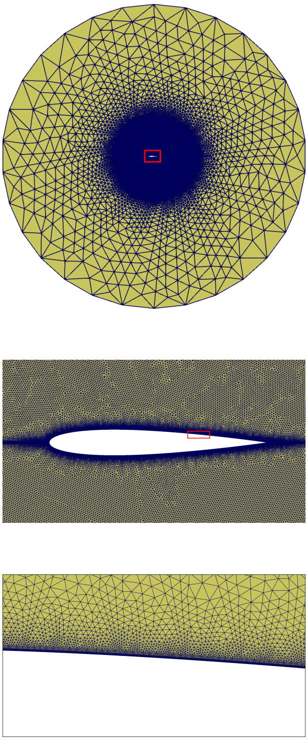

Figure 6.7: Mesh refinement for the NACA 0012 simulations.

Ma=0.5, Re=5,000

First we present the subsonic viscous flow simulation. Figure 6.8 displays density, Mach number and temperature distributions for the steady-state solution of this problem. Likewise, Figure 6.9 contains the chord-wise distributions of pressure and skin friction coefficients, comparing both fractional step and monolithic results with other researchers such as [172, 175, 176]. These are respectively computed from:

$$C_p = \frac{p - p_\infty}{\frac{1}{2}\rho_\infty \|\mathbf{u}\|_\infty^2}, \tag{6.30a}$$

$$C_f = \frac{\tau_{\mathrm{w}}}{\frac{1}{2}\rho_\infty \|\mathbf{u}\|_\infty^2}, \tag{6.30b}$$

where p_∞ is the inflow static pressure and

$$\tau_{\mathrm{w}} = (\boldsymbol{\sigma} \cdot \mathbf{n}) \cdot \mathbf{t}$$

is the wall stress, with **t** the tangent vector to the surface. It is observed that the results exhibit a clear agreement with the literature.

Additionally, the drag coefficient values are $C_d = 0.0548$ for the monolithic computations and $C_d = 0.0551$ for the fractional step counterpart, which are in line with the values reported by Mittal [175], $C_d = 0.0550$ and Venkatkrishnan [176], $C_d = 0.0554$. Finally, for the separation point, it is located at 82.7 % and 82.9 % of the chord from the leading edge, respectively for monolithic and fractional step algorithms. These results are summarized in Table 6.2 down below.

[176]: Venkatakrishnan (1990), "Viscous computations using a direct solver"

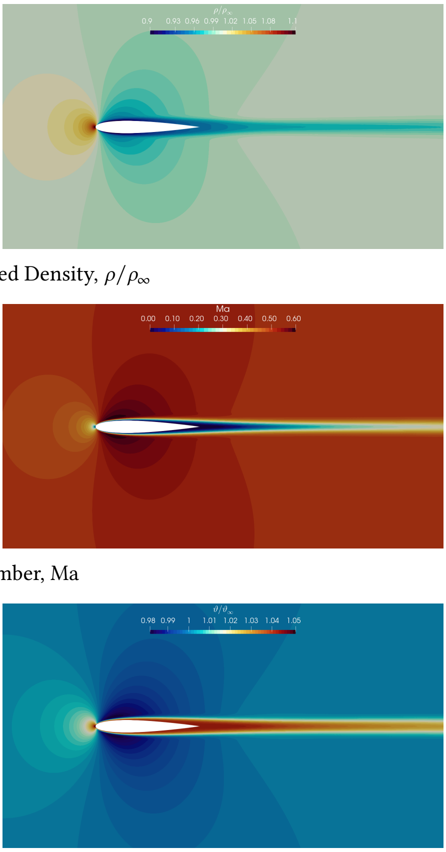

(a) Normalized Density, ρ/ρ_∞

(b) Mach number, Ma

(c) Normalized temperature, $\vartheta/\vartheta_\infty$

Figure 6.8: Subsonic flow over a NACA 0012 profile: (a) density, (b) Mach number and (c) temperature distributions around the airfoil computed with the second order version of the fractional step scheme.

Ma=0.85, Re=10,000

We switch now the conditions of the problem to a transonic regime with $\mathrm{Re} = 10,000$ and turn on the gradient-based

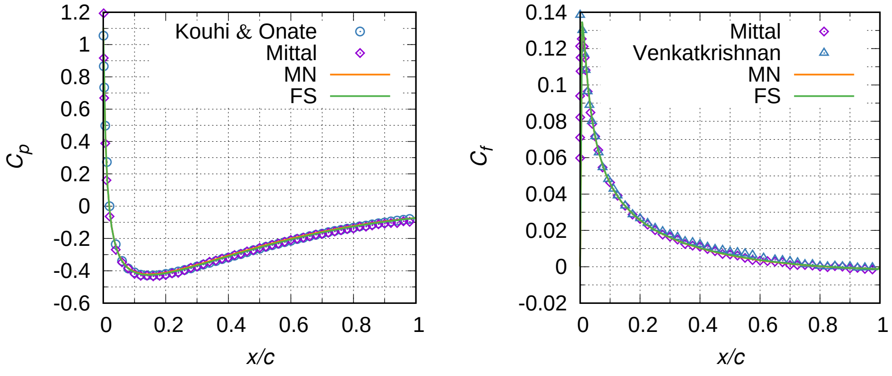

(a) Pressure coefficient

(b) Skin friction coefficient

Figure 6.9: Subsonic flow over a NACA 0012 profile: (a) Non-dimensional pressure coefficient, and (b) skin friction coefficient on the aerofoil.

Table 6.2: 2D differentially heated cavity: ratio of CPU time of the fractional step schemes over the monolithic formulations in the 2D chaotic case (second order schemes).

Ref.	C_d	x_s/c
Mittal [175]	0.0550	0.813
Venkatkrishnan [176]	0.0554	[0.810,0.825]
Present-MN	0.0548	0.827
Present-FS	0.0551	0.829

shock capturing operator with $C_{sc} = 0.25$. After an initial transient period is overcome, a fully developed periodic solution is established.

Figure 6.10 displays density, Mach number and temperature distributions once this periodic flow has been fully developed, and Figure 6.11 contains the pressure time history comparing fractional step and monolithic solutions. Both formulations obtain very similar results. The flow evolves as described in [177]: it originally expands from the front stagnation point and then the boundary layer thickness begins to increase until the interaction between the layer and the shock wave results in the separation of flow. It is to be noticed that the vortices are shed from both, the upper and the lower surfaces of the airfoil. Moreover, two different instability mechanisms are active in the wake region, one mainly associated with the shear layer (also known as Kelvin-Helmoltz mechanism), and the other one resulting from the interaction between the layer and the shock wave.

[177]: Bouhadji et al. (2003), "Organised modes and shock–vortex interaction in unsteady viscous transonic flows around an aerofoil. Part I: Mach number effect"

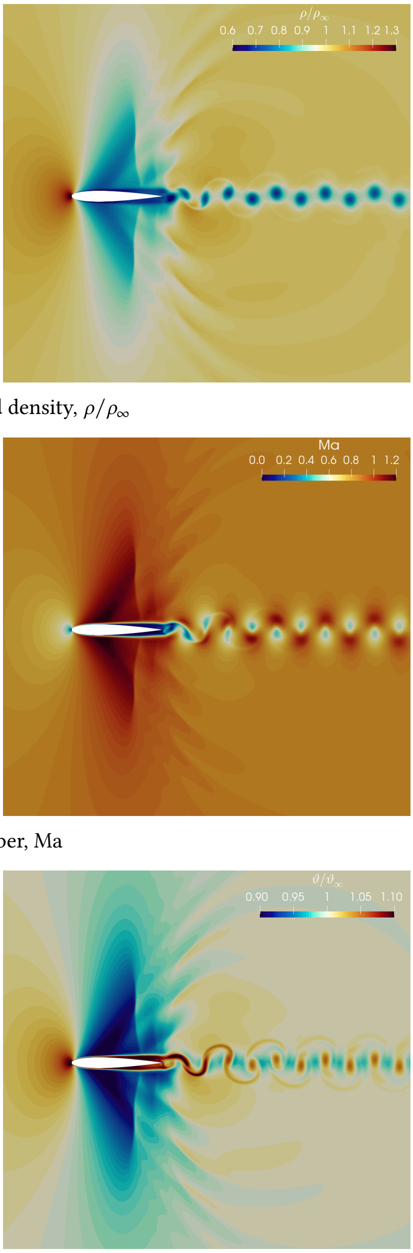

(a) Normalized density, ρ/ρ_∞

(b) Mach number, Ma

(c) Normalized temperature, $\vartheta/\vartheta_\infty$

Figure 6.10: Transonic flow over a NACA 0012 profile: (a) Density, (b) Mach number and (c) temperature distributions around the aerofoil computed with the second order version of the fractional step scheme.

6.6.5 3D flow over a sphere

In this final numerical example we model a 3D flow over a sphere. The purpose of this simulation is twofold. First, we use this example to show the applicability of the devel-

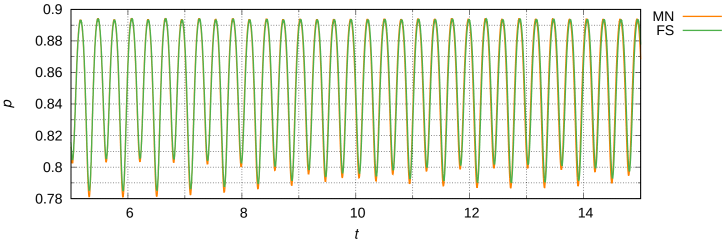

Figure 6.11: Transonic flow over a NACA 0012 profile: pressure time history for both formulations at point (3.5,0) located at the wake of the airfoil.

oped compressible formulation in complex 3D problems. Second, we will perform some simple tests in order to provide some insights on the actual computational savings that the fractional step implementation may offer with respect to the standard monolithic solver. We consider the flow around a sphere with

$$\mathrm{Re}_\infty = 5,000, \quad \text{and} \quad \mathrm{Ma}_\infty = \{0.25, 0.75\}.$$

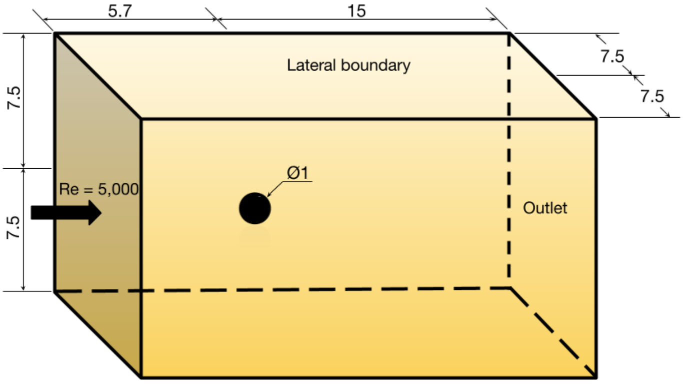

Figure 6.12: Flow around a sphere. Problem setup and domain specification.

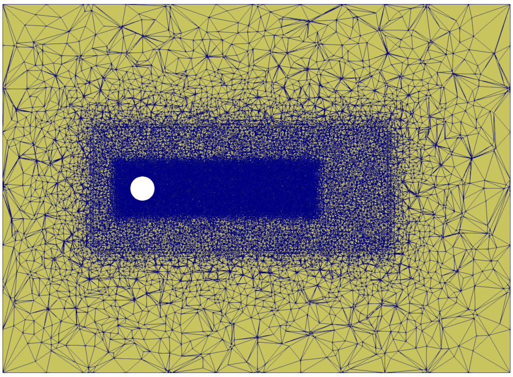

Figure 6.13: Flow around a sphere. Mesh cut.

The problem setup is shown in Figure 6.12. A uniform flow with the desired conditions impinges the left-inlet boundary, where density, velocity and temperature are prescribed. The lateral boundaries are defined as no-penetration and adiabatic, and the right-outflow boundary is traction free and adiabatic. The surface of the sphere is no-slip as well as adiabatic. As usual, the computations are initiated with free stream values. In order to build up the mesh, we first assign a size $h = 0.005$ over the sphere with uniform triangles. Likewise, two cylindrical refinement zones around and downstream of the sphere are introduced in order to better reproduce the wake of the flow, one with diameter of 2 m and the second one with diameter of 5 m. The remainder of the domain is filled with tetrahedral elements. A cut through the mesh is shown in Figure 6.13 in order to illustrate the interior of the domain. The mesh accounts for a total of ~ 5.8 million elements. Figure 6.14 shows streamlines just to give and idea of the features of the flow.

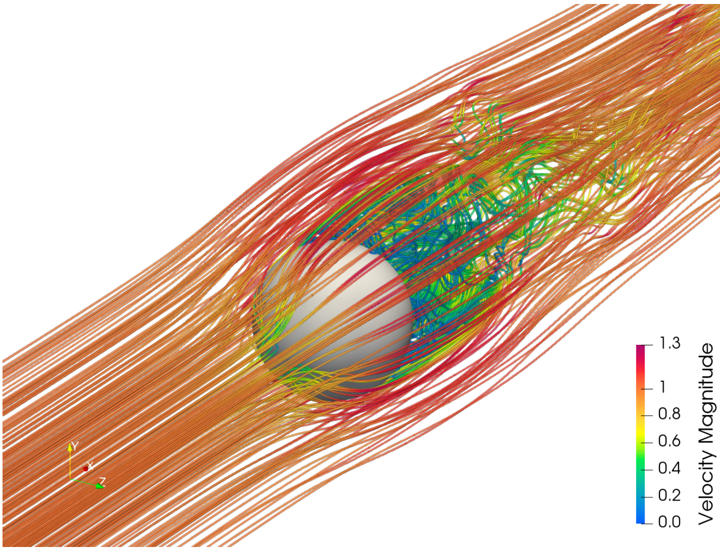

Figure 6.14: Flow around a sphere: stream lines for Ma = 0.25.

The left part in Table 6.3 shows the savings in CPU time of the fractional step algorithms (second order) for the two cases considered with respect to the monolithic formulation. A simple implementation over a series of time steps has been used. The savings are presented as the ratio between the CPU time of the fractional step scheme over the CPU time of the corresponding monolithic scheme. In addition, we collect the number of iterations needed by the solver to obtain the solution of the system of equations and the number of nonlinear iterations used to obtain converged results. In fractional step schemes, each variable requires a different

Table 6.3: Comparison between the number of nonlinear and solver iterations of the monolithic and of the second order fractional step algorithm using the BDF2 time integrator. Here, $\overline{\text{nni}}$ is the average number of nonlinear iterations to achieve convergence and $\overline{\text{nsi}}$ stands for the average number of iterations needed by the iterative algebraic solver.

Case	Time ratio	Monolithic	Fractional step		
		$\overline{\text{nni}}/\overline{\text{nsi}}$	$\overline{\text{nni}}_{\rho\mathbf{u}}/\overline{\text{nsi}}_{\rho\mathbf{u}}$	$\overline{\text{nsi}}_{\rho}$	$\overline{\text{nni}}_{\rho e}/\overline{\text{nsi}}_{\rho e}$
Ma=0.25	0.58	8/9	5/7	11	2/7
Ma=0.75	0.89	7/7	5/6	7	4/6

number of iterations to solve the corresponding linear system. Apart from the fact that the linear systems to be solved in the fractional step method are smaller and usually better conditioned, the main drawback of the monolithic formulation is that the total number of iterations of the linear system solver is driven by the slowest variable. This is at least our experience from our previous works on fractional step algorithms for incompressible, isentropic and compressible-primitive formulations (see the section of numerical results and conclusions in [55, 155, 169]). The general trend is that the slowest variable in those cases is the pressure. This point is illustrated by the first raw of Table 6.3. As expected, for the low Mach subsonic $\text{Ma}_{\infty} = 0.25$ case the slowest variable is the density (pressure). Not only there is a reduction in the computational cost but also the nonlinearities are solved in a better manner. However, the benefit of using a fractional step scheme in conservative variables degrades as the Mach number is progressively increased. As the problem is far from the incompressible behavior, the density stops being the slowest variable and then we observe that the number of iterations of the solver is basically the same for both monolithic and fractional step methodologies. This is why the obtained savings of the $\text{Ma}_{\infty} = 0.75$ case are not very important, although more important savings should be expected in very large scale problems.

6.7 Conclusions

In this chapter, we have introduced a fractional step technique to solve the compressible Navier-Stokes equations using conservative variables. The development of this methodology, which is up to second order in time, has been designed at the algebraic level, departing from the fully discretized monolithic problem both in space and in time and by using the extrapolation concept.

From the numerical viewpoint, the herein proposed fractional step compressible model is based on a stabilized VMS method and an implicit scheme to advance the solution in time. In addition, other ingredients were appended, such as the orthogonal and dynamic definition of subscales and the shock-captuting operator which is calculated by using the orthogonal projection onto the finite element space of the gradient of the solution.

First, we have shown that the fractional step method introduces an splitting error but it maintains the general temporal accuracy of the time integration scheme. Furthermore, the supersonic viscous flow over a cylinder and the classical flow over a plate have been used to test the performance of the algorithm in the supersonic regime, where the interaction of shocks and shear layers is relevant. Similarly, the NACA0012 flow problem was used to evaluate the behavior of the implementation in subsonic and transonic cases also with adequate results. Finally we have shown an involved 3D case and also we have provided some insights on the possible savings that a fractional step scheme may offer.

Afterword

The purpose of this section is to state an overall assessment of the different strategies developed in this project and to provide some possible topics that could be considered as future research. I found more appropriate to draw some conclusions individually in each of the chapters, particularly because Chapter 4, Chapter 5 and Chapter 6 all correspond, respectively, to different publications.

In this thesis we have developed different fractional step algorithms for compressible flow problems. Particularly, we developed algorithms for the isentropic Navier-Stokes problem and for both the compressible Navier-Stokes problem written in primitive and conservative variables. All the schemes were derived at the algebraic level, *i. e.*, once space and time discretizations were chosen and they are up to second order in time. Moreover, all of them follow the classical "pressure-correction" type of algorithms, commonly used in incompressible flow solvers, a field in which our research group has extensive experience.

From the theoretical standpoint, it could be particularly interesting to extend our algorithms to a third (or even higher) order method in time, *e. g.*, using a BDF3 integration scheme. This third order method could be in principle obtained by using only first order extrapolations, a procedure that can be interpreted as a Yosida scheme (see [53, 55] and specially [178]). This should be the first research line to be addressed in the near future and I consider that the code developed in this thesis should serve as the proper starting point.

[178]: Quarteroni et al. (1999), "Analysis of the Yosida method for the incompressible Navier–Stokes equations"

A different approach to derive fractional step algorithms is the socalled "velocity-correction" procedure, in which the velocity unknown is first extrapolated rather than the pressure (or density). The main advantage of this technique, at least when applied to incompressible problems, is that experience shows that extrapolations of velocity can be safely performed up to third order (we recall here the comment on pressure extrapolations from Section 4.6.2). Hence, the extension of the algorithms to third order is somehow straightforward. This could be done and then compared to third order "pressure-correction" methods.

As we have already stated in this thesis, there exists a vast literature regarding fractional step methods from incompressible flow problems, regardless the chosen procedure (velocity or pressure correction algorithms). In this scenario of incompressible problems, since the problem only contains pressure and velocity unknowns, there are just two possibilities to derive a segregation method at the algebraic level by means of the extrapolation concept: one either extrapolates first pressure or velocity. The same applies to the isentropic problem analyzed in Chapter 4. However, the full compressible models of Chapter 5 and Chapter 6 render the final algebraic systems with three different unknowns emanating from three equations. Hence, there are more possibilities to be explored in order to perform the extrapolations. This should be addressed in the future and compared with the algorithms here proposed, especially in the case of the problem written in conservative variables.

Particularly important in compressible flow simulations is the adopted time integration scheme. In this regard, we have just explored the application of classical BDF schemes up to second order, but our developments are in principle open, and other schemes could be easily attached. Due to the wide range of scales that the compressible Navier-Stokes problem expands, the selection of the time step size is crucial. Thus, we consider that the implementation of adaptive time stepping techniques would be a very important feature to add to the present code enabling the efficient simulation of practical applications (see *e. g.*, [179–181]). In fact, this is a research line of great interest in our group that could lead to the development of a new thesis.

Another important point in the simulation of compressible flows is the inclusion of non-reflecting boundary conditions, as we have specifically addressed in Chapter 4 and Chapter 5. In these chapters, we selected a weak imposition of Dirichlet boundary conditions via extrapolations of boundary terms and the application of the classical Sommerfeld boundary condition. Although the application of this approach was satisfactory for the simulations showcased in this thesis, this topic could be further investigated in order to develop a more direct approach for dealing with spurious wave reflections. As discussed, the literature here is really extensive, and different techniques could be implemented and compared.

Finally, for the case of the simulation of problems with shocks,

[179]: Pan et al. (2022), "Development of a Balanced Adaptive Time-Stepping Strategy Based on an Implicit JFNK-DG Compressible Flow Solver"
[180]: Peles et al. (2019), "Adaptive Time Steps for Compressible Flows Based on Dual-Time Stepping and a RK/Implicit Smoother"
[181]: Kalkote et al. (2019), "Towards developing an adaptive time stepping for compressible unsteady flows"

a formulation including an anisotropic shock capturing methodology could be investigated so that diffusion is efficiently introduced along the streamlines, rather than the isotropic strategy proposed in Section 6.4.1.

Bibliography

Here are the references in citation order.

[1] J. D. Anderson. *Fundamentals of Aerodynamics*. McGraw-Hill Education, 2021 (cited on page 7).

[2] J. Blazek. *Computational Fluid Dynamics: principles and applications*. Butterworth–Heinemann, 2015 (cited on page 7).

[3] G. K. Vallis. *Atmospheric and Oceanic Fluid Dynamics: Fundamentals and Large-Scale Circulation*. Cambridge University Presss, 2017 (cited on pages 7, 30).

[4] B. Cushman-Roisin and J. M. Beckers. *Introduction to Geophysical Fluid Dynamics*. Academic Press, 2011 (cited on page 7).

[5] G. K. Vallis. "Geophysical fluid dynamics: whence, whither and why?" In: *Proceedings. Mathematical, physical, and engineering sciences* 472.2192 (2016). DOI: 10.1098/rspa.2016.0140 (cited on page 7).

[6] O. C. Zienkiewicz, R. L. Taylor, and J. Z. Zhu. *The Finite Element Method: Its Basis and Fundamentals*. Butterworth-Heinemann, 2013 (cited on pages 10, 45).

[7] I. A. Magomedov, M. S. Khaliev, and A. A. Elmurzaev. "Application of Finite Element Analysis in medicine." In: *Journal of Physics: Conference Series* 1679.2 (2020), p. 022057. DOI: 10.1088/1742-6596/1679/2/022057 (cited on page 10).

[8] M. Driscoll. "The Impact of the Finite Element Method on Medical Device Design." In: *Journal of Medical and Biological Engineering* 39.2 (2019), pp. 171–172. DOI: 10.1007/s40846-018-0428-4 (cited on page 10).

[9] S. Godunov. "A difference scheme for numerical solution of discontinuous solution of hydrodynamic equations." In: *Matematicheskii Sbornik* 47 (1959), pp. 271–306 (cited on page 11).

[10] L. B. Lucy. "A numerical approach to the testing of the fission hypothesis." In: *Astronomical Journal* 82 (Dec. 1977), pp. 1013–1024. DOI: 10.1086/112164 (cited on page 11).

[11] R. A. Gingold and J. J. Monaghan. "Smoothed particle hydrodynamics: theory and application to non-spherical stars." In: *Monthly Notices of the Royal Astronomical Society* 181.3 (Dec. 1977), pp. 375–389. DOI: 10.1093/mnras/181.3.375 (cited on page 11).

[12] D. Violeau. *Fluid Mechanics and the SPH Method: Theory and Applications*. Oxford University Press, 2012 (cited on page 11).

[13] W. H. Reed and T. R. Hill. *Triangular mesh methods for the neutron transport equation*. Tech. rep. 1973 (cited on page 11).

[14] B. Cockburn. “Discontinuous Galerkin Methods for Convection-Dominated Problems.” In: *High-Order Methods for Computational Physics*. Ed. by Timothy J. Barth and Herman Deconinck. Berlin, Heidelberg: Springer Berlin Heidelberg, 1999, pp. 69–224. DOI: 10.1007/978-3-662-03882-6_2 (cited on page 11).

[15] F. Bassi and S. Rebay. “A High-Order Accurate Discontinuous Finite Element Method for the Numerical Solution of the Compressible Navier–Stokes Equations.” In: *Journal of Computational Physics* 131.2 (1997), pp. 267–279. DOI: https://doi.org/10.1006/jcph.1996.5572 (cited on page 11).

[16] Ruben Sevilla. “An implicit HDG method for linear convection-diffusion with dual time stepping.” In: *Journal of Computational Physics* 434 (2021), p. 110201. DOI: https://doi.org/10.1016/j.jcp.2021.110201 (cited on page 12).

[17] B. Cockburn and J. Gopalakrishnan. “The Derivation of Hybridizable Discontinuous Galerkin Methods for Stokes Flow.” In: *SIAM Journal on Numerical Analysis* 47.2 (2009), pp. 1092–1125. DOI: 10.1137/080726653 (cited on page 12).

[18] M. Woopen, T. Ludescher, and G. May. “A Hybridized Discontinuous Galerkin Method for Turbulent Compressible Flow.” In: *44th AIAA Fluid Dynamics Conference*. 2014. DOI: 10.2514/6.2014-2783 (cited on page 12).

[19] Camilo Bayona-Roa, Ramon Codina, and Joan Baiges. “Variational multiscale error estimators for the adaptive mesh refinement of compressible flow simulations.” In: *Computer Methods in Applied Mechanics and Engineering* 337 (2018), pp. 501–526. DOI: https://doi.org/10.1016/j.cma.2018.03.010 (cited on page 12).

[20] Z.J. Wang et al. “High-order CFD methods: current status and perspective.” In: *International Journal for Numerical Methods in Fluids* 72.8 (2013), pp. 811–845. DOI: https://doi.org/10.1002/fld.3767 (cited on page 12).

[21] J. Vila-Pérez et al. “Hybridisable Discontinuous Galerkin Formulation of Compressible Flows.” In: *Archives of Computational Methods in Engineering* 28.2 (Mar. 2021), pp. 753–784. DOI: 10.1007/s11831-020-09508-z (cited on page 12).

[22] F. Chalot and P.-E. Normand. “Higher-Order Stabilized Finite Elements in an Industrial Navier-Stokes Code.” In: *ADIGMA - A European Initiative on the Development of Adaptive Higher-Order Variational Methods for Aerospace Applications*. Ed. by Norbert Kroll et al. Berlin, Heidelberg: Springer Berlin Heidelberg, 2010, pp. 145–165 (cited on page 12).

[23] Ruben Sevilla, Oubay Hassan, and Kenneth Morgan. “An analysis of the performance of a high-order stabilised finite element method for simulating compressible flows.” In: *Computer Methods in Applied Mechanics and Engineering* 253 (2013), pp. 15–27. DOI: https://doi.org/10.1016/j.cma.2012.09.001 (cited on page 12).

[24] Jean-Camille Chassaing, Sofiane Khelladi, and Xesús Nogueira. “Accuracy assessment of a high-order moving least squares finite volume method for compressible flows.” In: *Computers & Fluids* 71 (2013), pp. 41–53. DOI: https://doi.org/10.1016/j.compfluid.2012.09.021 (cited on page 12).

[25] A. Jameson, W. Schmidt, and E. Turkel. “Numerical solution of the Euler equations by finite volume methods using Runge Kutta time stepping schemes.” In: *14th Fluid and Plasma Dynamics Conference*. 1981. DOI: 10.2514/6.1981-1259 (cited on page 13).

[26] R. Messahel et al. “A conservative multirate explicit time integration method for computation of compressible flows.” In: *Computers & Fluids* 229 (Oct. 2021), p. 105102 (cited on page 13).

[27] René van Buuren. “Time integration methods for compressible flow.” In: University of Twente, 1999 (cited on page 13).

[28] C. Bayona, J. Baiges, and R. Codina. “Variational multi-scale finite element solution of the compressible Navier–Stokes equations.” In: *International Journal of Numerical Methods for Heat and Fluid Flow* 26 (2015), pp. 1240–1271. DOI: 10.1108/HFF-11-2015-0483 (cited on pages 13, 55, 120, 150).

[29] C. Bayona, J. Baiges, and R. Codina. “Solution of low Mach number aeroacoustic flows using a Variational Multi-Scale finite element formulation of the compressible Navier–Stokes equations written in primitive variables.” In: *Computer Methods in Applied Mechanics and Engineering* 344 (2019), pp. 1073–1103. DOI: https://doi.org/10.1016/j.cma.2018.01.040 (cited on pages 13, 120, 132).

[30] A. J. Chorin. “A numerical method for solving incompressible viscous problems.” In: *Journal of Computational Physics* 2 (1967), pp. 12–26. DOI: https://doi.org/10.1006/jcph.1997.5716 (cited on page 14).

[31] A. J. Chorin. “Numerical solution of the Navier-Stokes equations.” In: *Mathematics of Computation* 22 (1968), pp. 745–762. DOI: https://doi.org/10.1090/S0025-5718-1968-0242392-2 (cited on page 14).

[32] R. Teman. “Sur l’approximation de la solution des equations de Navier–Stokes par la méthode des pas fractionaires (I).” In: *Archives for Rational Mechanics and Analysis* 32 (1969), pp. 135–153. DOI: https://doi.org/10.1007/BF00247678 (cited on page 14).

[33] R. Teman. “Sur l’approximation de la solution des equations de Navier–Stokes par la méthode des pas fractionaires (II).” In: *Archives for Rational Mechanics and Analysis* 34 (1969), pp. 377–385. DOI: https://doi.org/10.1007/BF00247696 (cited on page 14).

[34] J.L. Guermond and Jie Shen. “A new class of truly consistent splitting schemes for incompressible flows.” In: *Journal of Computational Physics* 192.1 (2003), pp. 262–276. DOI: https://doi.org/10.1016/j.jcp.2003.07.009 (cited on page 15).

[35] J. van Kan. “A Second-Order Accurate Pressure-Correction Scheme for Viscous Incompressible Flow.” In: *SIAM Journal on Scientific and Statistical Computing* 7.3 (1986), pp. 870–891. DOI: 10.1137/0907059 (cited on page 15).

[36] A. Prohl. “Advances in Numerical Mathematics.” In: *Projection and Quasi-Compressibility Methods for Solving the Incompressible Navier-Stokes Equations*. Springer, 1997. DOI: https://doi-org.recursos.biblioteca.upc.edu/10.1007/978-3-663-11171-9 (cited on page 15).

[37] J.-L. Guermond and L. Quartapelle. "On the approximation of the unsteady Navier–Stokes equations by finite element projection methods." In: *Numerische Mathematik* 80.2 (Aug. 1998), pp. 207–238. DOI: 10.1007/s002110050366 (cited on page 15).

[38] J.-L. Guermond and J. Shen. "On the error estimates for the rotational pressure-correction projection methods." In: *Mathematics of Computation* 73 (ember 2004), pp. 1719–1737. DOI: https://doi.org/10.1090/S0025-5718-03-01621-1 (cited on pages 15, 127).

[39] George Em Karniadakis, Moshe Israeli, and Steven A Orszag. "High-order splitting methods for the incompressible Navier-Stokes equations." In: *Journal of Computational Physics* 97.2 (1991), pp. 414–443. DOI: https://doi.org/10.1016/0021-9991(91)90007-8 (cited on page 15).

[40] Ramon Codina and Santiago Badia. "On some pressure segregation methods of fractional-step type for the finite element approximation of incompressible flow problems." In: *Computer Methods in Applied Mechanics and Engineering* 195.23 (2006). Incompressible CFD, pp. 2900–2918. DOI: https://doi.org/10.1016/j.cma.2004.06.048 (cited on page 15).

[41] J. Shen. "On error estimates of some higher order projection and penalty-projection methods for Navier-Stokes equations." In: *Numerische Mathematik* 62.1 (Dec. 1992), pp. 49–73. DOI: 10.1007/BF01396220 (cited on page 15).

[42] J Kim and P Moin. "Application of a fractional-step method to incompressible Navier-Stokes equations." In: *Journal of Computational Physics* 59.2 (1985), pp. 308–323. DOI: https://doi.org/10.1016/0021-9991(85)90148-2 (cited on page 15).

[43] J.-L. Guermond and L. Quartapelle. "On stability and convergence of projection methods based on pressure Poisson equation." In: *International Journal for Numerical Methods in Fluids* 26.9 (1998), pp. 1039–1053. DOI: https://doi.org/10.1002/(SICI)1097-0363(19980515)26:9<1039::AID-FLD675>3.0.CO;2-U (cited on page 15).

[44] J. Guermond, P. Minev, and J.Shen. "An overview of projection methods for incompressible flows." In: *Computer Methods in Applied Mechanics and Engineering* 195 (2006), pp. 6011–6045. DOI: https://doi.org/10.1016/j.cma.2005.10.010 (cited on page 15).

[45] L. G. Rebholz, A. Viguerie, and M. Xiao. "Analysis of Algebraic Chorin Temam splitting for incompressible NSE and comparison to Yosida methods." In: *Journal of Computational and Applied Mathematics* 365 (Feb. 2020), p. 112366 (cited on page 15).

[46] R. Codina. "Pressure stability in fractional step finite element methods for incompressible flows." In: *Journal of Computational Physics* 170 (2001), pp. 112–140. DOI: https://doi.org/10.1006/jcph.2001.6725 (cited on pages 15, 98, 159).

[47] J. B. Perot. "An analysis of the fractional step method." In: *Journal of Computational Physics* 108 (1993), pp. 51–58. DOI: https://doi.org/10.1006/jcph.1993.1162 (cited on pages 15, 98).

[48] Alfio Quarteroni, Fausto Saleri, and Alessandro Veneziani. "Factorization methods for the numerical approximation of Navier–Stokes equations." In: *Computer Methods in Applied Mechanics and Engineering* 188.1 (2000), pp. 505–526. DOI: https://doi.org/10.1016/S0045-7825(99)00192-9 (cited on pages 15, 16).

[49] S. Badia and R. Codina. "Convergence analysis of the FEM approximation of the first order projection method for incompressible flows with and without the inf-sup condition." In: *Numerische Mathematik* 107.4 (Oct. 2007), pp. 533–557. DOI: 10.1007/s00211-007-0099-5 (cited on pages 15, 16).

[50] S. Badia and R. Codina. "Algebraic Pressure Segregation Methods for the Incompressible Navier–Stokes Equations." In: *Archives of Computational Methods in Engineering* 15.3 (2007), pp. 1–52. DOI: 10.1007/s11831-008-9020-3 (cited on pages 15, 16, 72, 74, 76, 78, 98, 112, 117, 145, 158, 159).

[51] P. Gervasio and F. Saleri. "Algebraic Fractional-Step Schemes for Time-Dependent Incompressible Navier–Stokes Equations." In: *Journal of Scientific Computing* 27.1 (June 2006), pp. 257–269. DOI: 10.1007/s10915-005-9051-y (cited on pages 15, 16).

[52] P. Gervasio, F. Saleri, and A. Veneziani. "Algebraic fractional-step schemes with spectral methods for the incompressible Navier–Stokes equations." In: *Journal of Computational Physics* 214.1 (2006), pp. 347–365. DOI: https://doi.org/10.1016/j.jcp.2005.09.018 (cited on pages 15, 16).

[53] S. Badia and R. Codina. "Pressure segregation methods based on a discrete pressure Poisson equation. An algebraic approach." In: *International Journal for Numerical Methods in Fluids* 56 (2008), pp. 351–382. DOI: https://doi.org/10.1002/fld.1532 (cited on pages 16, 98, 145, 159, 175).

[54] A. Folch et al. "A fractional-step finite-element method for the Navier–Stokes equations applied to magma-chamber withdrawal." In: *Computers & Geosciences* 25.3 (Apr. 1999), pp. 263–275 (cited on page 16).

[55] E. Castillo and R. Codina. "First, second and third order fractional step methods for the three-field viscoelastic flow problem." In: *Journal of Computational Physics* 296 (2015), pp. 113–137. DOI: https://doi.org/10.1016/j.jcp.2015.04.027 (cited on pages 16, 98, 112, 139, 145, 158, 159, 172, 175).

[56] G. Hauke et al. "A segregated method for compressible flow computation.Part II: General divariant compressible fows." In: *International Journal for Numerical Methods in Fluids* 49 (2005), pp. 183–209. DOI: https://doi-org.recursos.biblioteca.upc.edu/10.1002/fld.999 (cited on pages 16, 112, 162, 164).

[57] J. M. Hérard and O. Hurisse. "A fractional step method to compute a class of compressible gas-liquid flows." In: *Computers & Fluids* 55 (2012), pp. 57–69. DOI: https://doi.org/10.1016/j.compfluid.2011.11.001 (cited on page 16).

[58] T. Gallouët, L. Gastaldo, and J. C. Latché R. Herbin. "An unconditionally stable pressure correction scheme for the compressible barotropic Navier–Stokes equations." In: *ESAIM: Mathematical Modelling and Numerical Analysis* 42.2 (2008), pp. 303–331. DOI: https://doi.org/10.1051/m2an:2008005 (cited on page 16).

[59] K. Liu and R. H. Pletcher. “A fractional step method for solving the compressible Navier–Stokes equations.” In: *Journal of Computational Physics* 226.2 (2007), pp. 1930–1951. DOI: https://doi.org/10.1016/j.jcp.2007.06.026 (cited on page 16).

[60] R. Codina, M. Vázquez, and O.C. Zienkiewicz. “A general algorithm for the compressible and incompressible flows. Part III: the semi–implicit form.” In: *International Journal for Numerical Methods in Fluids* 27 (1996), pp. 13–32. DOI: https://doi.org/10.1002/(SICI)1097-0363(199801)27:1/4<13::AID-FLD647>3.0.CO;2-8 (cited on pages 16, 17).

[61] S. Balay et al. *PETSc Web page*. http://www.mcs.anl.gov/petsc. 2015 (cited on pages 19, 85, 126, 159).

[62] U. Ayachit. *The ParaView Guide: A Parallel Visualization Application*. Kitware, 2015 (cited on page 19).

[63] W. Schroeder, K. Martin, and B. Lorensen. *The Visualization Toolkit*. Kitware, 2006 (cited on page 19).

[64] L. D. Landau and E. M. Lifshitz. *Fluid Mechanics*. Second Ed. Vol. 6. Course of Theoretical Physics. Pergamon, 1987 (cited on pages 21, 28).

[65] R. Aris. *Vectors, Tensors and the Basic Equations of Fluid Mechanics*. Dover Publications Inc., 1989 (cited on page 21).

[66] G. K. Batchelor. *An Introduction to Fluid Dynamics*. Cambridge Mathematical Library. Cambridge University Press, 2000 (cited on pages 21, 27).

[67] X. Oliver and C. Agelet de Saracibar. *Continuum Mechanics for Engineers. Theory and Problems*. Second Ed. UPC, 2017 (cited on pages 21, 23).

[68] G. A. Holzapfel. *Nonlinear Solid Mechanics: A Continuum Approach for Engineering*. John Wiley & Sons, 2000 (cited on pages 21, 23).

[69] T. L. Hill. *An introduction to statistical thermodynamics*. Dover books on physics. Dover publications, 1986 (cited on page 21).

[70] J. Donea et al. “Arbitrary Lagrangian–Eulerian methods.” In: *Encyclopedia of computational mechanics: 2nd edition* (2017), pp. 1–23. DOI: https://doi.org/10.1002/9781119176817.ecm2009 (cited on page 22).

[71] R. Nemer et al. “Stabilized finite element method for incompressible solid dynamics using an updated Lagrangian formulation.” In: *Computer Methods in Applied Mechanics and Engineering* 384 (2021), p. 113923. DOI: https://doi.org/10.1016/j.cma.2021.113923 (cited on page 22).

[72] I. Castañar, J. Baiges, and R. Codina. “A stabilized mixed finite element approximation for incompressible finite strain solid dynamics using a total Lagrangian formulation.” In: *Computer Methods in Applied Mechanics and Engineering* 368 (2020), p. 113164. DOI: https://doi.org/10.1016/j.cma.2020.113164 (cited on page 22).

[73] S. Osher and R. Fedkiw. *Level set methods and dynamic implicit surfaces*. Springer, 2006 (cited on page 23).

[74] E. Castillo, J. Baiges, and R. Codina. "Approximation of the two-fluid flow problem for viscoelastic fluids using the level set method and pressure enriched finite element shape functions." In: *Journal of Non-Newtonian Fluid Mechanics* 225 (2015), pp. 37–53. DOI: https://doi.org/10.1016/j.jnnfm.2015.09.004 (cited on page 23).

[75] I. G. Currie. *Fundamental mechanics of fluids.* McGraw-Hill Inc., 1976 (cited on page 23).

[76] C. Popa and S. S. Sritharan. "Fluid–Magnetic Splitting of the Magnetohydrodynamic Equations." In: *Mathematical Models and Methods in Applied Sciences* 13.6 (2003), pp. 893–917. DOI: https://doi.org/10.1142/S0218202503002763 (cited on page 25).

[77] R. Codina and N. Hernández–Silva. "Stabilized finite element approximation of the stationary MHD equations." In: *Computational Mechanics* 38 (2006), pp. 344–355. DOI: https://doi.org/10.1007/s00466-006-0037-x (cited on page 25).

[78] R. Codina, J. Principe, and M. Avila. "Finite element approximation of turbulent thermally coupled incompressible flows with numerical sub-grid scale modelling." In: *International Journal of Numerical Methods for Heat & Fluid Flow* 20 (2010), pp. 492–516. DOI: https://doi.org/10.1108/09615531011048213 (cited on pages 25, 135).

[79] L. Moreno, R. Codina, and J. Baiges. "Numerical simulation of non-isothermal viscoelastic fluid flows using a VMS stabilized finite element formulation." In: *Journal of Non-Newtonian Fluid Mechanics* 296 (2021), p. 104640. DOI: https://doi.org/10.1016/j.jnnfm.2021.104640 (cited on page 27).

[80] E. Castillo et al. "Stabilised Variational Multi-scale Finite Element Formulations for Viscoelastic Fluids." In: *Archives of Computational Methods in Engineering* 296 (2021), pp. 1987–2019. DOI: https://doi.org/10.1007/s11831-020-09526-x (cited on page 27).

[81] W. Sutherland. "The viscosity of gases and molecular force." In: *Philosophical Magazine* 5.36 (1893), pp. 507–531. DOI: https://doi.org/10.1080/14786449308620508 (cited on page 28).

[82] A. S. Dukhin and P. J. Goetz. "Bulk viscosity and compressibility measurement using acoustic spectroscopy." In: *Journal of Chemical Physics* 130 (2009). DOI: https://doi.org/10.1063/1.3095471 (cited on page 29).

[83] S. Chapman and T. G. Cowling. *The mathematical theory of non-uniform gases.* Cambridge University Press, Cambridge, 1991 (cited on page 31).

[84] J. O. Hirschfelder, C. F. Curtiss, and R. B. Bird. *Molecular theory of gases and liquids.* Wiley, 1954 (cited on page 31).

[85] B. R. Hollis. *Real-gas flow properties for NASA Langley research center aerothermodynamic facilities complex wind tunnels.* Tech. rep. NASA Langley Research Center, VA, United States, 1996 (cited on page 31).

[86] P. L. Lions. *Mathematical Topics in Fluid Dynamics, Volume 2. Compressible Models.* Oxford University Press, 1998 (cited on page 34).

[87] A. Huerta and J. Donea. *Finite Element Methods for flow problems.* John Wiley & Sons Ltd., 2003 (cited on page 35).

[88] J. Oliger and A. Sundstrom. “Theoretical and Practical Aspects of Some Initial Boundary Value Problems in Fluid Dynamics.” In: *SIAM Journal on Applied Mathematics* 35.3 (1978), pp. 419–446 (cited on page 35).

[89] T. J. Hughes. “Multiscale phenomena : Green’s functions, the Dirichlet-to-Neumann formulation, subgrid scale models, bubbles and the origins of stabilized methods.” In: *Computer Methods in Applied Mechanics and Engineering* 127.1 (1995), pp. 387–401. DOI: https://doi.org/10.1016/0045-7825(95)00844-9 (cited on page 37).

[90] T.J.R. Hughes et al. “The variational multiscale method–a paradigm for computational mechanics.” In: *Computer Methods in Applied Mechanics and Engineering* 166 (1998), pp. 3–24 (cited on page 37).

[91] J. VonNeumann and R. D. Richtmyer. “A Method for the Numerical Calculation of Hydrodynamic Shocks.” In: *Journal of Applied Physics* 21.3 (1950), pp. 232–237. DOI: 10.1063/1.1699639 (cited on page 37).

[92] D. W. Kelly et al. “A note on upwinding and anisotropic balancing dissipation in finite element approximations to convective diffusion problems.” In: *International Journal for Numerical Methods in Engineering* 15.11 (1980), pp. 1705–1711. DOI: https://doi.org/10.1002/nme.1620151111 (cited on page 37).

[93] A. N. Brooks and T. J.R. Hughes. “Streamline Upwind/Petrov-Galerkin formulations for convection dominated flows with particular emphasis on the incompressible Navier-Stokes equations.” In: *Computer Methods in Applied Mechanics and Engineering* 32.1 (1982), pp. 199–259. DOI: https://doi.org/10.1016/0045-7825(82)90071-8 (cited on page 37).

[94] T. Tezduyar and T. J. R. Hughes. “Finite element formulations for convection dominated flows with particular emphasis on the compressible Euler equations.” In: *Proceedings of AIAA 21st aerospace sciences meeting, AIAA Paper,* 83 (1983), pp. 1–25 (cited on page 37).

[95] G. Hauke and T. J. Hughes. “A comparative study of different sets of variables for solving compressible and incompressible flows.” In: *Computer Methods in Applied Mechanics and Engineering* 153.1 (1998), pp. 1–44. DOI: https://doi.org/10.1016/S0045-7825(97)00043-1 (cited on pages 38, 97).

[96] J. Douglas Jr. and T. F. Russell. “Numerical Methods for Convection-Dominated Diffusion Problems Based on Combining the Method of Characteristics with Finite Element or Finite Difference Procedures.” In: *SIAM Journal on Numerical Analysis* 19.5 (1982), pp. 871–885. DOI: 10.1137/0719063 (cited on page 38).

[97] J. Donea. “A Taylor–Galerkin method for convective transport problems.” In: *International Journal for Numerical Methods in Engineering* 20.1 (1984), pp. 101–119. DOI: https://doi.org/10.1002/nme.1620200108 (cited on page 38).

[98] R. Codina. "A stabilized finite element method for generalized stationary incompressible flows." In: *Computer Methods in Applied Mechanics and Engineering* 190.20 (2001), pp. 2681–2706. DOI: https://doi.org/10.1016/S0045-7825(00)00260-7 (cited on page 38).

[99] R. Codina. "Stabilized finite element approximation of transient incompressible flows using orthogonal subscales." In: *Computer Methods in Applied Mechanics and Engineering* 191 (2002), pp. 4295–4321. DOI: https://doi.org/10.1016/S0045-7825(02)00337-7 (cited on pages 38, 39, 49, 51, 58, 80, 117).

[100] J. L. Guermond. "Stabilization of Galerkin approximations of transport equations by subgrid modeling." en. In: *ESAIM: Mathematical Modelling and Numerical Analysis - Modélisation Mathématique et Analyse Numérique* 33.6 (1999), pp. 1293–1316 (cited on page 38).

[101] F. Brezzi et al. "A relationship between stabilized finite element methods and the Galerkin method with bubble functions." In: *Computer Methods in Applied Mechanics and Engineering* 96.1 (1992), pp. 117–129. DOI: https://doi.org/10.1016/0045-7825(92)90102-P (cited on page 38).

[102] F. Brezzi, D. Marini, and E. Süli. "Residual-free bubbles for advection-diffusion problems: the general error analysis." In: *Numer. Math.* 85 (2000), pp. 31–47. DOI: https://doi.org/10.1007/s002110050476 (cited on page 38).

[103] T. J.R. Hughes et al. "A multiscale discontinuous Galerkin method with the computational structure of a continuous Galerkin method." In: *Computer Methods in Applied Mechanics and Engineering* 195.19 (2006), pp. 2761–2787. DOI: https://doi.org/10.1016/j.cma.2005.06.006 (cited on page 38).

[104] R. Codina et al. "Time dependent subscales in the stabilized finite element approximation of incompressible flow problems." In: *Computer Methods in Applied Mechanics and Engineering* 196 (2007), pp. 2413–2430. DOI: https://doi.org/10.1016/j.cma.2007.01.002 (cited on pages 39, 49, 50).

[105] R. Codina and J. Principe. "Dynamic subscales in the finite element approximation of thermally coupled incompressible flows." In: *International Journal for Numerical Methods in Fluids* 54 (2007), pp. 707–730. DOI: https://doi.org/10.1002/fld.1481 (cited on pages 39, 50).

[106] B. Koobus and C. Farhat. "A variational multiscale method for the large eddy simulation of compressible turbulent flows on unstructured meshes–application to vortex shedding." In: *Computer Methods in Applied Mechanics in Engineering* 193.15 (2004), pp. 1367–1383 (cited on page 39).

[107] F. Van Der Bos, J. Van Der Vegt, and B. Geurts. "A multi-scale formulation for compressible turbulent flows suitable for general variational discretization techniques." In: *Computer Methods in Applied Mechanics in Engineering* 196.29 (2007), pp. 2863–2875 (cited on page 39).

[108] V. Levasseur et al. "An entropy-variable-based VMS/GLS method for the simulation of compressible flows on unstructured grids." In: *Computer Methods in Applied Mechanics in Engineering* 195.9 (2006), pp. 1154–1179 (cited on page 39).

[109] W. Dahmen et al. “Adaptive multiresolution finite volume discretization of the Variational Multiscale Method. General Framework.” In: *Inst. für Geometrie und Praktische Mathematik* (2011) (cited on page 39).

[110] T. J. R. Hughes, G. Scovazzi, and T. E. Tezduyar. “Stabilized Methods for Compressible Flows.” In: *Journal of Scientific Computing* 43 (2010), pp. 343–368. DOI: https://doi.org/10.1007/s10915-008-9233-5 (cited on page 40).

[111] F. Rispoli and R. Saavedra. “A stabilized finite element method based on SGS models for compressible flows.” In: *Computer Methods in Applied Mechanics and Engineering* 196 (2006), pp. 652–664. DOI: https://doi.org/10.1007/s10915-008-9233-5 (cited on pages 40, 164).

[112] S. Marras et al. “Simulations of moist convection by a variational multiscale stabilized finite element method.” In: *Journal of Computational Physics* 252 (2013), pp. 195–218 (cited on page 40).

[113] W. Hundsdorfer and J. G. Verwer. *Numerical Solution of Time-Dependent Advection-Diffusion-Reaction Equations*. Springer, 2003 (cited on page 43).

[114] R. Codina, J. Príncipe, and J. Baiges. “Subscales on the element boundaries in the variational two-scale finite element method.” In: *Computer Methods in Applied Mechanics and Engineering* 198 (2009), pp. 838–852. DOI: 10.1016/j.cma.2008.10.020 (cited on page 47).

[115] R. Codina et al. “Variational Multiscale Methods in Computational Fluid Dynamics.” In: *Encyclopedia of Computational Mechanics, Second Edition* (2018), pp. 1–28. DOI: https://doi.org/10.1002/9781119176817.ecm2117 (cited on pages 47, 49).

[116] J. Principe and R. Codina. “On the stabilization parameter in the subgrid scale approximation of scalar convection-diffusion-reaction equations on distorted meshes.” In: *Computer Methods in Applied Mechanics and Engineering* 199 (2010), pp. 1386–1402. DOI: https://doi.org/10.1016/j.cma.2009.08.011 (cited on page 48).

[117] Y. Bazilevs et al. “Variational multiscale residual-based turbulence modeling for large eddy simulation of incompressible flows.” In: *Computer Methods in Applied Mechanics and Enginneering* 197 (2007), pp. 173–201. DOI: https://doi.org/10.1016/j.cma.2007.07.016 (cited on page 49).

[118] T. J. R. Hughes, L. Mazzei, and K. E. Jansen. “Large eddy simulation and the variational multiscale method.” In: *Computing and Visualization in Science* 3 (2000), pp. 47–59. DOI: https://doi.org/10.1007/s007910050051 (cited on page 49).

[119] T. J. R. Hughes, A. A. Oberai, and L. Mazzei. “Large eddy simulation of turbulent channel flows by the variational multiscale method.” In: *Physics of Fluids* 13 (2001), pp. 1784–1799. DOI: https://doi.org/10.1063/1.1367868 (cited on page 49).

[120] S. Badia and R. Codina. “On a multiscale approach to the transient Stokes problem: Dynamic subscales and anisotropic space-time discretization.” In: *Applied Mathematics and Computation* 207 (2009), pp. 415–433. DOI: https://doi.org/10.1016/j.amc.2008.10.059 (cited on page 49).

[121] O. Colomes et al. “Assessment of variational multiscale models for the large eddy simulation of turbulent incompressible flows.” In: *Computer Methods in Applied Mechanics and Enginneering* 285 (2015), pp. 32–63. DOI: https://doi.org/10.1016/j.cma.2014.10.041 (cited on page 51).

[122] R. Codina. “Analysis of a stabilized finite element approximation of the Oseen equations using orthogonal subscales.” In: *Applied Numerical Mathematics* 58 (2008), pp. 264–283. DOI: https://doi.org/10.1016/j.apnum.2006.11.011 (cited on pages 52, 80).

[123] A. Aguirre, R. Codina, and J. Baiges. “A variational multiscale stabilized finite element formulation for Reissner-Mindlin plates and Timoshenko beams.” In: *Computer Methods in Applied Mechanics and Enginneering* (2021) (cited on page 52).

[124] C. Bailly, C. Bogey, and O. Marsden. “Progress in direct noise computation.” In: *Noise Notes* 9.3 (2010), pp. 31–48. DOI: https://doi.org/10.1260/1475-472X.9.1-2.123 (cited on page 55).

[125] M. J. Lighthill. “On sound generated aerodynamically I. General theory.” In: *Proceedings of the Royal Society – A. Mathematical, Physical and Engineering Sciences* 211.1107 (1952), pp. 564–587. DOI: https://doi.org/10.1098/rspa.1952.0060 (cited on page 56).

[126] J. Hardin and D. Pope. “An acoustic/viscous splitting technique for computational aeroacoustics.” In: *Theoretical and Computational Fluid Dynamics* 6.5-6 (1994), pp. 323–340. DOI: https://doi.org/10.1007/BF00311844 (cited on pages 56, 96).

[127] W. Z. Shen and J. N. Sørensen. “Aeroacoustic modelling of low-speed flows.” In: *Theoretical and Computational Fluid Dynamics* 13.4 (1999), pp. 271–289. DOI: https://doi.org/10.1007/s001620050118 (cited on pages 56, 96).

[128] W. Z. Shen, W. Zhu, and J. N. Sørensen. “Aeroacoustic Computations for Turbulent Airfoil Flows.” In: *American Institute of Aeronautics and Astronautics* 47.6 (2009), pp. 1518–1527. DOI: https://doi.org/10.2514/1.40399 (cited on pages 56, 96).

[129] W. Z. Shen, J. A. Michelsen, and J. N. Sørensen. “A collocated grid finite volume method for aeroacoustic computations of low-speed flows.” In: *Journal of Computational Physics* 196.1 (2004), pp. 348–366. DOI: https://doi.org/10.1016/j.jcp.2003.11.006 (cited on page 56).

[130] A. Pont et al. “Unified solver for fluid dynamics and aeroacoustics in isentropic gas flows.” In: *Journal of Computational Physics* 363 (2018), pp. 11–29. DOI: https://doi.org/10.1016/j.jcp.2018.02.029 (cited on pages 56, 58, 59, 63, 88, 104).

[131] E. Castillo and R. Codina. “Stabilized stress-velocity-pressure finite element formulations of the Navier-Stokes problem for fluids with non-linear viscosity.” In: *Computer Methods in Applied Mechanics and Engineering* 279 (2014), pp. 554–578. DOI: 10.1016/j.cma.2014.07.003 (cited on page 58).

[132] E. Castillo and R. Codina. “Finite element approximation of the viscoelastic flow problem: A non-residual based stabilized formulation.” In: *Computer & Fluids* 142 (2017), pp. 72–78. DOI: https://doi.org/10.1016/j.compfluid.2016.07.012 (cited on pages 58, 80).

[133] T. Colonius, S. K. Lele, and P. Moin. “Boundary conditions for direct computation of aerodynamic sound generation.” In: *American Institute of Aeronautics and Astronautics* 31.9 (1993), pp. 1574–1582. DOI: https://doi.org/10.2514/3.11817 (cited on pages 58, 97).

[134] P. Fosso et al. “Comparison of outflow boundary conditions for subsonic aeroacoustic simulations.” In: *International Journal of Numerical Methods in Fluids* 68(10) (2012), pp. 1207–1233. DOI: https://doi.org/10.1002/fld.2597 (cited on pages 58, 97).

[135] V. Granet et al. “Comparison of nonreflecting outlet boundary conditions for compressible solver on unstructured grids.” In: *American Institute of Aeronautics and Astronautics* 48(10) (2010), pp. 2348–2364. DOI: https://doi.org/10.2514/1.J050391 (cited on pages 58, 97).

[136] H. Espinoza, R. Codina, and S. Badia. “A Sommerfeld non-reflecting boundary condition for the wave equation in mixed form.” In: *Computer Methods in Applied Mechanics and Engineering* 276 (2014), pp. 122–148. DOI: https://doi.org/10.1016/j.cma.2014.03.015 (cited on pages 58, 64, 105).

[137] M. Avila, J. Principe, and R. Codina. “A finite element dynamical nonlinear subscale approximation for the low Mach number flow equations.” In: *Journal of Computational Physics* 230 (2011), pp. 7988–8009. DOI: https://doi.org/10.1016/j.jcp.2011.06.032 (cited on page 60).

[138] M. Juntunen and R. Stenbeg. “Nitche’s method for general boundary conditions.” In: *Mathematics of Computation* 78.267 (2009), pp. 1353–1374. DOI: 10.1090/s0025-5718-08-02183-2 (cited on page 66).

[139] H. Owen and R. Codina. “A third-order velocity correction scheme obtained at the discrete level.” In: *International Journal for Numerical Methods in Fluids* 69 (2012), pp. 57–72. DOI: https://doi.org/10.1002/fld.2535 (cited on pages 72, 112).

[140] R. Codina and A. Folch. “A stabilized finite element predictor–corrector scheme for the incompressible Navier–Stokes equations using a nodal–based implementation.” In: *International Journal for Numerical Methods in Fluids* 44 (2004), pp. 483–503. DOI: https://doi.org/10.1002/fld.648 (cited on pages 74, 114, 155).

[141] T. Chacón Rebollo. “A term by term stabilization algorithm for finite element solution of incompressible flow problems.” In: *Numerische Mathematik* 79 (1998), pp. 283–319. DOI: https://doi.org/10.1007/s002110050341 (cited on page 80).

[142] E. Castillo and R. Codina. “Dynamic term-by-term stabilized finite element formulation using orthogonal subgrid-scales for the incompressible Navier-Stokes problem.” In: *Computer Methods in Applied Mechanics and Engineering* 349 (2019), pp. 701–721. DOI: 10.1016/j.cma.2019.02.041 (cited on page 81).

[143] H. A. Van der Vorst. “Bi-CGSTAB: A fast and smoothly converging variant of Bi-CG for the solution of nonsymmetric linear systems.” In: *SIAM, Journal of Scientific and Statistical Computing* 13.2 (1992), pp. 631–644. DOI: https://doi.org/10.1137/0913035 (cited on pages 85, 126, 159).

[144] O. Guasch and R. Codina. "Computational aeroacoustics of viscous low speed flows using subgrid scale finite element methods." In: *Journal of Computational Acoustics* 17.3 (2009), pp. 309–330. DOI: https://doi.org/10.1142/S0218396X09003975 (cited on page 86).

[145] O. Guasch and R. Codina. "An algebraic subgrid scale finite element method for the convected Helmholtz equation in two dimensions with applications in aeroacoustics." In: *Computer Methods in Applied Mechanics and Engineering* 196 (2007), pp. 4672–4689. DOI: https://doi.org/10.1016/j.cma.2007.06.001 (cited on pages 86, 90).

[146] C. W. Rowley, T. Colonious, and A. J. Basu. "On self-sustained oscillations in two-dimensional compressible flow over rectangular cavities." In: *Journal of Fluid Mechanics* 455 (2002), pp. 315–346. DOI: 10.1017/S0022112001007534 (cited on page 92).

[147] G. A. Bres and T. Colonious. "Three–dimensional instabilities in compressible flow over open cavities." In: *Journal of Fluid Mechanics* 599 (2008), pp. 309–339. DOI: https://doi.org/10.1017/S0022112007009925 (cited on page 92).

[148] X. Gloerfelt, C. Bailly, and D. Juvé. "Direct computation of the noise radiated by a subsonic cavity flow and application of integral methods." In: *Journal of sound and vibration* 266 (2003), pp. 119–146. DOI: https://doi.org/10.1016/S0022-460X(02)01531-6 (cited on pages 92, 93).

[149] Y. Bazilevs et al. "Gas turbine computational flow and structure analysis with isogeometric discretization and a complex-geometry mesh generation method." In: *Computational Mechanics* 67 (2021), pp. 57–84. DOI: https://doi.org/10.1007/s00466-020-01919-w (cited on page 95).

[150] H. Lu et al. "Numerical investigation of effects of incisor angle on production of sibilant /s/." In: *Scientic Reports* 11.16720 (2021). DOI: https://doi.org/10.1038/s41598-021-96173-2 (cited on page 95).

[151] J. Wong, D. Darmofal, and J. Peraire. "The solution of the compressible Euler equations at low Mach numbers using a stabilized finite element algorithm." In: *Compute Methods in Applied Mechanics and Engineering* 190.43 (2001), pp. 5719–5737. DOI: https://doi.org/10.1016/S0045-7825(01)00193-1 (cited on page 96).

[152] L. Pesch and J. J. van der Vegt. "A discontinuous Galerking finite element discretization of the Euler equations for compressible and incompressible fluids." In: *Journal of Computational Physics* 11 (2008), pp. 5426–5446. DOI: https://doi.org/10.1016/j.jcp.2008.01.046 (cited on page 96).

[153] T. J. Hughes, L. Franca, and M. Mallet. "A new finite element formulation for computations fluid dynamics. I. Symmetric forms of the compressible Euler and Navier-Stokes equations and the second law of thermodynamics." In: *Computer Methods in Applied Mechanics and Engineering* 54.2 (1986), pp. 223–234. DOI: https://doi.org/10.1016/0045-7825(86)90127-1 (cited on page 97).

[154] T. Colonious. “Modeling artificial boundary conditions for compressible flow.” In: *Annual Review of Fluid Mechanics* 36 (2004), pp. 315–345. DOI: https://doi.org/10.1146/annurev.fluid.36.050802.121930 (cited on page 97).

[155] S. Parada, J. Baiges, and R. Codina. “A fractional step method for computational aeroacoustics using weak imposition of Dirichlet boundary conditions.” In: *Computers & Fluids* 197 (2020), p. 104374. DOI: https://doi.org/10.1016/j.compfluid.2019.104374 (cited on pages 98, 145, 159, 172).

[156] A. Salazar. “Energy propagation of thermal waves.” In: *European Journal of Physics* 27.6 (2006), pp. 1349–1355. DOI: 10.1088/0143-0807/27/6/009 (cited on page 105).

[157] P. R. Amestoy et al. “A Fully Asynchronous Multifrontal Solver Using Distributed Dynamic Scheduling.” In: *SIAM Journal on Matrix Analysis and Applications* 23.1 (2001), pp. 15–41 (cited on pages 127, 160).

[158] P. R. Amestoy et al. “Hybrid scheduling for the parallel solution of linear systems.” In: *Parallel Computing* 32.2 (2006), pp. 136–156 (cited on pages 127, 160).

[159] Y.S.K. Liow et al. “Sound generated in laminar flow past a two-dimensional rectangular cylinder.” In: *Journal of Sound and Vibration* 295.1–2 (2006), pp. 407–427. DOI: https://doi.org/10.1016/j.jsv.2006.01.014 (cited on page 130).

[160] B. Mahato, N. Ganta, and Y. G. Bhumka. “Direct simulation of sound generation by a two-dimensional flow past a wedge.” In: *Physics of Fluids* 30.096101 (2018). DOI: https://doi.org/10.1063/1.5039953 (cited on page 130).

[161] F. Margnat. “Hybrid prediction of the aerodynamic noise radiated by a rectangular cylinder at incidence.” In: *Computers & Fluids* 109 (2015). DOI: https://doi.org/10.1016/j.compfluid.2014.12.006 (cited on pages 131, 133).

[162] O. Inoue and N. Hatakeyama. “Sound generation by a two-dimensional circular cylinder in a uniform flow.” In: *Journal of Fluid Mechanics* 471 (2002), pp. 285–314. DOI: 10.1017/S0022112002002124 (cited on pages 131, 133).

[163] A. Laffite and F. Pérot. “Investigation of the Noise Generated by Cylinder Flows Using a Direct Lattice-Boltzmann Approach.” In: *15th AIAA/CEAS Aeroacoustics Conference (30th AIAA Aeroacoustics Conference)* (2009). DOI: https://doi.org/10.2514/6.2009-3268 (cited on pages 131, 133).

[164] N. Ganta, B. Mahato, and Y. G. Bhumka. “Analysis of sound generation by flow past a circular cylinder performing rotary oscillations using direct simulation approach.” In: *Physics of Fluids* 31.026104 (2019). DOI: https://doi.org/10.1063/1.5063642 (cited on pages 131, 133).

[165] M. A. Christon, P. M. Gresho, and S. B. Sutton. “Computational predictability of time-dependent natural convection flows in enclosures (including a benchmark solution).” In: *International Journal of Numerical Methods for Heat & Fluid Flow* 40.8 (2002), pp. 953–980. DOI: https://doi.org/10.1002/fld.395 (cited on page 133).

[166] T. J. R. Hughes and M. Mallet. “A new finite element formulation for computational fluid dynamics: III. The generalized streamline operator for multidimensional advective-diffusive systems.” In: *Computer Methods in Applied Mechanics and Engineering* 58.3 (1986), pp. 305–328 (cited on page 144).

[167] G. Le Beau and T. Tezduyar. “Finite element computation of compressible flows with the SUPG formulation.” In: *Army High Performance Computing Research Center* (1991) (cited on page 144).

[168] T. Tezduyar and M. Senga. “Stabilization and shock-capturing parameters in SUPG formulation of compressible flows.” In: *Computer Methods in Applied Mechanics and Engineering* 195.13 (2006), pp. 1621–1632 (cited on page 144).

[169] S. Parada, R. Codina, and J. Baiges. “Development of an algebraic fractional step scheme for the primitive formulation of the compressible Navier-Stokes equations.” In: *Journal of Computational Physics* 433 (2021), p. 110017. DOI: https://doi.org/10.1016/j.jcp.2020.110017 (cited on pages 145, 172).

[170] R. Codina. “Finite Element Approximation of the Convection-Diffusion Equation: Subgrid-Scale Spaces, Local Instabilities and Anisotropic Space-Time Discretizations.” In: *BAIL 2010- Boundary and Interior Layers, Computational and Asymptotic Methods* (2011), 85–97, Springer Berlin Heidelberg (cited on page 149).

[171] O.C. Zienkiewicz and R. Codina. “A general algorithm for the compressible and incompressible flows. Part I: The split, characteristic-based scheme.” In: *International Journal for Numerical Methods in Fluids* 20.8 - 9 (1995), pp. 869–885. DOI: https://doi.org/10.1002/fld.1650200812 (cited on pages 162, 164).

[172] M. Kouhi and E. Oñate. “An implicit stabilized finite element method for the compressible Navier–Stokes equations using finite calculus.” In: *Computational Mechanics* 56 (2015), pp. 113–129. DOI: https://doi.org/10.1007/s00466-015-1161-2 (cited on pages 162, 164, 166).

[173] F. Xu et al. “Compressible flows on moving domains: Stabilized methods, weakly enforced essential boundary conditions, sliding interfaces, and application to gas-turbine modeling.” In: *Computers & Fluids* 158 (2017), pp. 201–220 (cited on page 162).

[174] J.E. Carter. *Numerical solutions of the Navier–Stokes equations for the supersonic laminar flow over a two-dimensional compression corner.* Tech. rep. NASA, TR R-385, 1972 (cited on pages 162, 164).

[175] S. Mittal. “Finite element computation of unsteady viscous compressible flows.” In: *Computer Methods in Applied Mechanics and Engineering* 157 (1998), pp. 151–175. DOI: https://doi.org/10.1016/S0045-7825(97)00225-9 (cited on pages 164–168).

[176] V. Venkatakrishnan. “Viscous computations using a direct solver.” In: *Computers & Fluids* 18.2 (1990), pp. 191–204 (cited on pages 166–168).

[177] A. Bouhadji and M. Braza. “Organised modes and shock–vortex interaction in unsteady viscous transonic flows around an aerofoil. Part I: Mach number effect.” In: *Computer Methods in Applied Mechanics and Engineering* 32 (2003), pp. 1233–1260 (cited on page 168).

[178] Alfio Quarteroni, Fausto Saleri, and Alessandro Veneziani. "Analysis of the Yosida method for the incompressible Navier–Stokes equations." In: *Journal de Mathématiques Pures et Appliquées* 78.5 (1999), pp. 473–503. DOI: https://doi.org/10.1016/S0021-7824(99)00027-6 (cited on page 175).

[179] Yu Pan et al. "Development of a Balanced Adaptive Time-Stepping Strategy Based on an Implicit JFNK-DG Compressible Flow Solver." In: *Communications on Applied Mathematics and Computation* 4.2 (June 2022), pp. 728–757. DOI: 10.1007/s42967-021-00138-1 (cited on page 176).

[180] O. Peles and E. Turkel. "Adaptive Time Steps for Compressible Flows Based on Dual-Time Stepping and a RK/Implicit Smoother." In: *Journal of Scientific Computing* 81.3 (Dec. 2019), pp. 1409–1428. DOI: 10.1007/s10915-019-01024-y (cited on page 176).

[181] Nikhil Kalkote, Ashwani Assam, and Vinayak Eswaran. "Towards developing an adaptive time stepping for compressible unsteady flows." In: *International Journal of Numerical Methods for Heat & Fluid Flow* 29.2 (Jan. 2019), pp. 487–503. DOI: 10.1108/HFF-03-2018-0095 (cited on page 176).